UNIVERSITÀ DEGLI STUDI DI NAPOLI

FEDERICO II

DIPARTIMENTO DI MATEMATICA E

APPLICAZIONI "RENATO CACCIOPPOLI"

TESI DI DOTTORATO

ALBERTO TENORE

"FREE BOUNDARY PROBLEMS FOR MIXED-SPECIES BIOFILMS: MODELLING AND SIMULATION"

This PhD research was conducted as part of the National Operational Program for Research and Innovation 2014-2020, European Social Fund, Action I.1 "Innovative Doctorates with Industrial Characterization".

PhD Promoter

Prof. F. Capone,

Full Professor
Department of Mathematics and Applications "Renato Caccioppoli"
University of Naples "Federico II", Naples, Italy

International Scientific Partner

Dr. F. Fermoso, Instituto de la Grasa (CSIC), Seville, Spain

Industrial Partner

COGEI Srl, Naples, Italy

Thesis Committee

Thesis Supervisor

Dr. L. Frunzo,

Assistant Professor
Department of Mathematics and Applications "Renato Caccioppoli"
University of Naples "Federico II", Naples, Italy

Thesis Supervisor

Dr. M.R. Mattei,

Research fellow
Department of Mathematics and Applications "Renato Caccioppoli"
University of Naples "Federico II", Naples, Italy

Thesis Co-Supervisor

Dr. F. Fermoso,

Research fellow
Instituto de la Grasa
Spanish National Research Council (CSIC), Seville, Spain

Acknowledgments

I would like to express my gratitude to all the people I met during these three years as a PhD student. First of all, I thank my wonderful research group. I am deeply grateful to Prof. Berardino D'Acunto, for the immense passion and devotion that he places in the teaching and research activities, for the confidence he showed in me, for giving me the opportunity to experience the teaching activity. It was an honour for me to follow his courses during my university studies and to take part in his research meetings. I wish to acknowledge Prof. Florinda Capone, for being the promoter of my PhD, for the supervision and tutelage responsibilities, for the great availability she had towards me. I specially thank my supervisor Prof. Luigi Frunzo, for conveying to me the essence of the mathematical modelling starting from the preparation of my Master's thesis, for believing in my abilities, for helping and supporting me like an older brother in all scientific and practical obstacles of this experience. I would like to offer my special thanks to my supervisor Dr. Maria Rosaria Mattei, for her patience, for her suggestions, for all the scientific and moral support she has affectionately offer me. A few lines would not be enough to describe her importance in my research activity. I would like to share the merits of my scientific growth and of this thesis work with her. I wish to thank my Co-Supervisor Dr. Fernando Fermoso for welcoming me to the Instituto de la Grasa for my PhD period abroad, for his great hospitality and availability. Although this period was interrupted due to the health emergency caused by Covid-19, I enjoyed the few days spent at the Instituto, meeting a lot of nice people and working in a multidisciplinary research group. I would like to thank Dr. Vincenzo Luongo,

who has always behaved like a friend and has helped me in the realization of my first scientific article and supported me during my first scientific presentation at Ravello's school. I would like to extend my sincere thanks to my PhD colleagues, Daniele, Grazia and Fabiana, for the wonderful working atmosphere we lived, without envy, rivalry or competitions. Thanks to Daniele for sharing experiences, anxieties, joys and fears with me in these three years. Thanks to Grazia for cheering up my work days in the office, with jokes, conversations and laughter. Thanks to Fabiana for collaborating with me, for all the hours spent to discuss, reason and solve problems. I would like to thank my travel companion Domenico, who shared the nice experience in Seville with me and the lockdown period there. At the beginning of my PhD experience I had colleagues and supervisors, now I have got dear friends. Finally, I am deeply grateful to my family and my old friends, their support and love accompanied and inspired me during this amazing experience.

Abstract

English

This dissertation proposes a modelling study on biofilms, with a special interest in phototrophic biofilms, one of the most promising innovative biological technologies in the field of wastewater treatment.

Novel mathematical models are derived and presented here, with the aim of describing exhaustively the formation and the growth of planar and granular biofilms, specifically phototrophic-heterotrophic biofilms, anaerobic granular biofilms and oxygenic photogranules. The introduction of novel mathematical formulations allows to describe crucial aspects and processes of these ecosystems, never or not exhaustively explored by mathematical models present in literature.

Models presented here are formulated as one-dimensional free boundary problems, which describe the evolution of planar and granular biofilms. The processes taking place within the biofilm are modelled through systems of nonlinear partial differential equations (PDEs), derived using a continuum approach: non-linear hyperbolic PDEs model the advective transport and growth of sessile biomasses which constitute the biofilm, while quasi-linear parabolic PDEs govern the diffusive transport and conversion of soluble substrates, and the phenomena of microbial invasion by planktonic cells inhabiting the surrounding environment. The first proposed model consists of a free

boundary problem describing the role of planktonic cells in the formation and evolution of planar multispecies biofilms, by modelling the phenomena of initial attachment and microbial invasion. Moreover, a theorem of existence and uniqueness of the solutions, based on the fixed-point theorem, is presented. The second model is formulated as a free boundary problem which describes the ecology of phototrophic-heterotrophic biofilms. It considers the processes of microbial invasion and focuses on the metabolic activities of phototrophic and heterotrophic species, their interactions and main factors involved in this biofilm ecosystem, such as light conditions and attenuation, photoinhibition, phototrophic release of organic matter, production of extracellular polymeric substances (EPS). In order to model the process of initial formation and growth of anaerobic granular biofilms, known as *de novo* granulation, a free boundary problem is formulated within a spherical domain with radial symmetry. In this case, a multiscale approach is used, by modelling both the evolution of granular anaerobic biofilms and the dynamics of the bioreactor where such biofilms develop. Hence, such model allows to simulate the global treatment process occurring in anaerobic granular systems and to draw engineering conclusions. Finally, the latest model is aimed to describe for the first time the oxygenic photogranules (OPGs), biofilm granules composed of cyanobacteria and microalgae, recently recognised as an attractive biological technology to remove polluting compounds from wastewaters. As the previous one, this multiscale model is formulated as a spherical free boundary problem with radial symmetry, and allows to accurately describe the genesis and growth processes of oxygenic photogranules within a sequencing batch reactor (SBR) and to investigate the treatment efficiency of this system. The model considers the main biotic and abiotic factors involved, the symbiotic and competitive microbial mechanisms driving the treatment process, the metabolic differences between cyanobacteria and microalgae and the key role that cyanobacteria play in the photogranulation.

All models are integrated numerically through the development of original numerical softwares in MatLab platform. The main numerical methods used are the method

of characteristics, the Euler explicit method and the method of lines. Furthermore, the models presented are used to carry out numerical studies of relevant engineering, biological and ecological interest.

Italian

Questo lavoro di tesi propone uno studio di modellazione sui biofilm, con un interesse particolare verso i biofilm fototrofi, una delle tecnologie biologiche innovative più promettenti nel campo del trattamento delle acque reflue.

Nuovi modelli matematici sono derivati e presentati, con l'obiettivo di descrivere esaustivamente la formazione e la crescita di biofilm planari e granulari, in particolare biofilm fototrofi-eterotrofi, biofilm granulari anaerobici e fotogranuli ossigenici. L'introduzione di nuove formulazioni matematiche permette di descrivere aspetti e processi cruciali di questi ecosistemi, mai esplorati o esplorati in maniera non esaustiva dai modelli matematici presenti in letteratura.

I modelli qui presentati sono formulati come problemi a frontiera libera monodimensionali, che descrivono l'evoluzione di biofilm planari e granulari. I processi che avvengono all'interno dei biofilm sono modellati attraverso sistemi di equazioni alle derivate parziali non lineari (PDE), derivate utilizzando un approccio continuo: PDE iperboliche non lineari modellano il trasporto advettivo e la crescita delle biomasse sessili che costituiscono il biofilm, mentre PDE paraboliche quasi lineari governano il trasporto diffusivo e la conversione dei substrati solubili, ed i fenomeni di invasione microbica da parte delle cellule planctoniche che vivono nell'ambiente circostante. Il primo modello proposto si basa su un problema a frontiera libera che descrive il ruolo delle cellule planctoniche nella formazione ed evoluzione dei biofilm multispecie planari, modellando i fenomeni di attachment iniziale ed invasione microbica. Inoltre, viene presentato un teorema di esistenza e unicità delle soluzioni, basato sul teorema del punto fisso. Il secondo modello è formulato come un problema a frontiera libera

che descrive l'ecologia dei biofilm fototrofi-eterotrofi. Questo considera i processi di invasione microbica e si focalizza sulle attività metaboliche delle specie fototrofa ed eterotrofa, sulle loro interazioni e sui principali fattori coinvolti in questo ecosistema, come le condizioni e l'attenuazione della luce, la fotoinibizione, il rilascio fototrofo di sostanza organica, la produzione di sostanze polimeriche extracellulari (EPS). Al fine di modellare il processo di formazione iniziale e crescita dei biofilm granulari anaerobici, noto come granulazione *de novo*, viene formulato un problema a frontiera libera all'interno di un dominio sferico con simmetria radiale. In questo caso, viene utilizzato un approccio multiscala, modellando sia l'evoluzione dei biofilm granulari anaerobici sia le dinamiche del bioreattore nel quale tali biofilm si sviluppano. Pertanto, tale modello consente di simulare il processo di trattamento globale che si verifica nei sistemi granulari anaerobici e di trarre conclusioni ingegneristiche. Infine, l'ultimo modello è volto a descrivere per la prima volta i fotogranuli ossigenici (OPG), granuli di biofilm governati da cianobatteri e microalghe, recentemente riconosciuti come un'attrattiva tecnologia biologica per rimuovere composti inquinanti dalle acque reflue. Come il precedente, questo modello multiscala è formulato come un problema a frontiera libera sferico con simmetria radiale, e consente di descrivere accuratamente i processi di genesi e crescita dei fotogranuli ossigenici all'interno di un reattore SBR e di indagare l'efficienza di trattamento di questo sistema. Il modello considera i principali fattori biotici e abiotici coinvolti, i meccanismi microbici simbiotici e competitivi che guidano il processo di trattamento, le differenze metaboliche tra cianobatteri e microalghe ed il ruolo chiave che i cianobatteri svolgono nella fotogranulazione.

Tutti i modelli sono integrati numericamente tramite lo sviluppo di originali software numerici nella piattaforma MatLab. I principali metodi numerici utilizzati sono il metodo delle caratteristiche, il metodo esplicito di Eulero ed il metodo delle linee. Inoltre, i modelli presentati vengono utilizzati per eseguire inediti studi numerici di rilevante interesse ingegneristico, biologico ed ecologico.

Contents

List of Figures

List of Tables

Chapter 1

Introduction

1.1 Research context

Biofilms are complex biological aggregates that generate great scientific interest, mainly induced by their ability to remove polluting compounds from wastewaters. Understanding the essence of these ecosystems and their evolution is hugely difficult, due to the complexity of the processes and phenomena which occur and the multiplicity of biotic and abiotic factors involved. For these reasons, the study of biofilms represents a scientific challenge, which requires a synergistic approach involving different research fields, such as biology and microbiology, chemistry, ecology and engineering. In this multidisciplinary framework, some branches of applied mathematics, such as mathematical modelling and numerical analysis, have dealt with this topic in parallel to the experimental research activity. Over time, several mathematical models have been proposed to describe and portray the world of biofilms in a simplified, incisive and faithful way, by including and modelling the remarkable aspects and by leaving out the negligible and minor ones.

These models have applicability in the industrial field of wastewater treatment,

thanks to their ability to simulate and predict the functioning of biofilm systems and the biological processes involved. Specifically, these easy-to-use models are able to quickly provide a volume of information that cannot be achieved through experimental practices, due to the high costs and time required. Accordingly, they can effectively support activities of sizing, management and monitoring of full-scale plants.

A brief introduction to biofilms and continuum modelling of biofilms is provided in the following sections.

1.1.1 Biofilms

Biofilms are defined as microbial aggregates composed of a microbial community incorporated in a self-produced matrix of polymeric substances [47]. The solid matrix provides high density and resistance to these aggregates and protects the microbial living community from desiccation, oxidizing and external agents such as hydrodinamic stress and antibiotics [46]. In the voids and channels of this porous matrix, a liquid phase is found, where soluble compounds, essential for the metabolic activities of the microbial species, are dissolved. Biofilm high density generates microscale gradients of the concentration of soluble compounds and, therefore, leads to the formation of distinct ecological niches. This results in extremely heterogeneous aggregates, dominated by multilayer structures, where different microbial species are arranged in different layers, coexisting and interacting through a complex interplay of symbiotic and competitive mechanisms.

Biofilms are ubiquitous in nature as they can develop in natural, medical, and industrial settings [37], when ideal conditions for their microbial metabolic activity are found. Although the growth of biofilms is frequently unintentional and can have detrimental effects on the environment where it occurs, most of the scientific interest in biofilms comes from their artificial use in the engineering field [139]: under controlled conditions the formation of biofilms can be intentionally induced in wastewater treat-

ment systems, where they grow by degrading and therefore removing the unwanted substances, such as carbon, nutrients and heavy metals, from wastewaters. The formation and growth of biofilms are regulated by a number of physical and biochemical processes which include intense interactions and mass exchanges with the surrounding environment. First, the biofilm formation is initiated by the attachment process performed by pioneer planktonic cells, which attach on a living or inert solid surface, switch their phenotype from planktonic to sessile and form the first attached monolayer of biofilm [90]. The growth of the biofilm is then driven by the metabolic activity of sessile biomass: this grows by converting soluble compounds dissolved within the liquid phase of the biofilm. Such compounds diffuse into the biofilm from the surrounding environment or are produced within the biofilm during the metabolism of the sessile microbial community. On the other hand, detachment phenomena lead to sessile biomass losses, induced by external shear forces, substrates depletion and biomass decay [124]. Finally, biofilm dynamics can be influenced by other phenomena, such as the microbial invasion: specific planktonic cells have the ability to penetrate the porous matrix of the biofilm from the surrounding liquid medium and constitute new sessile biomass [117].

The most used mathematical model on biofilms has been introduced by Wanner and Gujer [132] and has deeply influenced the successive modelling research activity, by introducing assumptions and mathematical formulations frequently resumed in more recent biofilm models. This continuum model simulates the evolution of multispecies biofilms and is formulated as a free boundary problem applied to a 1D domain. Model equations are derived from mass conservation principles. In particular, the expansion of the free boundary domain is supposed to be the result of growth and decay processes, and detachment processes. Furthermore, the advective transport and growth of sessile biomass are modelled through nonlinear hyperbolic partial differential equations (PDEs) while the diffusive transport and conversion of soluble compounds are described through quasi-linear parabolic PDEs. Non-linearity derives from the intricate mathematical expressions introduced in the reaction terms, necessary to describe

the complexity and multiplicity of the biochemical transformations which regulate the biofilm dynamics. Over the years, the basic version of this model has been adapted in order to include additional phenomena such as microbial invasion [28]. Anyway, an exhaustive modelling description of the interactions between sessile and planktonic phenotypes is not present in the literature.

1.1.2 Phototrophic biofilms

In recent years, new technologies based on phototrophic biofilms have become widespread in the field of wastewater treatment. These kind of biofilms are governed by phototrophic microorganisms such as microalgae and cyanobacteria, and typically develop in freshwater [103] and marine [17] ecosystems, and sometimes in highly humid subaerial sites [128], on solid surfaces subject to appropriate light conditions and availability of nutrients. Moreover, high amounts of heterotrophic bacteria are frequently detected in these biofilms, supported by multiple and complex symbiotic mechanisms with phototrophic microorganisms, above all the phototrophic production of oxygen [50]. Due to their properties, phototrophic biofilms are cultivated in wastewater treatment systems under appropriate light conditions and allow to purify wastewaters by degrading carbon and nutrient compounds without the involvement of external sources of oxygen. Furthermore, phototrophic biomass deriving from wastewater treatments represents an ideal feedstock for other industrial applications such as the production of biofuels, chemicals, and nutraceuticals [53].

In this context, numerous experimental studies on photrotrophic biofilms have been performed to confirm their applicability and efficiency in the wastewater treatment field [94], to identify the factors driving their growth [35] and to investigate the mechanisms of interaction existing between phototrophs and heterotrophs [100, 143]. At the same time, some monospecies [21, 22, 67, 93] and multispecies [138, 84] mathematical models have been proposed to simulate the evolution of phototrophic biofilms and their

treatment performances. However, some aspects of phototrophic biofilms still remain unexplored. In particular, the intricate interplay of symbiotic and competitive microbial phenomena governing the biofilm growth appears to be considered in a partial and limited way, without the aim of achieving an exhaustive and accurate description of the ecology of these ecosystems.

1.1.3 Granular biofilms and oxygenic photogranules

Although biofilms typically form and grow attached to solid surfaces, specific environmental conditions can lead to the development of particular support free biofilms [123], known as granular biofilms or biofilm granules. These aggregates share the typical properties of biofilms in terms of density and composition, but they have a spherical structure and grow suspended in liquid environments. The process leading to the formation of biofilm granules is known as granulation and is initiated and regulated by mechanisms which are still not fully understood. Intense hydrodynamic conditions appear to be the main requirement for the success of the granulation process [69], despite some studies point out the key role of specific microbial species [92]. In the last decades, aerobic, anaerobic and anammox granular biofilms have found wide use in wastewater treatment systems [107, 95, 125].

Very recently, great attention has been paid to oxygenic photogranules (OPGs) [79], spherical granules constituted by a large phototrophic component which, as in the case of phototrophic biofilms growing attached to solid surfaces, produce oxygen necessary for the oxidation of polluting compounds present in wastewaters. In contrast to aerobic, anaerobic and anammox granules, which develop exclusively under intense hydrodynamic conditions, photogranules growth has been also observed under hydrostatic conditions [7]. Specifically, the growth of OPGs seems to be driven by cyanobacteria [2, 3], which first favor the initial photogranulation and then preserve the spherical structure of granules thanks to their filamentous structure, high EPS production and gliding motility.

Some modelling works have adapted the free boundary problem introduced by Wanner and Gujer to a spherical domain with radial symmetry, and have used this new formulation to correctly model the evolution of aerobic [32], anaerobic [88] and anammox [129] granular biofilms. Although such models focus on important aspects of the process, they neglect other equally significant elements. First, no work present in the literature reports a mathematical overview of the spherical free boundary model, by illustrating assumptions, mass balances, equations, initial and boundary conditions which define the model. Then, no modelling work focuses on the initial granulation process, which is ignored by neglecting attachment phenomena and considering biofilm granules already formed in the initial configuration. Furthermore, numerical studies on granular biofilms present in literature mainly focus on the treatment performance of the wastewater systems, while there is a lack of studies aimed at investigating ecological and biological aspects of the granules. Finally, since the engineering and biological interest in oxygenic photogranules is very recent, currently their development and the associated treatment processes have never been modelled.

1.2 Scope of the thesis

This dissertation deals with the mathematical modelling of biofilms, with a particular interest in phototrophic biofilms. Specifically, the modelling study of these microbial aggregates has been carried out through an interdisciplinary approach, arising from scientific collaborations with mathematicians, engineers and microbiologists. Two are the primary objectives pursued. The first is to describe the formation and growth of planar and granular biofilms, by modelling the main biological and ecological aspects of these ecosystems. Starting from this, the second objective consists in the modelling of innovative biofilm based systems devoted to wastewater treatment, by predicting and simulating the biological processes involved. For this purpose, the first part of the thesis (Chapters 2 and 3) focuses on the biofilm domain, and deals with the modelling

of specific aspects and phenomena partially or never addressed by models present in the literature, with the aim of achieving a comprehensive mathematical formulation of the mechanisms which govern the biofilm dynamics. These contents have been used to formulate new multiscale models (Chapters 4 and 5) which take into account both the microscale biofilm and the macroscale bioreactor and are able to predict the treatment process occurring in the biofilm systems.

In order to correctly describe the dimensional evolution of biofilms, all models presented are formulated within free boundary domains, which expand due to various phenomena such as attachment, detachment, invasion, microbial growth and decay.

In Chapter 2, a 1D free boundary model on the role of planktonic cells in biofilm formation and development is proposed, by modelling the initial attachment process and invasion phenomena by planktonic microbial cells present in the surrounding liquid medium. Furthermore, it is shown how the restrictions on ecological structure deriving from the mathematical formulation of Wanner and Gujer type models, reported and highlighted in [59], can be overcome through the modelling of microbial invasion phenomena. Finally, a theorem of existence and uniqueness of the solutions is presented for this model. Chapter 3 is devoted to the modelling of phototrophic biofilms, in particular the ecology of phototrophic-heterotrophic biofilms, describing how these two trophic species interact with each other and drive the evolution of these biofilms. In this context, the main factors involved in the process are considered and modelled, such as metabolic activities of microbial species, light conditions and their effects on the phototrophic growth, light attenuation across the biofilm, photoinhibition, phototrophic release of organic matter and EPS production. Chapter 4 presents a multiscale model on the formation and growth of granular biofilms within a completely mixed continuous reactor. It is developed in collaboration with Dr. Gavin Collins, from National University of Ireland (Galway, Ireland), who provided his scientific support in the biological and microbiological aspects of the work. Biofilm granules are modelled as spherical free boundary domains with radial symmetry. The mathematical formulation of the ini-

tial attachment, introduced in Chapter 2 for planar biofilms, is proposed here to model the granulation process. Moreover, the dynamics of soluble substrates and suspended biomasses have been taken into account. An exhaustive overview of the model has been carried out, by deriving equations starting from mass balances and by presenting all assumptions, variables, initial and boundary conditions involved. Furthermore, this model has been used to simulate the *de novo* granulation and the evolution of anaerobic granules. The mathematical formulations introduced in Chapters 2, 3 and 4 to model the attachment phenomena, the phototrophic metabolic activity, the microbial interactions between phototrophs and heterotrophs and the spherical free boundary problem with radial symmetry, are resumed in Chapter 5 to model for the first time oxygenic photogranules. This multiscale model allows to accurately describe the genesis and growth of oxygenic photogranules within a sequencing batch reactor (SBR) and to investigate the treatment efficiency of this system, by considering metabolic differences between cyanobacteria and microalgae, and the factors driving the process.

Due to the complexity and non-linearity of equations involved, all models in question have been numerically integrated through original softwares developed in MatLab platform. Hyperbolic PDEs have been integrated by using the method of characteristics, applied for the first time in the biofilm context by [27], while the Euler explicit method and the method of lines have been used to integrate parabolic PDEs. In Chapters 3, 4 and 5, original numerical studies of scientific interest are performed, to reveal the potential of the models and to investigate significant engineering, biological and ecological aspects of the processes described: the ecology of phototrophic-heterotrophic biofilms, anaerobic granules and oxygenic photogranules, the microbial interactions between phototrophs and other bacterial species, the effects of light on the growth of planar phototrophic biofilms and photogranules, the depurative performances of anaerobic granular systems and photogranules based systems. Numerical results are presented and discussed with the support of numerous figures. Some results are qualitatively compared with experimental evidences, while others suggest interesting perspectives

and conclusions that could be verified through future experimental studies. The output items shown include: evolution of dimension, relative abundance and microbial composition of 1D and spherical biofilms, spatial profiles of substrates and planktonic biomasses concentration, spatial profiles of light intensity across the biofilm, trends of the concentration of soluble substrates and suspended biomass within the reactor over time. Furthermore, model assumptions and characteristics are widely discussed, showing the model strengths and pointing out the model weaknesses that should be explored in possible future works. Conclusions and recommendation for future research are presented in Chapter 6.

Chapter 2

Free boundary problem for the role of planktonic cells in biofilm formation and development

2.1 Introduction

In recent years, the study of how the sessile and planktonic phenotypes interact in biofilm lifestyle has become a theme of intense interest and scrutiny [106]. Biofilms are microbial assemblies which commonly develop attached to abiotic or biotic surfaces. They are characterized by a solid matrix of extracellular polymeric substance (EPS) in which microorganisms are embedded [46]. The biofilm dynamics are deeply influenced by microbial mass exchanges between biofilm and the surrounding environment, which involve both the sessile and planktonic biomasses. The biofilm formation is initiated by pioneer microbial cells in planktonic form, which attach to a solid support through

This Chapter has been submitted to *Zeitschrift für angewandte Mathematik und Physik (ZAMP)* as: D'Acunto, B., Frunzo, L., Luongo, V., Mattei, M.R., Tenore, A. Free boundary problem for the role of planktonic cells in biofilm formation and development.

an initial attachment process. Such cells switch their mode of growth from planktonic to sessile and constitute the first sessile microbial colony [90], which develops and expands over time as a result of the microbial metabolic growth. Meanwhile, large EPS production by sessile cells confers high density and compactness to the aggregate and protects it from external agents. During the maturation stage, the high density induces large spatial gradients in biofilm properties, leading to numerous microenvironments and extremely heterogeneous microbial distributions. Specifically, new biological conditions arising within the biofilm can promote the phenomenon of microbial invasion: motile planktonic cells colonize the aggregate by penetrating the biofilm matrix, and proliferate as new sessile biomass where ideal conditions for their metabolic activity occur [117]. This means that the number of microbial species constituting the biofilm can increase over time, since microbial species initially not present can join the biofilm when new metabolic microniches arise. Furthermore, external shear forces, nutrients depletion and biomass decay lead to the detachment of cells from the biofilm colony into the surrounding medium [124]. Lastly, in the final stage of the biofilm lifecycle, microbial dispersal phenomena can occur: as a result of habitat decay (resource depletion and cell competition for space), planktonic cells, known as dispersed cells, are released in the surrounding environment, migrate to new surfaces and subsequently constitute new biofilm aggregates [77].

Despite the high amount of mathematical works on multispecies biofilms growth developed in the framework of the Wanner and Gujer model [132] or as multidimensional partial differential equation models [5, 24, 134, 39, 21], most of them completely neglect the attachment process in the initial phase of biofilm formation, since the initial data that prescribe location, size, and composition of colonies at the onset of the simulations are arbitrarily assigned. This strongly affects the biofilm development and maturation as highlighted by a recent work [102] where the attachment has been incorporated as a discrete stochastic process in a density-dependent diffusion-reaction model for cellulolytic biofilms. Furthermore, the Wanner-Gujer type models [132, 74, 51, 29]

can lead, in some cases, to ecological restrictions on the number of species constituting the biofilm [59]. Indeed, they are characterized by a restriction on the number of species that can inhabit the biofilm under the detachment regime: that is if a species is not initially present within the biofilm on the support, it will be washed out from the system. The free boundary problem introduced in this Chapter is intended to overcome these limitations by considering the initial biofilm formation mediated by planktonic cells as well as the colonization process. In particular, we present a one-dimensional continuous model considering two state variables representing the planktonic and sessile phenotypes and reproducing the transition from the former to the other in the biofilm lifecycle. The underlying model is a coupled hyperbolic-elliptic free boundary value problem with nonlocal effects. The attachment is modelled as a continuous, deterministic process which depends on the concentrations of the attaching species in the bulk liquid [29]. The colonization process which results in the establishment of new species in sessile form is modelled by considering an additional reaction term in the hyperbolic equations, which depends on the concentration of planktonic species within the biofilm [28]. The concentration of the planktonic species within the biofilm is governed by elliptic partial differential equations which describe their diffusion from the bulk liquid within the biofilm. A reaction term is considered to account for the conversion of the planktonic phenotype into the sessile mode of growth.

The Chapter is organized as follows. Section 2.2 introduces the mathematical background for the attachment process in the initial phase of multispecies biofilm formation, in the framework of the Wanner-Gujer approach to biofilm modelling [29]. The free boundary is constituted by the biofilm thickness and it is assumed to be initially zero. The growth of the attaching species is governed by nonlinear hyperbolic partial differential equations. The free boundary is governed by a first order differential equation that depends on attachment, detachment and biomass growth velocity. It is recalled that the free boundary velocity is greater than the characteristic velocity of the mentioned hyperbolic system during the first instants of biofilm formation. As a consequence, the

free boundary is a space-like line. The initial-boundary conditions for the microbial concentrations are assigned on this line and they are equal to the relative abundance of the species in the biomass attached to the biofilm-bulk liquid interface. The free boundary value problem is completed by a system of semi-linear elliptic partial differential equations that governs the quasi-static diffusion of substrates. In Section 2.3, a numerical experiment shows that the free boundary problem introduced in [29] needs to be generalized to eliminate any restriction on the number of species inhabiting the mature biofilm as described in [59]. Section 2.4 introduces the new free boundary problem which accounts for both the initial phase of biofilm formation and the diffusion and colonization of planktonic species within the biofilm. Section 2.5 introduces the integral version of the differential free boundary problem provided in Section 2.4, which is derived by adopting characteristics coordinates. An existence and uniqueness theorem of solutions is shown in Section 2.5 in the class of continuous functions. The proposed model is also solved numerically to simulate the biofilm evolution during biologically relevant conditions and provides interesting insights towards quantitative understanding of biofilm dynamics and ecology. Numerical results are reported in Section 2.6. Finally, the conclusions of the Chapter are outlined in Section 2.7.

2.2 Background

A free boundary approach was introduced in [29] for modelling the initial phase of the multispecies biofilm formation and growth in the framework of Wanner and Guyer model [132]. In this context, denoting by $X_i(z,t)$ the concentration of the generic bacterial species i, the one-dimensional multispecies biofilm growth is governed by the following system of nonlinear hyperbolic partial differential equations

$$\frac{\partial}{\partial t}X_i(z,t) + \frac{\partial}{\partial z}(u(z,t)X_i(z,t)) = \rho_i r_{M,i},\ i = 1, ..., n, \tag{2.1}$$

where $u(z,t)$ denotes the velocity of the microbial mass, $r_{M,i}$ the specific growth rate, and ρ_i the constant density. In addition, the substratum is assumed to be placed at $z = 0$. The function $r_{M,i}$ depends on $\mathbf{X} = (X_1, ..., X_n)$, and substrates S_j, $j = 1, ..., m$, as well $r_{M,i} = r_{M,i}(\mathbf{X}(z,t), \mathbf{S}(z,t)),\ \mathbf{S} = (S_1, ..., S_m)$.
$u(r,t)$ is governed by the following equation:

$$\frac{\partial u}{\partial z} = \sum_{i=1}^{n} r_{M,i},\ 0 < z \leq L(t),\ t > 0,\ u(0,t) = 0, \tag{2.2}$$

where $L(t)$ represents the biofilm thickness.

The substrate diffusion is governed by semi-linear parabolic partial differential equations that are usually considered in quasi-static conditions [74]

$$-D_j \frac{\partial^2 S_j}{\partial z^2} = r_{S,j}(\mathbf{X}(z,t), \mathbf{S}(z,t)),\ j = 1, ..., m, \tag{2.3}$$

where the functions $r_{S,j}$ denote the conversion rate of substrate j and D_j the diffusion coefficients assumed constant.

The biofilm thickness $L(t)$ represents the free boundary of the mathematical problem. Its evolution is governed by the following ordinary differential equation [132, 29, 23],

$$\dot{L}(t) = u(L,t) + \sigma_a(\boldsymbol{\psi}^*) - \sigma_d(L), \tag{2.4}$$

where σ_a denotes the attachment velocity of biomass from bulk liquid to biofilm and σ_d the detachment velocity of biomass from biofilm to bulk liquid. The function σ_a depends linearly on the concentrations ψ_i^*, $i = 1, ..., n$, $\boldsymbol{\psi}^* = (\psi_1^*, ..., \psi_n^*)$, of the microbial species in planktonic form present in the bulk liquid [132, 74, 29]. According to the experimental evidence, the ability of colonizing a clean surface is a feature of few microbial species, which are able to switch from their planktonic state, attach to the surface and start to secrete a polymeric matrix anchoring the cells to each other and to the surface. Even the formation of a single layer of cells can lead to a change

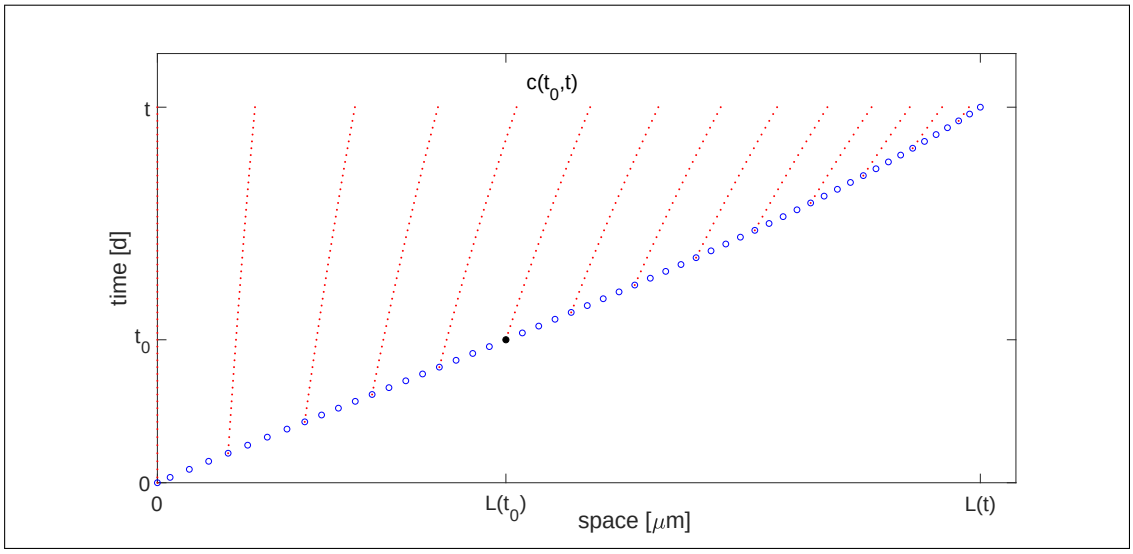

Figure 2.1: Time evolution of the free boundary with vanishing initial value and characteristic lines when $\sigma_a - \sigma_d > 0$. The free boundary is a space-like line. The blue dotted line denotes the free boundary evolution. Red dotted lines denote the characteristic-like lines.

on the electrostatic nature and mechanical properties of the surface, that can facilitate the attachment of new species that were initially unable to colonize the clean surface. According to [29], this is taken into account by considering in the formulation of the attachment flux $\sigma_a = \sum_{i=1}^{n} v_{a,i}\psi_i^*/\rho_i$ different attachment velocities $v_{a,i}$ for the single microbial species living in the liquid environment. Such velocities can be assigned constant or can be considered as functions of the environmental conditions affecting biofilm growth, that is substrate concentrations, biofilm composition itself, electrostatic and mechanical properties of the surface.

The function σ_d is usually assumed to be proportional to L^2: $\sigma_d = \delta L^2$, [1], where δ depends on the mechanical properties of the biofilm. In the initial phase of biofilm formation, where $L(0) = 0$, the attachment is the prevailing process and σ_d is very small, since so is L^2. Therefore, it is $\sigma_a - \sigma_d > 0$ and the free boundary velocity is greater than the characteristic velocity, $\dot{L}(t) > u(L,t)$. The free boundary is a space-like line, as illustrated in Fig. 2.1.

In the same figure, the characteristic-like lines of system (2.1) are also depicted. These

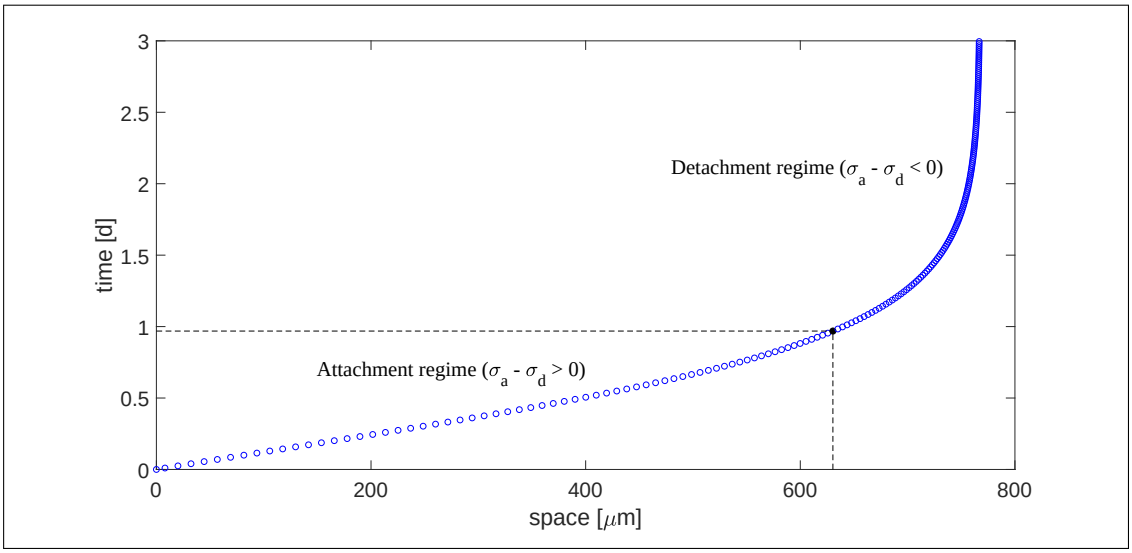

Figure 2.2: Time evolution of the free boundary with vanishing initial value. Note that the biofilm thickness undergoes both attachment ($\sigma_a - \sigma_d > 0$) and detachment regimes ($\sigma_a - \sigma_d < 0$), the latter prevailing for large L. The blue dotted line denotes the free boundary evolution.

lines, $z = c(t_0, t)$, are defined by the differential initial value problem

$$\frac{\partial c}{\partial t}(t_0, t) = u(c(t_0, t), t), \;\; c(t_0, t_0) = L(t_0). \tag{2.5}$$

For mature biofilms the free boundary L becomes large, the detachment is the prevailing process, it is $\sigma_a - \sigma_d < 0$ and the free boundary is a time-like line, Fig. 2.2.

The free boundary value problem (2.1)-(2.3) was discussed in [29] under the following initial-boundary conditions:

$$X_i(L(t), t) = X_{i,0}(t), \; i = 1, ..., n, \tag{2.6}$$

$$\frac{\partial S_j}{\partial z}(0, t) = 0, \; S_j(L, t) = S_j^*(t), \; j = 1, ..., m, \tag{2.7}$$

$$L(0) = 0. \tag{2.8}$$

In equations (2.6), $X_{i,0}(t)$ is the relative abundance of the species i in the biomass attached to the biofilm-bulk liquid interface [133]. More precisely, $X_{i,0}(t)$ can be evaluated as

$$X_{i,0}(t) = \frac{v_{a,i}\psi_i^*(t)}{\sum_{i=1}^n v_{a,i}\psi_i^*(t)}\rho_i,\ i = 1, ..., n, \tag{2.9}$$

where $\sigma_{a,i} = v_{a,i}\psi_i^*(t)$ denotes the attachment flux of the single species i and $\sigma_a = \sum_{i=1}^n v_{a,i}\psi_i^*(t)$ the total attachment flux. According to (2.9), the concentration of the microbial species at the biofilm-liquid interface $X_i(L(t), t)$ for a multispecies biofilm growing under attachment regime, depends on both the concentrations of the same species in planktonic form in the bulk liquid and their attachment propensity. Note that, when all the microbial species in the bulk liquid are characterized by the same attachment velocity, equations (2.9) reduces to

$$\frac{X_{i,0}(t)}{\rho_i} = \frac{\psi_i^*(t)}{\sum_{i=1}^n \psi_i^*(t)},$$

that is the volume fraction of the microbial species i at the biofilm-bulk liquid interface assumes the same value of the volume fraction within the bulk liquid. This reproduces the case of a biofilm that will be initially constituted by all microbial species inhabiting the surrounding liquid environment. However, going on with time the biofilm composition is affected by other factors such as substrate availability, specific microbial growth rate, detachment flux.

For what concerns substrate diffusion, the first boundary condition (2.7) is the no flux condition at substratum. The functions $S_j^*(t)$ in the second boundary condition (2.7) are prescribed functions in general.

2.3 Criticism

As outlined in [29], the model for the initial biofilm formation, summarized in the previous section, should be generalized to include the possibility that new attaching

bacterial species can move downward within the biofilm matrix and colonize the regions where the conditions for their growth are optimal. An example, referred to as *Case 1*, could help to better understand the question. To discuss this special problem, an equivalent expression will be used for equations (2.1), where X_i is replaced by the volume fraction f_i defined by

$$f_i(z,t) = X_i(z,t)/\rho_i,\ i = 1, ..., n, \tag{2.1}$$

subjected to the constraint

$$\sum_{i=1}^{n} f_i(z,t) = 1. \tag{2.2}$$

Considering (2.1) in (2.1) yields

$$\frac{\partial}{\partial t} f_i(z,t) + \frac{\partial}{\partial z}(u(z,t) f_i(z,t)) = r_{M,i},\ i = 1, ..., n. \tag{2.3}$$

For equations above, conditions (2.6) are replaced by

$$f_i(L(t),t) = f_{i,0}(t),\ i = 1, ..., n, \tag{2.4}$$

where

$$f_{i,0}(t) = X_{i,0}(t)/\rho_i. \tag{2.5}$$

Let us consider a three species and substrate biofilm $n = 3,\ m = 3$ growing under time-dependent conditions. In particular, the model simulates the case of a biofilm growing in a liquid environment initially inhabited by species ψ_1^* and ψ_2^* and continuously fed with substrates S_1 and S_2. At time $t = t_1 > 0$, a third species ψ_3^* is supposed to be fed into the system

$$\psi_i^*(t) = \psi_{i,0}^* > 0,\ 0 \le t \le T,\ i = 1, 2, \tag{2.6}$$

$$\psi_3^*(t) = \begin{cases} 0, & 0 \le t \le t_1, \\ \psi_{3,0}^* \frac{(t-t_1)^{10}}{t_1^{10/t_1}+(t-t_1)^{10}} > 0 & t_1 < t \le T. \end{cases} \tag{2.7}$$

Species ψ_1^* and ψ_2^* start to attach at $t = 0$ while the third at $t = t_1 > 0$

$$f_{i,0}(t) > 0,\ i = 1, 2,\ f_{3,0}(t) = 0,\ 0 \le t < t_1, \tag{2.8}$$

$$f_{i,0}(t) > 0,\ i = 1, 2, 3,\ t \ge t_1. \tag{2.9}$$

Functions $f_{i,0}(t)$ can be derived from equations (2.9), (2.6) and (2.7). Species f_1 and f_2 grow on substrate S_1 and S_2, respectively. Species f_1 by consuming substrate S_1 produces S_3, which is uptaken by f_3. All species are supposed to grow only in sessile form, and the reactor is considered as an infinite reserve of substrates and planktonic species ($S_j^*(t) = S_{j,0}^*$). The reaction terms $r_{M,i}$ and $r_{S,j}$ in equations (2.3) and (2.3) are modelled by using Monod type kinetics and are expressed as

$$r_{M,1} = \mu_{\max,1}\frac{S_1}{K_1+S_1}f_1,\ r_{M,2} = \mu_{\max,2}\frac{S_2}{K_2+S_2}f_2,\ r_{M,3} = \mu_{\max,3}\frac{S_3}{K_3+S_3}f_3, \tag{2.10}$$

$$r_{S,1} = -\frac{r_{M,1}}{Y_1}\rho_1,\ r_{S,2} = -\frac{r_{M,2}}{Y_2}\rho_2,\ r_{S,3} = \frac{r_{M,1}}{Y_1}\rho_1 - \frac{r_{M,3}}{Y_3}\rho_3. \tag{2.11}$$

The values of the kinetic parameters and boundary conditions used in the numerical simulations are reported in Table 2.1. All the sessile species are supposed to have the same density $\rho_i = \rho, i = 1, ..., n$. The simulation time adopted for the numerical experiment is $t = 10\ d$. We are aware that such simulation time will cover both the initial biofilm formation and the maturation phase where the detachment will be prevalent on the attachment flux. This choice is justified by the fact that we were interested in showing also the mature biofilm configuration, which is achieved under detachment regime. All numerical results are performed by using an original MatLab code. The method of

characteristics is used to track the biofilm expansion, while a finite difference approximation is adopted for the diffusion-reaction equations. The time to compute the values of the unknown variables is in the order of minutes to hours, depending on the specific target simulation time.

Parameter	**Definition**	**Unit**	**Value**
$\mu_{max,1}$	Maximum specific growth rate for f_1	d^{-1}	0.4
$\mu_{max,2}$	Maximum specific growth rate for f_2	d^{-1}	1.5
$\mu_{max,3}$	Maximum specific growth rate for f_3	d^{-1}	0.5
K_1	Half saturation constant for f_1 on S_1	$g\ m^{-3}$	1
K_2	Half saturation constant for f_2 on S_2	$g\ m^{-3}$	20
K_3	Half saturation constant for f_3 on S_3	$g\ m^{-3}$	1
Y_1	Yield of f_1 on S_1	$--$	0.4
Y_2	Yield of f_2 on S_2	$--$	0.9
Y_3	Yield of f_1 on S_1	$--$	0.9
D_1	Diffusion coefficient of S_1 in biofilm	$m^2\ d^{-1}$	10^{-5}
D_2	Diffusion coefficient of S_2 in biofilm	$m^2\ d^{-1}$	10^{-5}
D_3	Diffusion coefficient of S_3 in biofilm	$m^2\ d^{-1}$	10^{-5}
ρ	Biofilm density	$g\ m^{-3}$	5000
δ	Biomass shear constant	$m^{-1}\ d^{-1}$	2000
$S^*_{1,0}$	S_1 concentration in the bulk liquid	$g\ m^{-3}$	100
$S^*_{2,0}$	S_2 concentration in the bulk liquid	$g\ m^{-3}$	100
$S^*_{3,0}$	S_3 concentration in the bulk liquid	$g\ m^{-3}$	0
$\psi^*_{1,0}$	ψ^*_1 concentration in the bulk liquid	$g\ m^{-3}$	100
$\psi^*_{2,0}$	ψ^*_2 concentration in the bulk liquid	$g\ m^{-3}$	100
$\psi^*_{3,0}$	ψ^*_3 concentration in the bulk liquid	$g\ m^{-3}$	100
$v_{a,1}$	ψ^*_1 attachment velocity	$m\ d^{-1}$	$2.5 \cdot 10^{-2}$
$v_{a,2}$	ψ^*_2 attachment velocity	$m\ d^{-1}$	$2.5 \cdot 10^{-2}$
$v_{a,3}$	ψ^*_3 attachment velocity	$m\ d^{-1}$	$2.5 \cdot 10^{-2}$

Table 2.1: Kinetic parameters used for model simulations

Fig. 2.3 shows the free boundary evolution and the characteristic line $c(t_1, t)$ starting from $(L(t_1), t_1)$ up to $0.8d$ simulation time. Figs. 2.4 and 2.5 show the biofilm composition and substrate trends within the biofilm over time, under attachment and detachment regimes respectively.

The third species begins to adhere to the biofilm-bulk liquid interface at $t = t_1$. Substrates S_1 and S_2 are consumed within biofilm by species f_1 and f_2. As a consequence, favorable conditions for f_3 growth occurs within the inner biofilm region due to S_3 production. According to the uniqueness and existence theorem provided in [29], the third species is confined within the region $z > c(t_1, t)$ and does not colonize the region

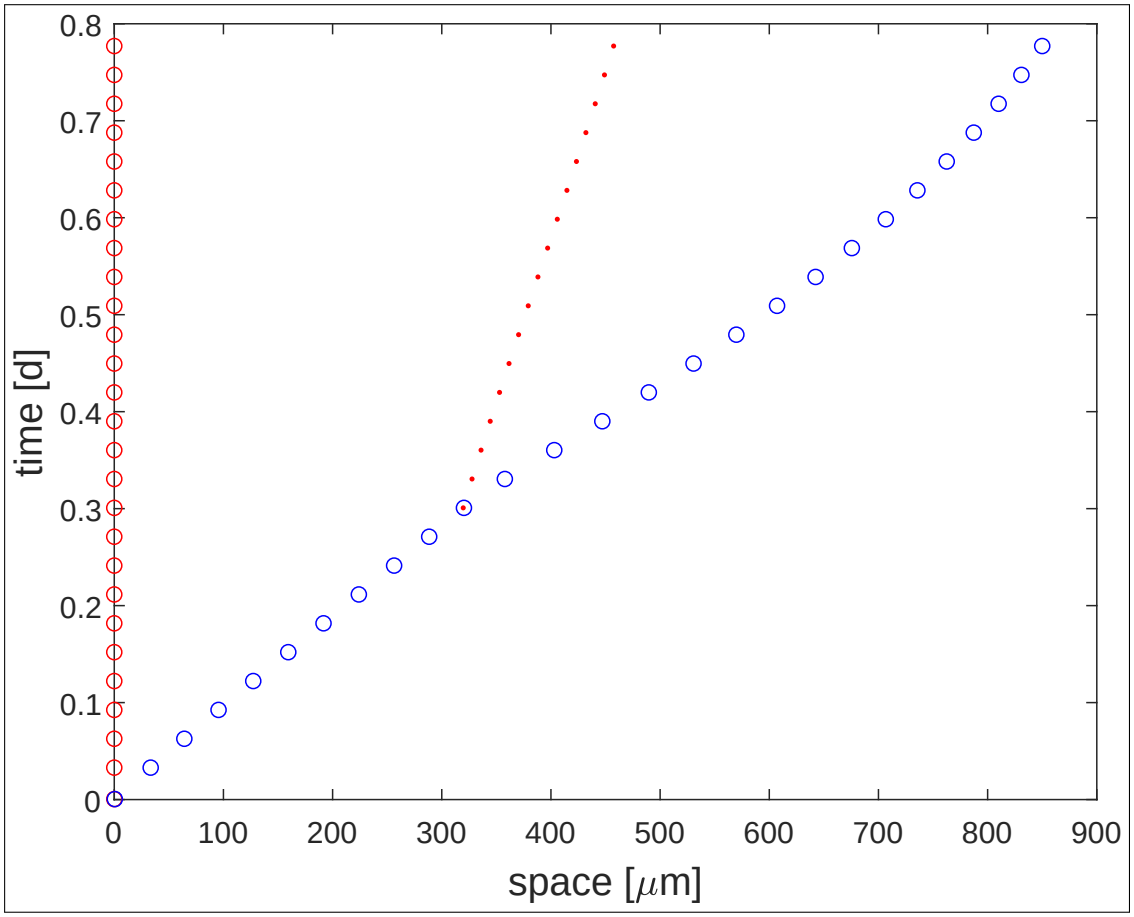

Figure 2.3: Time evolution of the free boundary (blue open dots) and the characteristic line $c(t_1, t)$ (red solid dots) under attachment regime ($\sigma_a - \sigma_d > 0$). Red open dots denote the characteristic line $c(0, t)$

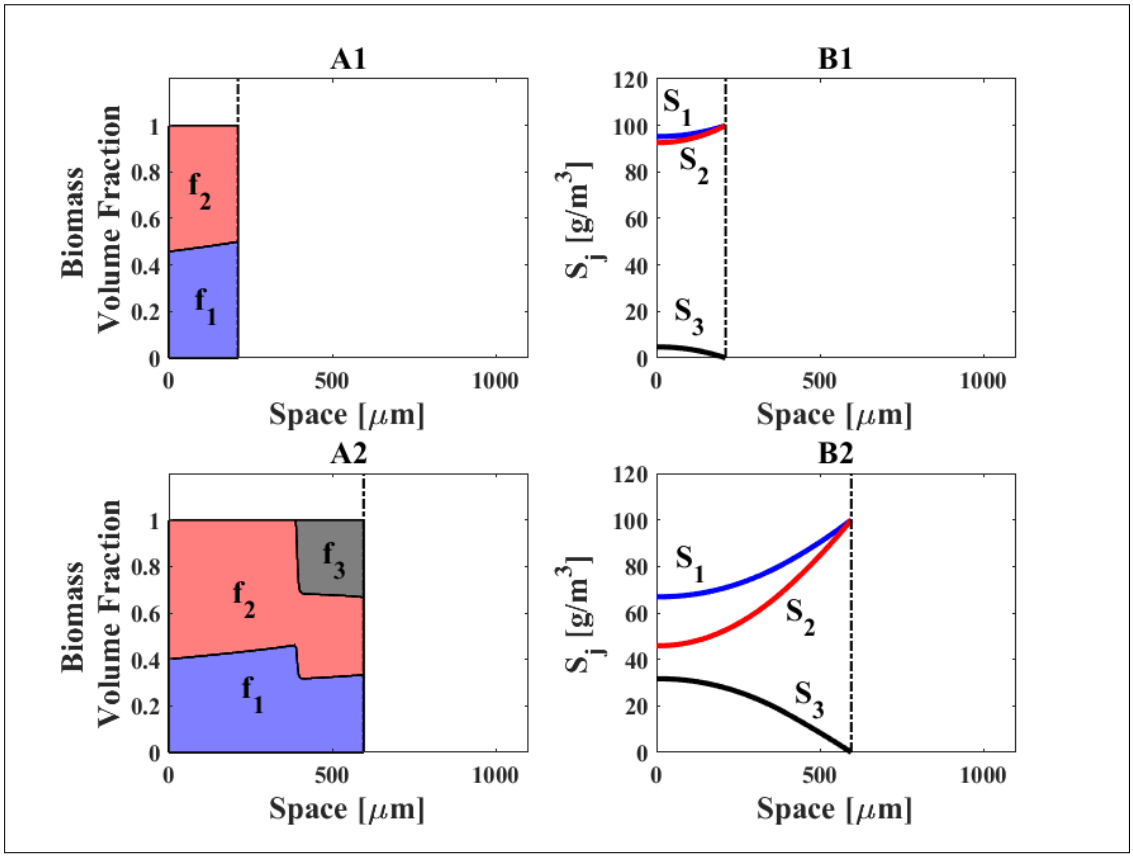

Figure 2.4: Biofilm composition (A1-A2) and substrate distribution (B1-B2) for *Case 1*, under attachment regime, at time $t = 0.25\ d$ (top) and $t = 0.50\ d$ (bottom).

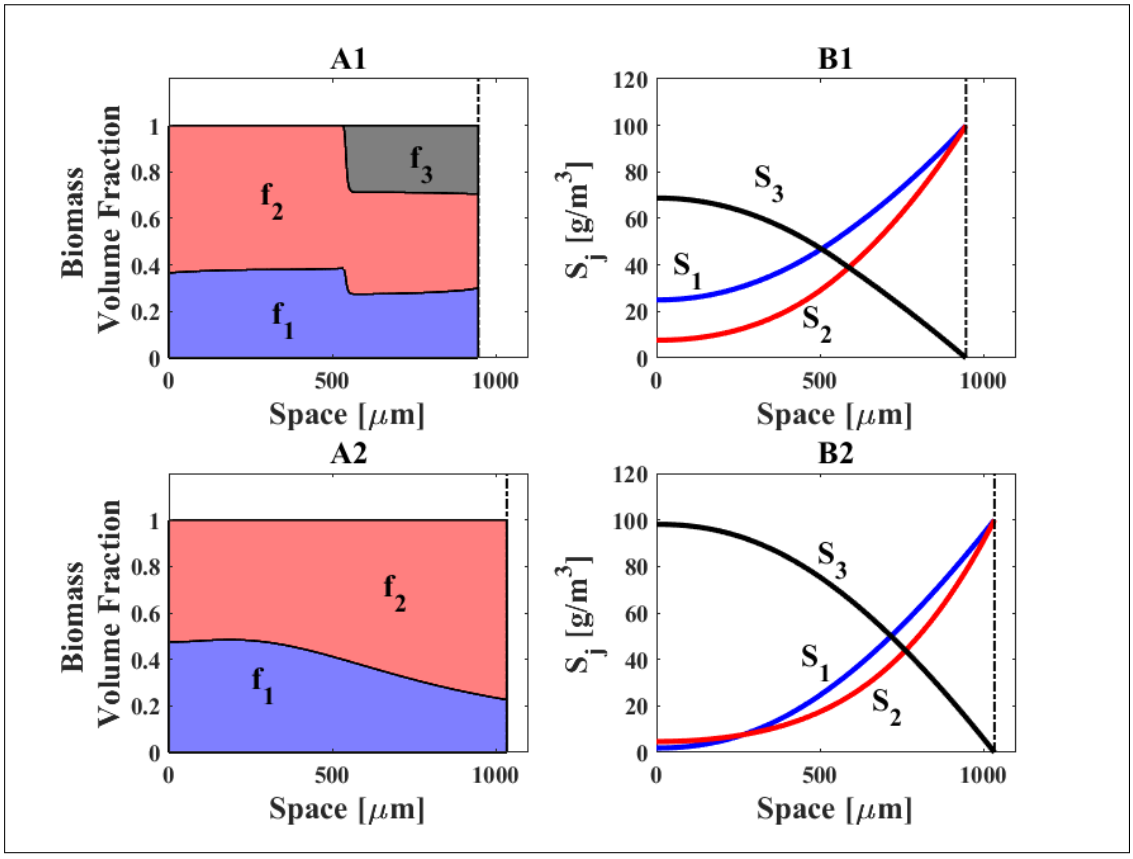

Figure 2.5: Biofilm composition (A1-A2) and substrate distribution (B1-B2) for *Case 1*, under detachment regime, at time $t = 1\ d$ (top) and $t = 10\ d$ (bottom).

$z < c(t_1, t)$ where there are favorable conditions for its growth

$$f_3(z,t) \begin{cases} = 0, & 0 \le z < c(t_1,t), \quad 0 \le t < t_1, \\ > 0, & z \ge c(t_1,t), \qquad t \ge t_1. \end{cases} \tag{2.12}$$

As shown in Figs. 2.4 and 2.5, the third species is unable to penetrate the inner biofilm region. Under detachment regime, its concentration tends to zero and it is completely washed out from the biofilm system. This is a well-known behavior of the model [132], as stated in [59]. The model introduced in this Chapter is intended to eliminate this great limitation.

2.4 Statement of the free boundary problem

This section presents the free boundary value problem for biofilm growth which considers its initial formation ($\sigma_a - \sigma_d > 0, L(0) = 0$) and the diffusion and colonization of the planktonic species within the biofilm. It is a generalization of the problem discussed in [74, 29] and it is obtained by developing some ideas introduced in [28]. Specifically, an additional state variable is considered, Ψ_i, $\mathbf{\Psi} = (\Psi_1, ..., \Psi_n)$, which represents the concentration of the planktonic species within the biofilm. The differential mass balance equations (2.1) are modified by adding a growth rate term r_i that takes into account for the colonizing bacterial species, and further equations are introduced for the diffusion of the planktonic species. The resulting model is able to overcome the criticism outlined in Sec. 2.3, as shown through the simple examples reported in Sec. 2.6.

The biofilm growth is governed by the following equations

$$\frac{\partial X_i}{\partial t} + \frac{\partial}{\partial z}(uX_i) = \rho_i r_{M,i}(\mathbf{X}, \mathbf{S}) + \rho_i r_i(\mathbf{\Psi}, \mathbf{S}),\ 0 \le z \le L(t),\ t > 0, i = 1, ..., n, \tag{2.1}$$

$$X_i(L(t), t) = X_{i,0}(t),\ t > 0,\ i = 1, ..., n, \tag{2.2}$$

$$\dot{L}(t) = u(L(t), t) + \sigma_a(\boldsymbol{\psi}^*),\ t > 0,\ L(0) = 0, \tag{2.3}$$

$$\frac{\partial u}{\partial z}(z,t) = G(\mathbf{X}(z,t), \mathbf{S}(z,t), \boldsymbol{\Psi}(z,t)),\ 0 < z \leq L(t),\ u(0,t) = 0, \tag{2.4}$$

where

$$G(\mathbf{X}(z,t), \mathbf{S}(z,t), \boldsymbol{\Psi}(z,t)) = \sum_{i=1}^{n} (r_{M,i} + r_i), \tag{2.5}$$

$$-D_j \frac{\partial^2 S_j}{\partial z^2} = r_{S,j}(\mathbf{X}(z,t), \mathbf{S}(z,t)),\ 0 < z < L(t),\ t > 0,\ j = 1, ..., m, \tag{2.6}$$

$$\frac{\partial S_j}{\partial z}(0,t) = 0,\ S_j(L,t)) = S_j^*(t),\ t > 0,\ j = 1, ..., m. \tag{2.7}$$

The diffusion of the colonizing species within the biofilm is governed by semi-linear parabolic partial differential equations that are considered in quasi-static conditions

$$-D_{\Psi,i} \frac{\partial^2 \Psi_i}{\partial z^2} = r_{\Psi,i}(\boldsymbol{\Psi}(z,t), \mathbf{S}(z,t)),\ 0 < z < L(t),\ t > 0,\ i = 1, ..., n, \tag{2.8}$$

where $r_{\Psi,i}$ indicates the conversion rate due to the switch from planktonic to sessile mode of growth and $D_{\Psi,i}$ is the diffusivity coefficient of the planktonic species within the biofilm. Diffusion equations for $\boldsymbol{\Psi}$ are considered in quasi-static conditions for the same reason as $\mathbf{S}$. Equations (2.8) are integrated with the following Neumann-Dirichlet boundary conditions

$$\frac{\partial \Psi_i}{\partial z}(0,t) = 0,\ \Psi_i(L,t) = \psi_i^*(t),\ t > 0,\ i = 1, ..., n, \tag{2.9}$$

where the no flux boundary conditions on the support are evident and the Dirichlet boundary conditions state that the values of the planktonic species on the free boundary are the same as in the bulk liquid.

Note that equation (2.3) refers to the initial phase of biofilm formation, when the detachment flux σ_d is negligible compared to σ_a. The free boundary $L(t)$ is a space-like line and equation (2.2) provides the initial conditions for the microbial species in sessile form on the free boundary. Conversely, during the maturation stage of biofilm growth the detachment flux is predominant and the free boundary is represented by a time-like line as stated in Sec. 2.2. The free boundary value problem referring to the mature phase of biofilm growth and considering the interaction between the planktonic and sessile phenotype through the colonization process has been investigated both qualitatively and numerically in [31, 30].

2.5 Uniqueness and existence theorem

According to [29], the differential free boundary problem (2.1)-(2.9) can be converted to an equivalent system of integral equations by using the characteristics introduced in (2.4). The integral problem is summarized below by using the following positions

$$\mathbf{x}(t_0,t) = \mathbf{X}(c(t_0,t),t), \;\; \mathbf{x}(x_1,...,x_n), \tag{2.10}$$

$$\mathbf{s}(t_0,t) = \mathbf{S}(c(t_0,t),t), \;\; \mathbf{s}(s_1,...,s_m), \tag{2.11}$$

$$\boldsymbol{\psi}(t_0,t) = \boldsymbol{\Psi}(c(t_0,t),t), \;\; \boldsymbol{\psi}(\psi_1,...,\psi_n), \tag{2.12}$$

The integral equations for x_i follow from (2.4),(2.1),(2.2),(2.4),(2.5)

$$x_i(t_0,t) = X_{i,0}(t_0) + \int_{t_0}^{t} F_i(\mathbf{x}(t_0,\tau),\mathbf{s}(t_0,\tau),\boldsymbol{\psi}(t_0,\tau))d\tau,\ 0 \le t_0 < t \le T,\ i = 1,...,n. \tag{2.13}$$

The integral equations for s_j follow from (2.6)-(2.7)

$$s_j(t_0,t) = \int_{t_0}^{t} d\theta \int_0^{\theta} F_{s,j}(\mathbf{x}(\tau,t), \mathbf{s}(\tau,t), \frac{\partial c}{\partial \theta}(\theta,t), \frac{\partial c}{\partial \tau}(\tau,t))d\tau$$

$$+S_j^*(t), \;\; 0 < t_0 < t \leq T, \; j = 1, ..., m, \tag{2.14}$$

where $F_{s,j}$ is defined in (2.22) at the end of this section. Similarly to $\mathbf{s}$, the integral equations for ψ_i follow from (2.8)-(2.9) and write

$$\psi_i(t_0,t) = \int_{t_0}^{t} d\theta \int_0^{\theta} F_{\psi,i}(\boldsymbol{\psi}(\tau,t), \mathbf{s}(\tau,t), \frac{\partial c}{\partial \theta}(\theta,t), \frac{\partial c}{\partial \tau}(\tau,t))d\tau$$

$$+\psi_i^*(t), \;\; 0 < t_0 < t \leq T, \; i = 1, ..., n, \tag{2.15}$$

where $F_{\psi,i}$ is defined in (2.23).

The integral equation for L follows from (2.4),(2.3),(2.4)

$$L(t_0) = \Sigma(t_0) + \int_0^{t_0} d\theta \int_0^{\theta} F_L(\mathbf{x}(\tau,\theta), \mathbf{s}(\tau,\theta), \boldsymbol{\psi}(\tau,\theta), \frac{\partial c}{\partial \tau}(\tau,\theta))d\tau, \; 0 < t_0 \leq T, \tag{2.16}$$

with $\Sigma(t_0)$ and F_L defined in (2.24)-(2.25).

The integral equations for $c(t_0,t)$ and $\partial c/\partial t_0$ can be obtained from (2.4),(2.3)-(2.5) rewritten in terms of characteristic coordinates

$$c(t_0,t) = \Sigma(t_0) + \int_0^{t_0} d\theta \int_0^{\theta} F_{c,1}(\mathbf{x}(\tau,\theta), \mathbf{s}(\tau,\theta), \boldsymbol{\psi}(\tau,\theta), \frac{\partial c}{\partial \tau}(\tau,\theta))d\tau$$

$$+ \int_{t_0}^{t} d\theta \int_0^{t_0} F_{c,1}(\mathbf{x}(\tau,\theta), \mathbf{s}(\tau,\theta), \boldsymbol{\psi}(\tau,\theta), \frac{\partial c}{\partial \tau}(\tau,\theta))d\tau, \;\; 0 < t_0 < t \leq T, \tag{2.17}$$

$$\frac{\partial c}{\partial t_0}(t_0,t) = \int_{t_0}^{t} F_{c,2}(\mathbf{x}(t_0,\theta),\mathbf{s}(t_0,\theta),\boldsymbol{\psi}(t_0,\theta),\frac{\partial c}{\partial t_0}(t_0,\theta))d\theta$$

$$+\sigma_a(\boldsymbol{\psi}^*(t_0)), \quad 0 < t_0 < t \leq T, \tag{2.18}$$

where

$$F_{c,1}(\mathbf{x}(\tau,\theta),\mathbf{s}(\tau,\theta),\boldsymbol{\psi}(\tau,\theta),\frac{\partial c}{\partial \tau}(\tau,\theta))$$

$$= G(\mathbf{x}(\tau,\theta),\mathbf{s}(\tau,\theta),\boldsymbol{\psi}(\tau,\theta))\frac{\partial c}{\partial \tau}(\tau,\theta), \tag{2.19}$$

$$F_{c,2}(\mathbf{x}(t_0,\theta),\mathbf{s}(t_0,\theta),\boldsymbol{\psi}(t_0,\theta),\frac{\partial c}{\partial t_0}(t_0,\theta))$$

$$= G(\mathbf{x}(t_0,\theta),\mathbf{s}(t_0,\theta),\boldsymbol{\psi}(t_0,\theta))\frac{\partial c}{\partial t_0}(t_0,\theta). \tag{2.20}$$

The functions introduced in equations (2.13)-(2.16) are defined below

$$F_i = \rho_i(r_{M,i} + r_i) - X_i G, \quad i = 1,...,n, \tag{2.21}$$

$$F_{s,j}(\mathbf{x}(\tau,t),\mathbf{s}(\tau,t),\frac{\partial c}{\partial \theta}(\theta,t),\frac{\partial c}{\partial \tau}(\tau,t))$$

$$= D_j^{-1} r_{S,j}(\mathbf{x}(\tau,t),\mathbf{s}(\tau,t))\frac{\partial c}{\partial \theta}(\theta,t)\frac{\partial c}{\partial \tau}(\tau,t), \tag{2.22}$$

$$F_{\psi,i}(\boldsymbol{\psi}(\tau,t),\mathbf{s}(\tau,t),\frac{\partial c}{\partial \theta}(\theta,t),\frac{\partial c}{\partial \tau}(\tau,t))$$

$$= D_{\psi,i}^{-1}\, r_{\psi,i}(\boldsymbol{\psi}(\tau,t),\mathbf{s}(\tau,t))\frac{\partial c}{\partial\theta}(\theta,t)\frac{\partial c}{\partial\tau}(\tau,t), \tag{2.23}$$

$$\Sigma(t_0) = \int_0^{t_0} \sigma_a(\boldsymbol{\psi}^*(\theta))d\theta, \tag{2.24}$$

$$F_L(\mathbf{x}(\tau,\theta),\mathbf{s}(\tau,\theta),\boldsymbol{\psi}(\tau,\theta)\frac{\partial c}{\partial\tau}(\tau,\theta)) = G(\mathbf{x}(\tau,\theta),\mathbf{s}(\tau,\theta),\boldsymbol{\psi}(\tau,\theta))\frac{\partial c}{\partial\tau}(\tau,\theta). \tag{2.25}$$

An existence and uniqueness theorem for the integral problem (2.13)-(2.18) can be proved in the space of the continuous functions as generalization of the results in [29].

Theorem 2.5.1. *Suppose that:*

(a) $x_i(t_0,t), s_j(t_0,t), \psi_i(t_0,t), c(t_0,t), c_{t_0}(t_0,t) \in C^0([0,\ T_1]\times[0,\ T_1]),\ T_1>0,$ $i=1,...,n,\ j=1,...,m$, and $L(t_0)\in C^0([0,\ T_1])$;

(b) $X_{i,0}(t_0), \sigma_a(\boldsymbol{\psi}^*(t_0)), S_j^*(t), \Psi_i^*(t) \in C^0([0,\ T_1]),\ i=1,...,n,\ j=1,...,m$;

(c) $|x_i - X_{i,0}| \le h_{x,i},\ i=1,...,n;\ |s_j - S_j^*| \le h_{s,j},\ j=1,...,m;\ |\psi_i - \psi_i^*| \le h_{\psi,i},\ i=1,...,n;\ |L-\Sigma| \le h_L;\ |c-\Sigma| \le h_{c,1};\ |c_{t_0}-\sigma_a| \le h_{c,2}$, *where* $h_{x,i}, h_{s,j}, h_{\psi,i}, h_L, h_{c,1}, h_{c,2}$ *are positive constants;*

(d) $F_i, i=1,...,n,\ F_{s,j}, j=1,...,m,\ F_{\psi,i}, i=1,...,n,\ F_L, F_{c,1}, F_{c,2}$ *are bounded and Lipschitz continuous with respect to their arguments*

$$M_i = \max|F_i|,\ i=1,...,n,\ M_{s,j} = \max|F_{s,j}|,\ j=1,...,m,$$

$$M_{\psi,i} = \max|F_{\psi,i}|,\ i=1,...,n,\ M_L = \max|F_L|,\ M_{c,1} = \max|F_{c,1}|,\ M_{c,2} = \max|F_{c,2}|,$$

$$|F_i(\mathbf{x},\mathbf{s},\boldsymbol{\psi}) - F_i(\tilde{\mathbf{x}},\tilde{\mathbf{s}},\tilde{\boldsymbol{\psi}})| \le \lambda_i\left[\sum_{k=1}^{n}|x_k-\tilde{x}_k| + \sum_{k=1}^{m}|s_k-\tilde{s}_k| + \sum_{k=1}^{n}|\psi_k-\tilde{\psi}_k|\right],\ i=1,...n,$$

$$|F_{s,j}(\mathbf{x},\mathbf{s},c_{t_0}) - F_{s,j}(\tilde{\mathbf{x}},\tilde{\mathbf{s}},\tilde{c}_{t_0})| \le \lambda_{s,j}\left[\sum_{k=1}^{n}|x_k-\tilde{x}_k|\right.$$

$$+\sum_{k=1}^{m}|s_k-\tilde{s}_k|+|c_{t_0}-\tilde{c}_{t_0}|\Bigg],\ j=1,...m,$$

$$|F_{\psi,i}(\boldsymbol{\psi},\mathbf{s},c_{t_0})-F_{\psi,i}(\tilde{\boldsymbol{\psi}},\tilde{\mathbf{s}},\tilde{c}_{t_0})|\leq\lambda_{\psi,i}\Bigg[\sum_{k=1}^{n}|\psi_k-\tilde{\psi}_k|$$

$$+\sum_{k=1}^{m}|s_k-\tilde{s}_k|+|c_{t_0}-\tilde{c}_{t_0}|\Bigg],\ i=1,...,n,$$

$$|F_L(\mathbf{x},\mathbf{s},\boldsymbol{\psi},c_{t_0})-F_L(\tilde{\mathbf{x}},\tilde{\mathbf{s}},\tilde{\boldsymbol{\psi}},\tilde{c}_{t_0})|\leq\lambda_L\Bigg[\sum_{k=1}^{n}|x_k-\tilde{x}_k|$$

$$+\sum_{k=1}^{m}|s_k-\tilde{s}_k|+\sum_{k=1}^{n}|\psi_k-\tilde{\psi}_k|+|c_{t_0}-\tilde{c}_{t_0}|\Bigg],$$

$$|F_{c,1}(\tau,t,\mathbf{x})-F_{c,1}(\tau,t,\tilde{\mathbf{x}})|\leq\lambda_{c,1}\left[\sum_{k=1}^{n}|x_k-\tilde{x}_k|+\sum_{k=1}^{m}|s_k-\tilde{s}_k|+\sum_{k=1}^{n}|\psi_k-\tilde{\psi}_k|+|c_{t_0}-\tilde{c}_{t_0}|\right],$$

$$|F_{c,2}(\tau,t,\mathbf{x})-F_{c,2}(\tau,t,\tilde{\mathbf{x}})|\leq\lambda_{c,2}\left[\sum_{k=1}^{n}|x_k-\tilde{x}_k|+\sum_{k=1}^{m}|s_k-\tilde{s}_k|+\sum_{k=1}^{n}|\psi_k-\tilde{\psi}_k|+|c_{t_0}-\tilde{c}_{t_0}|\right],$$

when $(t_0,t)\in[0,\ T_1]\times[0,\ T_1]$ *and the functions* x_i, s_j, ψ_i, L, c, c_{t_0} *satisfy the assumptions (a)-(c).*

Then, integral system (2.13)-(2.18) *has a unique solution* x_i, s_j, ψ_i, L, c, c_{t_0}, $\in C^0([0,\ T]\times[0,\ T])$, *where*

$$T=\min\left\{T_1,\frac{h_{x,1}}{M_1},...,\frac{h_{x,n}}{M_n},\sqrt{\frac{h_{s,1}}{M_{s,1}}},...,\sqrt{\frac{h_{s,m}}{M_{s,m}}},\sqrt{\frac{h_{\psi,1}}{M_{\psi,1}}},...,\sqrt{\frac{h_{\psi,n}}{M_{\psi,n}}},\sqrt{\frac{h_L}{M_L}},\sqrt{\frac{h_{c,1}}{2M_{c,1}}},\frac{h_{c,2}}{M_{c,2}}\right\}.$$

In addition,

$$aT^2+bT<1, \tag{2.26}$$

where

$$a=\sum_{j=1}^{m}\lambda_{s,j}+\sum_{i=1}^{n}\lambda_{\psi,i}+\lambda_L+2\lambda_{c,1},\ b=\sum_{i=1}^{n}\lambda_i+\lambda_{c,2}. \tag{2.27}$$

Proof. Denote by Ω the space of continuous functions $x_i(t_0,t)$, $s_j(t_0,t)$, $\psi_i(t_0,t)$,

$L(t_0)$, $c(t_0,t)$, $c_{t_0}(t_0,t)$, $t_0 \in [0,\ T]$, $t \in [0,\ T]$, and introduce the norm

$$||(\mathbf{x},\mathbf{s},\boldsymbol{\psi},L,c,c_{t_0})|| = \sum_{i=1}^{n}\max_{\Omega}|x_i| + \sum_{j=1}^{m}\max_{\Omega}|s_j| + \sum_{i=1}^{n}\max_{\Omega}|\psi_i|$$

$$+\max_{\Omega}|L| + \max_{\Omega}|c| + \max_{\Omega}|c_{t_0}|.$$

Consider the map $(\mathbf{x}^*,\mathbf{s}^*,\underline{\boldsymbol{\psi}}^*,L^*,c^*,c^*_{t_0}) = A(\mathbf{x},\mathbf{s},\boldsymbol{\psi},L,c,c_{t_0})$, where $(\mathbf{x}^*,\mathbf{s}^*,\underline{\boldsymbol{\psi}}^*,L^*,c^*,c^*_{t_0}) =$ RHS of equations (2.13)-(2.18). Let us prove that A maps Ω into itself. Indeed,

$$|x_i^* - X_{i,0}| \le M_i T \le h_{x,i},\ \ i = 1,...,n$$

$$|s_j^* - S_j^*| \le M_{s,j}T^2 \le h_{s,j},\ \ |\underline{\psi}_i^* - \psi_i^*| \le M_{\psi,i}T^2 \le h_{\psi,i},\quad i = 1,...,n,\ j = 1,...,m,$$

$$|L^* - \Sigma| \le M_L T^2 \le h_L,\ |c^* - \Sigma| \le 2M_{c,1}T^2 \le h_{c,1},\ |c^*_{t_0} - \sigma_a| \le M_{c,2}T \le h_{c,2}.$$

Consider $(\tilde{\mathbf{x}},\tilde{\mathbf{s}},\tilde{\boldsymbol{\psi}},\tilde{L},\tilde{c},\tilde{c}_{t_0}) \in \Omega$ and let $(\tilde{\mathbf{x}}^*,\tilde{\mathbf{s}}^*,\tilde{\boldsymbol{\psi}}^*,\tilde{L}^*,\tilde{c}^*,\tilde{c}^*_{t_0}) = A(\tilde{\mathbf{x}},\tilde{\mathbf{s}},\tilde{\boldsymbol{\psi}},\tilde{L},\tilde{c},\tilde{c}_{t_0})$. We easily obtain

$$|x_i^* - \tilde{x}_i^*| \le \lambda_i T||(\mathbf{x},\mathbf{s},\boldsymbol{\psi},L,c,c_{t_0}) - (\tilde{\mathbf{x}},\tilde{\mathbf{s}},\tilde{\boldsymbol{\psi}},\tilde{L},\tilde{c},\tilde{c}_{t_0})||,\ i = 1,...,n,$$

$$|s_j^* - \tilde{s}_j^*| \le \lambda_{s,j}T^2||(\mathbf{x},\mathbf{s},\boldsymbol{\psi},L,c,c_{t_0}) - (\tilde{\mathbf{x}},\tilde{\mathbf{s}},\tilde{\boldsymbol{\psi}},\tilde{L},\tilde{c},\tilde{c}_{t_0})||,\ j = 1,...,m,$$

$$|\underline{\psi}_i^* - \tilde{\psi}_i^*| \le \lambda_{\psi,i}T^2||(\mathbf{x},\mathbf{s},\boldsymbol{\psi},L,c,c_{t_0}) - (\tilde{\mathbf{x}},\tilde{\mathbf{s}},\tilde{\boldsymbol{\psi}},\tilde{L},\tilde{c},\tilde{c}_{t_0})||,\ i = 1,...,n,$$

$$|L^* - \tilde{L}^*| \le \lambda_L T^2||(\mathbf{x},\mathbf{s},\boldsymbol{\psi},L,c,c_{t_0}) - (\tilde{\mathbf{x}},\tilde{\mathbf{s}},\tilde{\boldsymbol{\psi}},\tilde{L},\tilde{c},\tilde{c}_{t_0})||,$$

$$|c^* - \tilde{c}^*| \le 2\lambda_{c,1}T^2||(\mathbf{x},\mathbf{s},\boldsymbol{\psi},L,c,c_{t_0}) - (\tilde{\mathbf{x}},\tilde{\mathbf{s}},\tilde{\boldsymbol{\psi}},\tilde{L},\tilde{c},\tilde{c}_{t_0})||,$$

$$|c^*_{t_0} - \tilde{c}^*_{t_0}| \le \lambda_{c,2}T||(\mathbf{x},\mathbf{s},\boldsymbol{\psi},L,c,c_{t_0}) - (\tilde{\mathbf{x}},\tilde{\mathbf{s}},\tilde{\boldsymbol{\psi}},\tilde{L},\tilde{c},\tilde{c}_{t_0})||.$$

Hence,

$$||(\mathbf{x}^*, \mathbf{s}^*, \underline{\boldsymbol{\psi}}^*, L^*, c^*, c^*_{t_0}) - (\tilde{\mathbf{x}}^*, \tilde{\mathbf{s}}^*, \tilde{\boldsymbol{\psi}}^*, \tilde{L}^*, \tilde{c}^*, \tilde{c}^*_{t_0})|| \leq \Lambda ||(\mathbf{x}, \mathbf{s}, \boldsymbol{\psi}, L, c, c_{t_0}) - (\tilde{\mathbf{x}}, \tilde{\mathbf{s}}, \tilde{\boldsymbol{\psi}}, \tilde{L}, \tilde{c}, \tilde{c}_{t_0})||,$$

where

$$\Lambda = aT^2 + bT.$$

Due to assumption (2.26) it is $\Lambda < 1$, proving Theorem 2.5.1.

2.6 Numerical applications

Numerical simulations have been performed to test the behavior of the model formulated in Sec. 2.4. Specifically, we have considered the same biofilm system of Sec. 2.3 composed of 3 microbial species and 3 dissolved substrates. The planktonic species present in the bulk liquid are able to initiate the biofilm formation through the attachment process, penetrate the biofilm matrix once constituted and establish where the most appropriate growth conditions are found. We have explored two ideal biological situations. In the first case the species ψ_3^* is not initially present in the bulk liquid but it arrives at time $t = t_1$ and starts to attach to the external surface of the biofilm as well as penetrate the biofilm matrix. In the second case, the species ψ_3^* is not able to attach to the biofilm surface ($v_{a,3} = 0$) but it can establish in sessile form through the colonization process. These biological situations will be referred to as *Case 2* and *Case 3*.

The reaction terms $r_{M,i}$ and $r_{S,j}$ in equations (2.1) and (2.6) have been adopted according to (2.10) and (2.11). The values for Ψ_i on the free boundary have been set according to (2.6) and (2.7). The values for S_j on the free boundary are reported in Table 2.1. The reaction terms concerning the colonization process in equations (2.1)

and (2.8) are modelled using Monod type kinetics and are expressed as

$$r_1 = \frac{k_{col,1}}{\rho}\frac{S_1}{K_1+S_1}\Psi_1,\ r_2 = \frac{k_{col,2}}{\rho}\frac{S_2}{K_2+S_2}\Psi_2,\ r_3 = \frac{k_{col,3}}{\rho}\frac{S_3}{K_3+S_3}\Psi_3, \tag{2.1}$$

$$r_{\Psi,1} = -\frac{\rho}{Y_{\Psi,1}}r_1,\ r_{\Psi,2} = -\frac{\rho}{Y_{\Psi,2}}r_2,\ r_{\Psi,3} = -\frac{\rho}{Y_{\Psi,3}}r_3 \tag{2.2}$$

where $k_{col,1}$, $k_{col,2}$, $k_{col,3}$ are the maximum colonization rates of motile species, and $Y_{\Psi,1}$, $Y_{\Psi,2}$, $Y_{\Psi,3}$ are the yields of the sessile species on planktonic ones. The values of such kinetic parameters and the diffusion coefficients for Ψ_i are reported in Table 2.2. Note that for these ideal biological situations, all the species are supposed to have colonization properties.

Parameter	**Definition**	**Unit**	**Value**
$k_{col,1}$	Maximum colonization rate for Ψ_1	d^{-1}	2.5
$k_{col,2}$	Maximum colonization rate for Ψ_2	d^{-1}	2.5
$k_{col,3}$	Maximum colonization rate for Ψ_3	d^{-1}	2.5
$Y_{\Psi,1}$	Yield of X_1 on Ψ_1	$--$	$2 \cdot 10^{-7}$
$Y_{\Psi,2}$	Yield of X_2 on Ψ_2	$--$	$2 \cdot 10^{-7}$
$Y_{\Psi,3}$	Yield of X_3 on Ψ_3	$--$	$2 \cdot 10^{-7}$
$D_{\Psi,1}$	Diffusion coefficient of Ψ_1 in biofilm	$m^2\ d^{-1}$	10^{-5}
$D_{\Psi,2}$	Diffusion coefficient of Ψ_2 in biofilm	$m^2\ d^{-1}$	10^{-5}
$D_{\Psi,3}$	Diffusion coefficient of Ψ_3 in biofilm	$m^2\ d^{-1}$	10^{-5}

Table 2.2: Invasion parameters used for model simulations

Numerical simulations have been performed for *Case 2* and *Case 3* by considering a final simulation time $T = 10\ d$. The results are summarized in Figs. 2.6-2.7 for *Case 2*, and in Figs. 2.8-2.9 for *Case 3*.

Case 2: Attachment and colonization of microbial species ψ_3^*

The results reported in Figs. 2.6 and 2.7 highlight model capability to reproduce both the attachment and colonization phenomena that strongly affect biofilm lifecycle. In particular, it is possible to notice that during the initial phase of biofilm formation,

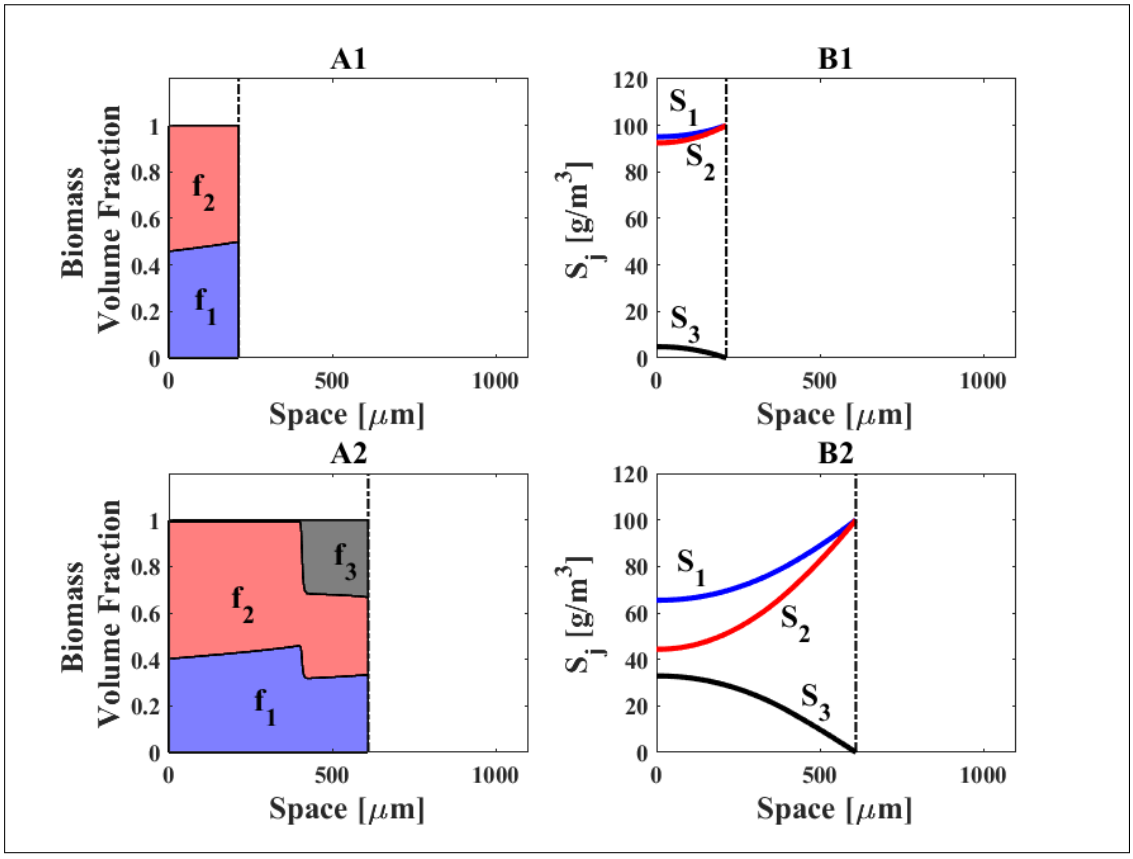

Figure 2.6: Biofilm composition (A1-A2) and substrate distribution (B1-B2) for *Case 2*, under attachment regime, at time $t = 0.25\ d$ (top) and $t = 0.50\ d$ (bottom).

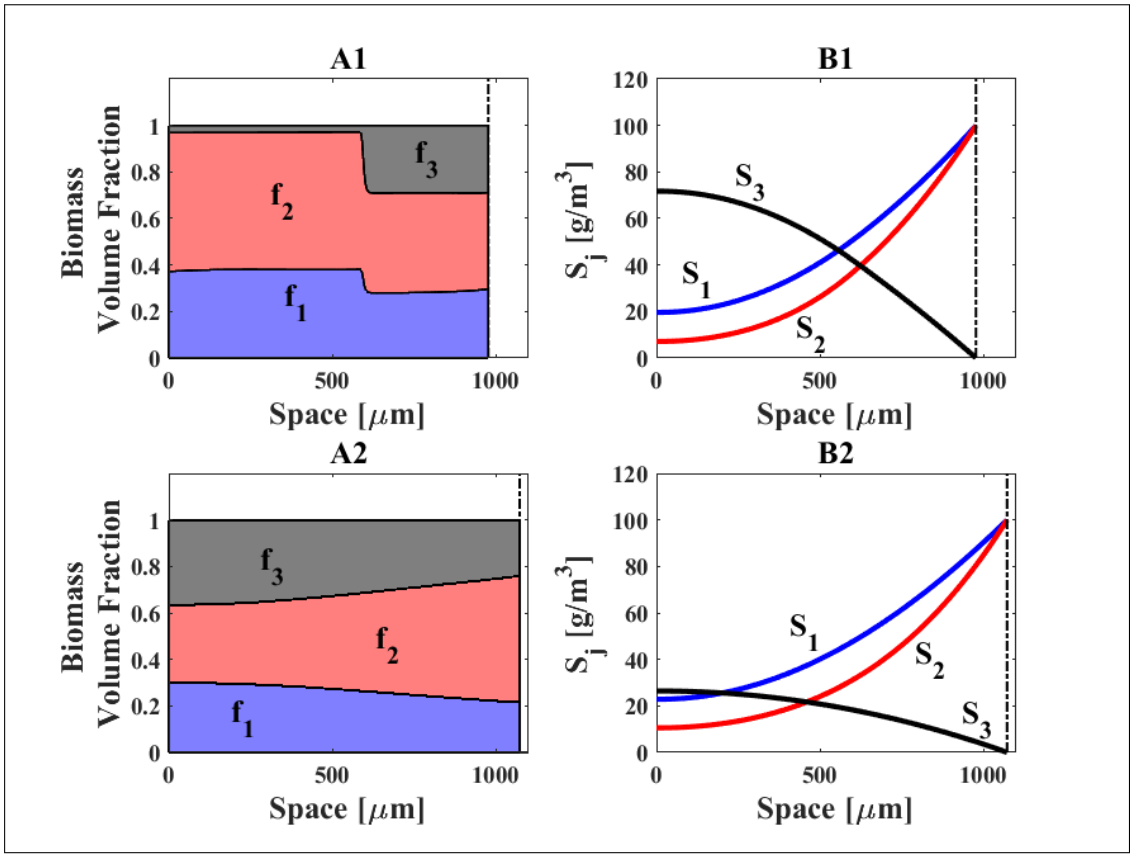

Figure 2.7: Biofilm composition (A1-A2) and substrate distribution (B1-B2) for *Case 2*, under detachment regime, at time $t = 1\ d$ (top) and $t = 10\ d$ (bottom).

the biofilm undergoes the same development illustrated in Sec. 2.3 and reported in Fig. 2.7. However, at time $t = 0.50\ d$ it is visible that the volume fraction of the third species f_3 is slightly positive even in the region $z < c(t_1, t)$ due to the colonization phenomenon (Fig. 2.6(A2)). Going on with the simulation time, f_3 increases all over the biofilm leading to a higher biofilm thickness at time $t = 1\ d$ (Fig. 2.7(A1)). At the final simulation time $t = 10\ d$ and under detachment regime, the biofilm is constituted by all the species inhabiting the bulk liquid (Fig. 2.7(A2)) conversely to the numerical results reported in Sec. 2.3 where the complete washout of species f_3 has been observed. The different biofilm stratification affects substrate trends as it is possible to notice that at the final simulation time, S_3 concentration is much lower when compared to the numerical example of pure attachment regime.

Case 3: Pure colonization of microbial species ψ_3^*

Figs. 2.8 and 2.9 illustrate the biofilm development and substrate trends when the species ψ_3^* is not able to attach to the biofilm surface, but it can penetrate the biofilm matrix and establish in sessile form. According to Figs. 2.8-2.9, numerical results reveal that for all simulation times the biofilm thickness is smaller compared to the pure attachment case. This contributes to have different substrate trends within the biofilm (Figs. 2.8-2.9(B1-B2)). In terms of biomass distribution, it is possible to notice that the third species grow in sessile form in the inner layers of the biofilm where there is the highest S_3 concentration. The biomass stratification and subtrate trends at the final simulation time resemble the one achieved for *Case 2*. Such results highlight an important feature of the model: the attachment and colonization phenomena are both dependent on the planktonic cells present in the bulk liquid. They can occur simultaneously reproducing the case of planktonic cells able to attach to the surface and penetrate the biofilm matrix. Conversely, the planktonic cells can be characterized by a certain motility which drives them to the biofilm region where there are the most appropriate conditions for their growth.

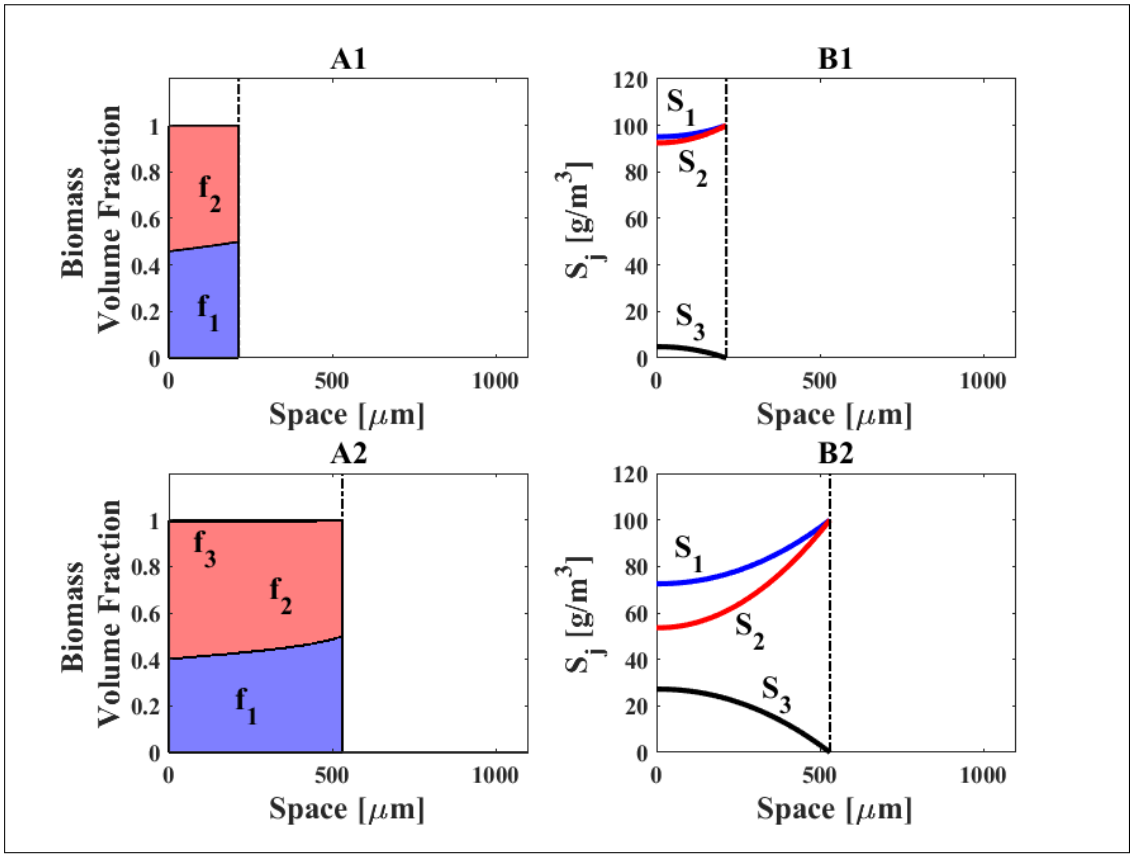

Figure 2.8: Biofilm composition (A1-A2) and substrate distribution (B1-B2) for *Case 3*, under attachment regime, at time $t = 0.25\ d$ (top) and $t = 0.50\ d$ (bottom).

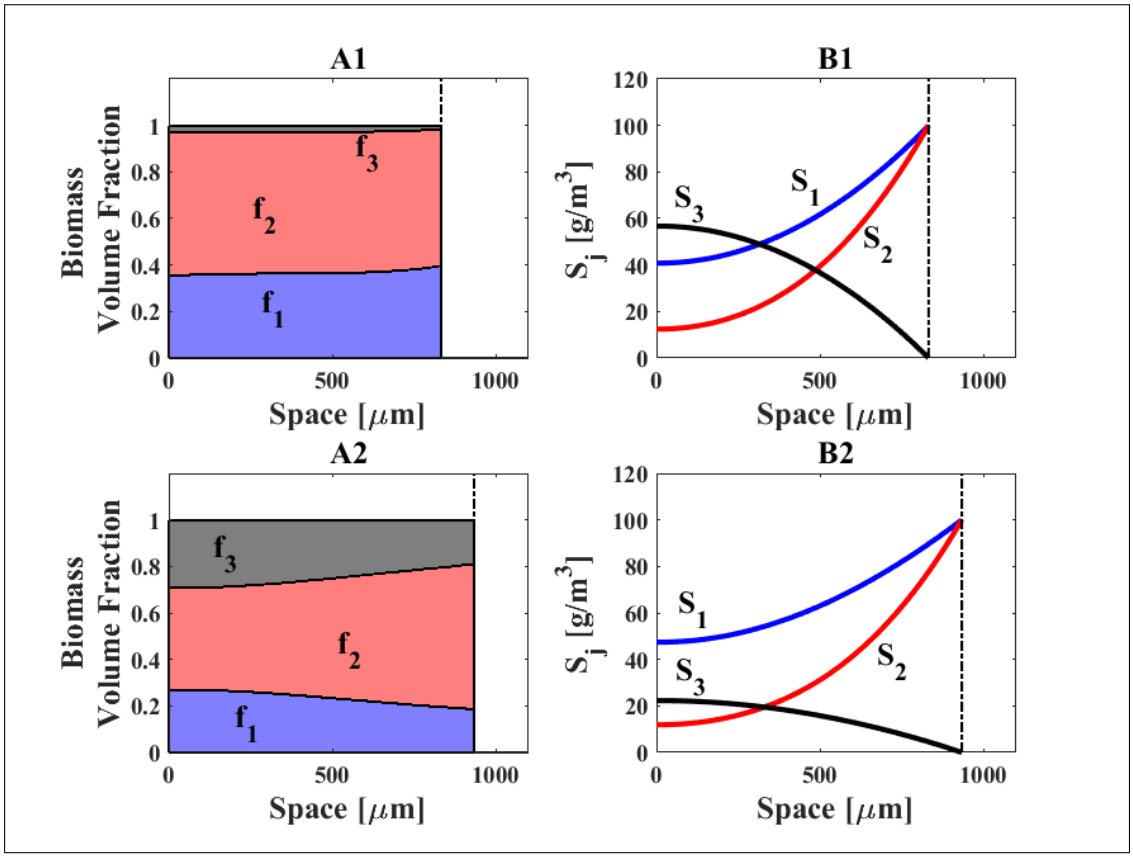

Figure 2.9: Biofilm composition (A1-A2) and substrate distribution (B1-B2) for *Case 3*, under detachment regime, at time $t = 1\ d$ (top) and $t = 10\ d$ (bottom).

2.7 Conclusion

The proposed model comprehensively describes the transition from planktonic to sessile phenotype which governs the biofilm dynamics. This allows to properly reproduce the evolution of biofilms starting from the initial formation and including the establishment and growth of new species. The criticism of Wanner and Gujer type models, discussed in [59], is here emphasized through a numerical example. Such models are not able to properly describe the growth of microbial species which do not participate in the initial biofilm formation attaching later to a pre-existing aggregate. The presented model is able to overcome this issue as it considers both the initial attachment phase and the growth of new sessile species within the biofilm mediated by the invasion process. The modelling of the initial phase of biofilm formation allows to describe the biofilm growth without arbitrarily fixing the initial composition of the biofilm. The existence and uniqueness of solutions is proved in the case of attachment regime. Numerical examples are provided to show model capability to reproduce the different stages of biofilm growth as affected by the planktonic phenotype. Future work may be related to the role of biofilm porosity on planktonic species diffusion and the qualitative analysis under detachment regime.

Chapter 3

Modelling the ecology of phototrophic-heterotrophic biofilms

3.1 Introduction

Biofilms are aggregates of microorganisms embedded in a self-produced matrix of polymeric compounds, frequently attached to a surface. Such aggregates can grow in a huge variety of aqueous and humid sites including living tissues, medical devices, industrial water systems, and natural aquatic systems [37]. Hence, understanding the complex mechanisms which drive the growth of biofilms appears to be crucial in different scientific fields. Microorganisms living in biofilms benefit of a broad range of ecological and physiological advantages including metabolites exchange, cellular communication and protection against desiccation, oxidizing, external agents (hydrodinamic stress, antibiotics etc.). Such protective benefits directly depend on their inherent structure [46, 89, 135]. In most cases, biofilms are mixotrophic ecosystems composed of

This Chapter is published as: Tenore, A., Mattei, M.R., Frunzo, L. (2021). Modelling the ecology of phototrophic-heterotrophic biofilms. Communications in Nonlinear Science and Numerical Simulation, 94, 105577.

various microbial species using different energy and carbon sources for growth and reproduction. Consequently, disparate antagonistic and synergistic interactions may arise among different trophic groups, modifying biofilm physical, chemical and biological properties [20, 104].

Biofilm formation and maturation derive from the interplay of different phenomena which involve continuous mass exchanges with the external environment: attachment, detachment, invasion and dispersal processes [75, 41]. In particular, invasion phenomena consist in the colonization of a pre-existing biofilm mediated by planktonic cells living in the surrounding environment [110]. Such planktonic cells have the ability to penetrate the porous matrix of the biofilm, invade the resident community and establish where conditions for their growth are optimal [117]. Accordingly, from an ecological point of view, invasion processes are essential to understand how the microbial community inhabiting the biofilm evolves over time. In general, the invasion of the biofilm by planktonic species depends on several factors, such as the biofilm structure, nutrient availability, the characteristics of the invading species and the resident community. Indeed, sometimes the presence of a specific microbial species in sessile form and its secretion of extracellular polymeric substances (EPS) may help other species to place and grow within the biofilm [100, 143].

In recent years, biofilm technologies have been widely used for industrial applications, in particular in the field of wastewater treatment: different microbial communities living in sessile form are able to degrade polluting compounds from industrial and urban wastewater. In addition, the development of a balanced mixotrophic biofilm system, in which different microbial species simultaneously assimilate different polluting compounds leads to higher bioreactor performances. In this perspective, phototrophic-heterotrophic biofilms are recognized as one of the most promizing biological technologies for the treatment of animal, municipal and mining wastewaters [94, 18]. Phototrophic microorganisms, such as cyanobacteria and microalgae, derive energy from light radiation and are able to synthesize organic compounds from inor-

ganic substances, while heterotrophic microorganisms, such as bacteria, require organic carbon for their metabolic activities. As a result of the metabolic properties of phototrophic and heterotrophic microorganisms, combined systems based on phototrophic-heterotrophic biofilms are able to remove efficiently primary nutrients (carbon, nitrogen, and phosphorus), heavy metals and micropollutants [80]. Moreover, phototrophic cultivations deriving from wastewater treatments may be used as feedstock in other industrial applications such as the production of fuels, chemicals, and nutraceuticals [53].

In this context, mathematical modelling can represent a crucial tool for monitoring, managing and sizing full-scale biofilm reactors. In order to correctly model the evolution of a phototrophic-heterotrophic biofilm it is necessary to take into account the main factors and biological dynamics involved. Above all, the phototrophic metabolism is based on the photosynthetic activity and, therefore, is highly dependent on the availability of light. However, excess light can inhibit photosynthesis leading to the destruction of the photosynthetic apparatus [71]. Moreover, in liquid environments where suitable conditions for both phototrophic and heterotrophic metabolic activities are found, light conditions govern the process of biofilm formation: as reported in [100], under high light conditions the initial colonizers of the substratum predominantly consisted of phototrophs, whereas at low light intensities, heterotrophs are the main initial colonizers. Hence, light intensity represents the key parameter in the process of genesis and evolution of a phototrophic biofilm.

Phototrophic and heterotrophic microorganisms coexist in a biofilm as a result of complex symbiotic relationships that make the presence of one species particularly convenient or even indispensable for the other [50, 98]. As shown in [100], the growth of phototrophic cells in sessile form is facilitated by the presence of heterotrophic pioneers. According to [143], this can be attributed to the heterotrophic secretion of EPS. Indeed, the EPS affects the physical, chemical and mechanical properties of the biofilm, and may establish ideal living conditions for planktonic microbial cells present in the surrounding environment.

In addition, the mutualistic network between phototrophs and heterotrophs is deeply based on metabolic interactions [6]. Using inorganic carbon, water and energy from light, phototrophs synthesize organic carbon for their cellular functions. Nevertheless, a fraction of photosynthetically fixed carbon is released as dissolved organic carbon (DOC) [14, 25, 60], which is an ideal substrate for the metabolic activity of heterotrophic species. This release is quantitatively variable and is supposed to depend on taxonomy, light and temperature [83, 144]. However, how these factors influence the phenomenon is not yet perfectly clear [15]. Dissolved oxygen is a further compound involved in the ecology of this biofilm. Oxygen produced in large amounts by phototrophs promotes processes of photorespiration which can compete and inhibit the photosyntetic activity [61]. At the same time, dissolved oxygen is required by the heterotrophic metabolism. Therefore, the presence of heterotrophs reduces the amount of oxygen and enhances the phototrophic growth [82]. Moreover, inorganic carbon (IC) produced by heterotrophic species can be required for photosyntetic activity [86]. Other mechanisms of interaction between these two trophic species can be mentioned, such as the release of particulate organic carbon (POC) by phototrophs, signals exchange, competition for any secondary compound in nutrient-poor environments [86]. Finally, when a phototrophic-heterotrophic biofilm develops under light stress conditions, heterotrophic biomass may have a positive shading effect on phototrophic growth.

Some mathematical models have been developed to describe the growth of a phototrophic biofilm under different approaches and paying attention to different aspects. Such models are based on partial differential equations and take into account the spatial variability of substrates and biomasses within the biofilm. Some of them adopted a free boundary approach [138, 84]. In particular, the biofilm growth in a plug-flow reactor is modeled in [84]. Meanwhile, the growth of a mixotrophic biofilm composed by phototrophic, heterotrophic and chemotrophic species aimed at wastewater treatment is described in [138]. Other models are based on the mixture theory and consider the phototrophs as the single active biomass in the biofilm: a fluid dynamic model on the

formation of cyanobacteria biofilms on the stone surfaces of ancient monuments is reported in [21, 22]; this model is resumed by [93] and extended to a generic phototrophic species investigating the main physiological mechanisms involved. Finally, a model for a porous substrate biofilm photobioreactor (PSBR) is developed in [67]. For the sake of completeness, other models based on ordinary differential equations have been focused on the growth of phototrophic and heterotrophic microorganisms in planktonic form [40, 81, 112]. None of these studies focused on modeling the ecology and evolution of the microbial colony.

This Chapter proposes a 1D model able to describe the ecology of a phototrophic-heterotrophic biofilm, the main processes, factors and microbial interactions which drive the biofilm dynamics. In particular, according to the continuum approach proposed in [132] for a multispecies biofilm and extended to the invasion processes in [28, 49, 30], biofilm growth, biomasses distribution, substrates diffusion and conversion, invasion and detachment processes are described with a set of partial differential equations. Moreover, the model reproduces the phenomena outlined in [100, 143, 13]:

- The positive effect of heterotrophic pioneers and their EPS secretion on the formation of the phototrophic biofilm. The pioneers are the microbial cells able to first colonize the substratum.
- The predominance of some microbial species in the biofilm evolution based on light conditions.
- The photoinhibition occurrence: the effect on phototrophic biomass and biofilm evolution and the positive shading contribution by heterotrophs to the phototrophic growth.
- The effect of organic carbon release by phototrophs on heterotrophic growth under different light and dissolved oxygen conditions.

The invasion process is modelled here for the first time as dependent on the abun-

dance of EPS in the biofilm. Main metabolic interactions between the two species are included in the model. The process of DOC release by phototrophs, introduced in [40] for suspended cultures, is here proposed in the biofilm case by introducing a release coefficient in the kinetic expression of phototrophic growth. The evolution of the biofilm and the distribution of biomass are investigated for different release fractions, light and dissolved oxygen conditions. Indeed, light intensity is included as a model variable. Specifically, light attenuation within the biofilm is supposed to follow a Lambert-Beer law, while an expression proposed by [115] is used to take into account the light dependency of phototrophic growth and the photoinhibition phenomenon. Finally, the modelling of the concentration boundary layer (CBL) is included to consider the effects of hydrodynamics condition on the mass transport of substrates.

The Chapter is organized as follows. In Section 3.2, the mathematical model is described by introducing all variables, equations, initial and boundary conditions. Numerical simulations and results are presented in Section 3.3 and discussed in Section 3.4. They explore the interactions between phototrophs and heterotrophs, such as the role of heterotrophic pioneers and their secretion of EPS on the phototrophic growth and the effects of organic carbon release by phototrophs on the invasion and growth of heterotrophic bacteria. Furthermore, the shading effect of heterotrophic species under photoinhibition conditions is investigated. Light turns out to be the key factor in the ecology of phototrophic-heterotrophic biofilms. Finally, a detailed description of the model reaction terms is given in Appendix A.

3.2 Mathematical Model

Based on a continuum approach, the mathematical model simulates the ecology of a phototrophic-heterotrophic biofilm. Biofilm is supposed to be attached to a solid support immersed in a liquid environment, such as the bulk liquid of a biofilm reactor or a natural ecosystem. The biofilm domain is supposed to be constituted by different micro-

bial species. The biofilm density ρ is assumed to be constant and equal for all species. Over time, biomass growth and detachment processes at biofilm-bulk liquid interface produce variation of the biofilm thickness. The CBL length is fixed at a constant value reproducing constant hydrodynamic conditions.

3.2.1 Model Components

The model is formulated as a free boundary problem for three state variables, expressed in terms of concentrations and function of time t and space z: sessile $X_i(z,t)$ and planktonic $\psi_i(z,t)$ species and soluble substrates $S_j(z,t)$ [28]. Moreover, light (expressed as intensity, I) is considered as an additional variable $I(z,t)$. By dividing sessile species concentration X_i by ρ, biomass volume fraction f_i is achieved. Notably, the volume fractions occupied by biomass are constrained to add up to unity, $\sum_{i=1}^{n} f_i = 1$ [96]. Inside the biofilm, sessile species grow using light and consuming soluble substrates which diffuse from the bulk liquid into the biofilm. Furthermore, under convenient environmental conditions, new species in planktonic form can colonize the biofilm shifting their phenotype from planktonic to sessile and competing with the resident species. The transport of soluble substrates and planktonic species is modeled through diffusion-reaction equations. The growth of microbial species in sessile form is described by hyperbolic equations. X_i, ψ_i and S_j interact with each other through non-linear reaction terms. Due to the particle size, the volume occupied by ψ_i is supposed to be negligible. Fig.3.1 shows the biological pattern described by the model. Biofilm is supposed to be constituted by 4 components: phototrophs X_1, heterotrophs X_2, EPS X_3 and inert X_4. Microbial growth, decay and colonization are the three kinetic processes taken into account. Note that all of them occur in water environments and water presence could be crucial in the success of these processes. However, given its abundance in the biofilm, water is expected to not influence biological rates and is

not included as a model variable. Phototrophic growth is driven by a complex combination of bio-chemical metabolic pathways [19]. For the purpose of this Chapter, the essential mechanism is considered: by using light I as energy source, phototrophs X_1 convert water, inorganic carbon S_1 and nitrates S_3 in energy-rich organic compounds used for cellular functions and oxygen S_4 as a waste product. Moreover, it is observed that phototrophs release a fraction of the photosynthetically fixed carbon in the form of dissolved organic carbon S_2 [25, 83, 52]. Notably, DOC release amount depends on several factors (e.g. taxonomy, cell size, light availability and temperature) [83, 144, 19] but contrasting results [83, 144, 113] do not allow to definitely establish the influence of these factors. From literature studies [14, 83, 144, 15, 52], different amount of DOC release are found. S_2 and S_4 which are released and produced by X_1 play an important role in the heterotrophic metabolic pathway. Indeed, heterotrophs X_2, under aerobic conditions, grow consuming S_2 and S_4. The heterotrophs are supposed to grow on reduced nitrogen which is not explicitely modelled as no limiting conditions are considered [100, 143, 13].

As reported extensively in the literature, both the metabolic activity of phototrophic X_1 and heterotrophic biomass X_2 in sessile form involve the production of EPS X_3 [42, 99]. The model considers such production proportional to the kinetic process of biomass growth [78]. In addition, inert biomass X_4 is included in the model as a product deriving from X_1 and X_2 decay. Finally, as already mentioned, the colonization of external species invading the biofilm is modeled. In particular, model takes into account planktonic phototrophs ψ_1 and heterotrophs ψ_2 diffusing within the biofilm and growing when the most appropriate environmental conditions are found.

In summary, model components are listed below:

$$f_i = \frac{X_i}{\rho},\ i = 1, 2, 3, 4,\ \mathbf{f} = (f_1, f_2, f_3, f_4), \tag{3.1}$$

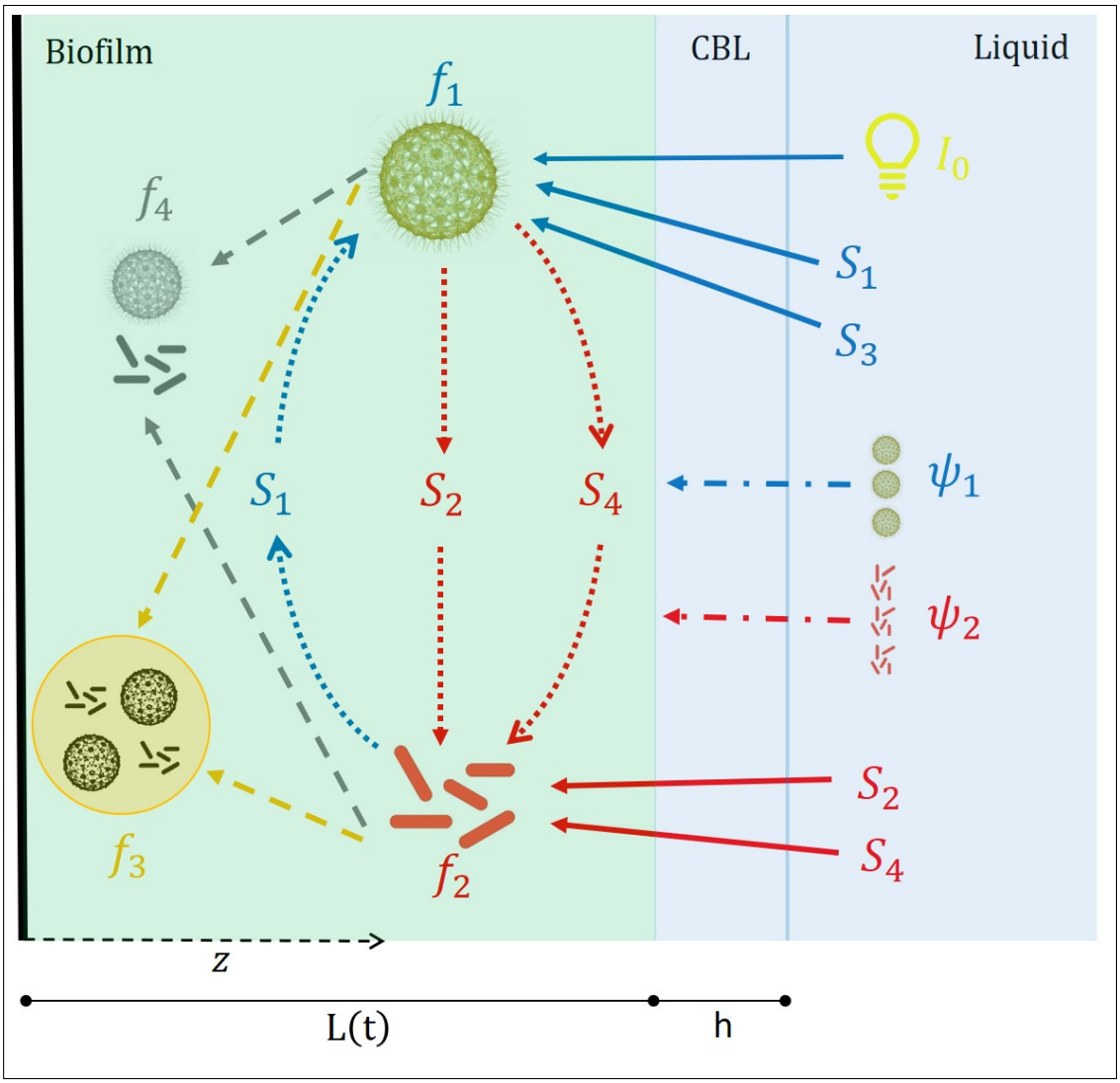

Figure 3.1: Schematic representation of the kinetic processes considered. Solid arrows: growth processes; dash arrows: decay and EPS production; dash-dot arrows: invasion processes; dot arrow: symbiotic growth process; blue arrows: phototrophic growth-related processes; red arrows: heterotrophic growth-related processes; orange arrows: EPS-related processes; grey arrows: decay processes. f_1: phototrophic biomass fraction. f_2: heterotrophic biomass fraction. f_3: EPS fraction. f_4: inert fraction. S_1: inorganic carbon. S_2: dissolved organic carbon. S_3: nitrate. S_4: dissolved oxygen. ψ_1: phototrophs in planktonic form. ψ_2: heterotrophs in planktonic form. I_0: incident light intensity. The domain of interest is constituted by: biofilm ($0 < z < L(t)$) and concentration boundary layer (CBL, $L(t) < z < L(t) + h$). $L(t)$: biofilm thickness. h: constant CBL thickness equal to $2 \cdot 10^{-4}$ m. z represents the spatial coordinate assumed perpendicular to the substratum.

$$\psi_i,\ i = 1, 2, 3, 4,\ \boldsymbol{\psi} = (\psi_1, \psi_2, \psi_3, \psi_4), \tag{3.2}$$

$$S_j,\ j = 1, 2, 3, 4,\ \mathbf{S} = (S_1, S_2, S_3, S_4). \tag{3.3}$$

Suspended EPS and inert are supposed to not have invasion properties and do not affect the biofilm evolution. Therefore ψ_3 and ψ_4 are set equal to zero in the biofilm and in the bulk liquid.

3.2.2 Equations

Assuming z as biofilm growth direction, perpendicular to the solid support (located at $z = 0$), the following non-linear hyperbolic PDEs describe the biomass growth in sessile form:

$$\frac{\partial f_i}{\partial t} + \frac{\partial}{\partial z}(u f_i) = r_{M,i}(z, t, \mathbf{f}, \mathbf{S}) + r_i(z, t, \boldsymbol{\psi}, \mathbf{f}, \mathbf{S}),\ i = 1, ..., 4,\ 0 \leq z \leq L(t),\ t > 0,$$

$$f_i(z, 0) = f_{i,0}(z),\ i = 1, ..., 4,\ 0 \leq z \leq L_0, \tag{3.4}$$

where $u(z, t)$ is the biomass velocity, $r_{M,i}(z, t, \mathbf{f}, \mathbf{S})$ and $r_i(z, t, \boldsymbol{\psi}, \mathbf{f}, \mathbf{S})$ are the specific growth rates due to sessile and planktonic species, respectively, $L(t)$ is the biofilm thickness and L_0 is the biofilm thickness for $t = 0$. Note that r_3 and r_4 are identically zero all over the biofilm as EPS and inert material have no invasion properties.

Biomass velocity represents the velocity of displacement of the microbial mass with respect to the z direction. It depends on the specific growth rate of the sessile species $r_{M,i}$ and the growth rates r_i due to the invasion process which induces the switch of

planktonic cells to a sessile mode of growth:

$$\frac{\partial u}{\partial z} = \sum_{i=1}^{4}(r_{M,i}(z,t,\mathbf{f},\mathbf{S}) + r_i(z,t,\boldsymbol{\psi},\mathbf{f},\mathbf{S})),\ 0 < z \leq L(t),\ t \geq 0,\ u(0,t) = 0. \quad (3.5)$$

The biofilm thickness evolution derives from the interplay of both negative and positive processes, namely biomass growth and detachment:

$$\dot{L}(t) = u(L(t),t) - \sigma_d(L(t)),\ t > 0,\ L(0) = L_0. \quad (3.6)$$

$\sigma_d(L(t))$ represents the detachment flux from biofilm to bulk liquid and is proportional to L^2 [1]:

$$\sigma_d(L(t)) = \lambda L^2(t), \quad (3.7)$$

where λ represents the constant detachment coefficient. Eq. (3.6) is derived from global mass balance considerations.

Soluble substrates and planktonic cells move from bulk liquid to the CBL to the biofilm. Therefore, non-linear parabolic PDEs are applied to CBL-biofilm domain describing S_j and ψ_i diffusion from bulk liquid into the biofilm. Assuming that biological conversion processes take place only in the biofilm, null reaction terms lead to homogeneous equations in CBL:

$$\frac{\partial \psi_i}{\partial t} - \frac{\partial}{\partial z}\left(D^B_{\psi,i}\frac{\partial \psi_i}{\partial z}\right) = r_{\psi,i}(z,t,\boldsymbol{\psi},\mathbf{f},\mathbf{S}),\ i = 1,...,4,\ 0 < z < L(t),\ t > 0,$$

$$\psi_i(z,0) = \psi_{i0}(z),\ i = 1,...,4,\ 0 \leq z \leq L_0,$$

$$\frac{\partial \psi_i}{\partial z}(0,t) = 0,\ i = 1,...,4,\ t > 0, \quad (3.8)$$

$$\frac{\partial \psi_i}{\partial t} - \frac{\partial}{\partial z}\left(D^L_{\psi,i}\frac{\partial \psi_i}{\partial z}\right) = 0,\ i = 1, ..., 4, L(t) < z < L(t) + h,\ t > 0,$$

$$\psi_i(z, 0) = \psi_{i0}(z),\ i = 1, ..., 4,\ L_0 \leq z \leq L_0 + h,$$

$$\psi_i(L(t) + h, t) = \psi_{iL},\ i = 1, ..., 4,\ t > 0, \tag{3.9}$$

where h is the CBL thickness, $D^B_{\psi,i}$ is the diffusivity coefficient of the planktonic species in biofilm, $D^L_{\psi,i}$ is the diffusivity coefficient of planktonic species in water and $r_{\psi,i}(z, t, \boldsymbol{\psi}, \mathbf{f}, \mathbf{S})$ is the conversion rate of motile species.

Similarly for soluble substrates:

$$\frac{\partial S_j}{\partial t} - \frac{\partial}{\partial z}\left(D^B_{S,j}\frac{\partial S_j}{\partial z}\right) = r_{S,j}(z, t, \mathbf{X}, \mathbf{S}),\ j = 1, ..., 4,\ 0 < z < L(t),\ t > 0,$$

$$S_j(z, 0) = S_{j0}(z),\ j = 1, ..., 4,\ 0 \leq z \leq L_0,$$

$$\frac{\partial S_j}{\partial z}(0, t) = 0,\ j = 1, ..., 4,\ t > 0, \tag{3.10}$$

$$\frac{\partial S_j}{\partial t} - \frac{\partial}{\partial z}\left(D^L_{S,j}\frac{\partial S_j}{\partial z}\right) = 0,\ j = 1, ..., 4, L(t) < z < L(t) + h,\ t > 0,$$

$$S_j(z, 0) = S_{j0}(z),\ j = 1, ..., 4,\ L_0 \leq z \leq L_0 + h,$$

$$S_j(L(t) + h, t) = S_{jL},\ j = 1, ..., 4,\ t > 0, \tag{3.11}$$

where $D^B_{S,j}$ is the diffusivity coefficient in biofilm, $D^L_{S,j}$ is the diffusivity coefficient in water and $r_{S,j}(z, t, \mathbf{X}, \mathbf{S})$ is the conversion rate of substrate j. Solution and flux continuity at CBL-biofilm interface are imposed for both soluble substrates and planktonic

species [30].

Besides soluble compounds, light is regarded as an additional factor influencing phototrophic growth processes. Light intensity is modelled as a function of time and space $I(z,t)$. Assigning a fixed light intensity I_0 at CBL-biofilm interface, a Lambert-Beer law describes the attenuation process across the biofilm:

$$I(z,t) = I_0 e^{-k_{tot}(L(t)-z)\rho}, \tag{3.12}$$

where k_{tot} is the light attenuation coefficient.

3.2.3 Reaction terms

Conversion rates for f_i, ψ_i and S_j complete the equation system. As consequence of biomass metabolism, each variable S_j is consumed and/or produced. Altogether, model considers 6 microbial processes: biomass growth due to planktonic and sessile species and decay, for both phototrophs and heterotrophs. The microbial metabolic activity leads to the formation of new biomass, EPS production and, in the case of phototrophs, DOC release. Similarly to [40], phototrophic release of DOC is taken into account by introducing the DOC release fraction γ_c while EPS production is considered by introducing the phototrophic EPS fraction $k_{EPS,1}$ [138] and heterotrophic EPS fraction $k_{EPS,2}$ [78].

Conversion rates for substrates, growth rates for suspended and sessile biomass are formulated as Monod-type kinetics [28, 138]. The decay rate is considered linear with respect to the concentration of the sessile microbial species. Oxygen inhibition for phototrophs is considered as in [67]. Moreover, the model considers the effects of light conditions and photoinhibition phenomena by including the optimum type expression proposed by [115] in the phototrophic kinetics.

As introduced in Section 3.1, the phototrophic growth is positively influenced by

the presence of EPS secreted by heterotrophs inhabiting the biofilm. In order to take into account this, the model proposes a new expression for the maximum colonization rate k_{col}, introduced in [28] as a constant value. In particular, in the case of phototrophs, $k_{col,1}$ is expressed as a function of the EPS volume fraction f_3 and, consequently, the specific growth rate of sessile phototrophs due to planktonic species r_1 turns into:

$$r_1 = k_{col,1}\frac{\psi_1}{\rho}\phi_{I,1}\frac{S_1}{K_{1,1}+S_1}\frac{S_3}{K_{3,1}+S_3}\frac{K_{4,1}^{in}}{K_{4,1}^{in}+S_4}, \tag{3.13}$$

$$k_{col,1} = k_{col,1,0}\,(1+f_3\,K_{aff}), \qquad \phi_{I,1} = \frac{I}{I_m}\,e^{(1-\frac{I}{I_m})}, \tag{3.14}$$

where I_m is the optimum light intensity, $K_{1,1}$ and $K_{3,1}$ and the half saturation constants of inorganic carbon and nitrates for phototrophs, respectively, $K_{4,1}^{in}$ is the inhibition constant for dissolved oxygen on photosyntethic growth, $k_{col,1,0}$ is the maximum colonization rate of phototrophs in absence of EPS material and K_{aff} is the coefficient of affinity EPS-phototrophic cells.

A detailed and comprehensive description of the reaction terms in Eq. (3.4), (3.8) and (3.10) is reported in Appendix A.

3.3 Numerical simulations

In order to test the model behaviour, numerical studies have been performed by using an original code developed on MatLab platform. Specifically, the method of characteristics is used to track the biofilm expansion, while a finite difference approximation is adopted for the diffusion-reaction equations. These numerical studies address the ecology of a biofilm composed of phototrophic and heterotrophic microbial species and investigate the main phenomena and factors involved in this ecosystem. The numerical simulations performed in this study are based on [100, 143, 13], and are aimed

at reproducing the experimental evidence reported in [100]. In particular, *Scenario 1* investigates the positive effect of heterotrophic pioneers and their secretion of EPS on the phototrophic invasion and biofilm formation; *Scenario 2* investigates the effect of light on biomass growth and biofilm evolution exploring favorable light conditions, photoinhibition phenomena and the role of heterotrophic species under light stress conditions; *Scenario 3* investigates how the release of DOC affects the heterotrophic invasion under different light and dissolved oxygen conditions.

For each simulation, constant Dirichlet conditions are assumed for soluble substrates and planktonic species within the bulk liquid at the right edge of the CBL ($z = L(t) + h$). The values adopted for S_{1L} and S_{3L} come from [100], while S_{2L} and S_{4L} are fixed to low values simulating an environment poor in organic carbon and oxygen. In all simulations, the initial biofilm thickness L_0 is set equal to $10^{-5}\ m$.

Kinetic parameters used for simulations are summarized in Tab.3.1. Furthermore, initial and boundary conditions are summarized in Tab.3.2, for each Scenario. Notably, diffusivity in biofilm is assumed to be 80% of diffusivity in water, in accordance with [132].

Some numerical results are reported in terms of mass of the species i within the biofilm, which is calculated as:

$$m_i(t) = \int_0^{L(t)} A\rho f_i(z,t)dz,\ i = 1, ..., n, \tag{3.15}$$

where A denotes the biofilm surface area, set equal to $1\ m^2$ for all numerical simulations.

3.3.1 Scenario 1 - Effect of heterotrophic pioneers and EPS secretion

As introduced in Section 3.1, some experimental works [100, 143] conclude that

Parameter	Definition	Unit	Value	Ref
$\mu_{max,1}$	Maximum specific growth rate for f_1	d^{-1}	2	[84]
$\mu_{max,2}$	Maximum specific growth rate for f_2	d^{-1}	4.8	[84]
$k_{d,1}$	Decay-inactivation rate for f_1	d^{-1}	0.1	[84]
$k_{d,2}$	Decay-inactivation rate for f_2	d^{-1}	0.1	[84]
$k_{EPS,1}$	EPS fraction produced by f_1	$--$	0.09	[138]
$k_{EPS,2}$	EPS fraction produced by f_2	$--$	0.18	[78]
$K_{1,1}$	IC half saturation constant for f_1	$kmol\ m^{-3}$	$4 \cdot 10^{-5}$	[138]
$K_{3,1}$	NO_3 half saturation constant for f_1	$kmol\ m^{-3}$	$1.2 \cdot 10^{-6}$	[138]
$K_{2,2}$	DOC half saturation constant for f_2	$kg(COD)\ m^{-3}$	$4 \cdot 10^{-3}$	[138]
$K_{4,2}$	O_2 half saturation constant for f_2	$kmol\ m^{-3}$	$3.125 \cdot 10^{-6}$	[132]
$K^{in}_{4,1,max}$	Max inhib. coeff. of O_2 on phototrophic growth	$kmol\ m^{-3}$	10^{-3}	[67]
K_{S_1/S_4}	Coeff. of effect of IC to O_2 ratio on O_2 inhib.	$--$	0.35	[67]
$D^L_{S,1}$	Diffusion coefficient of IC in water	$m^2\ d^{-1}$	$1.65 \cdot 10^{-4}$	[138]
$D^L_{S,2}$	Diffusion coefficient of DOC in water	$m^2\ d^{-1}$	$1.04 \cdot 10^{-4}$	[132]
$D^L_{S,3}$	Diffusion coefficient of NO_3 in water	$m^2\ d^{-1}$	$1.47 \cdot 10^{-4}$	[132]
$D^L_{S,4}$	Diffusion coefficient of O_2 in water	$m^2\ d^{-1}$	$1.73 \cdot 10^{-4}$	[138]
$k_{col,1,0}$	Maximum colonization rate for ψ_1	d^{-1}	$5 \cdot 10^{-2}$	(a)
$k_{col,2}$	Maximum colonization rate for ψ_2	d^{-1}	$5 \cdot 10^{-2}$	(a)
K_{aff}	Coeff. of microbial affinity EPS-phototrophs	$--$	$50 - 300$	(a)
$Y_{\psi,1}$	Yield of non-motile microrg. on motile species	$--$	0.05	(a)
$Y_{\psi,2}$	Yield of non-motile microrg. on motile species	$--$	0.05	(a)
$D_{\psi,1}$	Diffusion coefficient of ψ_1 in water	$m^2\ d^{-1}$	10^{-5}	(a)
$D_{\psi,2}$	Diffusion coefficient of ψ_2 in water	$m^2\ d^{-1}$	10^{-5}	(a)
I_m	Optimum light intensity	$kmol\ m^{-2}\ d^{-1}$	0.01814	[138]
I_0	Incident light intensity	$kmol\ m^{-2}\ d^{-1}$	$0.0013 - 0.12$	[100]
k_{tot}	Light attenuation coefficient	$m^2\ kg^{-1}$	210	[138]
γ_c	DOC release fraction	$--$	$0.05 - 0.3$	(a)
ρ	Biofilm density	$kg\ m^{-3}$	50	(a)
h	Concentration boundary layer thickness	m	$2 \cdot 10^{-4}$	(a)
λ	Biomass shear constant	$m^{-1}\ d^{-1}$	200	(a)

(a) Here introduced

Table 3.1: Kinetic parameters used for model simulations

the presence of heterotrophic pioneers can condition the surface support through their EPS production, facilitating and accelerating the growth and evolution of phototrophic biofilms. In this perspective, *Scenario 1* investigates this phenomenon through 2 different numerical studies (NS). The first one (NS1) compares the biofilm evolution in presence and absence of heterotrophic pioneers, respectively. As mentioned before, the pioneering microorganisms in a biofilm are the microbial cells which first colonize the solid support and contribute to the biofilm genesis. Therefore, the initial biomass is set to $f_{1,0} = f_{3,0} = f_{4,0} = 0, f_{2,0} = 1$ and $f_{1,0} = f_{2,0} = f_{3,0} = 0, f_{4,0} = 1$, respectively. The second study (NS2) examines the effects of the heterotrophic-produced EPS fraction $k_{EPS,2}$ and the affinity coefficient EPS-phototrophic cells K_{aff} on the model results in presence of heterotrophic pioneers ($f_{1,0} = f_{3,0} = f_{4,0} = 0, f_{2,0} = 1$). $k_{EPS,2}$ is varied from 0 to 0.4 and K_{aff} is varied from 50 to 300.

Parameter	*Scenario 1* Effects of heter. pioneers		*Scenario 2* Effects of light			*Scenario 3* Effects of DOC release		
	NS1	**NS2**	**NS3**	**NS4**	**NS5**	**NS6**	**NS7**	**NS8**
L_0 $[m]$	10^{-5}	10^{-5}	10^{-5}	10^{-5}	10^{-5}	10^{-5}	10^{-5}	10^{-5}
T $[d]$	20	20	35	35	15	20	20	20
$f_{1,0}$ $[--]$	0	0	0.7	0.7	varied*	1	1	1
$f_{2,0}$ $[--]$	varied*	1	0.3	0.3	varied*	0	0	0
$f_{3,0}$ $[--]$	0	0	0	0	0	0	0	0
$f_{4,0}$ $[--]$	varied*	0	0	0	0	0	0	0
$S_{1,0}$ $[kmol\ m^{-3}]$	0	0	0	0	0	0	0	0
$S_{2,0}$ $[kg\ m^{-3}]$	0	0	0	0	0	0	0	0
$S_{3,0}$ $[kmol\ m^{-3}]$	0	0	0	0	0	0	0	0
$S_{4,0}$ $[kmol\ m^{-3}]$	0	0	0	0	0	0	0	0
$\psi_{1,0}$ $[kg\ m^{-3}]$	0	0	0	0	0	0	0	0
$\psi_{2,0}$ $[kg\ m^{-3}]$	0	0	0	0	0	0	0	0
$S_{1,L}$ $[kmol\ m^{-3}]$	$3.33 \cdot 10^{-4}$	$3.33 \cdot 10^{-4}$	$3.33 \cdot 10^{-4}$	$3.33 \cdot 10^{-4}$	$3.33 \cdot 10^{-4}$	$3.33 \cdot 10^{-4}$	$3.33 \cdot 10^{-4}$	$3.33 \cdot 10^{-4}$
$S_{2,L}$ $[kg\ m^{-3}]$	$2 \cdot 10^{-3}$	$2 \cdot 10^{-3}$	$2 \cdot 10^{-3}$	$2 \cdot 10^{-3}$	$2 \cdot 10^{-3}$	$2 \cdot 10^{-3}$	$2 \cdot 10^{-3}$	$2 \cdot 10^{-3}$
$S_{3,L}$ $[kmol\ m^{-3}]$	$1.76 \cdot 10^{-2}$	$1.76 \cdot 10^{-2}$	$1.76 \cdot 10^{-2}$	$1.76 \cdot 10^{-2}$	$1.76 \cdot 10^{-2}$	$1.76 \cdot 10^{-2}$	$1.76 \cdot 10^{-2}$	$1.76 \cdot 10^{-2}$
$S_{4,L}$ $[kmol\ m^{-3}]$	$3.125 \cdot 10^{-5}$	$3.125 \cdot 10^{-5}$	$3.125 \cdot 10^{-5}$	$3.125 \cdot 10^{-5}$	$3.125 \cdot 10^{-5}$	$3.125 \cdot 10^{-5}$	$3.125 \cdot 10^{-5}$	varied*
$\psi_{1,L}$ $[kg\ m^{-3}]$	0.1	0.1	0.1	0.1	0	0.1	0.1	0.1
$\psi_{2,L}$ $[kg\ m^{-3}]$	0.1	0.1	0.1	0.1	varied*	0.1	0.1	0.1
$k_{EPS,2}$ $[--]$	0.18	varied*	0.18	0.18	0.18	0.18	0.18	0.18
K_{aff} $[--]$	100	varied*	100	100	100	100	100	100
I_0 $[kmol\ m^{-2}\ d^{-1}]$	0.0052	0.0052	varied*	varied*	0.1	0.0104	varied*	0.0104
γ_c $[--]$	0.05	0.05	0.05	0.05	0.05	varied*	varied*	varied*

*The values used are reported in the text

Table 3.2: Initial and boundary values and operating parameters adopted in model simulations

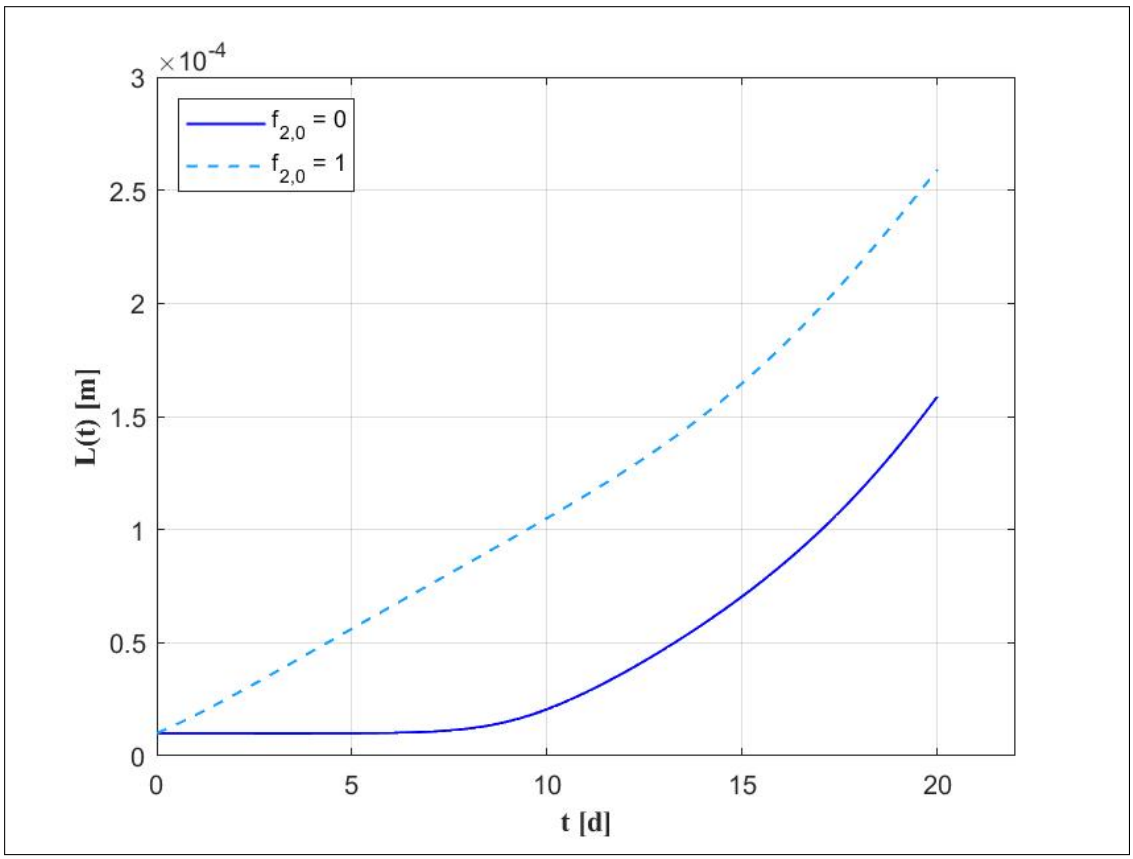

Figure 3.2: Scenario 1-NS1 (effects of heterotrophic pioneers on the phototrophic growth) - Biofilm thickness evolution over time in presence and absence of heterotrophic pioneers. Solid blue line: absence of heterotrophic pioneers (initial heterotrophic fraction $f_{2,0}$ equal to 0). Dash light blue line: presence of heterotrophic pioneers (initial heterotrophic fraction $f_{2,0}$ equal to 1). Incident light intensity $I_0 = 0.0052\ kmol\ m^{-2}\ d^{-1}$.

Numerical results are summarized in Fig.3.2, Fig.3.3 for NS1, and Fig.3.4 for NS2. In particular, the time evolution of the biofilm thickness (Fig.3.2) and of the phototrophic sessile mass (Fig.3.3) are shown, in presence and absence of heterotrophic pioneers. The dependence of the phototrophic invasion on the presence of heterotrophic species is clearly reproduced in these simulations. Indeed, the phototrophic biomass and the biofilm thickness grow faster when heterotrophic bacteria are present in the initial domain. These results qualitatively reproduce what is observed in [100]: the presence of sessile heterotrophic pioneers facilitates and intensifies the phototrophic growth in the biofilm. This experimental evidence proves positive interactions between phototrophs, heterotrophs and EPS and suggests new strategies to increase the efficiency of engineering applications based on phototrophic biofilms, such as wastewater treatment and bioenergy production. Indeed, the use of pioneering heterotrophs in the development of phototrophic biofilm cultures may lead to higher phototrophic productivities.

Fig.3.4 shows the results of NS2 in terms of biofilm thickness and microbial mass at $T = 20d$. Both the increase of the affinity coefficient and the EPS fraction produced by heterotrophs enhance the process of phototrophic invasion leading to an increase in phototrophic mass and biofilm thickness. The heterotrophic mass is not affected by K_{aff} while is sensitive to the variation of $k_{EPS,2}$, as it decreases linearly with $k_{EPS,2}$. Furthermore, it can be noted that for $k_{EPS,2} = 0$, the phototrophic mass is almost independent of K_{aff} value, since the EPS produced exclusively by phototrophs plays a limited role in the invasion process.

3.3.2 Scenario 2 - Effect of light and photoinhibition

Light is the main environmental factor governing the phototrophic metabolic activity and, consequently, the entire ecology of phototrophic-heterotrophic biofilms. *Scenario 2* investigates the effects of different light conditions, both favorable and inhibiting, on the phototrophic growth, and explores the positive role of heterotrophs under light stress

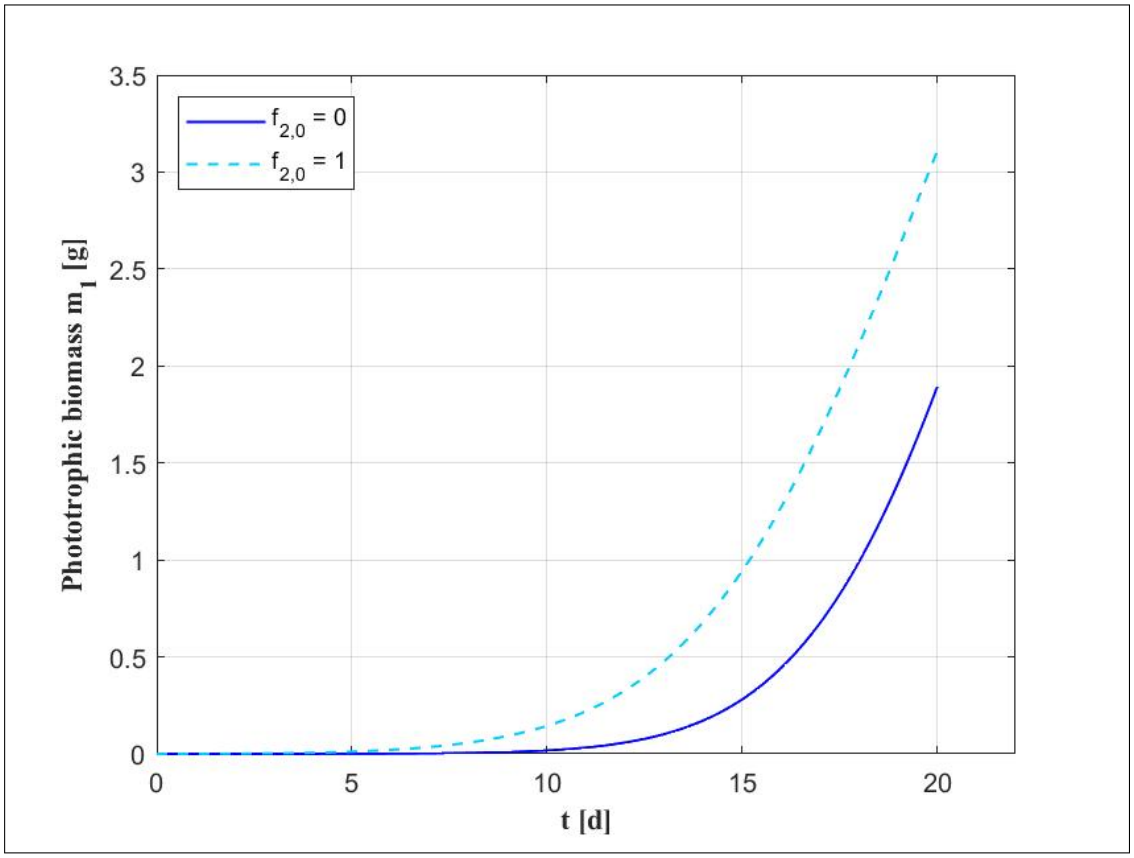

Figure 3.3: Scenario 1-NS1 (effects of heterotrophic pioneers on the phototrophic growth) - Phototrophic biomass m_1 evolution in presence (blue) and absence (light blue) of heterotrophic pioneers. Absence of heter. pioneers: initial heterotrophic fraction $f_{2,0}$ equal to 0. Presence of heter. pioneers: initial heterotrophic fraction $f_{2,0}$ equal to 1. Biofilm surface area $A = 1\ m^2$. Incident light intensity $I_0 = 0.0052\ kmol\ m^{-2}\ d^{-1}$.

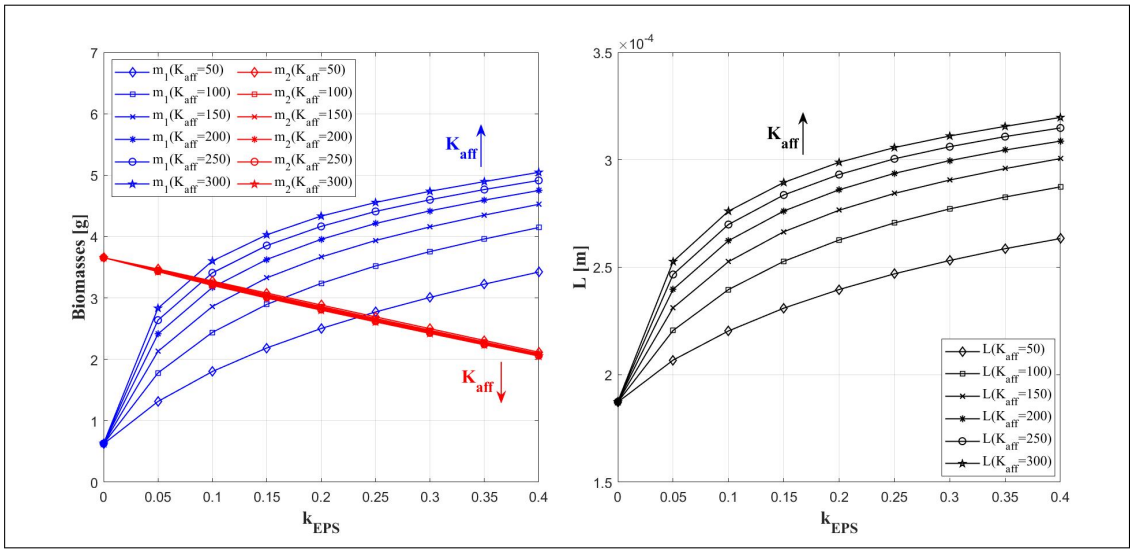

Figure 3.4: Scenario 1-NS2 (effects of heterotrophic EPS production and EPS-phototrophs affinity on phototrophic growth) - Amount [g] of phototrophic biomass (blue, left picture), heterotrophic biomass (red, left picture) and biofilm thickness (black, right picture) for different EPS-phototrophs affinity coefficient K_{aff} [50 - 300] and the heterotrophic EPS fraction $k_{EPS,2}$ [0 - 0.4], at $T = 20\ d$. Biofilm surface area $A = 1\ m^2$. Incident light intensity $I_0 = 0.0052\ kmol\ m^{-2}\ d^{-1}$. Initial biofilm composed exclusively of heterotrophs.

conditions. Three studies compose this Scenario. A first study (NS3) is carried out to investigate the effects of suboptimal incident light intensity I_0 on the biofilm growth. In this study, the incident light intensity values used in the experimental activity of [100] are adopted ($I_0 = 0.0013 - 0.0026 - 0.0052 - 0.0104\ kmol\ m^{-2}\ d^{-1}$, $I_0/I_{opt}\% = 7 - 14 - 29 - 57\%$). The initial biofilm domain is composed by 70% of phototrophs and 30% of heterotrophs ($f_{1,0} = 0.7$, $f_{2,0} = 0.3$, $f_{3,0} = f_{4,0} = 0$).

Results are reported in Figs.3.5, 3.6, 3.7. Fig.3.5 reports the evolution of the biofilm thickness $L(t)$. For all values of I_0, $L(t)$ increases linearly for about 15-20 days, after which the detachment process prevails and $L(t)$ remains almost constant. In the last days a modest decrease of $L(t)$ is observed for the simulations with $I_0 = 0.0052 - 0.0104\ kmol\ m^{-2}\ d^{-1}$. Indeed, in these cases the greater biofilm thickness leads to higher light attenuations and substrate consumptions. This corresponds to a reduction in the active biomass growth and an increase in the inert production. As a result, the biomass velocity decreases overall, as well as the thickness of the biofilm.

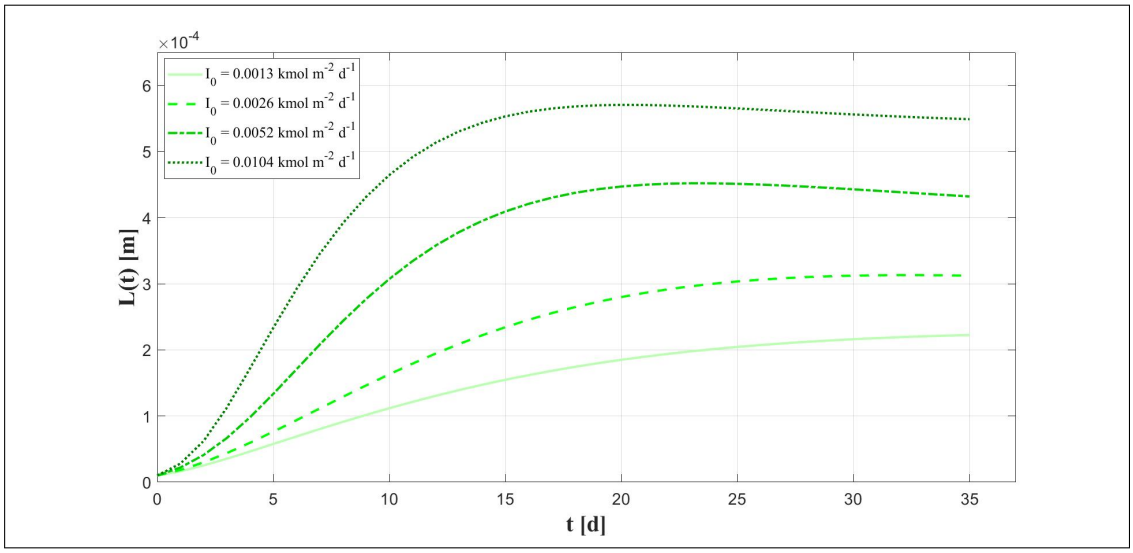

Figure 3.5: Scenario 2-NS3 (effects of suboptimal incident light intensity on biofilm growth) - Biofilm thickness evolution for four suboptimal values of incident light intensity I_0 [0.0013 - $0.0104\ kmol\ m^{-2}\ d^{-1}$]. Initial biofilm composed of 70% phototrophs and 30% heterotrophs.

Fig.3.6 shows the phototrophic biomass, the light dependency coefficient for phototrophs $\phi_{I,1}$ and the light intensity within the biofilm $I(z,t)$ for different values of I_0. Since the values considered for I_0 in these simulations are lower than I_m, photoinhibition phenomena do not come into play and light intensity is directly proportional to the phototrophic growth rate at each point of the biofilm. As consequence, for each time the higher is I_0 the higher are $L(t)$ and the phototrophic biomass in the biofilm. Moreover, the light conditions significantly influence the composition of the biofilm. The distribution of biomass within the biofilm can be observed in Fig.3.7 for $T = 35d$. When light intensity is low ($I_0 = 0.0013 - 0.0026\ kmol\ m^{-2}\ d^{-1}$), phototrophic growth is limited and the heterotrophic fraction is relevant in the biofilm. Instead, for high light intensities, the phototrophic growth rate is higher than the heterotrophic one, hence, the biofilm is mainly composed of phototrophic biomass. These results are qualitatively in agreement with the experimental results shown in [100]. Notably, most of the outer layer within the biofilm is occupied by active biomass ($f_1 + f_2$) which finds optimal conditions to grow. Conversely, due to the lack or shortage of soluble substrates and

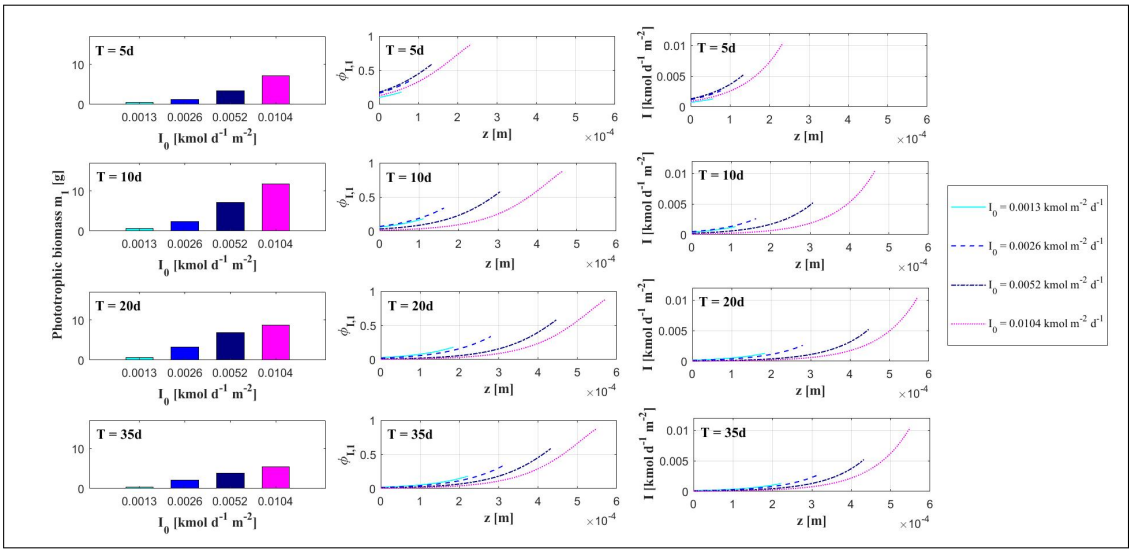

Figure 3.6: Scenario 2-NS3 (effects of suboptimal incident light intensity on biofilm growth) - Amount [g] of phototrophic biomass, light factor $\phi_{I,1}$ and light intensity within the biofilm $I(z,t)$ for four suboptimal values of incident light intensity I_0 [0.0013 - 0.0104 $kmol\ m^{-2}\ d^{-1}$], at $T = 5, 10, 20, 35\ d$. Biofilm surface area $A = 1\ m^2$. Initial biofilm composed of 70% phototrophs and 30% heterotrophs.

light, decay processes prevail in the inner part of biofilm and large amount of inert is produced.

The numerical studies NS4 and NS5 show the model results when photoinhibitory conditions arise. In NS4, biofilm evolution and phototrophic biomass growth are analyzed for different adversely high incident light intensities ($I_0 = 0.05 - 0.07 - 0.1 - 0.12\ kmol\ m^{-2}\ d^{-1}$). The initial biofilm domain is composed by 70% of phototrophs and 30% of heterotrophs ($f_{1,0} = 0.7, f_{2,0} = 0.3, f_{3,0} = f_{4,0} = 0$). The results of NS4 are summarized in Fig.3.8 and Fig.3.9. Fig.3.8 shows the evolution of biofilm thickness for different I_0 while Fig.3.9 shows the phototrophic mass, the light dependency coefficient for phototrophs $\phi_{I,1}$ and the light intensity within the biofilm $I(z,t)$.

From these results is clear that under light stress conditions, the increase in incident light intensity has negative effects on biofilm growth. At the beginning, high values of I_0 throughout the biofilm inhibit the phototrophic activity and modest variations of $L(t)$ are observed. Then, due to the slow biofilm growth, the light attenuation is improved in the innermost layers and phototrophs find better conditions to grow. This

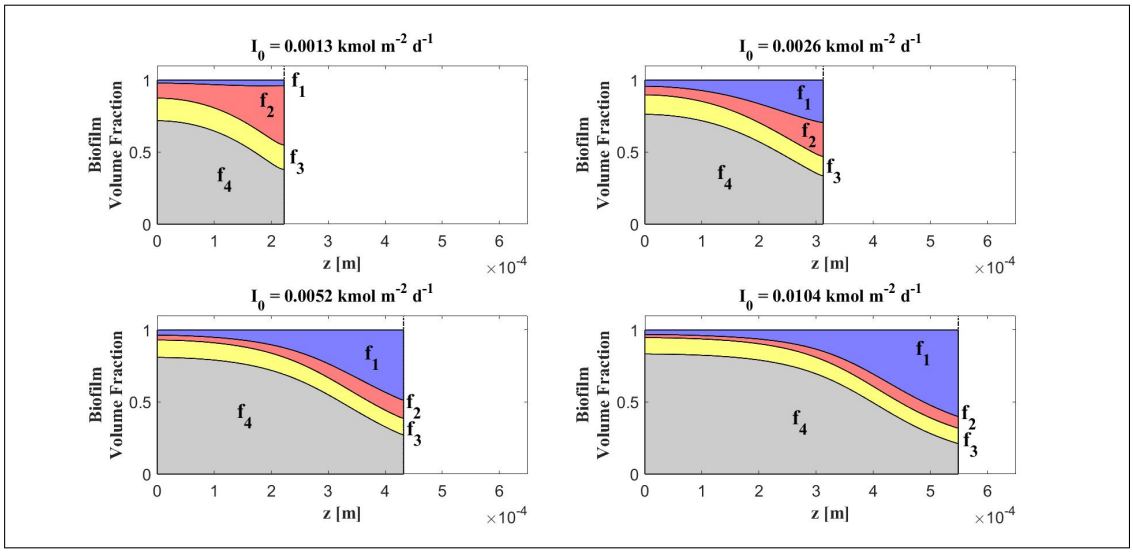

Figure 3.7: Scenario 2-NS3 (effects of suboptimal incident light intensity on biofilm growth) - Spatial distribution of biomass within the biofilm at $T = 35\ d$ for four suboptimal values of incident light intensity I_0: $0.0013\ kmol\ m^{-2}\ d^{-1}$ (top left), $0.0026\ kmol\ m^{-2}\ d^{-1}$ (top right), $0.052\ kmol\ m^{-2}\ d^{-1}$ (bottom left), $0.0104\ kmol\ m^{-2}\ d^{-1}$ (bottom right). f_1: phototrophs (blue), f_2: heterotrophs (red), f_3: EPS (yellow), f_4: inert (grey). Initial biofilm composed of 70% phototrophs and 30% heterotrophs.

behavior intensifies as I_0 increases. However, after 25 days the biofilm reaches similar steady-state thickness for all values of I_0 (Fig.3.8). Further interesting results concern the phototrophic mass variation over time. Phototrophic biomass develops faster when photoinhibition is reduced ($I_0 = 0.05 - 0.07\ kmol\ m^{-2}\ d^{-1}$). Nevertheless, for long times the maximum values of phototrophic mass are reached for higher I_0.

The numerical study NS5 is performed to investigate the heterotrophic shading contribution to the phototrophic growth under light stress conditions ($I_0 = 0.1\ kmol\ m^{-2}\ d^{-1}$). In particular, the biofilm evolution in presence (initial biofilm composition: $f_{1,0} = 0.7, f_{2,0} = 0.3, f_{3,0} = f_{4,0} = 0$) and absence of heterotrophic biomass (initial biofilm composition: $f_{1,0} = 1, f_{2,0} = f_{3,0} = f_{4,0} = 0$) are compared. In order to simulate the biofilm growth in absence of heterotrophic cells, $\psi_{2,L}$ is set equal to zero.

The biomass distribution is shown in Fig.3.10 at various simulation times. Results in presence and absence of heterotrophs are markedly different, suggesting that heterotrophs play a fundamental role in the growth of a phototrophic biofilm under light

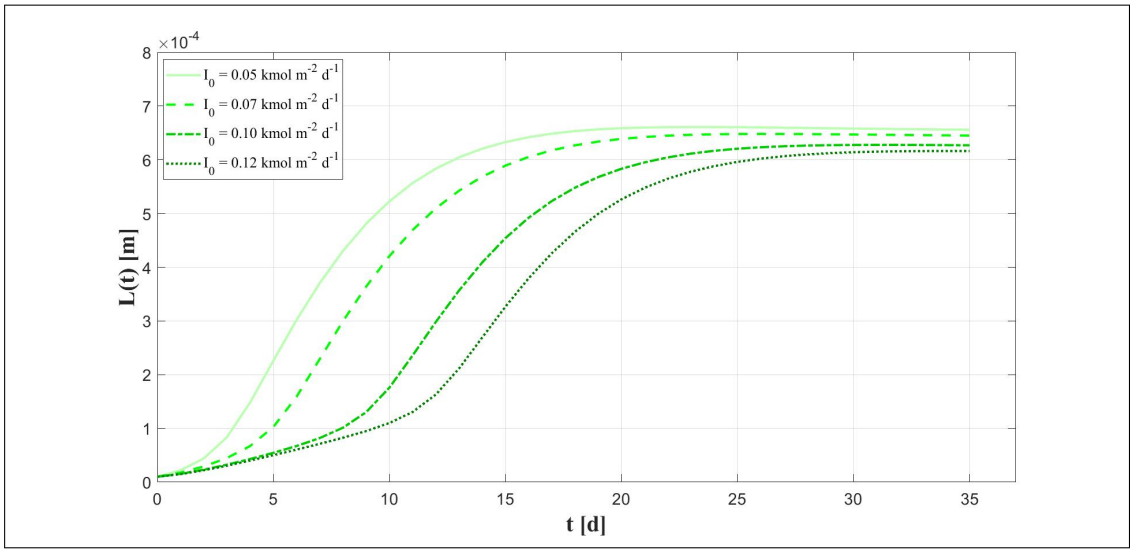

Figure 3.8: Scenario 2-NS4 (effects of light stress conditions on biofilm growth) - Biofilm thickness evolution for four photo-inhibiting values of incident light intensity I_0 [0.05 - 0.12 $kmol\ m^{-2}\ d^{-1}$]. Initial biofilm composed of 70% phototrophs and 30% heterotrophs.

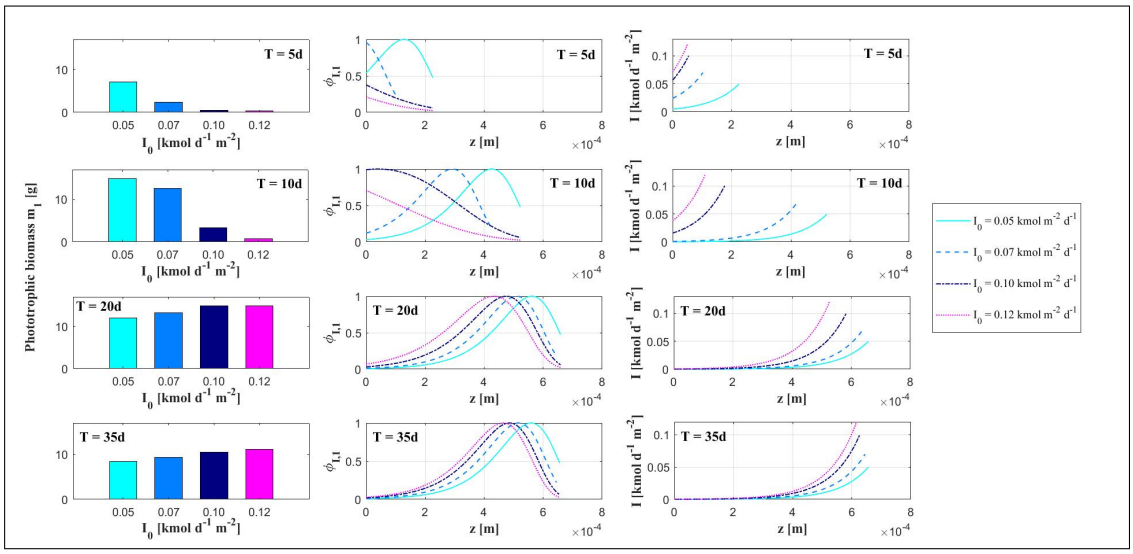

Figure 3.9: Scenario 2-NS4 (effects of light stress conditions on biofilm growth) - Amount [g] of phototrophic biomass, light factor $\phi_{I,1}$ and light intensity within the biofilm $I(z,t)$ for four photo-inhibiting values of incident light intensity I_0 [0.05 - 0.12 $kmol\ m^{-2}\ d^{-1}$], at $T = 5, 10, 20, 35\ d$. Biofilm surface area $A = 1\ m^2$. Initial biofilm composed of 70% phototrophs and 30% heterotrophs.

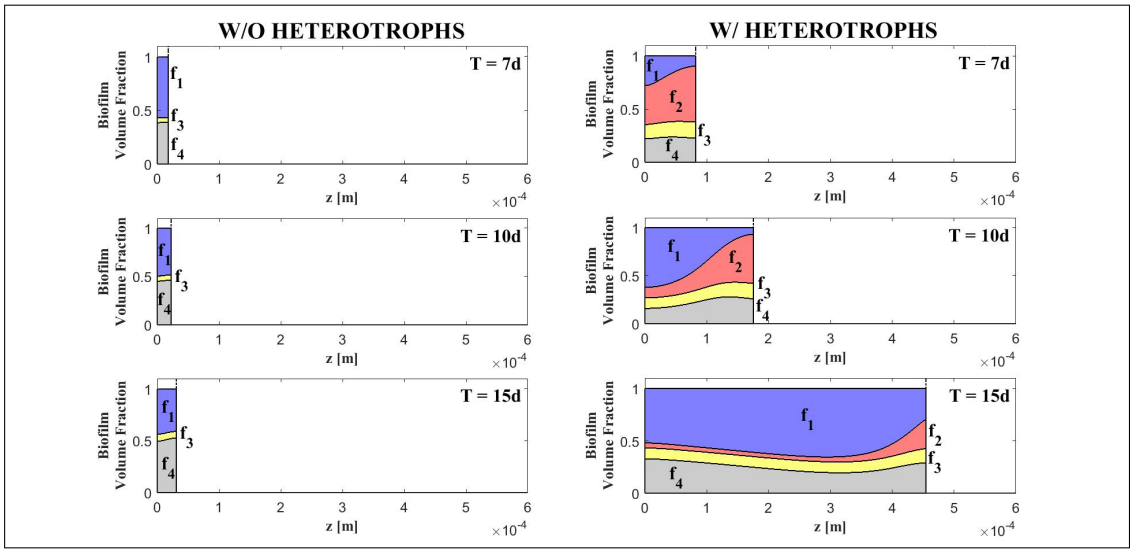

Figure 3.10: Scenario 2-NS5 (effects of heterotrophic shading contribution to phototrophic growth) - Spatial distribution of biomass within the biofilm in presence (right) and absence (left) of heterotrophic biomass both in sessile and planktonic state, under light stress conditions ($I_0 = 0.1\ kmol\ m^{-2}\ d^{-1}$), at $T = 7, 10, 15\ d$. f_1: phototrophs (blue), f_2: heterotrophs (red), f_3: EPS (yellow), f_4: inert (grey). Presence of heterotrophic biomass: initial biofilm is composed of 70% phototrophs and 30% heterotrophs. Absence of heterotrophic biomass: initial biofilm is composed exclusively of phototrophs, $\psi_{2,L} = 0\ kg\ m^{-3}$.

stress conditions. In both cases, the initial phototrophic metabolic activity is negatively affected by the critical light intensities. In absence of heterotrophs (left pictures), the limited phototrophic growth rate leads to limited biofilm velocities and a slow biofilm expansion. After 15 days the biofilm thickness is below $5 \cdot 10^{-5} m$. In presence of heterotrophs (right pictures), the biofilm velocity is increased by the heterotrophic metabolic activity, which is not affected by light conditions. Consequently, in the initial phase heterotrophs drive the expansion process of the biofilm which reaches an higher thickness than in the previous case. In the deepest part of the biofilm ideal light conditions for phototrophic growth develop. The result is a microbial stratification completely different from the one observed in absence of heterotrophic species: an high phototrophic biomass in the internal layers protected and shaded by an external layer populated mainly by heterotrophic biomass.

3.3.3 Scenario 3 - Effect of phototrophic organic carbon release

Scenario 3 focuses on the DOC-based interactions between the two species. As mentioned in Section 3.1, DOC release by phototrophs is a complex and variable phenomenon. In the model such release is considered by introducing the fraction of DOC released by phototrophs γ_c. Due to the high variability experimentally observed in this process, a numerical study NS6 with different values of γ_c is carried out. The initial biofilm domain is composed only by phototrophic species (initial biofilm composition: $f_{1,0} = 1, f_{2,0} = f_{3,0} = f_{4,0} = 0$). Due to the invasion process, heterotrophs colonize the domain and grow in sessile form. Two additional numerical studies NS7 and NS8 are performed to explore the coupled effect of γ_c and oxygen concentration in bulk liquid $S_{4,L}$ (NS7), and γ_c and incident light intensity I_0 (NS8) on model results.

Results of NS6 are proposed in Fig.3.11-3.12-3.13. In these simulations, a very low value of DOC is fixed at the interface biofilm-bulk liquid reproducing the growth of a biofilm immersed in environments poor in organic carbon. In this way, the metabolic release of DOC by phototrophs represents the main cause of the heterotrophic invasion process. Fig.3.11 shows the biomass distribution at different simulation times, for three values of γ_c. As expected, higher phototrophic DOC release results in higher heterotrophic fraction. In these simulations, biofilm growth is driven by phototrophic biomass, which accounts for most of the active biomass present in the biofilm. Accordingly, small variations in the biofilm thickness $L(t)$ observed for different phototrophic DOC releases mainly depend on the phototrophic metabolic activity: a higher release corresponds to a lower phototrophic growth rate and consequently a slightly lower thickness. Biofilm composition and trends of dissolved organic carbon and heterotrophic species in planktonic form are reported in Fig.3.12 for $\gamma_c = 0.30$. At $T = 5\ d$, the heterotrophic fraction within the biofilm is very small and the amount of DOC produced by phototrophs is higher than the one consumed by heterotrophs. Therefore, the values of DOC within the biofilm are higher than the boundary value

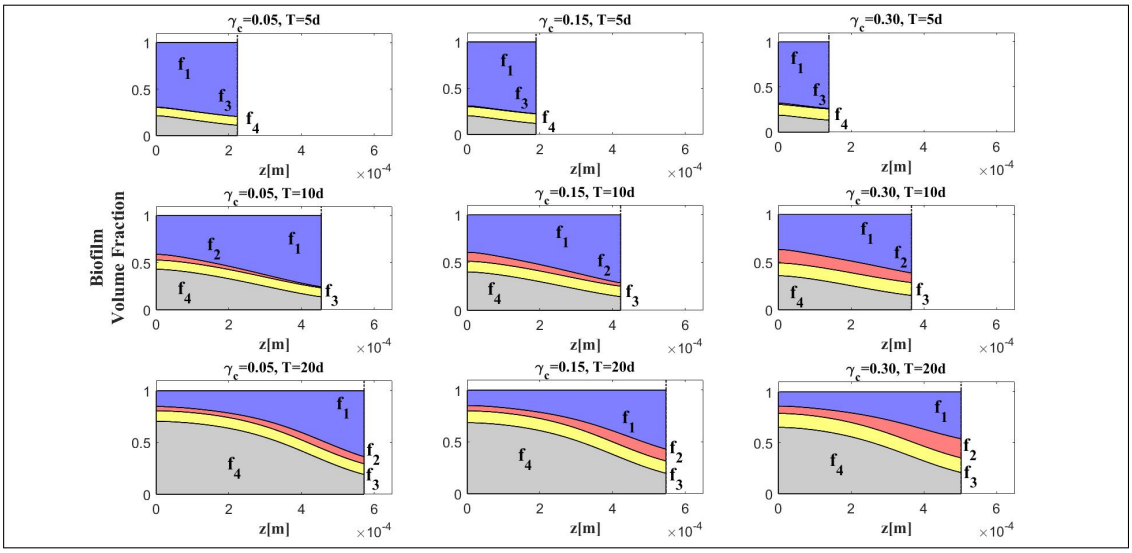

Figure 3.11: Scenario 3-NS6 (effects of DOC release fraction on heterotrophic invasion and growth) - Spatial distribution of biomass within the biofilm at $T = 5, 10, 20\ d$ for different phototrophic release fractions of dissolved organic carbon $\gamma_c = 0.05, 0.15, 0.30$. f_1: phototrophs (blue), f_2: heterotrophs (red), f_3: EPS (yellow), f_4: inert (grey). Incident light intensity $I_0 = 0.0104\ kmol\ m^{-2}\ d^{-1}$. Initial biofilm composed exclusively of phototrophs.

fixed at $z = L + h$. At later times ($T = 10\ d$ and $20\ d$), the heterotrophic fraction is more relevant due to invasion and growth processes. Consequently, DOC is consumed within the biofilm and the DOC profile reproduces the case of DOC values within the biofilm smaller than the fixed boundary value. Concerning planktonic heterotrophic cells (right column), the concentration of planktonic species decreases in the CBL (due to diffusion) and in the biofilm (due to diffusion and biological conversion).

Biofilm composition after 20 days is reported in Fig.3.13 for several values of γ_c. Note that, heterotrophic fraction is below 10-15% for any DOC release considered and could be higher in the case of bulk liquid richer in DOC. Finally, the release of DOC does not appear to influence the overall active biomass. Small increases in EPS occur when the abundance of heterotrophs increases.

Fig.3.14 summarize the results of NS7. Phototrophic and heterotrophic biomass and biofilm thickness are shown at $T = 20d$ for varying phototrophic DOC release fraction γ_c and incident light intensity I_0. The abundance of phototrophic biomass and

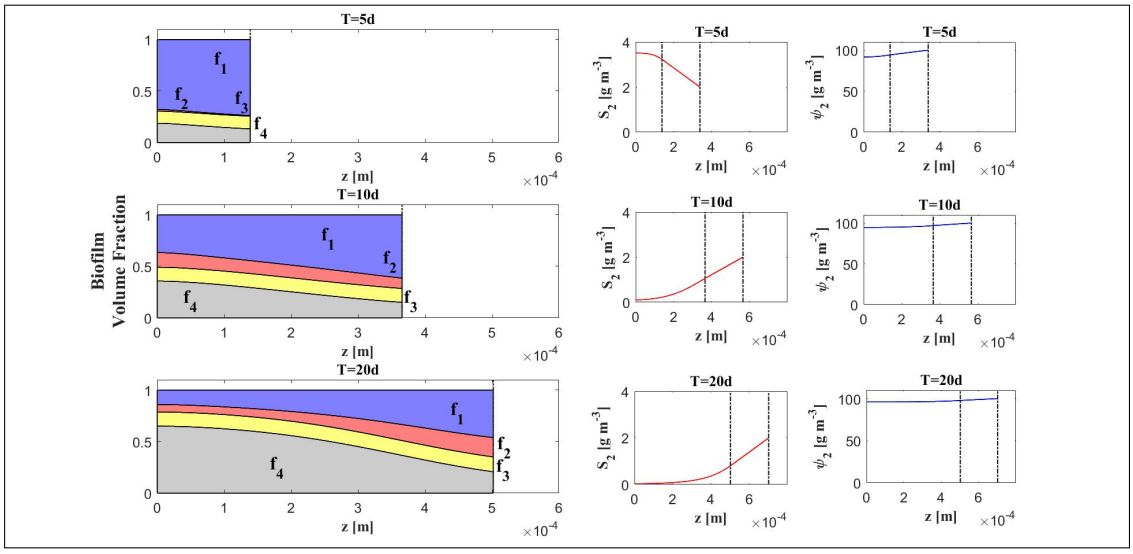

Figure 3.12: Scenario 3-NS6 (effects of DOC release fraction on heterotrophic invasion and growth) - Spatial distribution of biomass, dissolved organic carbon S_2 (red lines, central column) and heterotrophic species in planktonic form ψ_2 (blue lines, right column) within the biofilm, at $T = 5, 10, 20\ d$ for $\gamma_c = 0.30$. f_1: phototrophs (blue), f_2: heterotrophs (red), f_3: EPS (yellow), f_4: inert (grey). Incident light intensity $I_0 = 0.0104\ kmol\ m^{-2}\ d^{-1}$. Initial biofilm composed exclusively of phototrophs.

the biofilm expansion are highly sensitive to light conditions: the phototrophic growth is limited for modest I_0 and shows a considerable increase with increasing I_0. Being the biofilm growth driven by microbial growth, biofilm thickness follows a similar trend. Conversely, the heterotrophic metabolic activity does not depend on light energy and therefore, heterotrophic mass shows slow variations as I_0 varies. Such results confirm that light deeply affects the ecology of a phototrophic-heterotrophic biofilm. Furthermore, as γ_c increases, the phototrophic growth rate is reduced while heterotrophic mass goes up due to the greater DOC availability. Finally, for low I_0 values, the phototrophic metabolic activity and, consequently, the DOC released are limited and model results are less sensitive to the variation of γ_c.

Fig.3.15 reports the phototrophic and heterotrophic biomasses and biofilm thickness at $T = 20d$ for different γ_c values and dissolved oxygen concentrations in bulk liquid $S_{4,L}$ (NS8). It is clear that $S_{4,L}$ has almost no influence on heterotrophic growth because ideal oxygen conditions for their metabolism are guaranteed by phototrophic produc-

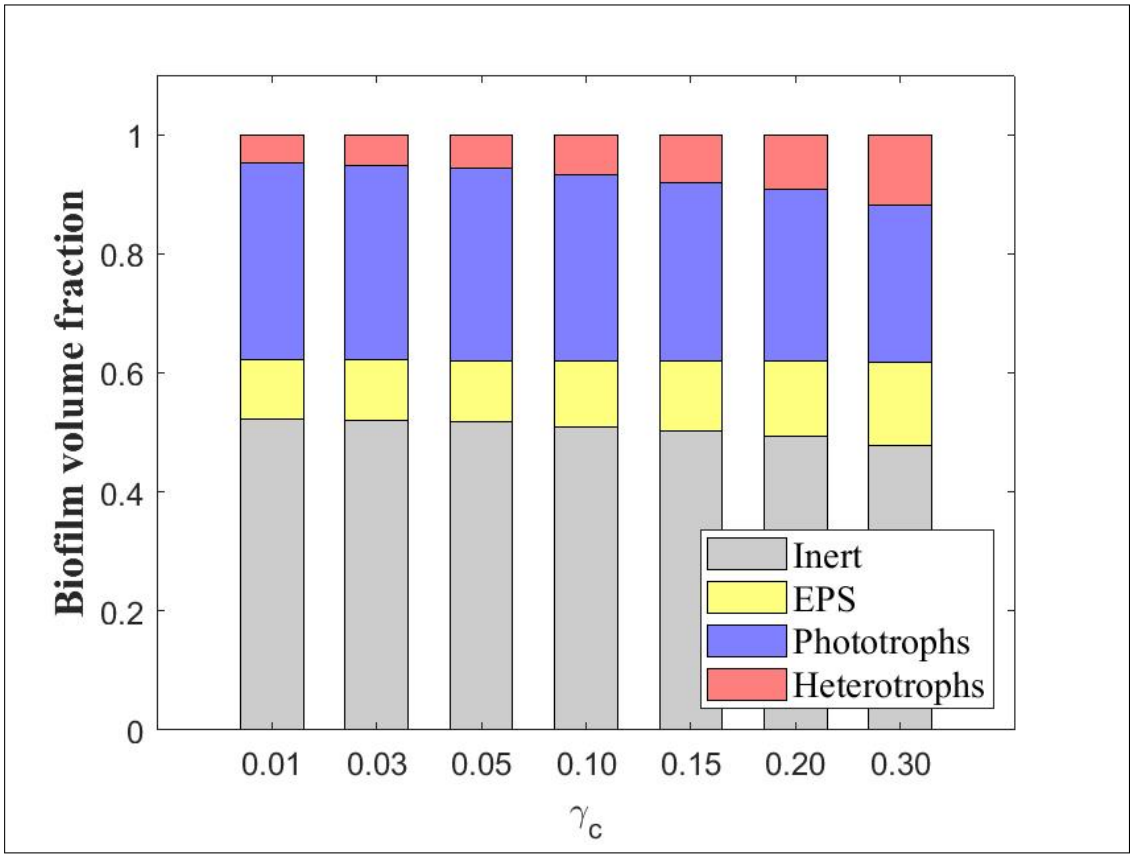

Figure 3.13: Scenario 3-NS6 (effects of DOC release fraction on heterotrophic invasion and growth) - Relative species abundance at $T = 20\ d$ for different phototrophic release fractions of dissolved organic carbon γ_c [0.01 - 0.30]. Blue: phototrophs; red: heterotrophs; yellow: EPS; grey: inert. Incident light intensity $I_0 = 0.0104\ kmol\ m^{-2}\ d^{-1}$. Initial biofilm composed exclusively of phototrophs.

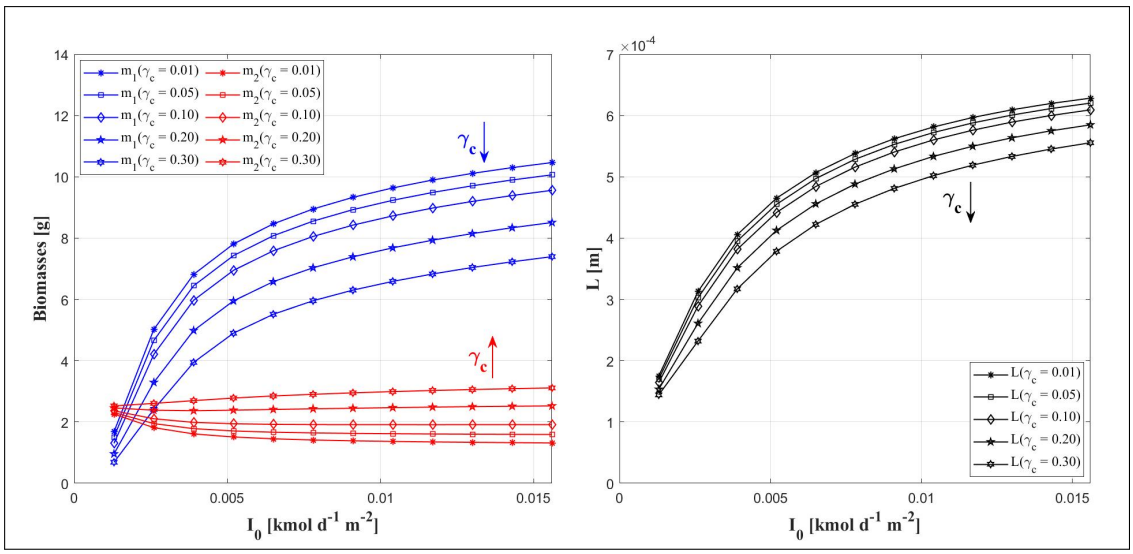

Figure 3.14: Scenario 3-NS7 (effects of DOC release fraction and light conditions on heterotrophic invasion and growth) - Amount [g] of phototrophic biomass (blue, left picture), heterotrophic biomass (red, left picture) and biofilm thickness (black, right picture) for different phototrophic release fractions of dissolved organic carbon γ_c [0.01 - 0.30] and incident light intensity I_0 [0.0013 - 0.0104 $kmol\ m^{-2}\ d^{-1}$], at $T = 20\ d$. Biofilm surface area $A = 1\ m^2$. Initial biofilm composed exclusively of phototrophs.

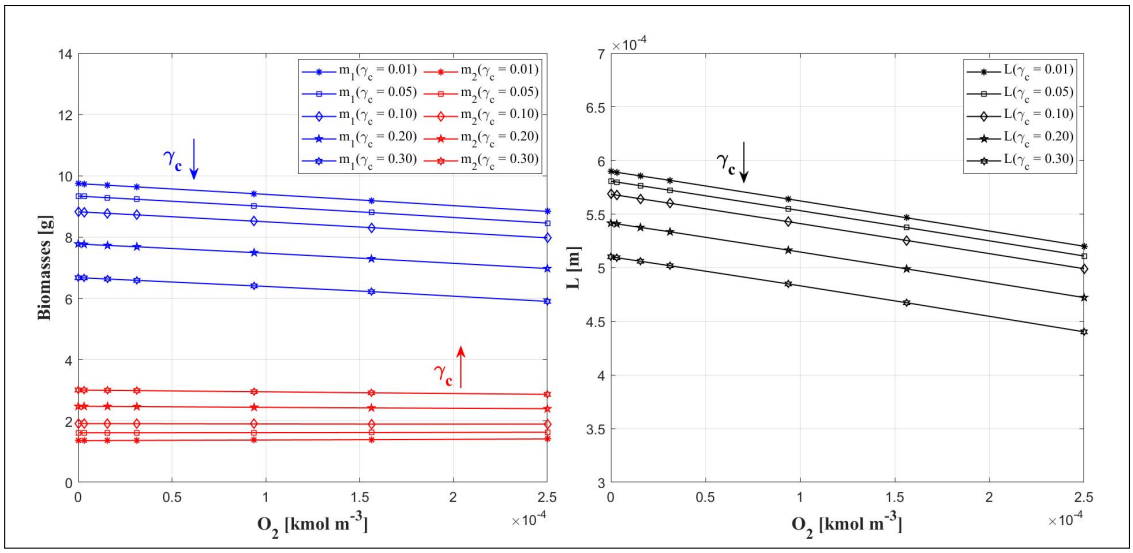

Figure 3.15: Scenario 3-NS8 (effects of DOC release fraction and oxygen conditions on heterotrophic invasion and growth) - Amount [g] of phototrophic biomass (blue, left picture), heterotrophic biomass (red, left picture) and biofilm thickness (black, right picture) for different phototrophic release fractions of dissolved organic carbon γ_c [0.01 - 0.30] and concentration of dissolved oxygen in bulk liquid $S_{4,L}$ [0 - $2.5 \cdot 10^{-4}\ kmol\ m^{-3}$], at $T = 20\ d$. Biofilm surface area $A = 1\ m^2$. Initial biofilm composed exclusively of phototrophs.

tions. In addition, phototrophic biomass and biofilm thickness are negatively influenced by $S_{4,L}$ due to the oxygen inhibition process on the phototrophic metabolism. However, the differences in terms of phototrophic biomass are not significant, suggesting that oxygen inhibition does not have relevant effects on phototrophic growth. Indeed, the oxygen inhibition coefficient depends on the ratio of inorganic carbon and dissolved oxygen and the adequate availability of inorganic carbon limits negative effects on phototrophic growth.

3.4 Discussion

We propose a mathematical model which simulate the growth and the ecology of a phototrophic-heterotrophic biofilm and the main phenomena involved. The biofilm is modelled as a one-dimensional free boundary domain which varies as a result of the processes of microbial growth, invasion and detachment. The invasion of the phototrophic species is set dependent on the EPS produced by the heterotrophic species in sessile form, so that the model reproduces the positive effects that heterotrophic pioneers have on the formation of a phototrophic biofilm.

This Chapter investigates the biofilm ecology under both suboptimal and light stress conditions and the role of heterotrophic pioneers and their secrection of EPS on the phototrophic growth. Moreover, the numerical studies explore the effects that the phototrophic release of DOC have on the biofilm evolution and species distribution under different light and dissolved oxygen conditions.

The results reported in Scenario 1 qualitatively reproduce what is observed in [100, 143]: the presence of sessile heterotrophic pioneers facilitates and intensifies the phototrophic growth in the biofilm. This experimental evidence proves positive interactions between phototrophs, heterotrophs and EPS and suggests new strategies to increase the efficiency of engineering applications based on phototrophic biofilms, such as wastewater treatment and bioenergy production. Indeed, the use of pioneering heterotrophs in

the development of phototrophic biofilm cultures may lead to higher phototrophic productivities. In Scenario 2, the model investigates the effects of light conditions on the biofilm ecology. All the results presented suggest that light is the major factor which influences phototrophic growth and evolution of the biofilm ecosystem. In agreement with the experimental results shown in [100], as the light intensity increases to the optimal value, we observe an increase in photosynthetic activity and phototrophic biomass abundance, and a consequent reduction in heterotrophic abundance. Conversely, incident light intensities higher than the optimal value initiate photoinhibition phenomena which lead to a decrease in phototrophic and biofilm growth. This result reveals that the model only partially reproduces the effects of photoinhibition. Indeed, according to experimental activity, photoinhibitory phenomena can even induce irreparable damage to the photosynthetic apparatus of the cell, endanging its reproduction [71]. Moreover, under light stress conditions, the biofilm may be highly vulnerable to incidental phenomena of desiccation, detachment or predation which could lead to complete washout. All these additional effects caused by the photoinhibition are not considered in this model, and as a consequence photoinhibition only leads to a delay in the biofilm growth. Furthermore, model results highlight the vital role of heterotrophic species under photoinhibition conditions, which provide a positive shading contribution to phototrophic growth. Such heterotrophic shading should be included among the syntrophic mechanisms existing between phototrophic and heterotrophic microorganisms in sessile form. Finally, Scenario 3 focuses on the effects that the phototrophic release of DOC has on the biofilm evolution and species distribution under different light and dissolved oxygen conditions. The abundance of heterotrophs within the biofilm is positively influenced by the phototrophic release of DOC, which guarantees the organic substrate necessary for the heterotrophic metabolism and confirms the syntrophic interaction between the two species [13]. Although high concentrations of dissolved oxygen can enhance photorespiration phenomena and reduce the rate of photosynthesis, this inhibiting effect is not quantitatively relevant in this study due to the significant presence

of inorganic carbon.

The model relies on a number of assumptions and focuses only on a specific ecosystem. Indeed, the model reproduces the evolution of the biofilm starting from a non-null initial configuration (already existing biofilm). Therefore, the definition of the initial biofilm thickness and microbial composition is required. The initial phase of biofilm formation by pioneering cells and flocs could be modelled by including the attachment process by planktonic microorganisms and by imposing a vanishing value as initial dimension of the domain [29].

The concentration of soluble substrates and planktonic species within the bulk liquid is assumed to be constant. However, their variation over time could be considered by introducing a system of ordinary differential equations based on mass balance which takes into account the inlet and outlet flow, and the exchange fluxes between the biofilm and the bulk liquid [30, 74]. In this way, the model could be adapted to a specific reactor configuration.

All simulations are carried out by setting a constant incident light intensity. The dynamic variation of light intensity due to the night-day cycle are neglected, since it occurs on a short time scale compared to the time periods investigated [40]. Consequently, phototrophic metabolic processes related to the dark period, such as dark respiration, are neglected.

The model takes into account the process of EPS secretion by phototrophs and heterotrophs, widely documented in the literature [138, 78]. Nevertheless, the experimental results reported are quantitatively discordant and this aspect should be further investigated.

In conclusion, the model may be applied to different fields, such as wastewater treatment and bioenergy production. Indeed, it is possible to reproduce the biological processes involved in these applications by setting appropriate values of the operating parameters and initial and boundary conditions. However, some parameters of the model, such as the invasion parameters, are unknown and have been assumed. Therefore, fu-

ture works should focus on the sensitivity analysis of the newly introduced parameters and the calibration and validation of the model using experimental data.

3.5 Appendix A

Conversion rates for f_i, ψ_i and S_j are needed to complete Eq. (3.4), (3.8) and (3.10). The model considers 6 microbial processes: biomass growth due to planktonic and sessile species and decay, for both phototrophs and heterotrophs.

The net biomass conversion rate due to sessile species $r_{M,i}$ is the difference between the growth rate $r_{G,i}$ and decay rate $r_{D,i}$:

$$r_{M,i} = \alpha_i r_{G,i} - r_{D,i},\ i = 1, 2, \tag{3.16}$$

where α_i is a positive coefficient ≤ 1 which takes into account the DOC release and the EPS production [78].

Growth rates due to sessile species are modelled with the following expression:

$$r_{G,i} = \mu_{\max,i}\ f_i \phi_{I,i} \prod_j \phi_{j,i},\ i = 1, 2, \tag{3.17}$$

where i indicates the phototrophic ($i = 1$) or heterotrophic ($i = 2$) biomass, $\mu_{\max,i}$ is the maximum specific growth rate, $\phi_{j,i}$ and $\phi_{I,i}$ are positive coefficients ≤ 1 considering dependence on soluble substrates and light, respectively. Such coefficients introduce non-linearity in the reaction terms and may be of three different types. Light dependency coefficient for phototrophs should consider the effects of photoinhibition phenomena: excess light can photoinhibit and reduce photosynthesis activity [71]. Therefore, as proposed by [115], the following optimum type expression is used:

$$\phi_{I,1} = \frac{I}{I_m}\, e^{(1-\frac{I}{I_m})}, \tag{3.18}$$

where I_m is the intensity at which maximum photosynthesis takes place (optimum light intensity). The heterotrophic growth rate does not depend on light intensity, hence, $\phi_{I,2} = 1$.

Furthermore, Monod-type kinetics are used as saturation coefficients:

$$\phi_{j,i} = \frac{S_j}{K_{j,i} + S_j}, \tag{3.19}$$

where $K_{j,i}$ represents the half saturation constant of the substrate j for biomass i. Finally, the inhibiting effect that some substrates may have on the microbial growth is considered with inhibition type coefficients:

$$\phi_{j,i} = \frac{K^{in}_{j,i}}{K^{in}_{j,i} + S_j}, \tag{3.20}$$

where $K^{in}_{j,i}$ represents the inhibition constant of the substrate j for biomass i.

Biomass decay processes are described by first-order kinetics:

$$r_{D,i} = k_{d,i}\, f_i, \;\; i = 1, 2, \tag{3.21}$$

where $k_{d,i}$ is the decay-inactivation rate for species i.

Finally, growth rates due to planktonic species are espressed by:

$$r_i = k_{col,i}\, \frac{\psi_i}{\rho} \phi_{I,i} \prod_j \phi_{j,i}, \;\; i = 1, 2, \tag{3.22}$$

where $k_{col,i}$ is the maximum colonization rate.

The kinetic rate expressions corresponding to each microbial process are listed below:

$$r_{G,1} = \mu_{\max,1} f_1 \frac{I}{I_m}\, e^{(1-\frac{I}{I_m})} \frac{S_1}{K_{1,1} + S_1} \frac{S_3}{K_{3,1} + S_3} \frac{K^{in}_{4,1}}{K^{in}_{4,1} + S_4}, \tag{3.23}$$

$$r_{G,2} = \mu_{\max,2} f_2 \frac{S_2}{K_{2,2} + S_2} \frac{S_4}{K_{4,2} + S_4}, \tag{3.24}$$

$$r_{D,1} = k_{d,1}\, f_1, \tag{3.25}$$

$$r_{D,2} = k_{d,2}\, f_2, \tag{3.26}$$

$$r_1 = k_{col,1} \frac{\psi_1}{\rho} \frac{I}{I_m}\, e^{(1-\frac{I}{I_m})} \frac{S_1}{K_{1,1} + S_1} \frac{S_3}{K_{3,1} + S_3} \frac{K_{4,1}^{in}}{K_{4,1}^{in} + S_4}, \tag{3.27}$$

$$r_2 = k_{col,2}\, \frac{\psi_2}{\rho} \frac{S_2}{K_{2,2} + S_2} \frac{S_4}{K_{4,2} + S_4}. \tag{3.28}$$

$K_{4,1}^{in}$ is the inhibition constant for dissolved oxygen on photosyntethic growth and is expressed as [67]:

$$K_{4,1}^{in} = K_{4,1,max}^{in} \frac{\frac{S_1}{S_4}}{K_{S_1/S_4} + \frac{S_1}{S_4}}, \tag{3.29}$$

where $K_{4,1,max}^{in}$ is the maximal inhibition coefficient of dissolved oxygen on phototrophic growth and K_{S_1/S_4} is the saturation coefficient representing the effect of IC to O_2 ratio on O_2 inhibition. All the reaction terms are expressed as:

$$r_{M,1} = (1 - k_{EPS,1} - \gamma_c)\, r_{G,1} - r_{D,1}, \tag{3.30}$$

$$r_{M,2} = (1 - k_{EPS,2})\, r_{G,2} - r_{D,2}, \tag{3.31}$$

$$r_{M,3} = k_{EPS,1}\, r_{G,1} + k_{EPS,2}\, r_{G,2}, \tag{3.32}$$

$$r_{M,4} = r_{D,1} + r_{D,2}, \tag{3.33}$$

$$r_{\psi,1} = -\frac{1}{Y_{\psi,1}}\, r_1\, \rho, \tag{3.34}$$

$$r_{\psi,2} = -\frac{1}{Y_{\psi,2}}\, r_2\, \rho, \tag{3.35}$$

$$r_{S,1} = \nu_{1,1}\, r_{G,1} + \nu_{2,1}\, r_{G,2}, \tag{3.36}$$

$$r_{S,2} = \gamma_c\, r_{G,1} + \nu_{2,2}\, r_{G,2}, \tag{3.37}$$

$$r_{S,3} = \nu_{1,3}\, r_{G,1}, \tag{3.38}$$

$$r_{S,4} = \nu_{1,4}\, r_{G,1} + \nu_{2,4}\, r_{G,2}, \tag{3.39}$$

where $Y_{\psi,1}$ and $Y_{\psi,2}$ are the yields of sessile species on planktonic species. The stoichiometric coefficients are reported in Table 3.3.

Parameter	**Unit**	**Value**	**Ref**
$\nu_{1,1}$	$kmol\ kg(COD)^{-1}$	-0.0313	[138]
$\nu_{2,1}$	$kmol\ kg(COD)^{-1}$	0.0198	[138]
$\nu_{2,2}$	$kg(COD)\ kg(COD)^{-1}$	-1.5873	[138]
$\nu_{1,3}$	$kmol\ kg(COD)^{-1}$	-0.0053	[138]
$\nu_{1,4}$	$kmol\ kg(COD)^{-1}$	0.0419	[138]
$\nu_{2,4}$	$kmol\ kg(COD)^{-1}$	-0.0184	[138]

Table 3.3: Stoichiometric parameters of the model

Chapter 4

Multiscale modelling of *de novo* anaerobic granulation

4.1 Introduction

Biofilms are complex, dense and compact aggregates composed by microbial cells immobilized in a self-produced matrix of extracellular polymeric substances (EPS) [46]. Several trophic groups coexist in such structures and deeply interact with each other through synergistic and antagonistic activities. Although natural biofilms typically develop as planar layers attached to suitable surfaces, under specific conditions the aggregation occurs due to the self-immobilization of cells into approximately spherical-shaped granules without the involvement of a surface [122]. The process leading to the formation of these aggregates is known as granulation. In particular, the term *de novo* granulation is used when the process is initiated by individual microbial cells and flocs, in opposition to the case in which the granulation process takes place starting from an

This Chapter has been submitted to the *Bulletin of Mathematical Biology* as: Tenore, A.,Russo, F., Mattei, M.R., D'Acunto, B., Collins, G., Frunzo, L. Multiscale modelling of *de novo* anaerobic granulation.

inoculum already in granular form.

In recent years, granular systems have become increasingly popular in the field of wastewater treatment. In particular, the sessile microbial species within the granules drive the purification process by converting the soluble substrates present in the liquid medium. Compared to suspended biomass of the conventional systems, the denser, stronger and more regular structure of the biofilm granules leads to better settling properties [69, 70] which allow higher biomass concentrations [9] and reduced-footprint reactors [69]. Furthermore, in contrast to other biofilm systems where sessile biomass develops on solid supports, granular systems are based on spherical and constantly moving microbial aggregates. Movement and shape mitigate boundary layer resistances and enhance the mass transfer of substrates across the biofilm granule [9]. For these reasons, granular biofilms have been successfully developed in different reactor configurations, for various processes, such as aerobic, anaerobic and partial nitritation-anammox treatments [123].

The main drawback of granular-based systems is represented by the start-up phase, due to the complexity of the mechanisms and phenomena which contribute to the success of the granulation process [66]. In the last years, many researchers have studied and explored this process and numerous theories have been proposed. Hydrodynamic conditions generated by the liquid up-flow velocity, the gas production, the particle-particle collision, the mixing systems and the reactor geometry are universally recognized as the key factors for the granulation process and the entire life cycle of the granules [123, 69, 64]. Indeed, suitable hydrodynamic conditions are needed to initiate the granulation process by promoting and improving the aggregation of suspended biomass [63] and, at the same time, avoiding its complete washout. Moreover, intense hydrodynamic conditions induce high shear forces on the granule surface which influence dimension, shape, structure and density of the granules [69, 34] and regulate a continuous process of aggregation and breaking which leads to the formation of an increasing number of granules. High shear forces are thought to stimulate the production

of EPS which represents a further beneficial factor for the granulation as it increases cell surface hydrophobicity [123]. Several studies also consider the granulation process as the result of an organized process driven by pioneering microbial species which have specific characteristics [92, 137].

In [92], various theories concerning the anaerobic sludge granulation are collected and described. The most widespread theory asserts that anaerobic granulation process is favoured by key microorganisms such as *Methanosaeta* [123, 92, 57, 43]. Such acetoclastic methanogens have filamentous structures and good adhering properties and initiate the granulation process by forming a central nucleus and favouring the immobilization of other methanogens and synergistically functioning bacterial groups [72, 142]. In this context, various studies [66, 141, 65] report that quorum sensing plays an essential role by regulating the transition of some *Methanosaeta* species from short to filamentous cells. In the initial phase, the nucleus presents a filamentous appearance and achieves a spherical shape due to the rolling effect of the hydraulic shear forces [123, 92]. In a second phase, the nucleus develops into a granule and acetogens and acidogens attach on its surface and grow syntrophically with acetoclastic methanogens [123, 92, 72, 126]. The result is a multiple, concentric layer structure with an archaeal core constituted by *Methanosaeta*. This theory is supported by several experimental evidences showing layered structures in anaerobic granules [108, 12, 26]. In any case, the granulation process still remains not fully understood and further studies on its complex biological aspects are necessary in order to optimize the efficiencies of this process.

In this framework, mathematical modelling represents a valuable tool to describe, explore and study the granulation process, the life cycle of the biofilm granules and the performances of granular-based systems. In the last years, the modelling of granular biofilm systems has stimulated a growing interest due to the relevance of this topic in engineering, biological and industrial fields. Numerous models have been proposed to mainly describe aerobic [32], anaerobic [88, 12, 44, 36] and anammox [129, 130, 127] processes involved in such systems. A first classification can be introduced according to

the approach used: continuum models simulate the evolution of the granular biofilm in a quantitative and deterministic way, while discrete models, such as individual-based [36, 91, 140] and cellular automata models [111], are able to represent the multidimensional structural heterogeneity of granular biofilm but provide results including elements of randomness and introduce stochastic effects into the solutions [76]. Most models of granular biofilms [88, 129, 12, 44, 130] are based on the continuum approach introduced by [132] for one-dimensional planar biofilms, and model the granule as a spherical free boundary domain, which evolves as a result of the microbial metabolic processes and the mass exchange with the surrounding environment. Among them, most describe the dynamic evolution of the granule fixing the final steady-state dimension [129, 12, 44, 130].

Anyway, some significant aspects of the granular biofilm growth are not considered exhaustively by the models present in the literature. According to [9], only two models [12, 109] consider the attachment process, which plays a key role in the formation and evolution of granular biofilms. No model takes into account the invasion process: the colonization of a pre-existing biofilm mediated by motile planktonic cells living in the surrounding environment, which can penetrate the porous matrix of the biofilm and convert to sessile biomass. Moreover, all continuum models fix a non-zero initial size of the domain and thus describe an initial configuration where the granular biofilm is already formed. Finally, according to the exclusion principle presented in [59], all biofilm models based on the basic version introduced in [132] lead to restrictions on ecological structure.

Concerning the aim and the numerical studies pursued in literature, most works focus on system performances by describing the biological purification process and the removal of soluble substrates from the wastewaters. Someone focuses on the biofilm granule, paying attention to the dimensional evolution [88] and to the distribution of sessile biomass within the biofilm at the steady-state [88, 129, 44, 130, 127]. However, no continuous model fully describes the *de novo* granulation process by considering the

initial formation and ecology of the biofilm granule. Only the individual-based model introduced by [36] focuses on the *de novo* formation of anaerobic granules based on a discrete approach.

In this Chapter, we propose a multiscale model which describes the *de novo* granulation process, and incorporates the mesoscopic granular biofilm processes within a continuous granular-based reactor. For this purpose, following the approach proposed in [73, 74] in the case of one-dimensional planar biofilms, the presented model couples the macroscopic reactor mass balances with the mesoscopic granular biofilm model here derived by using a continuum approach [132]. The model accounts for the growth of both granular attached and planktonic biomasses, and includes the main microbial exchange processes involved, such as attachment, detachment and invasion. The *de novo* granulation process is modelled by assuming that all biomass initially present in the reactor is in planktonic form. Mathematically, this corresponds to consider a vanishing initial value of the granule radius which represents the free boundary under the assumption of radial symmetry. The biofilm formation is initiated by the attachment process, which leads to consider a space-like free boundary. This mathematical problem has been discussed in [29] and is applied here for the first time to model the genesis of granular biofilms. The granule formation and expansion are governed by the following processes: microbial growth, attachment, invasion and detachment. Attachment initiates the life of biofilms and is regarded as the complex phenomenon whereby pioneering microbial cells in planktonic form attach to a surface and develop in the form of sessile aggregate [90]. However, as reported above, the formation of a biofilm granule is the result of the interaction and aggregation of microbial cells and flocs without the involvement of a surface. Therefore, in this Chapter, attachment is accounted as the flux of microbial mass which aggregates, switches its phenotype from planktonic to sessile and initiates the granulation. It is modelled as a linear function of the concentrations of the planktonic species, each of them characterized by a specific attachment velocity. The invasion process is included for the first time in the modelling of granular biofilms

by extending the mathematical formulation proposed in [28] for one-dimensional planar biofilms to a spherical domain. This allows to remove the restrictions on ecological structure highlighted in [59]. Furthermore, the bulk liquid is modelled as a perfectly mixed medium where soluble substrates and planktonic biomass are found and influenced by the operational parameters of the reactor, the microbial metabolic activities and the processes of mass exchange with the biofilm. The mathematical model has been derived for a generic granular-based reactor and applied to the anaerobic granulation process in order to test the model behaviour and study the genesis, evolution and ecology of anaerobic granules. Different numerical studies have been carried out to investigate how the granulation properties of the planktonic biomass, the biomass density of the granules, the shear forces and the composition of the influent wastewater can affect the evolution of the process. The results include the dimensional evolution and ecology of the granule, in terms of biomass distribution and relative abundance, and the variation of soluble substrates and planktonic biomass within the reactor.

The paper is organized as follows. In Section 4.2, the derivation of the model is carried out by presenting all assumptions, variables, equations, initial and boundary conditions. Section 4.3 describes the biological case to which the model is applied. Numerical studies are reported and discussed in detail in Section 4.4 and 4.5, respectively. Finally, the conclusions of the Chapter and the future goals are outlined in Section 4.6.

4.2 Mathematical Model

In this Chapter, the granular biofilm reactor is modelled as a completely mixed continuous system where N_G identical biofilm granules are immersed. As shown in Fig. 4.1, two different scales are considered in the model: the bioreactor macroscale and the granule mesoscale. Three components are considered within the granular biofilm: the sessile biomass which constitutes the solid matrix, the planktonic biomass which is found in the channels and voids and the soluble substrates dissolved in the liquid phase.

Meanwhile, planktonic biomass and soluble substrates are considered within the bulk liquid of the reactor. These components interact and influence each other as a result of biological, physical and chemical processes. In the following, the modelling of both the granule and reactor scales is discussed, introducing all the processes, assumptions, variables, equations, initial and boundary conditions involved.

4.2.1 Modelling granule scale

Under the assumption of radial symmetry, the biofilm granule is modelled as a spherical free boundary domain whose spatial evolution is completely described by the evolution of the radius $R(t)$. A vanishing initial value $R(0) = 0$ is considered to model the initial granulation. All variables involved in the biofilm modelling are considered as functions of time t and space r, where r denotes the radial coordinate. Consequently, the granule centre is located in $r = 0$.

The model takes into account the dynamics of three biofilm components, expressed in terms of concentration: n microbial species in sessile form $X_i(r,t)$; n microbial species in planktonic form $\psi_i(r,t)$; m dissolved substrates $S_j(r,t)$.

Volume occupied by soluble substrates and planktonic cells is considered negligible due to the small particle size and just sessile biomass is assumed to occupy biofilm volume. The density of the granule ρ is assumed to be constant and equal for all microbial species. By dividing sessile species concentration X_i by ρ, biomass volume fractions $f_i(r,t)$ are achieved. f_i are constrained to add up to unity [97]. The liquid component is not included as a model variable since the biofilm is supposed to be immersed in a liquid environment and the availability of liquid does not play any limiting role in the microbial metabolic activities. In summary, the model components which describe the

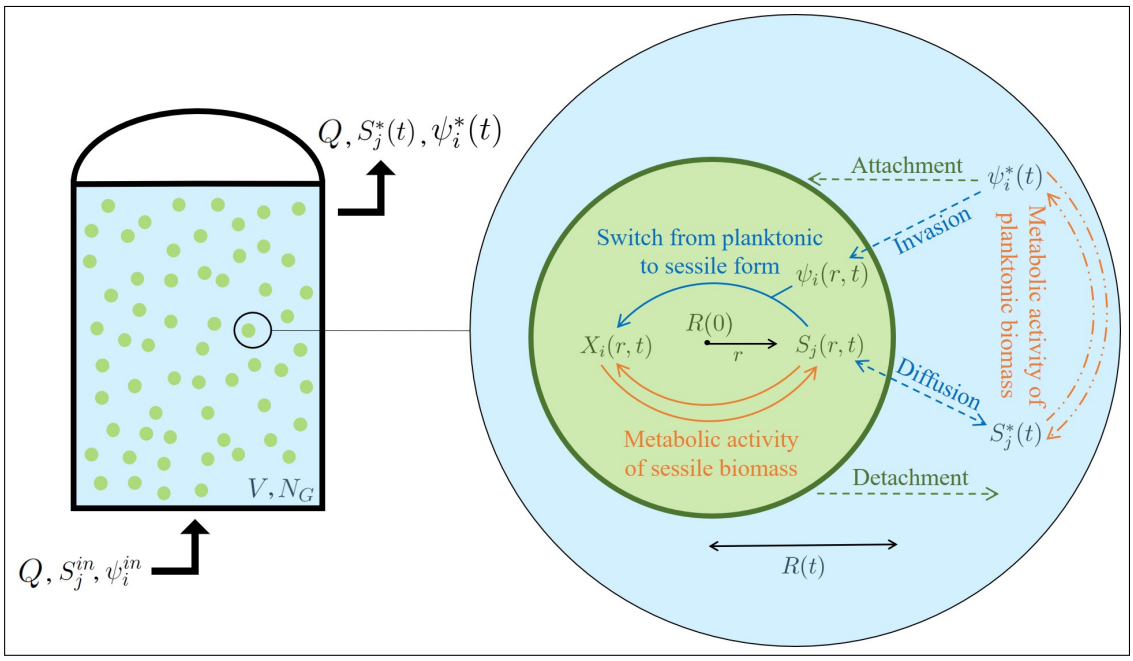

Figure 4.1: Multiscale representation of the model. The bioreactor is modelled as a perfectly mixed continuous system (on the left), having volume V, where N_G biofilm granules are immersed. The influent is characterized by constant values of flow rate Q and concentration of soluble substrates S_j^{in} and suspended biomasses ψ_i^{in}. The effluent is characterized by the same constant flow rate and by time-varying concentrations of soluble substrates $S_j^*(t)$ and suspended biomasses $\psi_i^*(t)$. Gas transfer is not included in the model. A focus on a single granule is presented on the right, with all processes considered in the model. The granule has a zero initial radius $R(0)$, which varies over time due to the effect of various microbial processes. Metabolic processes within the granule are carried out by the sessile biomass $X_i(r,t)$, which grows by converting the substrates dissolved in the biofilm liquid $S_j(r,t)$, while metabolic processes within the bulk liquid are carried out by the suspended biomasses $\psi_i^*(t)$, which grows by converting the substrates dissolved in the bulk liquid $S_j^*(t)$. The attachment process has been considered through a flux of suspended biomass from the bulk to the granule. The detachment process has been considered through a flux of sessile biomass from the granule to the bulk. Moreover, invasion processes are modelled: the planktonic biomass $\psi_i(r,t)$ invades the solid matrix of the granule and switches its phenotype from planktonic to sessile. Finally, process of diffusion of substrates across the granule is included in the model. Solid arrows: processes within the granule. Dash-dot arrows: processes within the bulk liquid. Dash arrows: exchange processes between granule and bulk liquid.

granular biofilm compartment are:

$$X_i,\ i = 1, ..., n,\ \mathbf{X} = (X_1, ..., X_n), \tag{4.1}$$

$$f_i = \frac{X_i}{\rho},\ i = 1, ..., n,\ \mathbf{f} = (f_1, ..., f_n), \tag{4.2}$$

$$\psi_i,\ i = 1, ..., n,\ \boldsymbol{\psi} = (\psi_1, ..., \psi_n), \tag{4.3}$$

$$S_j,\ j = 1, ..., m,\ \mathbf{S} = (S_1, ..., S_m). \tag{4.4}$$

Based on the continuum approach introduced in [132] for one-dimensional planar biofilms, a system of partial differential equations (PDEs) in a spherical free boundary domain is derived from mass balance considerations, under the assumption of radial symmetry. Hyperbolic PDEs model the distribution and growth of sessile biomass $f_i(r, t)$ and parabolic PDEs describe the diffusion and conversion of soluble substrates $S_j(r, t)$. Further parabolic PDEs govern the process of invasion and conversion of planktonic cells $\psi_i(r, t)$.

Based on the aggregation properties of the suspended biomass living in the bulk liquid, attachment phenomena govern the initial granulation process, while the further biofilm evolution is significantly affected by detachment phenomena. Attachment and detachment contribute to the microbial mass exchange occurring between granules and bulk liquid and are included in the model as continuous and deterministic processes. Finally, as introduced in [28] in the case of one-dimensional planar biofilm, the invasion process is considered to describe the phenomena of granule colonization by planktonic cells. Such cells penetrate the porous matrix of the biofilm from the surrounding medium and contribute to the development of the biofilm.

Under the assumption of radial symmetry, the mass balance set up for a generic

component in a differential volume of the spherical domain, leads to the following equation:

$$\frac{\partial c(r,t)}{\partial t} + \frac{1}{r^2}\frac{\partial}{\partial r}(r^2 J_r(r,t)) = r_c(r,t), \tag{4.5}$$

where $c(r,t)$ is the concentration of a generic component in the spherical domain, J_r is the advective and/or diffusive flux in the radial direction and $r_c(r,t)$ is the transformation term.

The transport of sessile biomass is modelled as an advective process. Hence, by expressing the advective flux of the i^{th} sessile microbial species in the radial direction as

$$J_{r,i}(r,t) = u(r,t)X_i(r,t), \tag{4.6}$$

where $u(r,t)$ is the biomass velocity, Eq.(4.5) applied to sessile microbial species within the granular biofilm domain takes the following hyperbolic form:

$$\frac{\partial X_i(r,t)}{\partial t} + \frac{1}{r^2}\frac{\partial}{\partial r}(r^2 u(r,t)X_i(r,t)) = \rho r_{M,i}(r,t,\mathbf{X},\mathbf{S}) + \rho r_i(r,t,\boldsymbol{\psi},\mathbf{S}),$$

$$i = 1,...,n,\ 0 \leq r \leq R(t),\ t > 0, \tag{4.7}$$

where $r_{M,i}(r,t,\mathbf{X},\mathbf{S})$ and $r_i(r,t,\boldsymbol{\psi},\mathbf{S})$ are the specific growth rates due to sessile and planktonic species, respectively.

By dividing Eq.(4.7) by ρ and by considering $f_i = \frac{X_i}{\rho}$ yields

$$\frac{\partial f_i(r,t)}{\partial t} + \frac{1}{r^2}\frac{\partial}{\partial r}(r^2 u(r,t)f_i(r,t)) = r_{M,i}(r,t,\mathbf{f},\mathbf{S}) + r_i(r,t,\boldsymbol{\psi},\mathbf{S}),$$

$$i = 1, ..., n,\ 0 \leq r \leq R(t),\ t > 0, \tag{4.8}$$

$$\frac{\partial f_i(r,t)}{\partial t} + f_i(r,t)\frac{\partial u(r,t)}{\partial r} + \frac{2u(r,t)f_i(r,t)}{r} + u(r,t)\frac{\partial f_i(r,t)}{\partial r} = r_{M,i}(r,t,\mathbf{f},\mathbf{S}) + r_i(r,t,\boldsymbol{\psi},\mathbf{S}),$$

$$i = 1, ..., n,\ 0 \leq r \leq R(t),\ t > 0. \tag{4.9}$$

Summing Eq.(4.9) over all i and considering $\sum_{i=1}^{n} f_i = 1$, it follows:

$$\frac{\partial u(r,t)}{\partial r} = -\frac{2u(r,t)}{r} + G(r,t,\mathbf{f},\mathbf{S},\boldsymbol{\psi}), 0 < r \leq R(t),\ t > 0, \tag{4.10}$$

where $G(r,t,\mathbf{f},\mathbf{S},\boldsymbol{\psi}) = \sum_{i=1}^{n}(r_{M,i}(r,t,\mathbf{f},\mathbf{S}) + r_i(r,t,\boldsymbol{\psi},\mathbf{S}))$.

This differential equation governs the evolution of the biomass velocity $u(r,t)$.

By imposing the flux of the i^{th} sessile microbial species equal to 0 at $r = 0$, it follows from Eq.(4.6) that $u(0,t) = 0$. Considering this result and integrating Eq.(4.10), the integral expression of $u(r,t)$ is achieved:

$$u(r,t) = \frac{1}{r^2}\int_0^r r'^2 G(r',t,\mathbf{f},\mathbf{S},\boldsymbol{\psi})dr',\ 0 < r \leq R(t),\ t > 0. \tag{4.11}$$

Substituting Eq.(4.10) into Eq.(4.9) yields

$$\frac{\partial f_i(r,t)}{\partial t} + u(r,t)\frac{\partial f_i(r,t)}{\partial r} = r_{M,i}(r,t,\mathbf{f},\mathbf{S}) + r_i(r,t,\boldsymbol{\psi},\mathbf{S}) - f_i(r,t)G(r,t,\mathbf{f},\mathbf{S},\boldsymbol{\psi}),$$

$$i = 1, ..., n,\ 0 \leq r \leq R(t),\ t > 0. \tag{4.12}$$

Eq.(4.12) describes the transport and growth of the sessile microbial species i across

the granular biofilm under the assumption of radial symmetry.

Compared to the equation reported in [132] for a planar biofilm, Eq.(4.12) presents a different expression of $u(r,t)$ and the additional reaction term $r_i(r,t,\boldsymbol{\psi},\mathbf{S})$ due to the invasion phenomenon.

In the same way as for sessile microbial species, Eq.(4.5) can be applied to soluble substrates and planktonic species. In these cases, the transport of planktonic biomass and soluble substrates is modelled as a diffusive process and the fluxes of the i^{th} planktonic species and the j^{th} soluble substrate in the radial direction are expressed as

$$J_{r,\psi_i}(r,t) = -D_{\psi,i}\frac{\partial \psi_i(r,t)}{\partial r}, \tag{4.13}$$

and

$$J_{r,j}(r,t) = -D_{S,j}\frac{\partial S_j(r,t)}{\partial r}, \tag{4.14}$$

where $D_{\psi,i}$ and $D_{S,j}$ denote the diffusivity coefficient of the planktonic species i and the soluble substrate j in the biofilm, respectively.

Then, parabolic diffusion-reaction PDEs are derived from Eq.(4.5):

$$\frac{\partial \psi_i(r,t)}{\partial t} - D_{\psi,i}\frac{\partial^2 \psi_i(r,t)}{\partial r^2} - \frac{2D_{\psi,i}}{r}\frac{\partial \psi_i(r,t)}{\partial r} = r_{\psi,i}(r,t,\boldsymbol{\psi},\mathbf{S}),$$

$$i = 1,...,n,\ 0 < r < R(t),\ t > 0, \tag{4.15}$$

$$\frac{\partial S_j(r,t)}{\partial t} - D_{S,j}\frac{\partial^2 S_j(r,t)}{\partial r^2} - \frac{2D_{S,j}}{r}\frac{\partial S_j(r,t)}{\partial r} = r_{S,j}(r,t,\mathbf{f},\mathbf{S}),$$

$$j = 1,...,m,\ 0 < r < R(t),\ t > 0, \tag{4.16}$$

where $r_{\psi,i}(r,t,\boldsymbol{\psi},\mathbf{S})$ is the conversion rate of planktonic species i and $r_{S,j}(r,t,\mathbf{f},\mathbf{S})$

is the conversion rate of soluble substrate j.

The free boundary evolution is described by the variation of the radius $R(t)$ over time. This is affected by microbial growth and processes of attachment and detachment occurring at the surface of the biofilm. In particular, as in Chapter 2, the attachment flux of the i^{th} suspended species is supposed to be linearly dependent on the concentration of the suspended species i in the bulk liquid $\psi_i^*(t)$ and is expressed as:

$$\sigma_{a,i}(t) = \frac{v_{a,i}\psi_i^*(t)}{\rho},\ i = 1, ..., n, \tag{4.17}$$

where $v_{a,i}$ is the attachment velocity of the suspended species i.

By summing Eq.(4.17) over all suspended species, the total attachment flux is achieved:

$$\sigma_a(t) = \frac{\sum_{i=1}^{n} v_{a,i}\psi_i^*(t)}{\rho}. \tag{4.18}$$

The detachment is modelled as a quadratic function of the granule radius $R(t)$ [1]:

$$\sigma_d(t) = \lambda R^2(t), \tag{4.19}$$

where λ is the detachment coefficient and is supposed to be equal for all microbial species.

The global mass balance on the spherical domain gives:

$$\frac{\partial}{\partial t}\int_0^{R(t)} 4\pi r^2 \rho dr = \rho A(t)(\sigma_a(t) - \sigma_d(t)) + \int_0^{R(t)} 4\pi r^2 \rho G(r, t, \mathbf{f}, \mathbf{S}, \boldsymbol{\psi}) dr, \tag{4.20}$$

where $A(t)$ is the area of the spherical granule and is equal to $4\pi R^2(t)$.

By dividing Eq.(4.20) by $4\pi\rho$ and by considering $u(R(t), r)$ from Eq.(4.11), it fol-

lows:

$$\frac{\partial}{\partial t}\int_0^{R(t)} r^2 dr = R^2(t)(\sigma_a(t) - \sigma_d(t)) + \int_0^{R(t)} r^2 G(r,t,\mathbf{f},\mathbf{S},\boldsymbol{\psi})dr, \tag{4.21}$$

$$\frac{1}{3}\frac{\partial R^3(t)}{\partial t} = R^2(t)(\sigma_a(t) - \sigma_d(t)) + R^2(t)u(R(t),t), \tag{4.22}$$

$$\dot{R}(t) = \sigma_a(t) - \sigma_d(t) + u(R(t),t). \tag{4.23}$$

The latter equation governs the time evolution of the free boundary domain.

The total mass of the sessile community and the mass of the i^{th} sessile microbial species within the granule can be calculated as follows:

$$m_i(t) = \int_0^{R(t)} 4\pi r^2 \rho f_i(r,t)dr,\ i = 1,...,n, \tag{4.24}$$

$$m_{tot}(t) = \sum_{i=1}^{n} m_i(t) = \frac{4}{3}\pi\rho R^3(t). \tag{4.25}$$

4.2.2 Modelling reactor scale

As already mentioned, the reactor is modelled as a completely mixed continuous system. Thus, all the quantities referring to the bulk liquid dynamics are equal at every point and are dependent on time. The variables considered in the bulk liquid are n planktonic biomasses and m soluble substrates, both expressed in terms of concentration ($\psi_i^*(t)$ and $S_j^*(t)$, respectively). Such concentrations vary over time due to biological processes, operational parameters of the reactor and mesoscopic granule processes.

In summary, the model components which describe the bulk liquid compartment are:

$$\psi_i^*,\ i = 1, ..., n,\ \boldsymbol{\psi}^* = (\psi_1^*, ..., \psi_n^*), \tag{4.26}$$

$$S_j^*,\ j = 1, ..., m,\ \mathbf{S}^* = (S_1^*, ..., S_m^*). \tag{4.27}$$

Accordingly, a system of ordinary differential equations (ODEs) derived from mass balance considerations is considered to describe the dynamics of suspended biomass and soluble substrates within the bulk liquid:

$$V\dot{\psi}_i^*(t) = Q(\psi_i^{in} - \psi_i^*(t)) - A(t)N_G D_{\psi,i}\frac{\partial \psi_i(R(t),t)}{\partial r} + r_{\psi,i}^*(t, \boldsymbol{\psi}^*, \mathbf{S}^*) - \sigma_{a,i}(t)\rho A(t)N_G,$$

$$i = 1, ..., n\ \ t > 0, \tag{4.28}$$

$$V\dot{S}_j^*(t) = Q(S_j^{in} - S_j^*(t)) - A(t)N_G D_{S,j}\frac{\partial S_j(R(t),t)}{\partial r} + r_{S,j}^*(t, \boldsymbol{\psi}^*, \mathbf{S}^*),$$

$$j = 1, ..., m,\ \ t > 0. \tag{4.29}$$

where V is the volume of the bulk liquid assumed equal to the reactor volume, Q is the continuous flow rate, ψ_i^{in} is the concentration of the planktonic species i in the influent, S_j^{in} is the concentration of the substrate j in the influent, $r_{\psi,i}^*(t, \boldsymbol{\psi}^*, \mathbf{S}^*)$ and $r_{S,j}^*(t, \boldsymbol{\psi}^*, \mathbf{S}^*)$ are the conversion rates for ψ_i^* and S_j^*, respectively.

Eq.(4.28) represents the mass balance of the i^{th} microbial species in suspended form. In particular, the mass variation within the reactor (first member) is due to the continuous mass flow in and out of the reactor (first term of the second member), the

exchange flux between the bulk liquid and the granular biofilms (second term of the second member), the growth and decay in the bulk liquid (third term of the second member), the exchange flux related to attachment processes (fourth term of the second member). Notably, no contribution by detachment to suspended species is considered in Eq.(4.28). Indeed, detachment phenomena within granular biofilm-based reactors involve large pieces of granule which detach from the mother granule. Such biofilm pieces can attach to existing granules, constitute new granules or disintegrate and become suspended biomass. Due to the uncertainty and complexity of such mechanisms, any contribution by detachment to suspended or attached biomass is neglected and may be considered in future works.

Similarly, Eq.(4.29) represents the mass balance of the j^{th} soluble substrate. In this case, the mass variation within the reactor (first member) is due to the continuous mass flow in and out of the reactor (first term of the second member), the exchange flux between the bulk liquid and the granular biofilms (second term of the second member) and the consumption and/or production occurring in the bulk liquid and mediated by the suspended biomass (third term of second member).

4.2.3 Initial and boundary conditions

The processes involved in a granular biofilm reactor are described by Eqs.(4.10), (4.12), (4.15), (4.16), (4.23), (4.28) and (4.29). In order to integrate such equations, it is necessary to specify initial and boundary conditions.

As mentioned above, the *de novo* granulation is modelled by considering an initial configuration whereby only suspended biomass is supposed to be present in the reactor. Hence, a vanishing initial condition is coupled to Eq.(4.23) which describes the variation of the granule radius over time:

$$R(0) = 0. \tag{4.30}$$

Being applied to the bulk liquid domain, Eq.(4.28) and Eq.(4.29) also need initial conditions:

$$\psi_i^*(0) = \psi_{i,0}^*,\ i = 1, ..., n, \tag{4.31}$$

$$S_j^*(0) = S_{j,0}^*,\ j = 1, ..., m, \tag{4.32}$$

where $\psi_{i,0}^*$ and $S_{j,0}^*$ are the initial concentrations of the i^{th} suspended species and the j^{th} soluble substrate within the bulk liquid, respectively.

Eqs.(4.10), (4.12), (4.15) and (4.16) refer to the biofilm domain and do not require to specify initial conditions, since the extension of the biofilm domain is zero at $t = 0$.

The boundary condition of the Eq.(4.12) at the interface granule-bulk liquid $r = R(t)$ depends on the sign of the mass flux at the interface. When the free boundary is a space-like line ($\sigma_a - \sigma_d > 0$), there is a mass flux from bulk liquid to biofilm, thus the boundary condition depends on the concentration of suspended biomass in the bulk liquid:

$$f_i(R(t), t) = \frac{v_{a,i}\psi_i^*(t)}{\sum_{i=1}^{n} v_{a,i}\psi_i^*(t)},\ i = 1, ..., n,\ t > 0. \tag{4.33}$$

Meanwhile, when the free boundary is a time-like line ($\sigma_a - \sigma_d < 0$), the boundary condition for Eq.(4.12) is not needed because there is a mass flux from biofilm to bulk liquid and the biomass concentration at the interface is regulated exclusively by the internal points of the biofilm domain.

For both parabolic systems (4.15) and (4.16), a no-flux condition is fixed at the granule centre $r = 0$, while boundary conditions at the interface biofilm-bulk liquid $r = R(t)$ are related to the solutions of Eq.(4.28) and Eq.(4.29), which represent the

Equations	**Initial conditions**	**Boundary conditions**	
	$t=0$	$r=0$	$r=R(t)$
$\frac{\partial f_i(r,t)}{\partial t}+u(r,t)\frac{\partial f_i(r,t)}{\partial r}=r_{M,i}(r,t,\mathbf{f},\mathbf{S})+r_i(r,t,\boldsymbol{\psi},\mathbf{S})+$			$f_i(R(t),t)=\frac{v_{a,i}\psi_i^*(t)}{\sum_{i=1}^n v_{a,i}\psi_i^*(t)}$
$-f_i(r,t)G(r,t,\mathbf{f},\mathbf{S},\boldsymbol{\psi}))$			when $\sigma_a-\sigma_d>0$
$\frac{\partial \psi_i(r,t)}{\partial t}-D_{\psi,i}\frac{\partial^2\psi_i(r,t)}{\partial r^2}-\frac{2D_{\psi,i}}{r}\frac{\partial\psi_i(r,t)}{\partial r}=r_{\psi,i}(r,t,\boldsymbol{\psi},\mathbf{S})$		$\frac{\partial\psi_i}{\partial r}(0,t)=0$	$\psi_i(R(t),t))=\psi_i^*(t)$
$\frac{\partial S_j(r,t)}{\partial t}-D_{S,j}\frac{\partial^2 S_j(r,t)}{\partial r^2}-\frac{2D_{S,j}}{r}\frac{\partial S_j(r,t)}{\partial r}=r_{S,j}(r,t,\mathbf{f},\mathbf{S}))$		$\frac{\partial S_j}{\partial r}(0,t)=0$	$S_j(R(t),t))=S_j^*(t)$
$\frac{\partial u(r,t)}{\partial r}=-\frac{2u(r,t)}{r}+G(r,t,\mathbf{f},\mathbf{S},\boldsymbol{\psi})$		$u(0,t)=0$	
$\dot{R}(t)=\sigma_a(t)-\sigma_d(t)+u(R(t),t)$	$R(0)=0$		
$V\dot{\psi}_i^*(t)=Q(\psi_i^{in}-\psi_i^*(t))-A(t)N_G D_{\psi,i}\frac{\partial\psi_i(R(t),t)}{\partial r}+$ $+r_{\psi,i}^*(t,\boldsymbol{\psi}^*,\mathbf{S}^*)-\sigma_{a,i}(t)\rho A(t)N_G$	$\psi_i^*(0)=\psi_{i,0}^*$		
$V\dot{S}_j^*(t)=Q(S_j^{in}-S_j^*(t))-A(t)N_G D_{S,j}\frac{\partial S_j(R(t),t)}{\partial r}+$ $+r_{S,j}^*(t,\boldsymbol{\psi}^*,\mathbf{S}^*)$	$S_j^*(0)=S_{j,0}^*$		

Table 4.1: Model equations and initial and boundary conditions

concentrations of planktonic species and soluble substrates within the bulk liquid:

$$\frac{\partial\psi_i}{\partial r}(0,t)=0,\ \psi_i(R(t),t))=\psi_i^*(t),\ i=1,...,n,\ t>0, \tag{4.34}$$

$$\frac{\partial S_j}{\partial r}(0,t)=0,\ S_j(R(t),t))=S_j^*(t),\ j=1,...,m,\ t>0. \tag{4.35}$$

Finally, as previously mentioned, the boundary condition for Eq.(4.10) is given by:

$$u(0,t)=0,\ t>0. \tag{4.36}$$

In conclusion, the model is based on Eqs.(4.10), (4.12), (4.15), (4.16), (4.23), (4.28), (4.29), and initial and boundary conditions Eqs.(4.30)-(4.36). All equations and initial

and boundary conditions on which the model is based are summarized in Table 4.1. The reaction terms of these equations depend on the specific biological case considered and describe the complex biological interplay taking place between sessile biomass $X_i(r,t)$, planktonic biomass $\psi_i(r,t)$ and soluble substrates $S_j(r,t)$ within the biofilm and suspended biomass $\psi_i^*(t)$ and soluble substrates $S_j^*(t)$ within the bulk liquid.

4.3 Modelling *de novo* anaerobic granulation

The mathematical model described in the previous section can be applied to any granular biofilm system by defining appropriate variables, parameters, initial and boundary conditions and reaction terms of the equations based on the biological processes involved.

In this Chapter, the model is applied to study the process of *de novo* granulation and the ecology of granules in an anaerobic reactor. Anaerobic digestion (AD) is a biological process extensively used to manage liquid and solid wastes and produce fuels. It is a low-cost and renewable technology based on a complex multi-step process where different microbial species convert organic substances in methane-rich biogas. During the last decades, the AD process has been implemented in granular biofilm systems, where the microbial community forms dense biofilm granules which offer several operational advantages compared to conventional suspended systems.

As introduced in Section 4.1, many theories are proposed to explain and motivate the granulation process and several factors are included among the causes, above all the hydrodynamic conditions of the reactor [123, 69, 64]. Many studies report the fundamental role played by methanogenic species which facilitate the formation of the granule nucleus due to their filamentous structure and their abilities to produce EPS and to use quorum sensing strategies [123, 66, 141, 65]. To model this aspect, different attachment velocities are used depending on the microbial species.

The following variables, expressed in terms of concentrations, are included in the

model:

- 5 sessile microbial species within the biofilm: sugar fermenters X_{Su}, butyrate consumers X_{Bu}, propionate consumers X_{Pro}, acetoclastic methanogens X_{Ac}, inert material X_I.
- 4 planktonic species within the biofilm: sugar fermenters ψ_{Su}, butyrate consumers ψ_{Bu}, propionate consumers ψ_{Pro}, acetoclastic methanogens ψ_{Ac}.
- 5 soluble substrates within the biofilm: sugar S_{Su}, butyrate S_{Bu}, propionate S_{Pro}, acetate S_{Ac} and methane S_{CH_4}.
- 4 suspended species within the bulk liquid: sugar fermenters ψ^*_{Su}, butyrate consumers ψ^*_{Bu}, propionate consumers ψ^*_{Pro}, acetoclastic methanogens ψ^*_{Ac}.
- 5 soluble substrates within the bulk liquid: sugar S^*_{Su}, butyrate S^*_{Bu}, propionate S^*_{Pro}, acetate S^*_{Ac} and methane $S^*_{CH_4}$.

Suspended inert is not modelled as it is supposed to play no role in the life cycle of the granular biofilm (inactive biomass is supposed to have neither metabolic activity nor attachment and invasion properties).

The model considers an influent flow composed exclusively of dissolved substrates. Therefore, extracellular biological and non-biological processes of conversion of complex organic matter into soluble compounds, known as disintegration and hydrolysis, are neglected. The main intracellular processes are taken into account both in the biofilm and in the bulk liquid: acidogenesis, acetogenesis and methanogenesis. The kinetic expressions of the biological processes involved in the model are taken from [11]. In particular, each growth process leads to the formation of new biomass, consumption and/or production of one or more soluble substrates. Each decay process implies the death of active biomass which turns into inert material. Within the biofilm, sessile sugar fermenters X_{Su} grow by converting sugar S_{Su} into butyrate S_{Bu}, propionate S_{Pro} and

acetate S_{Ac} (acidogenesis process). Butyrate S_{Bu} and propionate S_{Pro} are consumed by sessile butyrate consumers X_{Bu} and sessile propionate consumers X_{Pro}, respectively, and acetate S_{Ac} is produced (acetogenesis process). Lastly, acetate is converted into methane S_{CH_4} by sessile acetoclastic methanogens X_{Ac} (methanogenesis process). The same biological processes are supposed to occur in the bulk liquid where the suspended biomasses ψ_i^* consume or produce the soluble substrates S_j^*. Furthermore, the decay of any sessile biomass is considered to produce inert material (X_I) which represents inactive biomass and accumulates in the biofilm. The decay processes are also considered for suspended species in the bulk liquid.

The suspended active species present in the bulk liquid are also modelled in the granule domain as planktonic cells ψ_i which populate the voids of the solid matrix and contribute to the growth of the corresponding sessile species as a result of the invasion phenomena.

All the reaction terms of the model equations are listed below. The specific growth rates within the biofilm due to sessile biomass $r_{M,i}$ in Eq.(4.10) and Eq.(4.12) are modelled as Monod-type kinetics:

$$r_{M,i} = f_i(\mu_{\max,i}\frac{S_i}{K_i + S_i} - k_{d,i}),\ i \in I_B, \tag{4.37}$$

where $I_B = [Su, Bu, Pro, Ac]$ is the index set, $\mu_{\max,i}$ is the maximum net growth rate for biomass i, K_i is the affinity constant of the consumed substrate for biomass i and $k_{d,i}$ is the decay constant for biomass i.

The inert formation rate is give by the sum of the decay rates of each active species, modelled as first order kinetic:

$$r_{M,I} = \sum_{i \in I_B} f_i\ k_{d,i}. \tag{4.38}$$

The specific growth rates within the biofilm due to planktonic cells r_i in Eq.(4.10) and Eq.(4.12) are defined as:

$$r_i = k_{col,i}\ \frac{\psi_i}{\rho}\frac{S_i}{K_i + S_i},\ i \in I_B, \tag{4.39}$$

where $k_{col,i}$ is the maximum colonization rate of motile species i and ρ is the granule density.

The conversion rates for planktonic cells due to the invasion process $r_{\psi,i}$ in Eq.(4.15) are expressed by:

$$r_{\psi,i} = -\frac{1}{Y_{\psi,i}} r_i\ \rho,\ i \in I_B, \tag{4.40}$$

where $Y_{\psi,i}$ denotes the yield of non-motile species i on corresponding motile species.

While, the conversion rates for soluble substrates within the biofilm $r_{S,j}$ in Eq.(4.16), with $j \in [Su, Bu, Pro, Ac, CH_4]$, are listed below:

$$r_{S,Su} = -\frac{\mu_{\max,Su}}{Y_{Su}}\frac{S_{Su}}{K_{Su} + S_{Su}} f_{Su}\ \rho, \tag{4.41}$$

$$r_{S,Bu} = -\frac{\mu_{\max,Bu}}{Y_{Bu}}\frac{S_{Bu}}{K_{Bu} + S_{Bu}} f_{Bu}\ \rho + g_{Su,Bu}\frac{(1 - Y_{Su})}{Y_{Su}}\mu_{\max,Su}\frac{S_{Su}}{K_{Su} + S_{Su}} f_{Su}\ \rho, \tag{4.42}$$

$$r_{S,Pro} = -\frac{\mu_{\max,Pro}}{Y_{Pro}}\frac{S_{Pro}}{K_{Pro} + S_{Pro}} f_{Pro}\ \rho + g_{Su,Pro}\frac{(1 - Y_{Su})}{Y_{Su}}\mu_{\max,Su}\frac{S_{Su}}{K_{Su} + S_{Su}} f_{Su}\ \rho, \tag{4.43}$$

$$r_{S,Ac} = -\frac{\mu_{\max,Ac}}{Y_{Ac}}\frac{S_{Ac}}{K_{Ac}+S_{Ac}}f_{Ac}\,\rho + g_{Su,Ac}\frac{(1-Y_{Su})}{Y_{Su}}\mu_{\max,Su}\frac{S_{Su}}{K_{Su}+S_{Su}}f_{Su}\,\rho +$$

$$+g_{Bu,Ac}\frac{(1-Y_{Bu})}{Y_{Bu}}\mu_{\max,Bu}\frac{S_{Bu}}{K_{Bu}+S_{Bu}}f_{Bu}\,\rho + g_{Pro,Ac}\frac{(1-Y_{Pro})}{Y_{Pro}}\mu_{\max,Pro}\frac{S_{Pro}}{K_{Pro}+S_{Pro}}f_{Su}\,\rho, \tag{4.44}$$

$$r_{S,CH_4} = \frac{(1-Y_{Ac})}{Y_{Ac}}\mu_{\max,Ac}\frac{S_{Ac}}{K_{Ac}+S_{Ac}}f_{Ac}\,\rho, \tag{4.45}$$

where Y_{Su}, Y_{Bu}, Y_{Pro}, Y_{Ac}, denote the yields of sugar fermenters, butyrate consumers, propionate consumers and acetoclastic methanogens on the corrisponding substrate consumed, $g_{Su,Bu}$, $g_{Su,Pro}$, $g_{Su,Ac}$ are the stoichiometric fractions of butyrate, propionate and acetate produced from sugar, $g_{Bu,Ac}$ and $g_{Pro,Ac}$ are the stoichiometric fractions of acetate produced from butyrate and propionate.

Moreover, the conversion rates of suspended biomasses $r^*_{\psi,i}$ within the bulk liquid in Eq.(4.28) are defined as:

$$r^*_{\psi,i} = \psi^*_i(\mu_{\max,i}\frac{S^*_i}{K_i+S^*_i} - k_{d,i}),\ i \in I_B, \tag{4.46}$$

while, the conversion rates of soluble substrates $r^*_{S,j}$ within the bulk liquid in Eq.(4.29), with $j \in [Su, Bu, Pro, Ac, CH_4]$, are listed below:

$$r^*_{S,Su} = -\psi^*_{Su}\frac{\mu_{\max,Su}}{Y_{Su}}\frac{S^*_{Su}}{K_{Su}+S^*_{Su}}, \tag{4.47}$$

$$r^*_{S,Bu} = -\psi^*_{Bu}\frac{\mu_{\max,Bu}}{Y_{Bu}}\frac{S^*_{Bu}}{K_{Bu}+S^*_{Bu}} + g_{Su,Bu}\frac{(1-Y_{Su})}{Y_{Su}}\psi^*_{Su}\mu_{\max,Su}\frac{S^*_{Su}}{K_{Su}+S^*_{Su}}, \tag{4.48}$$

Parameter	Definition	Unit	Value	Ref
$\mu_{max,Su}$	Max specific growth rate for sugar fermenters	d^{-1}	3	[11]
$\mu_{max,Bu}$	Max specific growth rate for butyrate consumers	d^{-1}	1.2	[11]
$\mu_{max,Pro}$	Max specific growth rate for propionate consumers	d^{-1}	0.52	[11]
$\mu_{max,Ac}$	Max specific growth rate for acetoclastic methanogens	d^{-1}	0.4	[11]
$k_{d,Su}$	Decay-inactivation rate for sugar fermenters	d^{-1}	0.02	[11]
$k_{d,Bu}$	Decay-inactivation rate for butyrate consumers	d^{-1}	0.02	[11]
$k_{d,Pro}$	Decay-inactivation rate for propionate consumers	d^{-1}	0.02	[11]
$k_{d,Ac}$	Decay-inactivation rate for acetoclastic methanogens	d^{-1}	0.02	[11]
K_{Su}	Sugar half saturation coeff. sugar fermenters	$gCOD\, m^{-3}$	500	[11]
K_{Bu}	Butyrate half saturation coeff. butyrate consumers	$gCOD\, m^{-3}$	300	[11]
K_{Pro}	Propionate half saturation coeff. propionate consumers	$gCOD\, m^{-3}$	300	[11]
K_{Ac}	Acetate half saturation coeff. acetoclastic methanogens	$gCOD\, m^{-3}$	150	[11]
Y_{Su}	Yield of sugar fermenters on sugar	$--$	0.10	[11]
Y_{Bu}	Yield of butyrate consumers on butyrate	$--$	0.06	[11]
Y_{Pro}	Yield of propionate consumers on propionate	$--$	0.04	[11]
Y_{Ac}	Yield of acetoclastic methanogens on acetate	$--$	0.05	[11]
$g_{Su,Bu}$	Fraction of butyrate from sugar	$--$	0.13	[11]
$g_{Su,Pro}$	Fraction of propionate from sugar	$--$	0.27	[11]
$g_{Su,Ac}$	Fraction of acetate from sugar	$--$	0.41	[11]
$g_{Bu,Ac}$	Fraction of acetate from butyrate	$--$	0.80	[11]
$g_{Pro,Ac}$	Fraction of acetate from propionate	$--$	0.57	[11]
$D_{S,Su}$	Diffusion coefficient of sugar in biofilm	$m^2\, d^{-1}$	$4.63 \cdot 10^{-5}$	[116]
$D_{S,Bu}$	Diffusion coefficient of butyrate in biofilm	$m^2\, d^{-1}$	$6.01 \cdot 10^{-5}$	[116]
$D_{S,Pro}$	Diffusion coefficient of propionate in biofilm	$m^2\, d^{-1}$	$7.33 \cdot 10^{-5}$	[116]
$D_{S,Ac}$	Diffusion coefficient of acetate in biofilm	$m^2\, d^{-1}$	$8.36 \cdot 10^{-5}$	[116]
D_{S,CH_4}	Diffusion coefficient of methane in biofilm	$m^2\, d^{-1}$	$10.3 \cdot 10^{-5}$	[116]
$k_{col,i}$	Max colonization rate of i^{th} planktonic species	d^{-1}	0.001	(a)
$Y_{\psi,i}$	Yield of non-motile microorganisms on motile species	$--$	0.001	(a)
$D_{\psi,i}$	Diffusion coeff of i^{th} planktonic species in biofilm	$m^2\, d^{-1}$	10^{-5}	(a)
$v_{a,Su}$	Attachment velocity of suspended species ψ_{Su}	$m\, d^{-1}$	$3 \cdot 10^{-3}$	(a)
$v_{a,Bu}$	Attachment velocity of suspended species ψ_{Bu}	$m\, d^{-1}$	$3 \cdot 10^{-3}$	(a)
$v_{a,Pro}$	Attachment velocity of suspended species ψ_{Pro}	$m\, d^{-1}$	$3 \cdot 10^{-3}$	(a)
$v_{a,Ac}$	Attachment velocity of suspended species ψ_{Ac}	$m\, d^{-1}$	$150 \cdot 10^{-3}$	(a)
ρ	Biofilm density	$gCOD\, m^{-3}$	120000	(a)
λ	Detachment coefficient	$m^{-1}\, d^{-1}$	10	(a)
V	Reactor volume	m^3	400	(a)
Q	Volumetric flow rate	$m^3\, d^{-1}$	600	(a)
N_G	Number of granules in the reactor	$--$	$2.4 \cdot 10^{10}$	(a)

(a) Assumed

Table 4.2: Kinetic, stoichiometric and operating parameters used for numerical simulations

$$r^*_{S,Pro} = -\psi^*_{Pro}\frac{\mu_{\max,Pro}}{Y_{Pro}}\frac{S^*_{Pro}}{K_{Pro}+S^*_{Pro}} + g_{Su,Pro}\frac{(1-Y_{Su})}{Y_{Su}}\psi^*_{Su}\mu_{\max,Su}\frac{S^*_{Su}}{K_{Su}+S^*_{Su}}, \tag{4.49}$$

$$r^*_{S,Ac} = -\psi^*_{Ac}\frac{\mu_{\max,Ac}}{Y_{Ac}}\frac{S^*_{Ac}}{K_{Ac}+S^*_{Ac}} + g_{Su,Ac}\frac{(1-Y_{Su})}{Y_{Su}}\psi^*_{Su}\mu_{\max,Su}\frac{S^*_{Su}}{K_{Su}+S^*_{Su}} +$$

$$+g_{Bu,Ac}\frac{(1-Y_{Bu})}{Y_{Bu}}\psi^*_{Bu}\mu_{\max,Bu}\frac{S^*_{Bu}}{K_{Bu}+S^*_{Bu}}+g_{Pro,Ac}\frac{(1-Y_{Pro})}{Y_{Pro}}\psi^*_{Pro}\mu_{\max,Pro}\frac{S^*_{Pro}}{K_{Pro}+S^*_{Pro}}, \tag{4.50}$$

$$r^*_{S,CH_4}=\frac{(1-Y_{Ac})}{Y_{Ac}}\psi^*_{Ac}\mu_{\max,Ac}\frac{S^*_{Ac}}{K_{Ac}+S^*_{Ac}}. \tag{4.51}$$

The values used for all stoichiometric and kinetic parameters are reported in Table 4.2.

4.4 Numerical simulations and results

Numerical simulations are performed to describe the formation and evolution of anaerobic granular biofilms, to study the ecological succession occurring in the granule and explore the effects of the main factors on the process. In particular, five numerical studies are carried out: the first numerical study (NS1) describes the *de novo* granulation process in a reactor fed with a wastewater influent rich in sugar; the second study (NS2) investigates the effect of influent composition on granule evolution and ecology; the third study (NS3) explores the role of the attachment phenomenon on the biofilm granule evolution; the fourth study (NS4) investigates the effects of the biomass density on the transport of soluble substrates and, consequently, on the growth and stratification of biomass within the granule; lastly, the fifth study (NS5) simulates the effects of different detachment regimes on granule dimension and dynamics. The values used for the parameters under study are presented in Table 4.3 for all numerical studies.

The initial concentration of the soluble substrates in the bulk liquid $S^*_{j,0}$ is assumed the same as the wastewater influent. No microbial biomass is present in the influent flow ($\psi^{in}_i=0$), while the reactor inoculum is modelled by setting the initial concentration of suspended biomass in the bulk liquid $\psi^*_{i,0}$. In particular, it is considered that the granular

Parameter	**NS1**	**NS2**	**NS3**	**NS4**	**NS5**
	RUN1	RUN2 - RUN4	RUN5 - RUN13	RUN14 - RUN17	RUN18 - RUN25
S_{Su}^{in} $[gCOD\,m^{-3}]$	3500	$varied^1$	3500	3500	3500
S_{Bu}^{in} $[gCOD\,m^{-3}]$	0	$varied^1$	0	0	0
S_{Pro}^{in} $[gCOD\,m^{-3}]$	0	$varied^1$	0	0	0
S_{Ac}^{in} $[gCOD\,m^{-3}]$	0	$varied^1$	0	0	0
$S_{CH_4}^{in}$ $[gCOD\,m^{-3}]$	0	$varied^1$	0	0	0
$\psi_{Su,0}^{*}$ $[gCOD\,m^{-3}]$	300	$varied^1$	300	300	300
$\psi_{Bu,0}^{*}$ $[gCOD\,m^{-3}]$	50	$varied^1$	50	50	50
$\psi_{Pro,0}^{*}$ $[gCOD\,m^{-3}]$	50	$varied^1$	50	50	50
$\psi_{Ac,0}^{*}$ $[gCOD\,m^{-3}]$	100	$varied^1$	100	100	100
$v_{a,Su}$ $[m\,d^{-1}]$	$3 \cdot 10^{-3}$	$3 \cdot 10^{-3}$	$varied^1$	$3 \cdot 10^{-3}$	$3 \cdot 10^{-3}$
$v_{a,Bu}$ $[m\,d^{-1}]$	$3 \cdot 10^{-3}$	$3 \cdot 10^{-3}$	$varied^1$	$3 \cdot 10^{-3}$	$3 \cdot 10^{-3}$
$v_{a,Pro}$ $[m\,d^{-1}]$	$3 \cdot 10^{-3}$	$3 \cdot 10^{-3}$	$varied^1$	$3 \cdot 10^{-3}$	$3 \cdot 10^{-3}$
$v_{a,Ac}$ $[m\,d^{-1}]$	$150 \cdot 10^{-3}$	$150 \cdot 10^{-3}$	$varied^1$	$150 \cdot 10^{-3}$	$150 \cdot 10^{-3}$
ρ $[gCOD\,m^{-3}]$	120000	120000	120000	$varied^1$	120000
λ $[m^{-1}\,d^{-1}]$	10	10	10	10	$varied^1$
T $[d]$	300	300	300	300	300

[1] The values used are reported in the text

Table 4.3: Initial and boundary conditions and operating parameters adopted in numerical studies

reactor is inoculated with the sludge coming from a conventional AD reactor and fed with the same wastewater influent. Therefore, the initial concentrations of suspended species in the bulk liquid (representative of the inoculum) are derived from numerical results of an ADM1-based model.

In granular reactors, intense hydrodynamic conditions shall improve the aggregation of suspended particles and the formation of granules. Consequently, for all the simulations reported in this Chapter, the reactor volume V and the influent flow rate Q are assumed constant and equal to $400\ m^3$ and $600\ m^3 d^{-1}$, respectively, leading to high hydrodynamic velocities and a very low constant hydraulic retention time (HRT = $0.667\ d$). Such value is within the range of HRT values typical of granular biofilm systems [68]. Moreover, the organic loading rate (OLR), defined as the amount of daily organic matter treated per unit reactor volume, is set equal to $5.25\ kg\ m^{-3}\ d^{-1}$. The number of granules N_G is calculated in order to have a reactor filled by biofilm granules for approximately 25% of volume once the granules have reached the steady-state dimension.

In accordance with [132], diffusivity of soluble substrates in biofilm is assumed to be 80% of diffusivity in water. The diffusion coefficients in water for all soluble substrates are taken from [116], see Table 4.2.

The model has been integrated numerically by developing an original code in MatLab platform. The method of characteristics has been used to track the biofilm expansion, while the method of lines has been adopted for the diffusion-reaction PDEs. A first-order approximation has been used for the reactor balance equations of ψ_i^* and S_j^*. The time to compute the values of the unknown variables is in the order of hours. Simulations are run for a set target simulation time T, fixed to $300\ d$. This time interval guarantees to achieve the steady-state configuration for all model variables: concentration of soluble substrates $S_j^*(t)$ and suspended biomasses $\psi_i^*(t)$ in the bulk liquid; granule dimension $R(t)$; sessile biomass fractions $f_i(r,t)$, concentration of soluble substrates $S_j(r,t)$ and planktonic species $\psi_i(r,t)$ within the biofilm.

4.4.1 NS1 - Process of granular anaerobic digestion

The first numerical study (NS1) describes the *de novo* granulation process occurring in a granular reactor fed with an organic load of sugar: $S_{Su}^{in} = 3500\ g\ m^{-3}$, $S_{Bu}^{in} = S_{Pro}^{in} = S_{Ac}^{in} = S_{CH_4}^{in} = 0$ (RUN1). The initial concentration of the suspended biomasses (reactor inoculum) is derived from an ADM1-based model following the procedure introduced above: $\psi_{Su,0}^* = 300\ g\ m^{-3}$, $\psi_{Bu,0}^* = \psi_{Pro,0}^* = 50\ g\ m^{-3}$, $\psi_{Ac,0}^* = 100\ g\ m^{-3}$.

Numerical results are summarized in Figs. 4.2-4.5. In Fig. 4.2 the evolution of the granule radius $R(t)$ over time is reported. As can be seen, a vanishing initial value is assigned to $R(t)$ at $t = 0$ ($R(0) = 0$). During the first days, the granulation process has its maximum intensity and the granule dimension increases. The variation of $R(t)$ is almost exhausted during the first 70-100 days, after which it reaches a steady-state value of about $1\ mm$.

In Fig. 4.3 the distribution of sessile species within the granule is shown at different

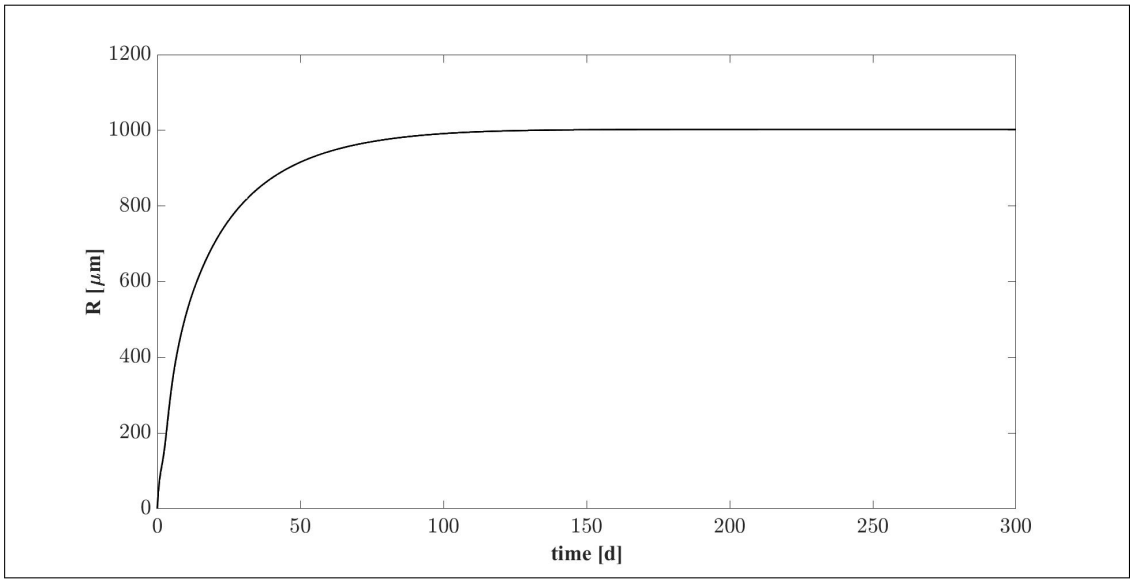

Figure 4.2: NS1 - Biofilm radius evolution over time. Wastewater influent composition: $S_{Su}^{in} = 3500\ g\ m^{-3}$ (Sugar), $S_{Bu}^{in} = 0$ (Butyrate), $S_{Pro}^{in} = 0$ (Propionate), $S_{Ac}^{in} = 0$ (Acetate), $S_{CH_4}^{in} = 0$ (Methane).

times. After $5\ d$ the granule has a radius of about $0.3\ mm$ and is constituted mostly by acidogens (blue) which are favoured by the high concentration of sugar initially present in the bulk liquid. However, the granule core is also composed of methanogens (red) which have high propensity to attach due to their filamentous structures and aggregation properties. At $T = 15\ d$, the consumption of sugar and the production of volatile fatty acids (VFAs) in large amount by acidogenesis affects the biomass distribution: the methanogenic core grows while the acidogens occupy the outer layer of the granule, and the acetogens (green) and inert (black) fractions starts to be visible. For later times (40-$70\ d$), the radius almost reaches the steady-state value, a significant amount of inert material accumulates especially in the innermost part of the domain, homogeneous fractions of methanogens and acetogens are found throughout the granule except the outermost part, where a thin layer of acidogens is established.

Fig. 4.4 presents the mass trend of each microbial species within the granule over time. This result confirms the microbial succession described above. The biofilm is initially constituted predominantly by acidogens m_{Su} (blue) and methanogens m_{Ac} (red). Their mass within the biofilm achieves a maximum and then decreases to a steady-state

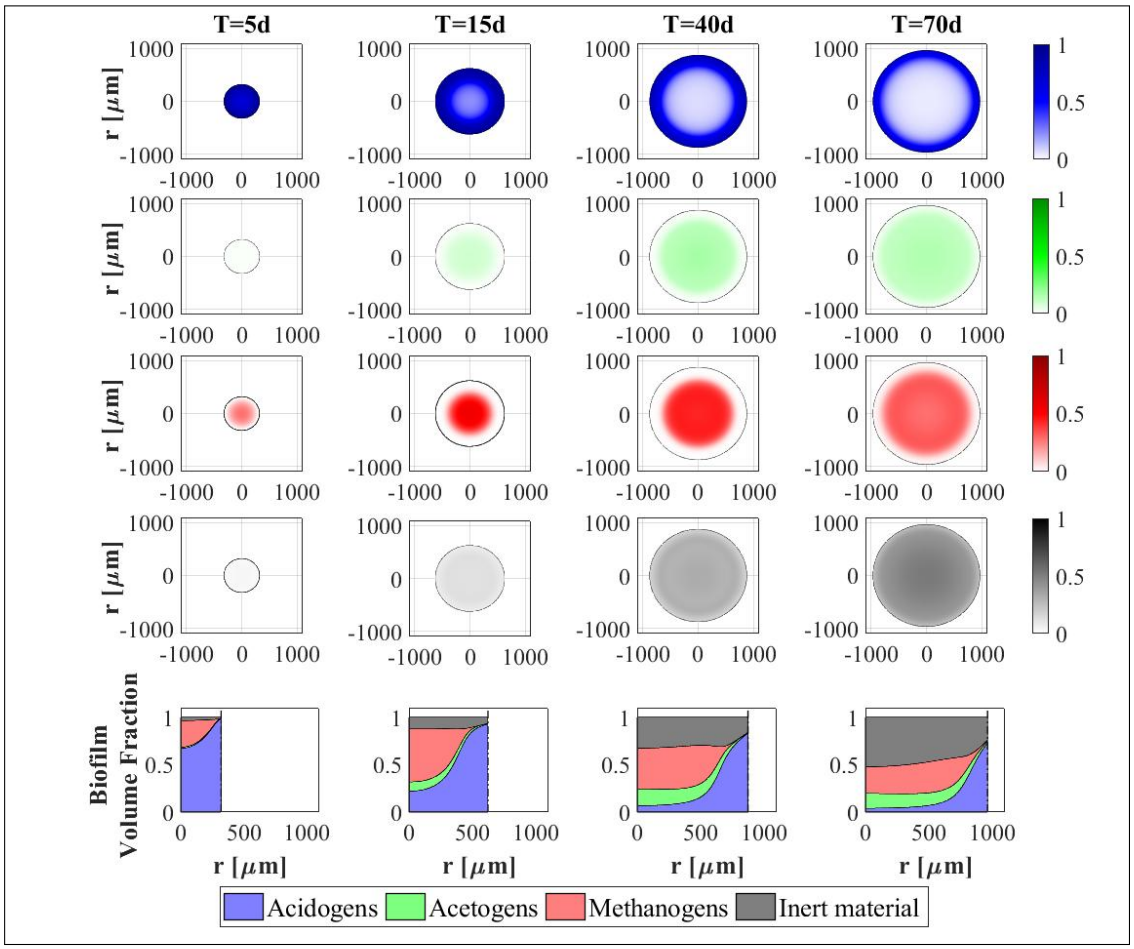

Figure 4.3: NS1 - Microbial species distribution in the diametrical section and across the radius of the granule, at $T = 5d$, $T = 15d$, $T = 40d$ and $T = 70d$. Wastewater influent composition: $S_{Su}^{in} = 3500\ g\ m^{-3}$ (Sugar), $S_{Bu}^{in} = 0$ (Butyrate), $S_{Pro}^{in} = 0$ (Propionate), $S_{Ac}^{in} = 0$ (Acetate), $S_{CH_4}^{in} = 0$ (Methane).

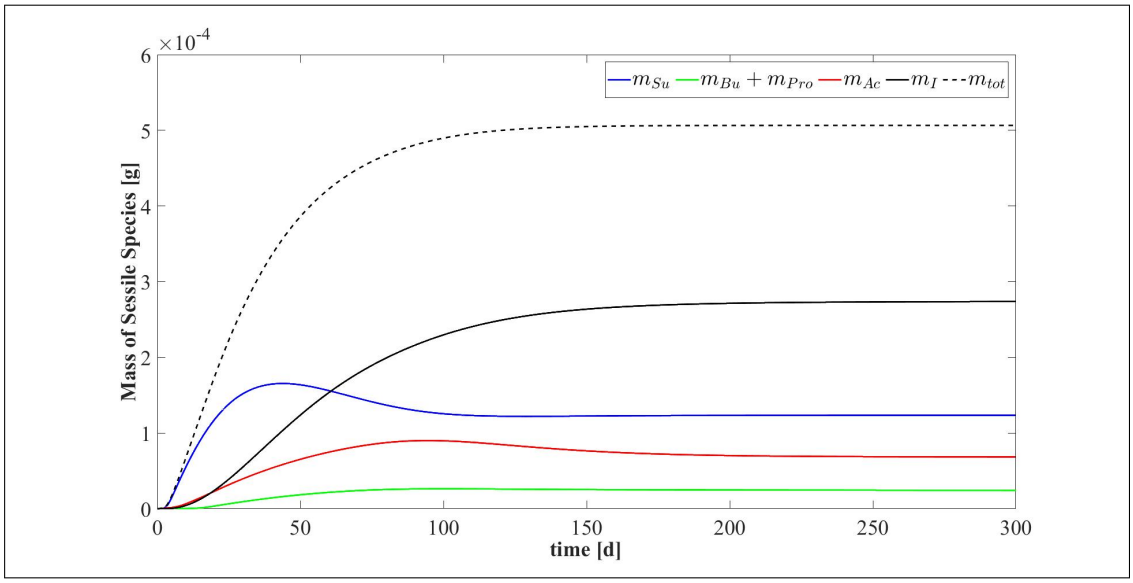

Figure 4.4: NS1 - Evolution of mass of sessile species within the granule. m_{Su}: mass of sugar fermenters, m_{Bu}: mass of butyrate consumers, m_{Pro}: mass of propionate consumers, m_{Ac}: mass of acetoclastic methanogens, m_{tot}: total sessile mass. Wastewater influent composition: $S_{Su}^{in} = 3500\ g\ m^{-3}$ (Sugar), $S_{Bu}^{in} = 0$ (Butyrate), $S_{Pro}^{in} = 0$ (Propionate), $S_{Ac}^{in} = 0$ (Acetate), $S_{CH_4}^{in} = 0$ (Methane).

value when the substrates required by their metabolism (sugar and acetate, respectively) are limited and the decay process prevails. The growth process of acetogens $m_{Bu}+m_{Pro}$ and the accumulation of inert m_I are slower and take place in a longer time. However, all microbial species exhibit steady-state values 150-170 days after the granule genesis. Furthermore, the total microbial mass m_{tot} (dashed black line) follows the trend of the radius reported in Fig. 4.2. Indeed, assuming a constant density ρ, the variation of mass within the granule is related to the variation of volume.

Lastly, the trends of soluble substrates and suspended biomass within the bulk liquid are shown in Fig. 4.5. In the initial phase, the biofilm granules are small, and the consumption and production of soluble substrates are governed by suspended biomass. In particular, suspended sugar fermenters ψ_{Su}^* (blue in Fig. 4.5-bottom) degrade sugar S_{Su}^* (blue in Fig. 4.5-top) and produce VFAs: butyrate S_{Bu}^* (green in Fig. 4.5-top), propionate S_{Pro}^* (magenta in Fig. 4.5-top) and acetate S_{Ac}^* (red in Fig. 4.5-top). Meanwhile, the concentration of all suspended biomasses within the bulk liquid is reduced due to

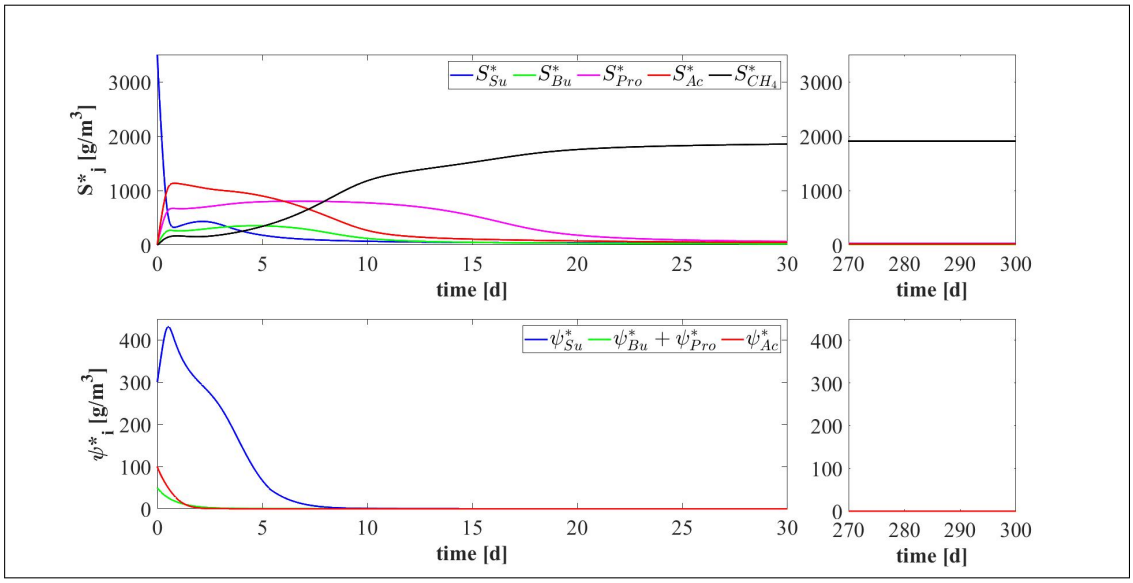

Figure 4.5: NS1 - Evolution of soluble substrates (top) and suspended biomass (bottom) concentrations within the bulk liquid. S^*_{Su}: Sugar, S^*_{Bu}: Butyrate, S^*_{Pro}: Propionate, S^*_{Ac}: Acetate, $S^*_{CH_4}$: Methane, ψ^*_{Su}: Sugar fermenters, ψ^*_{Bu}: Butyrate consumers, ψ^*_{Pro}: Propionate consumers, ψ^*_{Ac}: Acetoclastic methanogens. Wastewater influent composition: $S^{in}_{Su} = 3500\ g\ m^{-3}$ (Sugar), $S^{in}_{Bu} = 0$ (Butyrate), $S^{in}_{Pro} = 0$ (Propionate), $S^{in}_{Ac} = 0$ (Acetate), $S^{in}_{CH_4} = 0$ (Methane).

two distinct phenomena: part is converted in sessile biomass during the granulation process and part is rapidly washed out due to unfavourable hydrodynamic conditions (low HRT). For these reasons, no microbial species in suspended form is present within the reactor after 5-7 days. After the washout of the suspended biomass, the substrates trend is influenced exclusively by the sessile metabolic activity: the residual sugar S^*_{Su} and VFAs (S^*_{Bu}, S^*_{Pro} and S^*_{Ac}) are consumed with different velocities according to the consumption rate of the corresponding sessile microbial species and significant amount of methane $S^*_{CH_4}$ (black in Fig. 4.5-top) is produced. After 30 days substrates concentrations within the bulk liquid reach a steady-state value. High concentrations of methane (end product of the AD process) and negligible concentrations of sugar and VFAs are found inside the reactor and in the effluent.

4.4.2 NS2 - Effects of wastewater influent composition

The results presented in the previous section describe the dynamic evolution and the steady-state configuration of anaerobic granular biofilms growing in a sugar-fed reactor. However, the composition of the wastewater influent affects the granulation process and regulates the ecological succession and the growth of the individual species. Since the wastewater influents treated in anaerobic granular systems originate from various applications and present variable compositions of the organic load, it is interesting to compare the model results for different types of wastewater influent. In particular, in this study (NS2) different influent compositions and reactor inocula are set as model input: (RUN2: $S_{Su}^{in} = 2000\ g\ m^{-3}$, $S_{Bu}^{in} = S_{Pro}^{in} = S_{Ac}^{in} = 500\ g\ m^{-3}$, $S_{CH_4}^{in} = 0$, $\psi_{Su,0}^{*} = 170\ g\ m^{-3}$, $\psi_{Bu,0}^{*} = \psi_{Pro,0}^{*} = 40\ g\ m^{-3}$, $\psi_{Ac,0}^{*} = 100\ g\ m^{-3}$; RUN3: $S_{Su}^{in} = S_{Bu}^{in} = S_{Pro}^{in} = S_{Ac}^{in} = 880\ g\ m^{-3}$, $S_{CH_4}^{in} = 0$, $\psi_{Su,0}^{*} = 70\ g\ m^{-3}$, $\psi_{Bu,0}^{*} = 50\ g\ m^{-3}, \psi_{Pro,0}^{*} = 40\ g\ m^{-3}$, $\psi_{Ac,0}^{*} = 110\ g\ m^{-3}$; RUN4: $S_{Su}^{in} = S_{CH_4}^{in} = 0$, $S_{Bu}^{in} = S_{Pro}^{in} = S_{Ac}^{in} = 1170\ g\ m^{-3}$, $\psi_{Su,0}^{*} = 0$, $\psi_{Bu,0}^{*} = 60\ g\ m^{-3}, \psi_{Pro,0}^{*} = 40\ g\ m^{-3}$, $\psi_{Ac,0}^{*} = 110\ g\ m^{-3}$). These cases have been compared with the case of reactor fed with only sugar (RUN1). The results are summarized in Figs. 4.6-4.10.

Fig. 4.6 shows the trend of the granule radius $R(t)$ over time. In the four cases, granules of different sizes are formed. These differences are related to the sessile biomass growth which varies according to the substrates present in the wastewater influent. Specifically, sessile growth is affected by anabolic and catabolic pathways of the microbial metabolism: the yield of acidogens on sugar Y_{Su} is higher than the yields of the other species, thus, the amount of acidogenic biomass grown per unit of substrate consumed is higher than the other species. Therefore, the steady-state dimension of the granule increases with increasing sugar concentration in the influent S_{Su}^{in}. For $S_{Su}^{in} = 0$ (RUN4), the granule achieves the smallest dimension.

The distribution of sessile biomass within the granule in the four cases is reported in Fig. 4.7, at $T = 70\ d$. As the sugar concentration in the influent S_{Su}^{in} increases, the

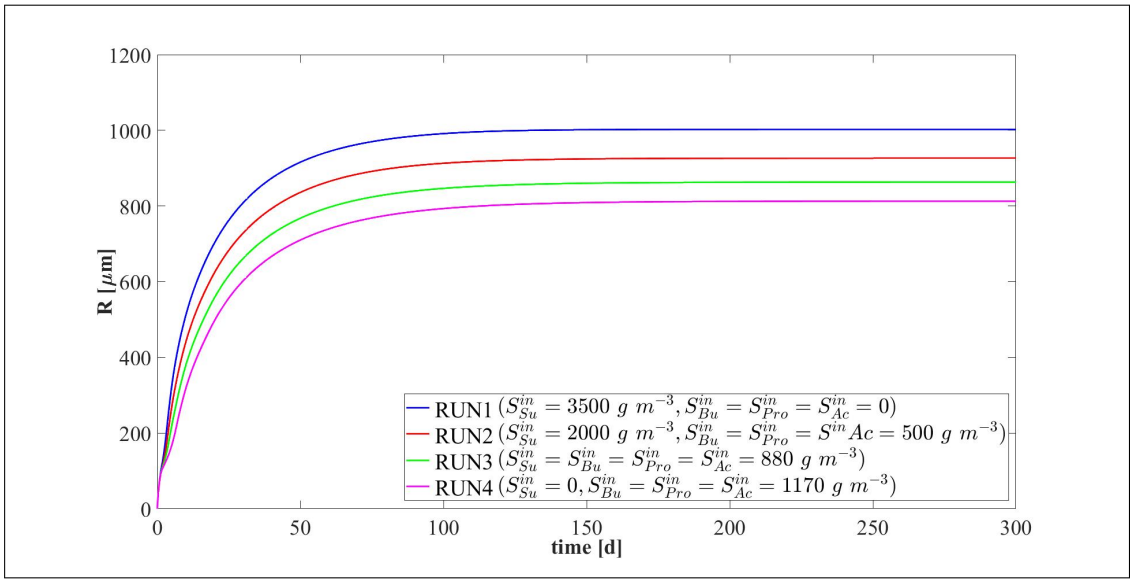

Figure 4.6: NS2 - Biofilm radius evolution over time for different wastewater influent compositions. S_{Su}^{in}: Sugar, S_{Bu}^{in}: Butyrate, S_{Pro}^{in}: Propionate, S_{Ac}^{in}: Acetate, $S_{CH_4}^{in}$: Methane.

fraction of acidogens f_{Su} (blue) increases, especially in the outer part of the granule, where there is maximum availability of substrate. When the sugar concentration S_{Su}^{in} decreases from $3500\ g\ m^{-3}$ (RUN1) to $880\ g\ m^{-3}$ (RUN3), the acidogenic fraction present in the external part of the biofilm significantly reduces. Obviously, no acidogens are found within the granule when sugar is absent in the wastewater influent (RUN4). In addition, as the concentration of butyrate S_{Bu}^{in}, propionate S_{Pro}^{in} and acetate S_{Ac}^{in} in the influent increases going from RUN1 to RUN4, an increase in the fractions of acetogens $f_{Bu} + f_{Pro}$ (green) and methanogens f_{Ac} (red) is observed.

The relative abundance of sessile microbial species is reported for different simulation times in Fig. 4.8. When sugar is present in the influent (RUN1, RUN2, RUN3), the initial phase of the granulation is governed by acidogens (which have a higher growth rate) and methanogens (which have high attachment properties). The acidogenic fraction (blue) reaches a maximum after $7\ d$ and then decreases when the availability of sugar in the bulk liquid reduces. When sugar is not present in the influent (RUN4), the granulation process is dominated by methanogens (red) and acetogens in small amounts (green). In all four cases, the maximum fraction of methanogens is observed at the be-

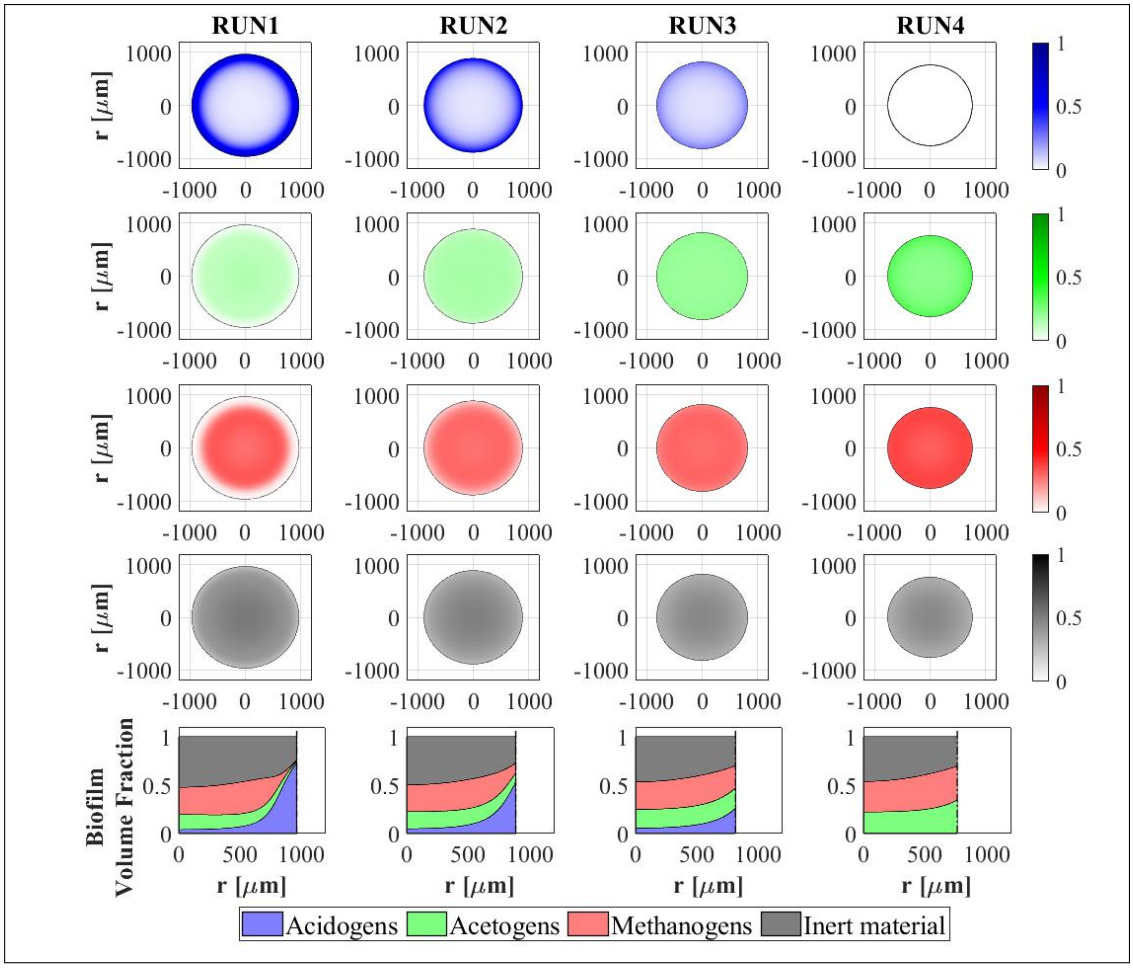

Figure 4.7: NS2 - Microbial species distribution in the diametrical section and across the radius of the granule at $T = 70d$, for different wastewater influent compositions. RUN1: $S_{Su}^{in} = 3500\ g\ m^{-3}$, $S_{Bu}^{in} = S_{Pro}^{in} = S_{Ac}^{in} = S_{CH_4}^{in} = 0$; RUN2: $S_{Su}^{in} = 2000\ g\ m^{-3}$, $S_{Bu}^{in} = S_{Pro}^{in} = S_{Ac}^{in} = 500\ g\ m^{-3}$, $S_{CH_4}^{in} = 0$; RUN3: $S_{Su}^{in} = S_{Bu}^{in} = S_{Pro}^{in} = S_{Ac}^{in} = 880\ g\ m^{-3}$, $S_{CH_4}^{in} = 0$; RUN4: $S_{Su}^{in} = 0$, $S_{Bu}^{in} = S_{Pro}^{in} = S_{Ac}^{in} = 1170\ g\ m^{-3}$, $S_{CH_4}^{in} = 0$. S_{Su}^{in}: Sugar, S_{Bu}^{in}: Butyrate, S_{Pro}^{in}: Propionate, S_{Ac}^{in}: Acetate, $S_{CH_4}^{in}$: Methane.

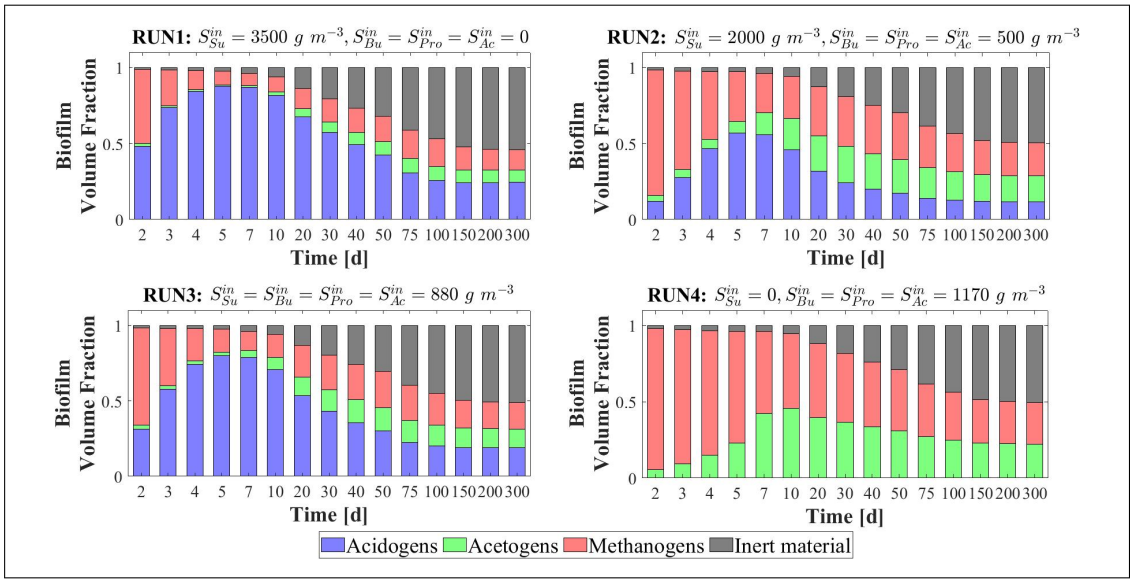

Figure 4.8: NS2 - Relative abundances of microbial species within the granule at several instant time under different wastewater influent compositions. S_{Su}^{in}: Sugar, S_{Bu}^{in}: Butyrate, S_{Pro}^{in}: Propionate, S_{Ac}^{in}: Acetate, $S_{CH_4}^{in}$: Methane.

ginning of the process due to their granulation properties. Then, the methanogenic fraction reduces due to the decay process and the competition with acidogens and acetogens. Furthermore, the acetogenic fraction is negligible in all cases during the initial phase of the granulation and grows when other microbial species become less competitive, and sugar is converted to butyrate and propionate. The microbial relative abundances related to the steady-state value confirm the results introduced in Fig. 4.7: the fraction of acidogens increases with the increase of the sugar in the influent; the fractions of methanogens and acetogens increase with increasing VFAs in the influent; in all cases, inactive biomass (black) represents approximately 50 % of the total sessile biomass within the granule.

The model results related to the bulk liquid are summarized in Fig. 4.9 and Fig. 4.10, which show how the concentration of soluble substrates and suspended biomass changes over time. As reported in Fig. 4.9, the composition of the wastewater influent affects the trend of the substrates mostly in the initial phase. In all cases, the AD process is completed in about 30 days: sugar (blue), butyrate (green), propionate (magenta) and acetate (red) are totally consumed and the concentration of methane (black) achieves a

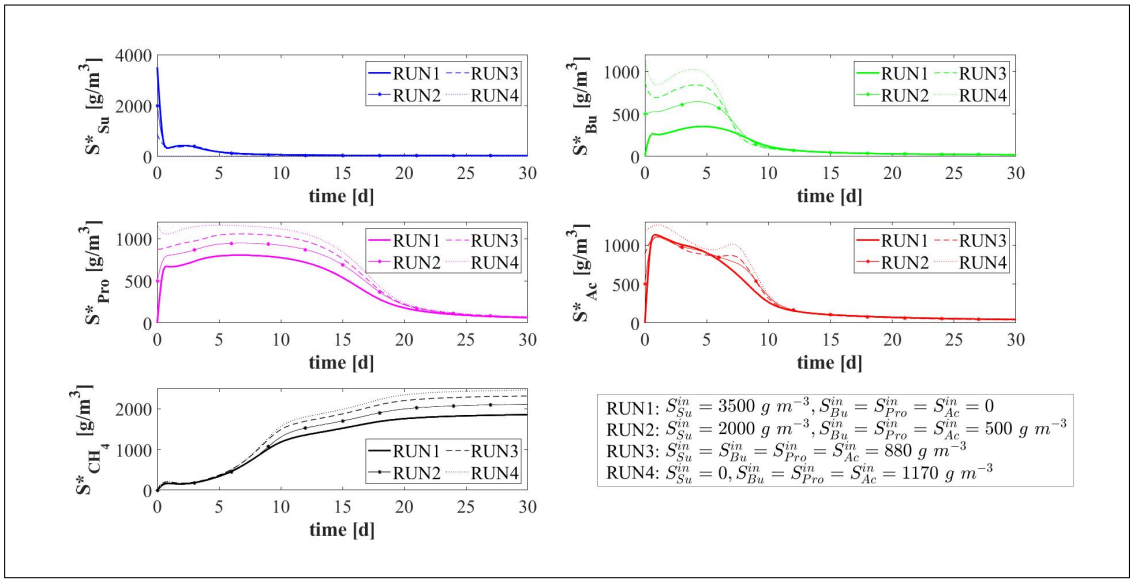

Figure 4.9: NS2 - Evolution of soluble substrates concentrations within the bulk liquid for different wastewater influent compositions. S^*_{Su}: Sugar, S^*_{Bu}: Butyrate, S^*_{Pro}: Propionate, S^*_{Ac}: Acetate, $S^*_{CH_4}$: Methane.

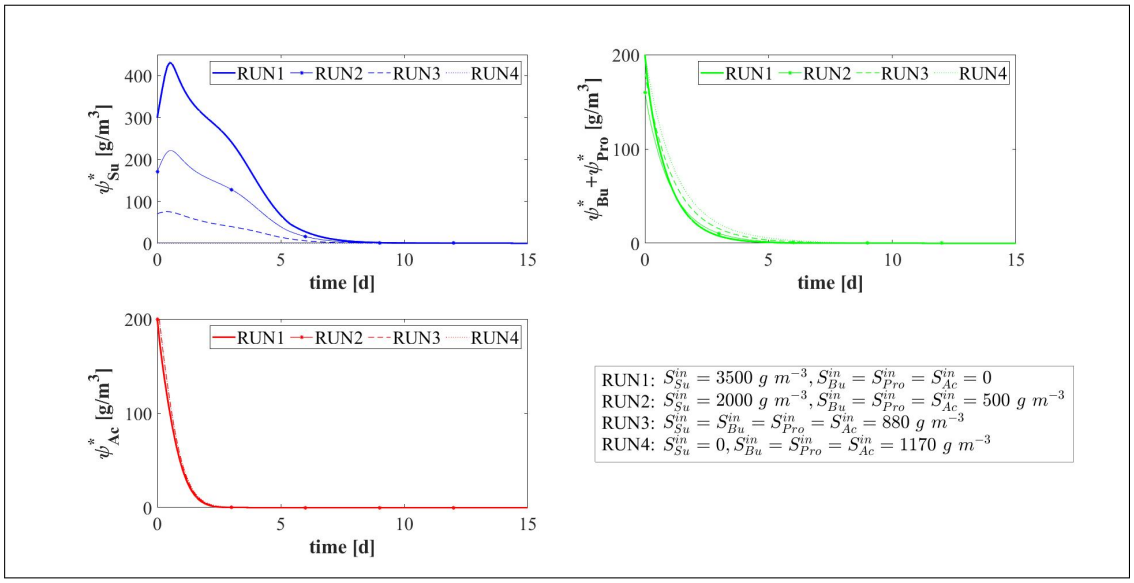

Figure 4.10: NS2 - Evolution of suspended biomass concentrations within the bulk liquid for different wastewater influent compositions. ψ^*_{Su}: Sugar fermenters, ψ^*_{Bu}: Butyrate consumers, ψ^*_{Pro}: Propionate consumers, ψ^*_{Ac}: Acetoclastic methanogens.

steady-state value. Notably, different productions of methane are observed as the composition of the influent changes. Concerning the concentration of suspended biomass shown in Fig. 4.10, the concentration of acidogens (blue) is affected by the composition of the influent in the initial phase of the granulation process (0-7 days). Conversely, the concentration of acetogens (green) and methanogens (red) in suspended form have low growth rates and are washed out due to the dilution phenomenon even when significant concentrations of VFAs are present in the influent.

4.4.3 NS3 - Effects of attachment properties

The characteristics of the microbial community play a fundamental role in the anaerobic granulation process. In particular, such process is highly affected by the attachment properties of the suspended biomass present in the reactor. The attachment properties of microbial cells depend on several factors such as hydrodynamic conditions inside the reactor, cell dimension, cell structure, ability to produce EPS and ability to use quorum sensing strategies. In this regard, several studies report that quorum sensing regulates the formation of filamentous cells frequently involved in anaerobic granular reactors, such as *Methanosaeta* [141, 65]. As reported in [66], some quorum sensing molecule-promoted filamentous cells of *Methanosaeta harundinacea* enhance the reactor performance, improve the granulation, and immobilize other synergistically functioning bacterial groups.

In the management of full-scale reactors, several strategies are pursued to reduce the duration of time of granule formation and improve the efficiency of the wastewater treatment process. For example, the direct addition of the quorum sensing molecule acyl homoserine lactone (AHL) during granule formation might remarkably improve the granulation process in anaerobic granular reactors [66, 141, 33]. Furthermore, bioaugmentation is regarded as a promising method to improve the granulation velocity and reduce the time required for the start-up of full-scale plants [54, 85, 58]. It consists in

the addition of selected microbial cultures with high self-aggregation ability within the reactor [10]. Overall, such strategies positively alter the attachment properties of the suspended microbial community.

In this framework, an interesting and original numerical study (NS3) is conducted to investigate the effects of biomass attachment properties on the process of granule formation. For this purpose, nine simulations (RUN5 - RUN13) are carried out with different attachment velocities $v_{a,i}$. The nine values of $v_{a,i}$ used are chosen by increasing and reducing the default values (presented in Table 4.2) through different multiplication factors $(0.05, 0.1, 0.25, 0.5, 1, 2, 3, 4, 5)$. The concentration of soluble substrates in the wastewater influent S_j^{in} and the initial concentration of suspended biomasses within the reactor $\psi_{i,0}^*$ set for this numerical study are the same used in NS1 and are reported in Table 4.3.

The results of this study are reported in Figs. 4.11-4.15. The evolution of the granule radius $R(t)$ over time is shown in Fig. 4.11. From Fig. 4.11 (right) it is clear that different attachment velocities $v_{a,i}$ lead to different growth rates of the granule in the initial phase of the process: when the inoculated microbial community is more inclined to grow in sessile form, the granulation process occurs faster and the granule reaches earlier the steady-state dimension. However, such steady-state dimension is not dependent on the attachment velocity. Indeed, the profiles of $R(t)$ for different $v_{a,i}$ get closer over time and reach the same steady-state value.

Fig. 4.12 and Fig. 4.13 report the mass and the relative abundance of the different sessile microbial species within the granule, respectively. Again, relevant differences concern the initial phase ($T = 10$-$20\ d$), when the total sessile mass, proportional to the granule dimension, is higher in the case of more intense attachment process. However, after long times both the total sessile mass and the relative abundance of individual microbial species within the granule are no longer affected by $v_{a,i}$ and all simulations achieve the same steady-state configuration.

Other interesting results refer to the effects that the attachment process has on the

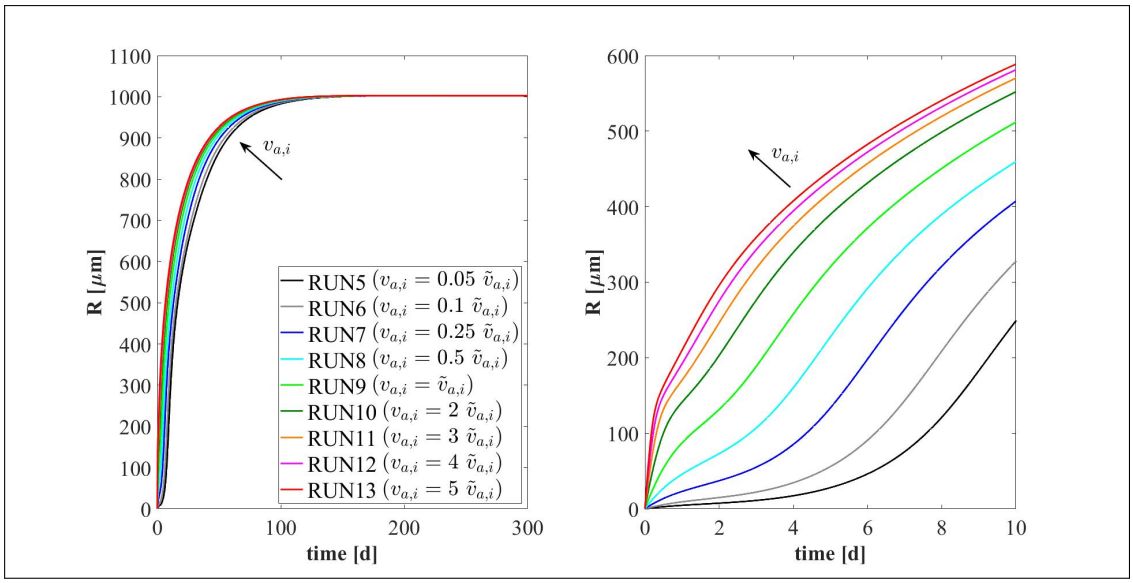

Figure 4.11: NS3 - Biofilm radius evolution over time for different attachment velocities $v_{a,i}$ (left), with a focus on the first 10 days (right). $\tilde{v}_{a,i}$: value of attachment velocity of the i^{th} suspended species set in RUN1. Wastewater influent composition: $S_{Su}^{in} = 3500\ g\ m^{-3}$ (Sugar), $S_{Bu}^{in} = 0$ (Butyrate), $S_{Pro}^{in} = 0$ (Propionate), $S_{Ac}^{in} = 0$ (Acetate), $S_{CH_4}^{in} = 0$ (Methane).

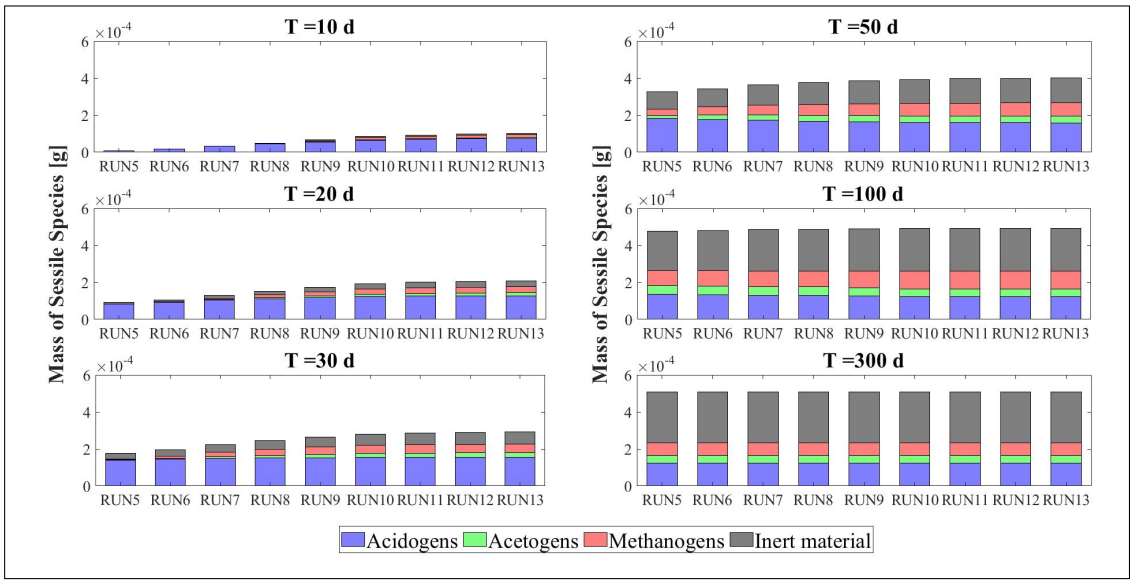

Figure 4.12: NS3 - Mass of microbial species within the granule at $T = 10d$, $T = 20d$, $T = 30d$, $T = 50d$, $T = 100d$ and $T = 300d$ under different attachment velocities $v_{a,i}$. RUN5: $v_{a,i} = 0.05\ \tilde{v}_{a,i}$, RUN6: $v_{a,i} = 0.1\ \tilde{v}_{a,i}$, RUN7: $v_{a,i} = 0.25\ \tilde{v}_{a,i}$, RUN8: $v_{a,i} = 0.5\ \tilde{v}_{a,i}$, RUN9: $v_{a,i} = \tilde{v}_{a,i}$, RUN10: $v_{a,i} = 2\ \tilde{v}_{a,i}$, RUN11: $v_{a,i} = 3\ \tilde{v}_{a,i}$, RUN12: $v_{a,i} = 4\ \tilde{v}_{a,i}$, RUN13: $v_{a,i} = 5\ \tilde{v}_{a,i}$. $\tilde{v}_{a,i}$: value of attachment velocity of the i^{th} suspended species set in RUN1. Wastewater influent composition: $S_{Su}^{in} = 3500\ g\ m^{-3}$ (Sugar), $S_{Bu}^{in} = 0$ (Butyrate), $S_{Pro}^{in} = 0$ (Propionate), $S_{Ac}^{in} = 0$ (Acetate), $S_{CH_4}^{in} = 0$ (Methane).

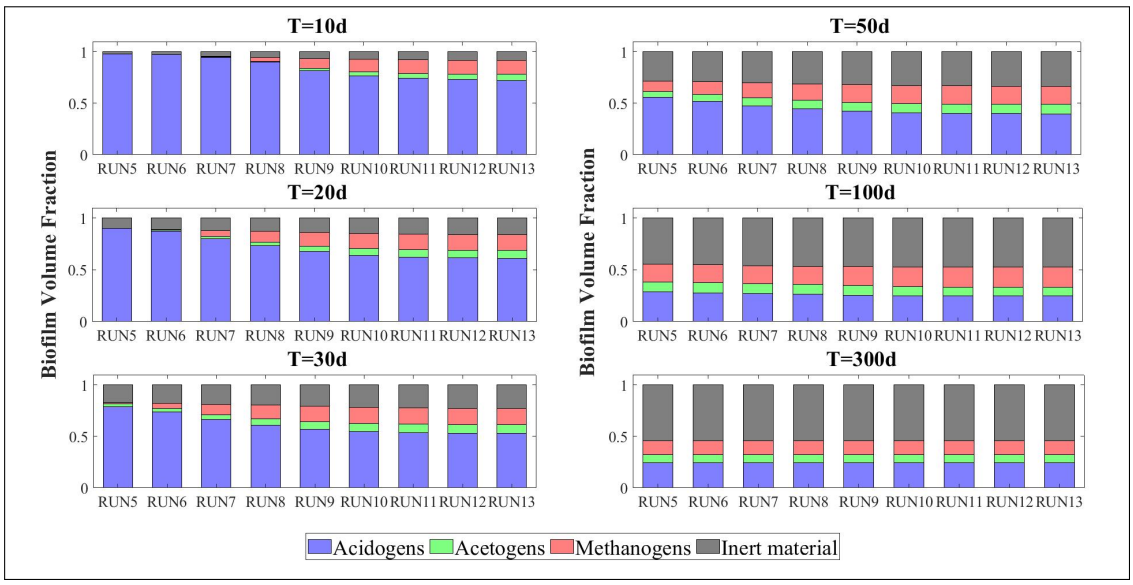

Figure 4.13: NS3 - Relative abundances of microbial species within the granule at $T = 10d$, $T = 20d$, $T = 30d$, $T = 50d$, $T = 100d$ and $T = 300d$ under different attachment velocities $v_{a,i}$. RUN5: $v_{a,i} = 0.05\ \tilde{v}_{a,i}$, RUN6: $v_{a,i} = 0.1\ \tilde{v}_{a,i}$, RUN7: $v_{a,i} = 0.25\ \tilde{v}_{a,i}$, RUN8: $v_{a,i} = 0.5\ \tilde{v}_{a,i}$, RUN9: $v_{a,i} = \tilde{v}_{a,i}$, RUN10: $v_{a,i} = 2\ \tilde{v}_{a,i}$, RUN11: $v_{a,i} = 3\ \tilde{v}_{a,i}$, RUN12: $v_{a,i} = 4\ \tilde{v}_{a,i}$, RUN13: $v_{a,i} = 5\ \tilde{v}_{a,i}$. $\tilde{v}_{a,i}$: value of attachment velocity of the i^{th} suspended species set in RUN1. Wastewater influent composition: $S_{Su}^{in} = 3500\ g\ m^{-3}$ (Sugar), $S_{Bu}^{in} = 0$ (Butyrate), $S_{Pro}^{in} = 0$ (Propionate), $S_{Ac}^{in} = 0$ (Acetate), $S_{CH_4}^{in} = 0$ (Methane).

suspended biomass ψ_i^* (Fig. 4.14) and soluble substrates S_j^* (Fig. 4.15) within the reactor. The concentration profiles of the suspended acetogens $\psi_{Bu}^* + \psi_{Pro}^*$ (green) and methanogens ψ_{Ac}^* (red) in the bulk liquid shown in Fig. 4.14 are not very sensitive to the variation of $v_{a,i}$. Indeed, the reduction of the suspended biomass ψ_i^* depends on two phenomena: attachment and dilution. The reduction of $\psi_{Bu}^*, \psi_{Pro}^*$ and ψ_{Ac}^* occurs in the initial phase of the process, when the granules are small and the attachment flux of suspended biomass (proportional to the granule surface $A(t)$) has limited effects on the properties of the bulk liquid. On the other hand, the dilution process is prominent: the hydrodynamic conditions (high flow rate, low HRT) and the slow metabolic growth (due to low maximum growth rates and substrate unavailability) lead to the washout of suspended acetogens and methanogens. Such dilution process is not affected by microbial attachment properties and therefore leads to similar profiles by varying $v_{a,i}$. Conversely, the suspended acidogens ψ_{Su}^* (blue) have higher growth rates and optimal conditions to grow (sugar-rich influent), hence, they populate the reactor for longer times and decrease mainly due to the granulation process, which is strongly influenced by $v_{a,i}$. Consequently, different values of $v_{a,i}$ correspond to different profiles of suspended acidogens ψ_{Su}^*: the higher $v_{a,i}$, the faster the reduction of the concentration ψ_{Su}^* in the bulk liquid.

Fig. 4.15 shows the trend of soluble substrates within the reactor. As just mentioned, in the first few days the granules have small dimensions and the consumption and production of soluble substrates mainly depend on the metabolic activity of the suspended biomass. Consequently, in the initial phase the trends of soluble substrates are not affected by attachment conditions. For later times, the granule size and the amount of sessile biomass within the reactor increase and the trend of the substrates becomes more sensitive to $v_{a,i}$: for small values of $v_{a,i}$ the concentrations of soluble substrates reach steady-state conditions in 40-50 days while for high values of $v_{a,i}$ they require half of the time to reach a steady-state configuration.

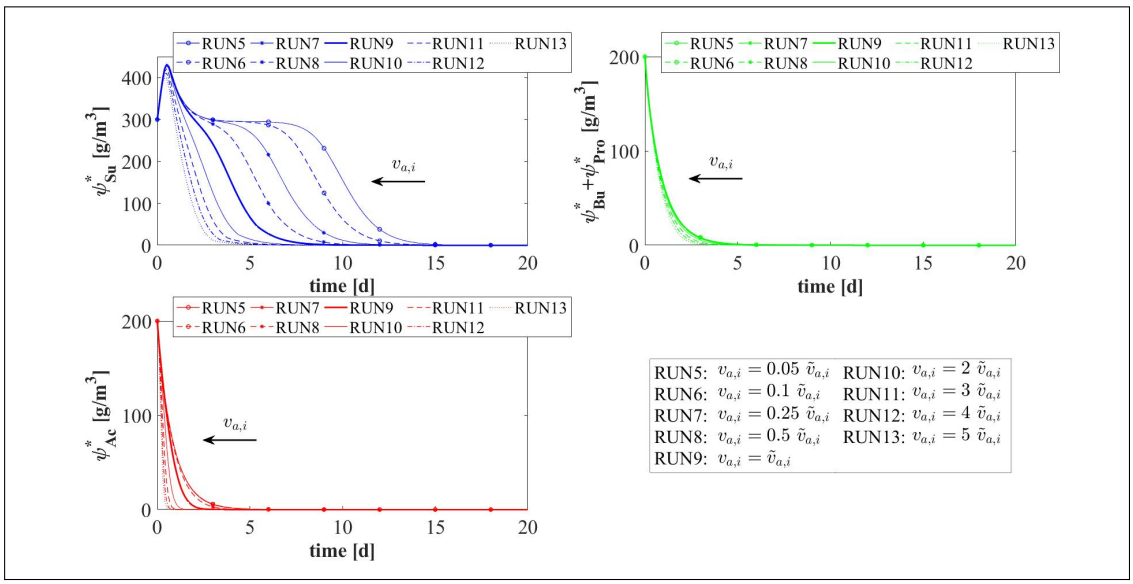

Figure 4.14: NS3 - Evolution of suspended biomass concentrations within the bulk liquid for different attachment velocities $v_{a,i}$. ψ^*_{Su}: Sugar fermenters, ψ^*_{Bu}: Butyrate consumers, ψ^*_{Pro}: Propionate consumers, ψ^*_{Ac}: Acetoclastic methanogens. $\tilde{v}_{a,i}$: value of attachment velocity of the i^{th} suspended species set in RUN1. Wastewater influent composition: $S^{in}_{Su} = 3500\ g\ m^{-3}$ (Sugar), $S^{in}_{Bu} = 0$ (Butyrate), $S^{in}_{Pro} = 0$ (Propionate), $S^{in}_{Ac} = 0$ (Acetate), $S^{in}_{CH_4} = 0$ (Methane).

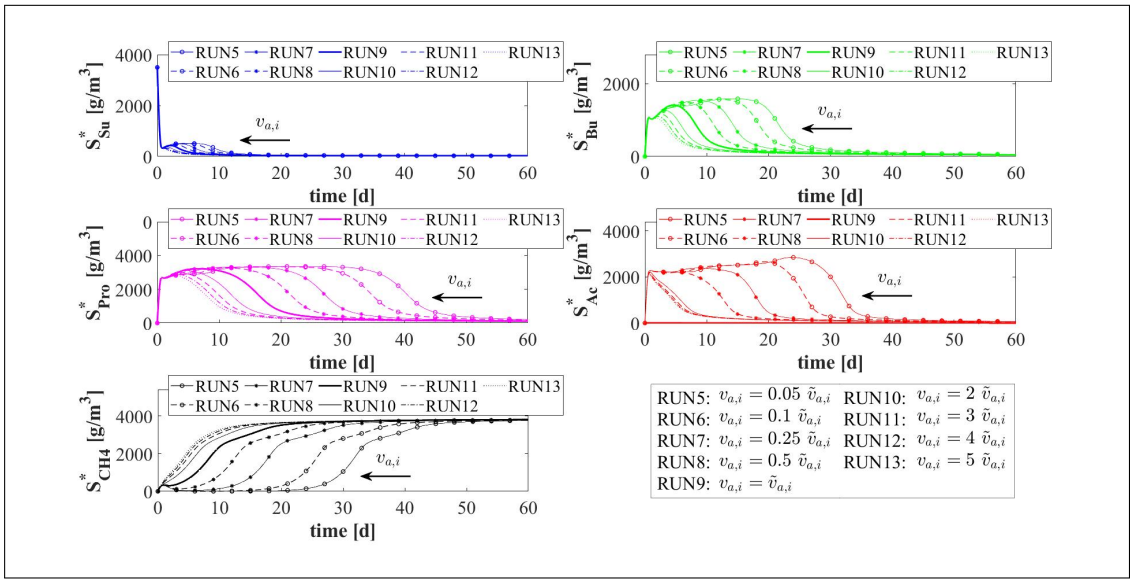

Figure 4.15: NS3 - Evolution of soluble substrates concentrations within the bulk liquid for different attachment velocities $v_{a,i}$. S^*_{Su}: Sugar, S^*_{Bu}: Butyrate, S^*_{Pro}: Propionate, S^*_{Ac}: Acetate, $S^*_{CH_4}$: Methane. $\tilde{v}_{a,i}$: value of attachment velocity of the i^{th} suspended species set in RUN1. Wastewater influent composition: $S^{in}_{Su} = 3500\ g\ m^{-3}$ (Sugar), $S^{in}_{Bu} = 0$ (Butyrate), $S^{in}_{Pro} = 0$ (Propionate), $S^{in}_{Ac} = 0$ (Acetate), $S^{in}_{CH_4} = 0$ (Methane).

4.4.4 NS4 - Effects of biomass density

Biomass density of the granules involved in granular biofilm systems is highly variable due to several factors, such as hydrodynamic conditions, shear forces, EPS production. Firstly, high shear forces lead to stronger and denser granules, while weaker and more porous granule structures develop for lower shear forces [69, 34, 118]. Moreover, EPS production is generally thought to increase cell surface hydrophobicity and promote the formation of a sticky matrix which favours the attachment of new cells or flocs [123]. Thus, EPS positively influences the granulation process, contributing to maintain the structural integrity of the biofilm matrix and improve the biomass density.

Biomass density is a crucial property of granular biofilms because it regulates the mass transfer, the consumption of soluble substrates within the granules and consequently the growth of microbial species and granule dynamics. As a result, granules of different densities typically have different dimensions and are characterized by different microbial stratifications.

In this context, a numerical study (NS4) is performed to describe the evolution of biofilm granules with different biomass densities. Four simulations (RUN14 - RUN17) are carried out using four different values of biomass density ρ (RUN14: $\rho = 20000\ g\ m^{-3}$, RUN15: $\rho = 70000\ g\ m^{-3}$, RUN16: $\rho = 120000\ g\ m^{-3}$, RUN17: $\rho = 170000\ g\ m^{-3}$). The concentration of soluble substrates in the wastewater influent S_j^{in} and the initial concentration of suspended biomasses within the reactor $\psi_{i,0}^*$ set for this numerical study are the same used in NS1 and are reported in Table 4.3. Numerical results are summarized in Figs. 4.16-4.18.

The evolution of the granule radius $R(t)$ and of the phototrophic sessile mass m_{tot} are shown in Fig. 4.16. It is clear that higher is the biomass density of the granule, smaller is the steady-state radius achieved. This is due to different mass transfer conditions occurring within the granule: higher biomass densities entail higher flux of soluble substrates exchanged between bulk liquid and granules. For this reason, for higher den-

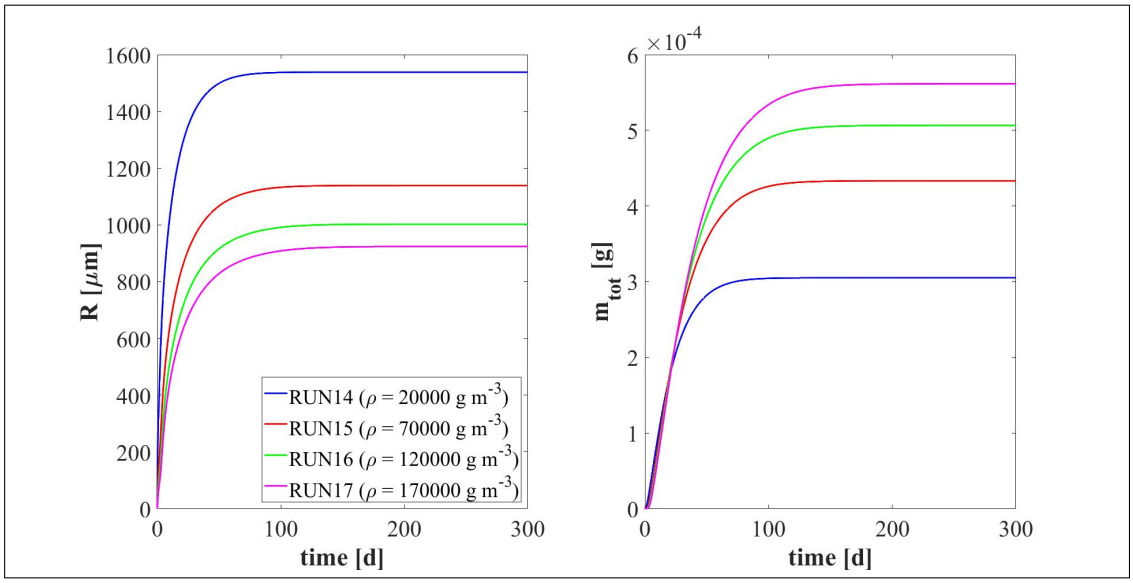

Figure 4.16: NS4 - Evolution of the biofilm radius $R(t)$ and of the total sessile mass m_{tot} for different biomass densities ρ. Wastewater influent composition: $S_{Su}^{in} = 3500\ g\ m^{-3}$ (Sugar), $S_{Bu}^{in} = 0$ (Butyrate), $S_{Pro}^{in} = 0$ (Propionate), $S_{Ac}^{in} = 0$ (Acetate), $S_{CH_4}^{in} = 0$ (Methane).

sities, the substrates in the bulk liquid are consumed faster and the metabolic growth rates driving the growth of the granule are on average lower. This leads to smaller granules, in accordance with [69].

The microbial ecology for the four values of ρ and at $T = 70\ d$ is reported in Fig. 4.17. As can be seen, granules with different densities have different microbial distributions. In particular, when $\rho = 20000\ g\ m^{-3}$ (RUN14) an homogeneous distribution is observed: although acidogens (blue) have a tendency to gather in the outermost layers and methanogens (red) and acetogens (green) have the tendency to populate the internal part, the microbial distribution within the granule is fairly homogeneous. This is due to the mass transfer of the soluble substrates within the granule: a low biomass density leads to small gradients of soluble substrates across the granule and an homogeneous growth of the different microbial species is observed throughout the biofilm. As the density of the biofilm increases (RUN15-RUN17), the gradient of soluble substrates across the biofilm increases and the layered distribution of the biomass is clearer and visible: acidogens are strictly confined in the outer layer while acetogens and methanogens are

mostly present in the inner part. These results are in agreement with the experimental evidence reported in [12].

In Fig. 4.18 the mass (left) and the relative abundance (right) of the sessile microbial species within the biofilm are shown at the steady-state condition ($T = 300\ d$). Higher biomass density leads higher amount (left) and fractions (right) of dead biomass accumulated as inert (black).

4.4.5 NS5 - Effects of erosive detachment

The evolution of the granule dimension is the result of a dynamic equilibrium between biomass growth, attachment of new biomass and detachment process. The detachment flux is essentially related to the erosion process occurring on the granule surface, due to the effect of the hydrodynamic shear forces developing in the reactor [8]. These forces are highly variable due to the influence of several factors, such as liquid upflow velocity, gas production, particle-particle collision, eventual mixing systems and geometry of the reactor [69, 118].

In this perspective, it is interesting to investigate the role of detachment phenomena induced by shear stress on the anaerobic granulation process and study its effects on the granule dimension and, consequently, on the distribution, amount and relative abundance of sessile biomass within the granule. For this purpose, the fifth and last study (NS5) is carried out based on 8 simulations (RUN18 - RUN25) with 8 different values of the detachment coefficient λ, in order to simulate different shear stress conditions. The values used are $\lambda = 4, 8, 12, 16, 20, 24, 28, 32\ m^{-1}\ d^{-1}$. The concentration of soluble substrates in the wastewater influent S_j^{in} and the initial concentration of suspended biomasses within the reactor $\psi_{i,0}^*$ set for this numerical study are the same used in NS1 and are reported in Table 4.3.

It should be noted that, contrary to the attachment, the detachment phenomenon increases as the biofilm dimension increases and has a negligible effect on the initial

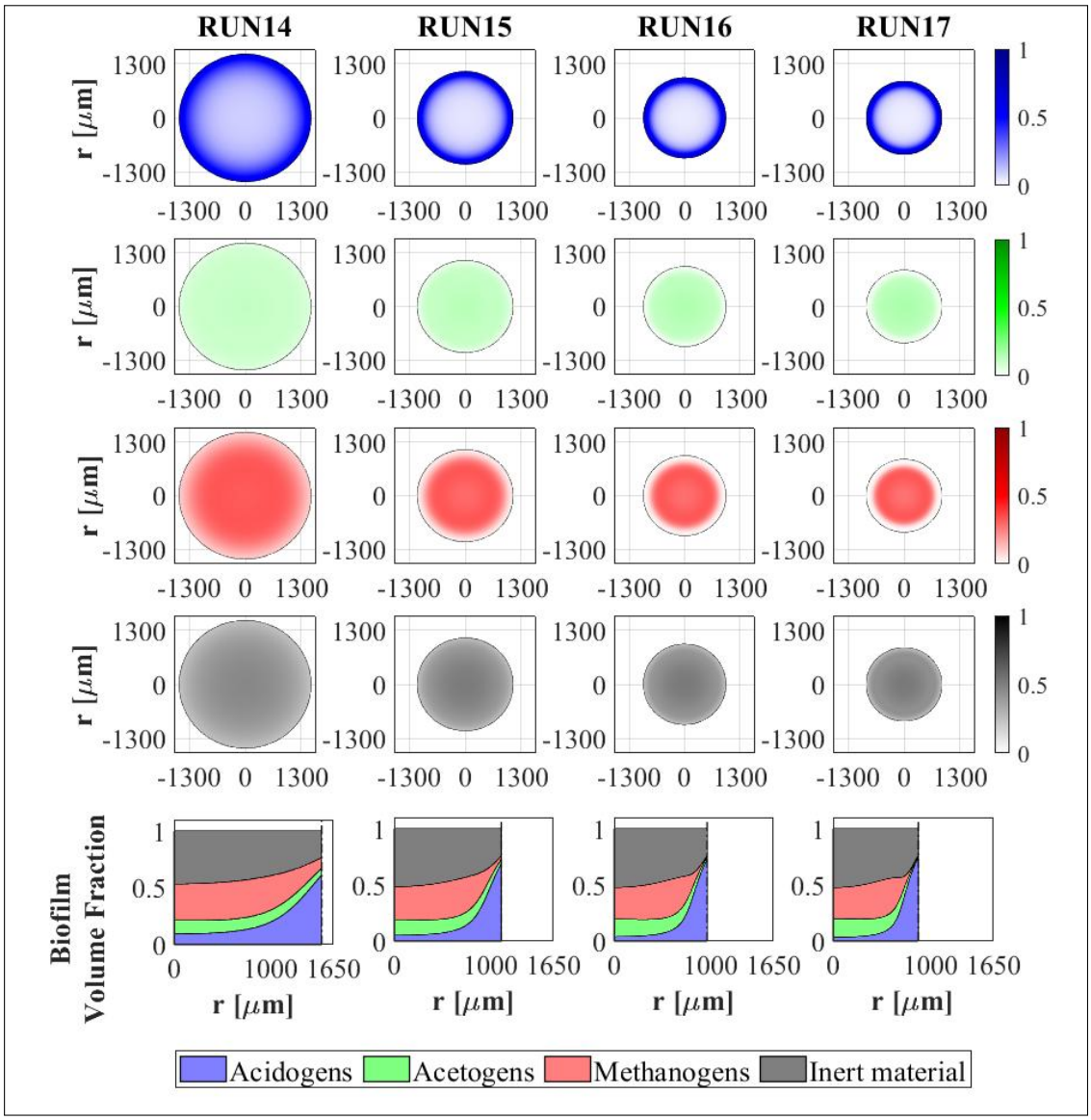

Figure 4.17: NS4 - Microbial species distribution in the diametrical section and across the radius of the granule at $T = 70d$, for different biomass densities. RUN14: $\rho = 20000\ g\ m^{-3}$, RUN15: $\rho = 70000\ g\ m^{-3}$, RUN16: $\rho = 120000\ g\ m^{-3}$, RUN17: $\rho = 170000\ g\ m^{-3}$. Wastewater influent composition: $S_{Su}^{in} = 3500\ g\ m^{-3}$ (Sugar), $S_{Bu}^{in} = 0$ (Butyrate), $S_{Pro}^{in} = 0$ (Propionate), $S_{Ac}^{in} = 0$ (Acetate), $S_{CH_4}^{in} = 0$ (Methane).

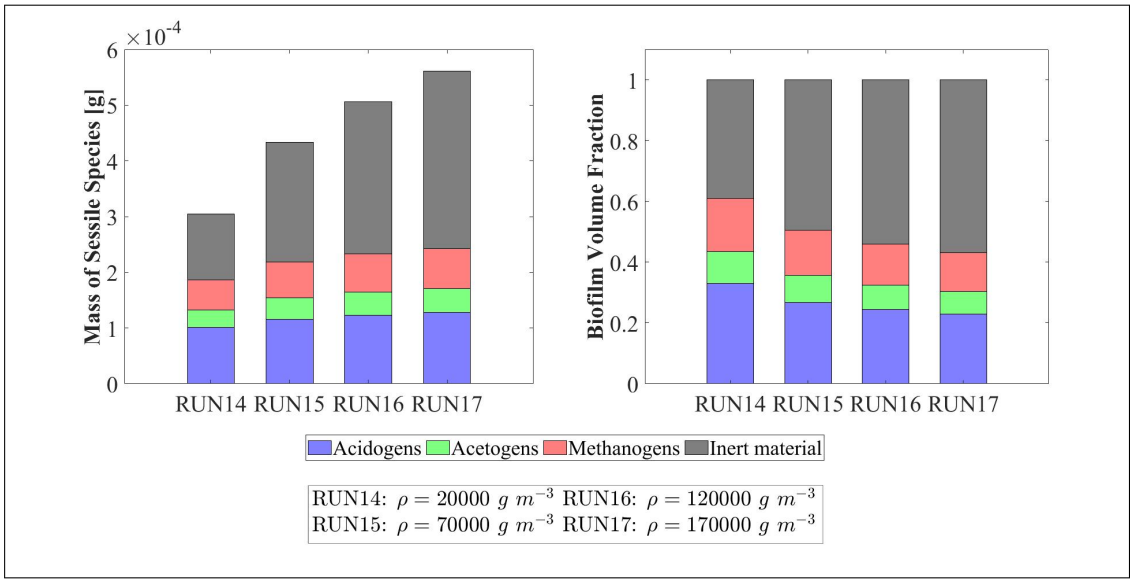

Figure 4.18: NS4 - Mass (left) and relative abundances (right) of microbial species within the granule at $T = 300d$ for different biomass densities ρ. Wastewater influent composition: $S_{Su}^{in} = 3500\ g\ m^{-3}$ (Sugar), $S_{Bu}^{in} = 0$ (Butyrate), $S_{Pro}^{in} = 0$ (Propionate), $S_{Ac}^{in} = 0$ (Acetate), $S_{CH_4}^{in} = 0$ (Methane).

phase of the granulation process ($\sigma_d(t) = \lambda R^2(t)$). For this reason, the study does not focus on the initial biofilm formation but investigates the long-term effects of the detachment process.

Fig. 4.19 summarizes the effects that different detachment conditions have on the variation of the granule radius $R(t)$ over time and on the granule steady-state dimension. As explained above, the formation and the initial evolution of the granule are not affected by the detachment phenomenon. Indeed, it is clear that the trend of $R(t)$ is not influenced by λ until $T = 10$-$20\ d$. When the granule reaches a $600\ \mu m$ radius, it becomes very sensitive to the detachment coefficient: as λ increases, the erosion phenomenon increases, and a smaller steady-state granule dimension is achieved. However, the steady-state granule radius has a less than linear behaviour with increasing λ. Furthermore, in the case of positive attachment flux, steady-state $R(t)$ tends asymptotically to 0 for λ tending towards an infinite value. Indeed, when $R(t) = 0$ the detachment flux is null (see Eq.4.19) and any positive value of attachment flux is enough to trigger the expansion of the spherical free boundary domain.

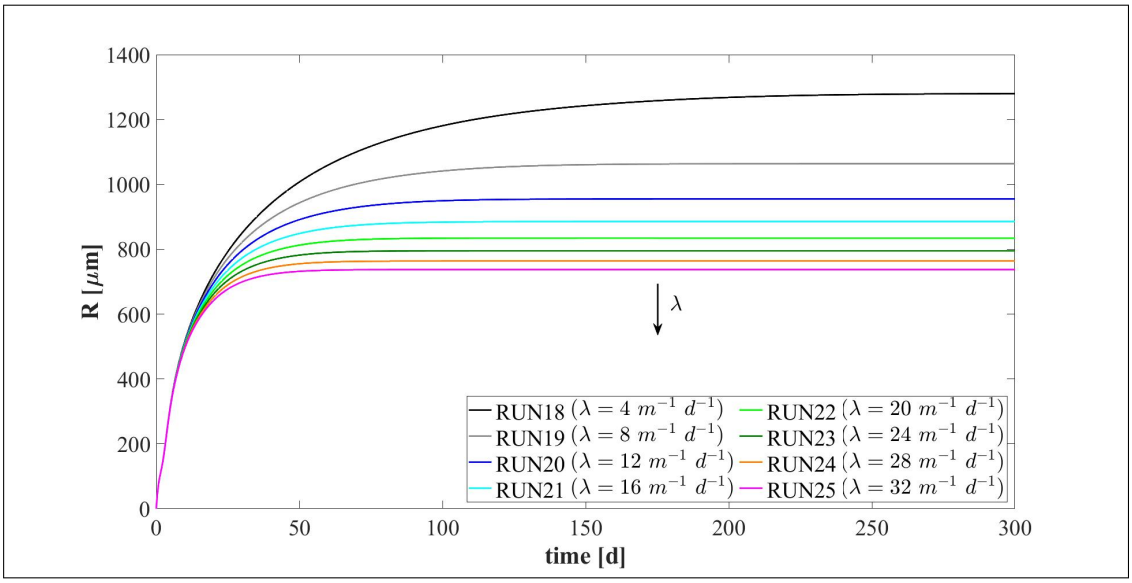

Figure 4.19: NS5 - Biofilm radius evolution over time for different detachment coefficients λ. Wastewater influent composition: $S_{Su}^{in} = 3500\ g\ m^{-3}$ (Sugar), $S_{Bu}^{in} = 0$ (Butyrate), $S_{Pro}^{in} = 0$ (Propionate), $S_{Ac}^{in} = 0$ (Acetate), $S_{CH_4}^{in} = 0$ (Methane).

Fig. 4.20 presents the distribution of sessile biomasses within the granule under four different detachment conditions ($\lambda = 4, 8, 16, 32\ m^{-1}\ d^{-1}$), at $T = 70\ d$. As λ increases, an increase in the active biomass fraction $f_{Su} + f_{Bu} + f_{Pro} + f_{Ac}$ and a reduction in the inert material f_I occur within the granule. Moreover, for all λ values the granule is mainly composed of acidogens (blue) in the external layers, and methanogens (red) and acetogens (green) in the internal nucleus. This distribution appears more evident when the granule is larger (low λ) and there are higher gradients of soluble substrates along the radius.

Finally, Fig. 4.21 reports the steady-state mass (top) and the relative abundance (bottom) of sessile microbial species within the granule under different detachment conditions, at $T = 300\ d$. Since the density is constant and equal in all simulations, the total sessile mass within the granule is directly proportional to the granule dimension. Then, a higher value of detachment coefficient λ leads to a smaller granule and consequently, a smaller sessile mass both overall and for individual species (Fig. 4.21-top). The relative abundances shown in Fig. 4.21 (bottom) confirm the results presented in Fig. 4.20: higher erosion conditions lead to smaller granules which are characterized

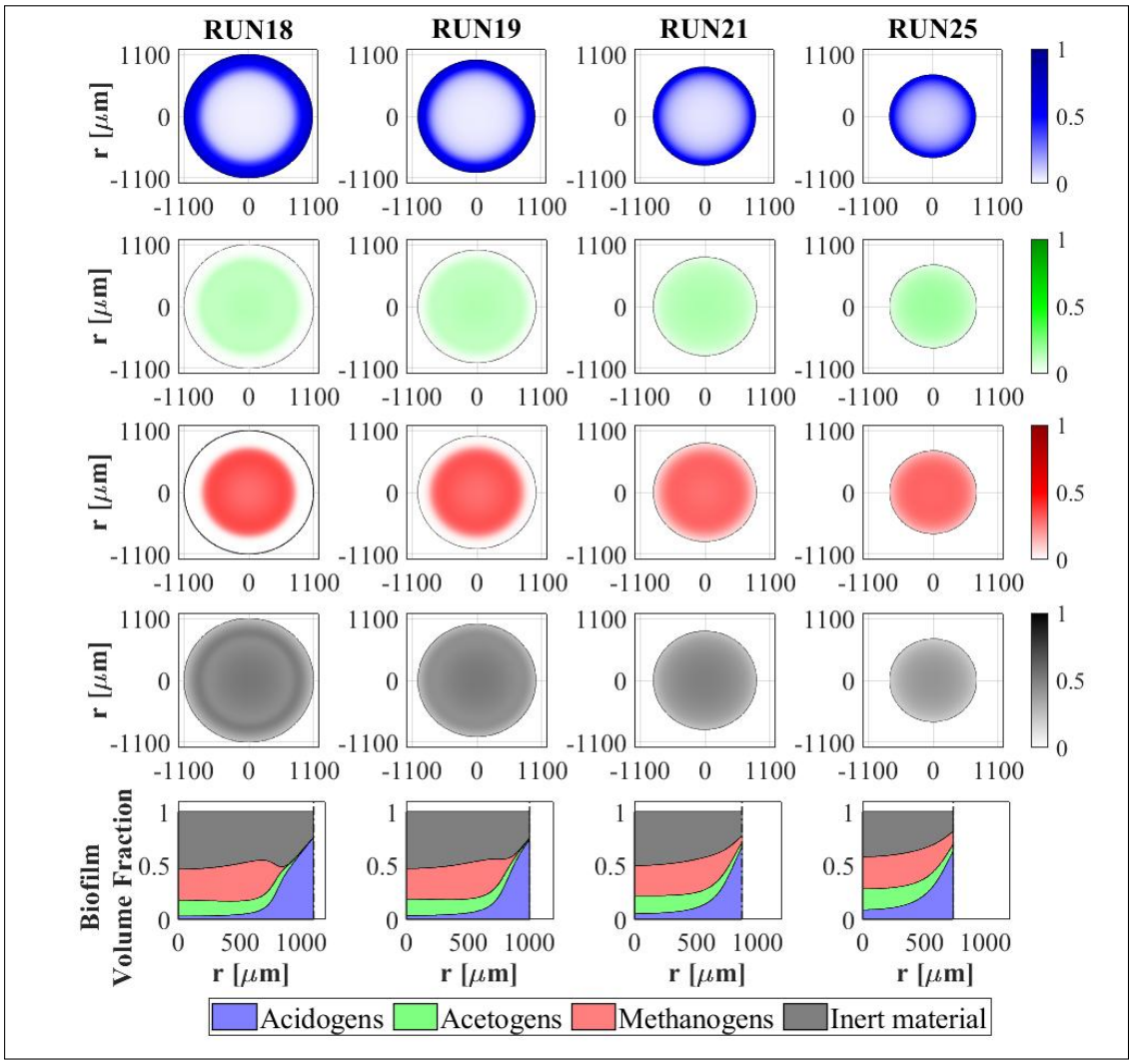

Figure 4.20: NS5 - Microbial species distribution in the diametrical section and across the radius of the granule at $T = 70d$, for different detachment coefficients. RUN18: $\lambda = 4\ m^{-1}\ d^{-1}$, RUN19: $\lambda = 8\ m^{-1}\ d^{-1}$, RUN21: $\lambda = 16\ m^{-1}\ d^{-1}$, RUN25: $\lambda = 32\ m^{-1}\ d^{-1}$. Wastewater influent composition: $S_{Su}^{in} = 3500\ g\ m^{-3}$ (Sugar), $S_{Bu}^{in} = 0$ (Butyrate), $S_{Pro}^{in} = 0$ (Propionate), $S_{Ac}^{in} = 0$ (Acetate), $S_{CH_4}^{in} = 0$ (Methane).

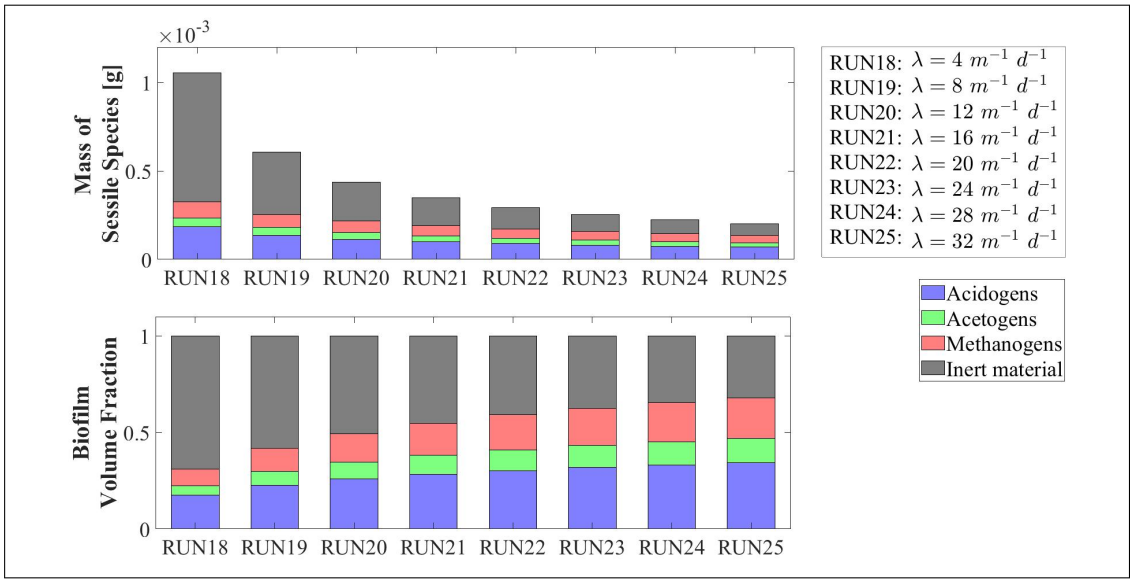

Figure 4.21: NS5 - Mass (top) and relative abundances (bottom) of microbial species within the granule at $T = 300d$ for different detachment coefficients λ. Wastewater influent composition: $S_{Su}^{in} = 3500\ g\ m^{-3}$ (Sugar), $S_{Bu}^{in} = 0$ (Butyrate), $S_{Pro}^{in} = 0$ (Propionate), $S_{Ac}^{in} = 0$ (Acetate), $S_{CH_4}^{in} = 0$ (Methane).

by a higher fraction of active biomass.

4.5 Discussion

4.5.1 Model assumptions

An anaerobic granular biofilm reactor is an extremely complex and heterogeneous multiphase biological system characterized by properties that vary over time and space. This system is constituted by a liquid medium where an assorted microbial community is immersed. Most of this community is organized into granular aggregates: spherical-shaped biological structures with variable densities composed of several microbial species in sessile form which enhance the spatial heterogeneity. The life cycle of the *de novo* granules includes an initial phase of granulation which leads to the granule formation, a maturation phase in which the granule size increases and a final phase of breaking. The pieces of biofilm deriving from the breaking of a granule may in turn originate new granules. During this evolution, the granule is affected by complex phenomena which

radically influence its structure and suddenly change its properties: attachment processes of suspended biomass, metabolic growth and decay of sessile biomass, particle-particle interactions, EPS secretion, gas production, invasion processes by planktonic cells, detachment processes induced by intense hydrodynamic conditions and shear stress. The combination of these factors leads to a biological community consisting of a number of granules that vary over time, which differ from one another in size, density and microbial distribution. In addition, the location inside the reactor influences the characteristics of the granules. Indeed, due to the geometry and the hydrodynamic conditions of these systems, gradients in the concentrations of soluble substrates establish along the reactor and amplify the differences between the granules located at different points of the system. However, in some cases mixing devices are added to the system, in order to enhance the movement of the sludge and to reduce the gradients without increasing the flow rate and velocity.

Given its physical and biological complexity, the mathematical modelling of an anaerobic granular-based system necessarily requires the introduction of some model assumptions. In this perspective, the model presented in this Chapter describes the anaerobic granular system as a domain having a constant liquid volume where a fixed number of granules is immersed. All granules are assumed to have identical evolution and properties (same size, same density, same constituents). The single granule is modelled as a spherical, continuous free boundary domain having a biomass density constant in time and space. Under the assumption of perfect mixing, the properties of the bulk liquid, in particular the concentration of soluble substrates and suspended biomass, are supposed to be the same at every point and vary only over time. The attachment is modelled as a continuous, deterministic process which depends linearly on the concentration of the suspended biomass. The detachment process is modelled as a continuous mass flux that detaches from the granule due to the effect of shear-induced erosion. Due to the uncertainty about the form of detached biomass, its contribution to suspended and sessile biomass is neglected. Moreover, since the mechanisms lead-

ing to the breaking of the granule are not perfectly clear, breaking phenomena are not included in the model. The process of invasion by planktonic cells present in the bulk liquid is modelled as a diffusive transport across the granule. This eliminates the restrictions on the granule ecological structure that could be generated in particular cases, and guarantees the growth of each sessile microbial species where optimal conditions for its metabolism occur. Finally, suspended substrates in the wastewater influent, gas transfer processes and EPS production are neglected as they are not significant for the purposes of the numerical investigation presented in this Chapter: qualitatively studying the anaerobic granulation process, the evolution of the granules over time and the related ecological succession.

It is emphasized that all assumptions introduced in the model do not compromise the reliability of the numerical results which correctly reproduce the *de novo* anaerobic granulation process and are qualitatively in accordance with several experimental studies present in literature.

4.5.2 Dimension, microbial distribution, ecology of biofilm granules and evolution of bulk liquid characteristics

As mentioned above, the dimensional evolution of the granule is described through the expansion of a spherical free boundary domain, whose radius varies over time. In particular, the *de novo* granulation process is modelled starting from an initial condition where all the biomass present in the reactor is in suspended form and there are no biofilm granules. Subsequently, the attachment process of the suspended biomass initiates the granulation process and the granules begin to grow. The evolution of the granule over time is governed by the positive contributions of sessile metabolic growth and attachment flux of suspended biomass and by the negative contribution of the erosive detachment flux. In the initial phase of the process, the size of the granule grows exponentially due to the high availability of substrates which leads to high rates of ses-

sile metabolic growth, the high attachment flux induced by the presence of suspended biomass within the bulk liquid and the negligible detachment flux, proportional to the granule size ($\sigma_d(t) = \lambda R^2(t)$). Later, the concentrations of soluble substrates and the suspended biomass within the bulk liquid reduce. This leads to a reduction in metabolic growth and attachment flux. In addition, the detachment flux intensifies as a result of the granule size increase. Consequently, the growth of the granule decreases until it reaches a steady-state value regulated by the balance between the positive and negative mass fluxes.

Numerical studies carried out show that the evolution of the granule dimension and its equilibrium value are deeply influenced by some factors, such as hydrodynamic shear stress, mass transfer of soluble substrates, composition of the influent and attachment properties of the suspended biomass present in the inoculum. The model results presented in NS5 report that the granule dimension is governed by the shear forces: high shear forces produce an intense erosion on the granule surface and limit its growth. This qualitative result is fully in agreement with the literature [69, 118, 8]. Since the shear forces depend on the hydrodynamic conditions occurring within the reactor, the model suggests that different particle distributions can be achieved by regulating the hydrodynamic regime in the reactor. As reported in NS2, the composition of the influent can affect the size of the granule due to the anabolic pathway of the species involved in the process. For example, the consumption of sugar induces a larger growth of sessile biomass compared to the consumption of the other substrates. As a result, for equal OLR, an influent with higher concentrations of sugar leads to the growth of more sessile biomass and larger dimensions of the granules. NS4 reports that larger amount of soluble substrates is consumed in denser granules, per unit of volume, therefore the metabolic growth rates decrease faster and lead to smaller equilibrium dimensions, in accordance with [69]. Finally, NS3 suggests that the attachment properties of the suspended biomass regulate the evolution of the granule, especially in the initial phase of biofilm formation. More precisely, when the suspended biomass is more prone to form

biofilm structures and to grow in sessile form, the granulation process is more intense, and the granules grow faster.

In addition, the model describes the microbial ecology that develops in the granule and shows the distribution of the different microbial species. In the initial phase, the granulation process is governed by acidogenic and methanogenic species. This is in agreement with several studies [123, 92, 57] which report that methanogens play a fundamental role in the formation of the initial nucleus of the granule. Indeed, some methanogenic cells have a filamentous morphology [123] and ability to use quorum sensing strategies [66, 141, 65] which improve their attachment properties and increase the efficiency of the granulation process. At the same time, acidogens have higher growth rates than other species, therefore they are present in large amount within the granule since the beginning of the process. Acidogens and methanogens exhibit the tendency to grow in different areas of the granule: the first in the outermost layer and the second in the inner part. This distribution becomes more evident over time. In particular, when the granule is mature, it is constituted by a large internal part populated by methanogens shielded by a thin external layer of acidogens. For long times, a homogeneous growth of acetogens and inert material deriving from the biomass decay is also observed. Many experimental studies [108, 12] show a microbial distribution within the anaerobic granules similar to the results proposed by the model.

However, the model suggests that some factors such as the composition of the influent, the biomass density and the hydrodynamic shear forces developing in the reactor can radically affect the microbial distribution. For example, NS2 shows that in the case of higher concentration of sugar within the wastewater influent, the granules that develop during the process show larger amount of acidogenic biomass. Conversely, when only VFAs are present in the influent, acidogens do not develop and methanogens and acetogens dominate the granule. Furthermore, the model qualitatively reproduces the microbial distribution observed by [12] in granules of different densities (study NS4). The biomass density deeply influences the mass transfer of the soluble substrates and

therefore the microbial ecology. Accordingly, low densities lead to small gradients of soluble substrates across the granule and a homogeneous distribution of the microbial species is observed throughout the biofilm. More pronounced gradients develop within denser granules, leading to a more stratified distribution of biomass. According to NS5 study, shear stress conditions appear to be an additional factor affecting the microbial distribution in an anaerobic granule, playing an important role especially on the amount of active and inactive biomass: as mentioned above, intense shear forces result in the formation of small granules where there is high availability of substrates and the active biomass prevails over the inactive one; lower shear forces induces the formation of larger granules populated by high amount of inactive biomass which accumulates in the innermost zone of the granule due to lack or shortage of soluble substrates.

Furthermore, the model describes how the granulation process influences the characteristics of the bulk liquid and the effluent, in particular the concentration of suspended biomasses and soluble substrates. The suspended biomasses are present in the inoculum initially introduced in the reactor and represent the microbial community that initiates the granulation process. In the first few days, the concentration of suspended biomass decreases rapidly as a consequence of attachment and dilution. The first concerns the aggregation of suspended biomass which converts to sessile form and contribute to create granular structures. The second is the result of the hydrodynamic regime established in the reactor. As already reported, the HRT of granular-based systems is fixed small enough to guarantee hydrodynamic conditions and shear forces optimal for the granulation process. Such HRT values are highly unfavourable for suspended biomass, which has short retention time to grow and consequently is diluted. After a few days, the suspended biomass is completely washed out. Note that this result also derives from the assumption that biomass detached from the biofilm due to erosive phenomena does not constitute new suspended biomass. Suspended acidogens remain in the bulk liquid longer than other species due to their higher growth rate. Soluble substrates are produced or consumed in the bulk liquid due to the effect of suspended

and sessile biomass. In the initial phase, the granules are small and the substrates are converted mainly by suspended biomass. Subsequently, when the size of the granules increases and the suspended biomass has already been washed out, the trend of the substrates in the bulk liquid is governed by the granular biomass. Note that soluble substrates and suspended biomasses achieve the steady-state values in a shorter time than sessile biomass within the granule. The effluent results to be purified at the steady-state, with the complete conversion of sugar and VFAs into methane.

Obviously, the trend of suspended biomass and soluble substrates within the bulk liquid is influenced by the influent composition (study NS2). Furthermore, NS3 shows that the attachment properties of the suspended microbial community initially present in the reactor deeply affect the velocity of the *de novo* granulation process. When the granulation process occurs faster, the conversion rate of substrates is higher, and the process reaches the steady-state in a shorter time. Accordingly, the model results confirm that improving attachment properties by regulating hydrodynamic conditions, by adding substances which stimulate the quorum sensing [66, 141] or by adopting bioaugmentation strategies [85, 58] allows to speed up the process and reduce the long start-up times of anaerobic granular systems, which represent a critical issue in the operation of granular-based systems.

4.6 Conclusions

In this Chapter, a mathematical model able to reproduce the *de novo* granulation process involved in a generic granular biofilm system has been introduced. It is presented the derivation of the model equations which govern the expansion of the granule, the growth of sessile biomass, the transport of substrates and planktonic cells within the granule, under the assumption of radial symmetry. Such equations have been derived from mass balances considerations in the framework of continuum mechanics. Processes of growth and decay of attached and suspended biomass, attachment from bulk

liquid to biofilm, detachment from biofilm to bulk liquid, invasion of planktonic cells, conversion and diffusion of soluble substrates are modelled. The model has been applied to anaerobic granular systems in order to test its qualitative behaviour and study the process of formation and evolution of the granular biofilm in this case of biological and engineering interest. The model takes into account the different contribution that individual microbial species can provide to the granulation process. For example, in the anaerobic case, the model is able to consider the fundamental role that some species of methanogens play in the granulation process by setting appropriate values of attachment velocity. The results shown describe exhaustively the anaerobic granulation process, the main properties of the granules such as the dimensional evolution, the ecology, the biomass distribution, the relative abundance and the evolution of the bulk liquid characteristics (soluble substrates and suspended biomass). Finally, further numerical studies have been carried out to investigate the effects of some significant factors on the process.

The most interesting observations resulting from the numerical studies are reported below:

- The anaerobic granule presents a typical microbial stratification: methanogens and acetogens populate the innermost layers of the granule and are shielded by a thin external layer of acidogens; the thickness of these layers depends on multiple factors (composition of the wastewater influent, biomass density, detachment forces).

- Intense hydrodynamic conditions and short HRT typical of granular biofilm systems limit the growth of suspended biomass, which has short retention times to grow and is washed out.

- The wastewater influent composition affects the evolution, ecology and microbial stratification of the granules.

- The attachment properties of the suspended biomass considerably influence the start-up period of the system. Strategies such as controlling hydrodynamic conditions, quorum sensing stimulation, bioaugmentation can reduce this period and enhance the start-up efficiency.

- The density of biomass regulates the mass transfer of soluble substrates and consequently the microbial distribution within the granule: denser granules have a more layered structure while less dense granules have a more homogeneous structure.

- Shear forces have a large impact on the granule size and the ratio of active to inactive biomass: higher shear forces lead to smaller granules constituted by larger fractions of active biomass.

The results shown are qualitatively in accordance with the experimental evidence from the literature. Accordingly, this model is able to correctly simulate both the formation and maturation of anaerobic granules by focusing on both the transient and the steady-state. From an engineering point of view, this leads to conclude that the model proves to be a useful tool both in the start-up and in the purification process of anaerobic granular biofilm systems. Furthermore, the model can be applied to any biological process which takes place in a granular-based system by choosing the suitable model variables and kinetic expressions.

In any case, some model parameters such as the values of the attachment velocities of the suspended biomass are introduced here for the first time and should be calibrated and validated on the basis of experimental data. Finally, in a future work, the detachment process leading to the breaking of the granule and the consequent formation of new granules could be included in the model, in order to describe the entire life cycle of biofilm granules.

Chapter 5

Multiscale modelling of oxygenic photogranules

5.1 Introduction

Nowadays, great interest is addressed to innovative biological systems in the field of wastewater treatment, aimed to improve treatment efficiencies and, at the same time, reduce the operating and development costs of traditional systems. In this context, several studies have been carried out to investigate treatment potentialities of granular biofilms [123, 87]. Biofilm granules are described as spherical, dense aggregate composed by microbial organisms embedded in a self-produced matrix of extracellular polymeric substances (EPS). The process leading to the biofilm granule formation is known as granulation and consists in the aggregation of microbial cells and flocs under particular conditions. The microorganisms living in biofilm granules can degrade polluting compounds present in wastewaters and required by their metabolism. Compared to conventional biomass flocs, biofilm granules have higher densities, which lead to mi-

This Chapter will be submitted as: Tenore, A., Mattei, M.R., Frunzo, L. Multiscale modelling of oxygenic photogranules.

croscale gradients of the substrates concentration and, consequently, to the formation of different microbial niches along the radius [136]. As a result, biofilm granules are extremely heterogeneous ecosystems populated by a broad diversity of microbial species. Specifically, the complexity, variability and multiplicity of microbial metabolic activities lead to a dense and intricate network of symbiotic and competitive interactions between the microbial species of granule ecosystem.

For several years, full-scale biological systems based on aerobic, anaerobic and anammox granular biofilms have been developed [107, 95, 125], while only more recently, attention has been paid to oxygenic photogranules (OPGs) [79, 114], biofilm granules developed in presence of light and constituted by a relevant phototrophic component. OPGs-based systems have huge advantages compared to conventional systems. Above all, they do not require aeration and this leads to lower energy costs compared to all aerobic systems. Indeed, the phototrophic production of O_2 meets the demand of heterotrophic and nitrifying bacteria and allows the oxidation of carbon and nitrogen compounds without the need of external O_2 sources [79]. Due to their high density, photogranules have settling properties better than suspended biomass and this leads to easy the separation of biomass from treated water and to reduce the footprint of the plants [2], and allows to reach higher biomass concentrations without risk of re-suspension [9]. Specifically, OPGs-based systems are convenient compared to systems based on phototrophic suspended biomass, in which the main drawback is represented by the complex and expensive separation phase, base on harvesting procedures [101]. Moreover, contrary to biofilm systems based on sessile biomass attached to solid supports, OPGs-based systems involve sessile biomass arranged in spherical and constantly moving granules and this mitigates boundary layer resistances and enhances the mass transfer of substrates across the biofilm photogranule [9]. Finally, photogranules biomass deriving from wastewater treatments represents a renewable energy source to be used in industrial applications such as the production of biofuels, chemicals, and nutraceuticals [79].

The granulation process is complex and not fully understood. Over time, several theories have been proposed to explain the formation process of aerobic, anaerobic and anammox biofilm granules [92, 16]. In this context, hydrodynamic conditions are regarded as the key factor of the process [69], although some works assign a decisive role to specific microbial species [92]. In the case of oxygenic photogranules, some experimental evidences have highlighted their formation in batch reactors, under hydrostatic conditions [79, 7]. In this regard, the discriminating factor in the photogranulation process appears to be the presence of cyanobacteria [79, 2, 3]. Due to their motility and filamentous structure, cyanobacteria are able to arrange in mat-like layers which encloses other microbial species in rigid, spherical structures [7]. Some studies have reported high chance of success of the photogranulation process in the case of inocula rich in cyanobacteria, which reduces drastically in the case of inocula poor in cyanobacteria [55].

Although full-scale OPGs-based systems have not yet been developed, many experimental studies based on lab scale systems have been carried out to investigate the main aspects of the OPGs formation and their treatment potential [79, 7, 114, 38, 4]. As well as aerobic granules, photogranules are cultivated in sequencing batch reactors (SBRs). The experimental results recommend this system as one of the most promising technologies in the field of wastewater treatment [2, 55].

Several models have been proposed to describe the dynamics of phototrophic biofilms growing on solid supports and investigate the main mechanisms which drive the process [21, 22, 67, 93, 138, 84], while others models have focused on the description of aerobic, anaerobic or anammox biofilm granules [32, 88, 129], by considering a spherical geometry with radial symmetry. Nevertheless, since the engineering and biological interest in this topic is recent, modelling works on OPGs are not present in the literature. In this framework, this Chapter introduces a mathematical model which describes the OPGs-based system and the formation and evolution of OPGs. In order to model the process correctly and comprehensively, a number of modelling novelties have been in-

troduced the following. Such novelties have a multidisciplinary value and can be easily adapted to different contexts.

Based on a continuum approach [132], the model couples the granular biofilm model to the mass balances within an SBR reactor. The granular biofilm model is formulated as a free boundary problem applied to a spherical domain with radial symmetry and is based on partial differential equations derived in Chapter 4. As introduced in [29], a vanishing value is set as the initial granule dimension, in order to describe the evolution of the granular biofilm from its genesis, initiated by the attachment process. Furthermore, a number of identical granules (modelled as explained above) are supposed to be immersed in an SBR reactor, modelled through a system of first order impulsive ordinary differential equations (IDEs) [45].

To correctly model oxygenic photogranules, it is necessary to differentiate cyanobacteria from microalgae. Models that take into account the growth of phototrophic biomass in engineering systems include all phototrophic species under a common model component, and suppose the entire phototrophic community to have the same metabolic activity. Indeed, the different phototrophic groups have similar functions in the phototrophic systems modelled and the engineering purposes do not require their distinction. Nevertheless, as previously introduced, cyanobacteria play a key role in the process of formation and growth of photogranules, due to characteristics and abilities that microalgae lack. Therefore, cyanobacteria and microalgae are modelled as two distinct components, taking into account the main differences in metabolic activity [120], attachment properties [79] and light harvesting [2, 3, 121]. Specifically, as mentioned above, it is realistically assumed that cyanobacteria govern the granulation process due to their excellent attachment properties and promote also the presence of other species within the granules. Consequently, a novelty has been introduced in the attachment modelling: the attachment velocities of all suspended microbial species are not assumed to be constant, as in the previous Chapter, but functions of the concentration of suspended cyanobacteria present in the system.

Light influences the metabolic activity of cyanobacteria and microalgae and is included as a model variable. Such variable is modelled as a piecewise-constant time function within the reactor, to simulate the day-night cycle, and as a function of time and space within the granule, by considering attenuation phenomena through the Lambert-Beer law. The metabolic activity of cyanobacteria and microalgae has been modelled by taking into account the main processes and factors: photoautotrophic pathways with consumption of ammonium or nitrates in light conditions [138], heterotrophic pathway in dark conditions [131], release of dissolved organic matter [40], photoinhibition phenomena [115], inhibition of oxygen on the photosynthetic activity [67]. In addition to cyanobacteria and microalgae, other microbial components have been assumed to compose the biofilm granule: aerobic and anoxic heterotrophic bacteria, nitrifying bacteria, EPS and inert material. Moreover, the diffusion and conversion of the following soluble substrates are considered: inorganic carbon (IC), organic carbon (DOC), nitrates (NO_3), ammonia (NH_3), oxygen (O_2). The modelling of all these components allows to include in the model the main positive and negative microbial interactions taking place in the photogranule ecosystem, which are discussed in the following sections.

The model has been integrated numerically, to investigate the main biological aspects of OPGs evolutions and the performances of OPGs-based systems, under different influent compositions and light conditions.

5.2 Mathematical Model

This model describes the evolutionary process of oxygenic photogranules in an SBR reactor, starting from their formation, induced by the granulation of the suspended biomass present in the reactor. Specifically, following the approach used in Chapter 4 in order to model anaerobic granules, this system has been modelled by considering two distinct compartments: N_G biofilm granules and the liquid medium of the reactor. Such compartments are closely related as they exchange significant mass fluxes of

soluble substrates and biomass. Consequently, two distinct but related submodels have been developed to describe these compartments, both based on specific assumptions, equations and variables.

5.2.1 Submodel 1: Granular Biofilm

The model introduced in Chapter 4 is used to describe the growth of the granular biofilm, maintaining the same equations and assumptions. It is assumed that all granules are subject to same phenomena, therefore, at any time it is possible to identify in the system N_G granules having same properties (density, dimension, microbial composition etc.). Specifically, each granule has been modelled as a spherical free boundary domain with radial symmetry, which evolves due to the growth of sessile biomass, the attachment flux from liquid medium to granule σ_a and detachment flux from granule to liquid medium σ_d. Thus, the spatial variability of the quantities involved can be fully described by the radial coordinate r, locating the granule centre at $r = 0$.

The components considered within the biofilm granule, expressed in terms of concentration, are the sessile biomasses constituting the solid matrix $X_i(r,t)$ and the soluble substrates dissolved in the liquid present in the voids $S_j(r,t)$. Due to the small particle size of soluble substrates, they are supposed to occupy no volume and only sessile biomass contributes to the biofilm volume. All sessile microbial species are supposed to have the same constant density ρ and the volume fraction of each individual species is achieved by dividing its concentration X_i by ρ. Notably, the fractions of volume occupied by biomass are constrained to add up to unity, $\sum_{i=1}^{n} f_i = 1$ [97].

A system of hyperbolic PDEs describes the transport and growth of sessile microbial species within the granule:

$$\frac{\partial f_i(r,t)}{\partial t} + u(r,t)\frac{\partial f_i(r,t)}{\partial r} = r_{M,i}(r,t,\mathbf{f},\mathbf{S}) - f_i(r,t)\sum_{i=1}^{n} r_{M,i}(r,t,\mathbf{f},\mathbf{S}),$$

$$i = 1, ..., n, 0 \leq r \leq R(t),\ t > 0, \tag{5.1}$$

$$f_i(R(t), t) = \frac{v_{a,i}\psi_i^*(t)}{\sum_{i=1}^n v_{a,i}\psi_i^*(t)},\ i = 1, ..., n,\ t > 0,\ \sigma_a - \sigma_d > 0, \tag{5.2}$$

where $r_{M,i}(r, t, \mathbf{f}, \mathbf{S})$ is the growth rate of the i^{th} sessile biomass, $v_{a,i}$ is the attachment velocity and $\psi_i^*(t)$ is the concentration within the liquid medium of the i^{th} suspended biomass, while $u(r, t)$ is the biomass velocity and is governed by the following equation:

$$\frac{\partial u(r,t)}{\partial r} = -\frac{2u(r,t)}{r} + \sum_{i=1}^{n} r_{M,i}(r, t, \mathbf{f}, \mathbf{S}),\ 0 < r < R(t),\ t > 0, \tag{5.3}$$

$$u(0, t) = 0,\ t > 0. \tag{5.4}$$

Eq. 5.2 represents the boundary condition for Eq. 5.1 at the interface granule-liquid medium and holds only when attachment flux is higher than detachment flux. Indeed, in the opposite case, the biomass concentration at the interface is regulated exclusively by the internal points of the biofilm domain, and the boundary condition is not needed. The evolution of the free boundary domain is described by the radius of the biofilm granule $R(t)$ which varies according to the following equation, derived by the global mass balance on the granule volume:

$$\dot{R}(t) = \sigma_a(t) - \sigma_d(t) + u(R(t), t), \tag{5.5}$$

$$R(0) = 0. \tag{5.6}$$

In order to model the formation of the granular biofilm, all biomass is initially supposed in suspended form by setting a vanishing value as initial condition of $R(t)$.

The granulation process is initiated by the attachment flux of suspended biomass, assumed linearly dependent on the concentration of suspended biomasses within the liquid medium $\psi_i^*(t)$:

$$\sigma_a(t) = \sum_{i=1}^{n} \sigma_{a,i}(t) = \frac{\sum_{i=1}^{n} v_{a,i}\psi_i^*(t)}{\rho}. \tag{5.7}$$

Meanwhile, the detachment flux is modelled as [1]

$$\sigma_d(t) = \lambda R^2(t), \tag{5.8}$$

where λ is the constant detachment coefficient.

The soluble substrates diffuse and convert in the granule and are governed by the following system of parabolic PDEs:

$$\frac{\partial S_j(r,t)}{\partial t} - D_{S,j}\frac{\partial^2 S_j(r,t)}{\partial r^2} - \frac{2D_{S,j}}{r}\frac{\partial S_j(r,t)}{\partial r} = r_{S,j}(r,t,\mathbf{f},\mathbf{S}),$$

$$j = 1,...,m, 0 < r < R(t),\ t > 0, \tag{5.9}$$

$$\frac{\partial S_j}{\partial r}(0,t) = 0,\ S_j(R(t),t)) = S_j^*(t),\ j = 1,...,m,\ t > 0, \tag{5.10}$$

where $D_{S,j}$ is the diffusion coefficient in biofilm, $r_{S,j}(r,t,\mathbf{f},\mathbf{S})$ is the conversion rate and $S_j^*(t)$ is the concentration of substrate j in the liquid medium.

5.2.2 Submodel 2: Sequencing batch reactor (SBR)

The second submodel has been developed to describe the sequencing batch reactor (SBR) where the growth of the photogranules occurs. SBR reactors are based on a cyclic operation, in which the wastewater influent is fed and treated discontinuously: in the first phase (filling) a volume of wastewater is fed within the reactor; in the second

phase (reaction), such volume is biologically treated by means of the biomass present in the system; the biomass-liquid separation takes place in the third phase (settling); lastly, in the last phase (emptying) the purified supernatant leaves the reactor, which is refilled with a new wastewater volume to be treated. The model components considered in the liquid medium are the concentrations of suspended biomasses $\psi_i^*(t)$ and the concentrations of soluble substrates $S_j^*(t)$.

To model this system some assumptions have been introduced:

- The filling, settling and emptying phases take place instantaneously and influence the process through an instantaneous change of state of the system, therefore the cycle time corresponds to the reaction time.
- The reactor is completely mixed, hence, the variables involved are functions of time and not of space.
- The volume of granular and suspended biomass is neglected (the reactor volume is equal to the liquid volume).
- All sessile biomass remains in the reactor during the emptying phase (100% settling efficiency of biofilm granules); suspended biomass has a partial settling efficiency; soluble substrates are dissolved in the liquid and do not settle.
- During the emptying phase the reactor is only partially emptied (emptying/refilling ratio less than 1).

Mathematically, the SBR configuration is modelled through a system of first order impulsive ordinary differential equations (IDEs) [45]. Each impulsive differential equation is based on three components: the continuous-time differential equation which governs the state of the system between impulses; the impulse equation, which describes an impulsive jump and is defined by a jump function at the instant the impulse occurs; and the jump criterion, which defines a set of jump events in which the impulse equation is active [45]. These equations have been applied to $\psi_i^*(t)$ and $S_j^*(t)$:

$$V\dot{\psi}_i^*(t) = -\sigma_{a,i}(t)\rho A(t)N_G + r^*_{\psi,i}(t, \boldsymbol{\psi}^*, \mathbf{S}^*),$$

$$t \in [0,T],\ t \neq t_k,\ \psi_i^*(0) = \psi^*_{i,0},\ i = 1, ..., n, \tag{5.11}$$

$$V\dot{S}_j^*(t) = -A(t)N_G D_{S,j}\frac{\partial S_j(R(t),t)}{\partial r} + r^*_{S,j}(t, \boldsymbol{\psi}^*, \mathbf{S}^*),$$

$$t \in [0,T],\ t \neq t_k,\ S_j^*(0) = S^*_{j,0},\ j = 1, ..., m, \tag{5.12}$$

$$\Delta\psi_i^*(t_k) = \psi_i^*(t_k^+) - \psi_i^*(t_k^-) = -\gamma\psi_i^*(t_k^-),\ k = 1, ..., h,\ i = 1, ..., n, \tag{5.13}$$

$$\Delta S_j^*(t_k) = S_j^*(t_k^+) - S_j^*(t_k^-) = -\omega S_j^*(t_k^-) + \omega S_j^{in},\ k = 1, ..., h,\ j = 1, ..., m, \tag{5.14}$$

where $r^*_{\psi,i}(t, \boldsymbol{\psi}^*, \mathbf{S}^*)$ and $r^*_{S,j}(t, \boldsymbol{\psi}^*, \mathbf{S}^*)$ are the conversion rates for ψ_i^* and S_j^*, respectively; V is the reactor volume; $A(t)$ is the area of the spherical granule and is equal to $4\pi R^2(t)$; $\psi^*_{i,0}$ and $S^*_{j,0}$ are the initial concentrations of the i^{th} suspended species and the j^{th} soluble substrate within the liquid medium, respectively; S_j^{in} is the concentration of the j^{th} substrate in the influent; γ is the fraction of suspended biomass removed during the emptying; ω is the emptying/refilling ratio; $0 = t_0 < t_1 < t_2 < ... < t_h < t_{h+1} = T$, $t_{k+1} - t_k = \tau$; τ is the duration of a cycle; $\psi_i^*(t_k^+)$, $S_j^*(t_k^+)$, $\psi_i^*(t_k^-)$, $S_j^*(t_k^-)$ are the right and left limits of ψ_i^* and S_j^* at time t_k.

5.2.3 Model components

As already introduced in Section 5.1, the formation process of oxygenic photogranules is strongly influenced by the presence of cyanobacteria in the inoculum and this requires to introduce a mathematical differentiation between cyanobacteria and microalgae, which are here defined as two distinct model components. Consequently, the components supposed to constitute the solid matrix of the biofilm are (expressed in terms of concentrations): cyanobacteria $X_C(r,t)$, microalgae $X_A(r,t)$, heterotrophic bacteria $X_H(r,t)$, nitrifying bacteria $X_N(r,t)$, EPS $X_{EPS}(r,t)$ and inert material $X_I(r,t)$. The soluble substrates supposed to be dissolved within the liquid phase of the granules are (expressed in terms of concentrations): inorganic carbon $S_{IC}(r,t)$, organic carbon $S_{DOC}(r,t)$, nitrates $S_{NO_3}(r,t)$, ammonium $S_{NH_4}(r,t)$ and dissolved oxygen $S_{O_2}(r,t)$. The same soluble substrates are considered in the bulk liquid and their concentration is expressed as $S_j^*(t)$, $j \in \{IC, DOC, NO_3, NH_4, O_2\}$. The suspended microbial species supposed to populate the bulk liquid are (expressed in terms of concentrations): cyanobacteria $\psi_C^*(t)$, microalgae $\psi_A^*(t)$, heterotrophic bacteria $\psi_H^*(t)$ and nitrifying bacteria $\psi_N^*(t)$. Inert material formation and EPS production are processes occuring also within the bulk liquid, on account of suspended biomass. Indeed, beyond the key role in biofilm growth, EPS contributes to the formation of suspended flocs [62]. In any case, it is likely to assume that EPS production by suspended biomass is much lower than sessile production [62] and it has been neglected. Furthermore, inert material in suspended form does not play any role on the evolution of granules and on system performances, therefore it has been not included in the model. Heterotrophic bacteria include aerobic heterotrophs which grow by consuming oxygen and anoxic heterotrophs which grow by consuming nitrates and are inhibited by oxygen. Since cyanobacteria and microalgae need light to develop their metabolic activity, light intensity $I(r,t)$ has been included as a model variable. I is assumed to be constant and equal at every point of the bulk liquid, while it attenuates within the granules following the

Lambert-Beer law:

$$I(r,t) = I_0\, e^{-k_{tot}(R(t)-r)\rho},\ 0 \le r \le R(t),\ t > 0, \tag{5.15}$$

where I_0 is the fixed light intensity at the granule surface and k_{tot} is the light attenuation coefficient.

5.2.4 Modelling attachment

The photogranulation process is governed by cyanobacteria in suspended form which aggregate due to the motility, the filamentous structure and their ability to secrete EPS. During this process, cyanobacteria envelop other microbial species leading to granules populated by an assorted microbial community [7]. This process is modelled in a deterministic way, through an attachment flux of suspended biomass, which contributes to the formation and growth of the granule. In particular, cyanobacteria attachment flux is assumed proportional to the concentration and the attachment velocity of suspended cyanobacteria (ψ_C^* and $v_{a,C}$, respectively):

$$\sigma_{a,C}(t) = v_{a,C}\frac{\psi_C^*(t)}{\rho}. \tag{5.16}$$

With regard to the attachment flux of other species, a new expression is here introduced to take into account the role of cyanobacteria. For this reason, the attachment flux of microalgae, heterotrophs and nitrifiers takes the following form:

$$\sigma_{a,i}(t) = v_{a,i}(\psi_C^*(t))\frac{\psi_i^*(t)}{\rho},\ i \in \{A,H,N\}, \tag{5.17}$$

$$v_{a,i}(\psi_C^*(t)) = \frac{v_{a,i}^0\psi_C^*(t)}{K_C + \psi_C^*(t)},\ i \in \{A,H,N\}, \tag{5.18}$$

where $v_{a,i}^0$ is the maximum attachment velocity of the i^{th} suspended species and K_C is the cyanobacteria half saturation constant on the attachment of microalgae, het-

erotrophs and nitrifiers.

5.2.5 Microbial kinetics of cyanobacteria and microalgae

In general, the metabolic activity of microalgae and cyanobacteria is extremely complex and species-specific and can be characterized by photoautotrophic, heterotrophic and mixotrophic pathways [104], depending on a multitude of factors, such as taxonomy, light conditions, alternation of light and dark, temperature, availability of nutrients [19]. For the engineering and ecological purposes of this Chapter, the main processes have been modelled, believed to describe on average the metabolism of typical, heterogeneous communities of microalgae and cyanobacteria.

In the presence of light, metabolism of microalgae and cyanobacteria is supposed photoautotrophic and based on photosynthetic activity: using light energy, cyanobacteria and microalgae grow by consuming IC and NH_3, release DOC and O_2 and secrete EPS. In lack or shortage of NH_3, cyanobacteria and microalgae are supposed to grow by using NO_3 as a nitrogen source [138]. The model takes into account the inhibition induced by the presence of O_2 on photosynthetic activity. In absence of light, cyanobacteria and microalgae are supposed to have a heterotrophic metabolic activity: they grow by consuming O_2, DOC and NH_3 and produce IC.

In addition to the different granulation ability, some differences in the metabolic kinetics of cyanobacteria and microalgae has been considered, based on literature. As reported in [105], although microalgae and other microbial species contribute to the EPS production, cyanobacteria are seen as the main EPS contributors throughout the biofilm development. The model takes into account this evidence by considering a higher production of EPS by cyanobacteria compared to microalgae and other species. In accordance with [120], the maximum growth rate of cyanobacteria has been assumed lower than microalgae. Furthermore, differences in the harvesting and utilization of light are widely documented in the literature [2, 3, 121]: the optimal light intensity for

the photoautotrophic metabolic activity of cyanobacteria is lower than microalgae and their adaptability to extreme light conditions appears to be enhanced. These differences are take into account by setting the parameters of the light dependency coefficient [115] based on the phototrophic microbial species and by introducing the additional parameter η_i in the original formulation, which represents adaptability to non-optimal light conditions:

$$\phi_{I,i}(r,t) = (\frac{I(r,t)}{I_{opt,i}})_i^{\eta} \, e^{(1-(\frac{I(r,t)}{I_{opt,i}})_i^{\eta})}, \; i \in \{C, A\}, \; 0 \leq r \leq R(t), \; t > 0, \tag{5.19}$$

where $I_{opt,i}$ is the optimum light intensity and η_i is the coefficient of adaptability to light. Specifically, $\eta_C < \eta_A = 1$.

This formulation of the light dependence coefficient has been chosen because it also takes into account the phenomenon of photoinhibition, which limits photoautotrophic growth in adversely high light conditions.

5.2.6 Metabolic microbial interactions

The active biomasses (cyanobacteria, microalgae, heterotrophs and nitrifiers) grow by converting the soluble substrates, decay turning into inert material and secrete EPS. Due to their metabolic demand, biomasses cooperate and/or compete with each other. The most relevant interactions have been included in the model. As previously mentioned, the metabolic activity of cyanobacteria and microalgae is affected by light. Consequently, their interactions with the other species constituting the microbial community of the granule change according to light conditions provided in the system. In the presence of light, cyanobacteria and microalgae promote the growth of nitrifiers and aerobic heterotrophs by producing O_2 and the growth of aerobic and anoxic heterotrophs by releasing DOC, while compete with nitrifiers for IC. Moreover, in the absence or shortage of NH_3, they grow on NO_3, competing with anoxic heterotrophs. In dark

conditions, cyanobacteria and microalgae produce IC for nitrifiers, while compete with aerobic heterotrophs and nitrifiers for O_2 and with all heterotrophs for DOC. In return, heterotrophic bacteria produce IC necessary for the metabolism of cyanobacteria, microalgae and nitrifiers. Lastly, the latter produce NO_3 necessary for anoxic heterotrophs and for cyanobacteria and microalgae (in lack or shortage of reduced nitrogen).

All the biological processes are included in the model through the reaction terms of Eqs. 5.1, 5.3, 5.9, 5.11 and 5.12. The expressions of such terms are reported in Appendix A.

5.3 Numerical studies

The model has been coded and implemented in MatLab, and integrated through numerical methods. Specifically, the method of characteristics has been used to track the biofilm expansion, a finite difference approximation has been adopted for the diffusion-reaction PDEs and a first-order approximation is used for the reactor impulsive equations. The time to compute the values of the unknown variables is in the order of hours to days, depending on the specific target simulation time T.

The numerical results on both the photogranule and the reactor scales have been analyzed. In this regard, three different numerical studies have been carried out and discussed in the following paragraphs. The first has been focused on the treatment of a typical municipal wastewater and both the treatment process and the microbial characteristics of the biofilm granules have been investigated. In the second study, different types of influent wastewaters have been considered, to check the elasticity of the system and to study how the influent composition affect the microbial distribution within the granules. Finally, the third study looks into the process under different light conditions and how these govern the microbial growth, with particular attention to the dualism between microalgae and cyanobacteria.

Parameter	Definition	Unit	Value	Ref
$q_{max,A}$	Maximum specific O_2 production rate by A	$kmol(O_2)kgCOD^{-1}d^{-1}$	0.074	[138]
$q_{max,C}$	Maximum specific O_2 production rate by C	$kmol(O_2)kgCOD^{-1}d^{-1}$	0.037	(a)
$\mu_{max,H}$	Maximum specific growth rate for H	d^{-1}	4.8	[84]
$\mu_{max,N}$	Maximum specific growth rate for N	d^{-1}	1	[84]
$k_{d,A}$	Decay-inactivation rate for A	d^{-1}	0.1	[138]
$k_{d,C}$	Decay-inactivation rate for C	d^{-1}	0.1	[138]
$k_{d,H}$	Decay-inactivation rate for H	d^{-1}	0.1	[138]
$k_{d,N}$	Decay-inactivation rate for N	d^{-1}	0.1	[138]
$K_{A,IC}$	IC half saturation coeff. for A	$kmol(IC)\ m^{-3}$	10^{-4}	[138]
$K_{A,DOC}$	DOC half saturation coeff. for A	$kg(COD)\ m^{-3}$	$5 \cdot 10^{-3}$	[138]
$K_{A,NO3}$	NO_3 half saturation coeff. for A	$kmol(NO_3)\ m^{-3}$	$1.2 \cdot 10^{-6}$	[138]
$K_{A,NH3}$	NH_3 half saturation coeff. for A	$kmol(NH_3)\ m^{-3}$	$1.2 \cdot 10^{-6}$	[138]
$K_{A,I}$	Light inhibition coefficient for A	$kmol(e^-)\ m^{-2}\ d^{-1}$	$8 \cdot 10^{-5}$	[138]
$K_{C,IC}$	IC half saturation coeff. for C	$kmol(IC)\ m^{-3}$	10^{-4}	[138]
$K_{C,DOC}$	DOC half saturation coeff. for C	$kg(COD)\ m^{-3}$	$5 \cdot 10^{-3}$	[138]
$K_{C,NO3}$	NO_3 half saturation coeff. for C	$kmol(NO_3)\ m^{-3}$	$1.2 \cdot 10^{-6}$	[138]
$K_{C,NH3}$	NH_3 half saturation coeff. for C	$kmol(NH_3)\ m^{-3}$	$1.2 \cdot 10^{-6}$	[138]
$K_{C,I}$	Light inhibition coefficient for C	$kmol(e^-)\ m^{-2}\ d^{-1}$	$8 \cdot 10^{-5}$	[138]
$K_{H,DOC}$	DOC half saturation coeff. for H	$kg(COD)\ m^{-3}$	$4 \cdot 10^{-3}$	[138]
$K_{H,NO3}$	NO_3 half saturation coeff. for H	$kmol(NO_3)\ m^{-3}$	$3.6 \cdot 10^{-5}$	[138]
$K_{H,NH3}$	NH_3 half saturation coeff. for H	$kmol(NH_3)\ m^{-3}$	$3.6 \cdot 10^{-6}$	[56]
$K_{H,O2}$	O_2 half saturation coeff. for H	$kmol(O_2)\ m^{-3}$	$6.25 \cdot 10^{-6}$	[138]
$K_{N,IC}$	IC half saturation coeff. for N	$kmol(IC)\ m^{-3}$	10^{-4}	[138]
$K_{N,NH3}$	NH_3 half saturation coeff. for N	$kmol(NH_3)\ m^{-3}$	$7 \cdot 10^{-5}$	[138]
$K_{N,O2}$	O_2 half saturation coeff. for N	$kmol(O_2)\ m^{-3}$	$1.56 \cdot 10^{-5}$	[138]
$K^{in}_{O2,max}$	Max inhibition coefficient of O_2 on A and C	$kmol(O_2)\ m^{-3}$	10^{-3}	[67]
$K_{R_{CO2/O2}}$	Half saturation coeff. for O_2 inhibition	$--$	0.35	[67]
Y_H	Yield of H on DOC	$kg(COD)\ kg(COD)^{-1}$	0.63	[138]
Y_N	Yield of N on NO_3	$kg(COD)\ kg(NO_3 - N)^{-1}$	0.24	[138]
Y_{DOC}	Yield of A and C on DOC	$kg(COD)\ kg(COD)^{-1}$	0.5	(a)

(a) Assumed

Table 5.1: Kinetic parameters

The treatment process takes place in an SBR reactor, where the wastewater is fed discontinuously and treated through a cycle which is repeated over time. The duration of each cycle has been set at six hours ($\tau = 0.25\ d$), as in the experiments carried out in [2]. Each cycle is based on a first phase of darkness (three hours), when no light source is provided to the system, followed by a phase of light (three hours) when the reactor is supposed to be homogeneously illuminated in every points. In particular, in the first two studies, the incident light intensity I_0 is fixed at $0.008\ kmol\ m^{-2}\ d^{-1}$, similar to [2, 38]. As noted in [2], this value favors the growth of cyanobacteria at the expense of microalgae, and therefore guarantees greater chances of success of the granulation process. Instead, a number of I_0 values have been used in the last study and they will

Parameter	Definition	Unit	Value	Ref
$\phi_{EPS,A}$	Relative rate of EPS formation to A production	$--$	0.1	(a)
$\phi_{EPS,C}$	Relative rate of EPS formation to C production	$--$	0.3	(a)
$k_{EPS,H}$	EPS fraction produced by H	$--$	0.18	[78]
$k_{EPS,N}$	EPS fraction produced by N	$--$	0.075	[78]
k_{DOC}	DOC release fraction by A and C	$--$	0.05	[119]
k_{La}	O_2 mass transfer coefficient	d^{-1}	23.3	[84]
$S_{O2,sat}$	O_2 saturation concentration in bulk liquid	$kmol(O_2)\ m^{-3}$	$2.4 \cdot 10^{-4}$	[84]
$I_{opt,A}$	Optimum light intensity for A	$kmol(e^-)\ m^{-2}\ d^{-1}$	0.01728	[48]
$I_{opt,C}$	Optimum light intensity for C	$kmol(e^-)\ m^{-2}\ d^{-1}$	0.00864	(a)
η_A	Coeff. of adaptability to non-optimal light for A	$--$	1	(a)
η_C	Coeff. of adaptability to non-optimal light for C	$--$	0.6	(a)
k_{tot}	Light attenuation coefficient	$m^2\ kg^{-1}$	210	[138]
$D_{S,IC}$	Diffusion coefficient of IC in biofilm	$m^2\ d^{-1}$	$1.32 \cdot 10^{-4}$	[138]
$D_{S,DOC}$	Diffusion coefficient of DOC in biofilm	$m^2\ d^{-1}$	$0.83 \cdot 10^{-4}$	[132]
$D_{S,NO3}$	Diffusion coefficient of NO_3 in biofilm	$m^2\ d^{-1}$	$1.18 \cdot 10^{-4}$	[138]
$D_{S,NH3}$	Diffusion coefficient of NH_3 in biofilm	$m^2\ d^{-1}$	$1.49 \cdot 10^{-4}$	[132]
$D_{S,O2}$	Diffusion coefficient of O_2 in biofilm	$m^2\ d^{-1}$	$1.75 \cdot 10^{-4}$	[132]
$v_{a,C}$	Attachment velocity of ψ_C^*	$m\ d^{-1}$	$5 \cdot 10^{-3}$	(a)
$v_{a,A}^0$	Attachment velocity of ψ_A^*	$m\ d^{-1}$	$5 \cdot 10^{-4}$	(a)
$v_{a,H}^0$	Attachment velocity of ψ_H^*	$m\ d^{-1}$	$5 \cdot 10^{-4}$	(a)
$v_{a,N}^0$	Attachment velocity of ψ_N^*	$m\ d^{-1}$	$5 \cdot 10^{-4}$	(a)
K_C	Half saturation coeff. of ψ_C^* on ψ_A^*, ψ_H^*,ψ_N^* attachment	$kg(COD)\ m^{-3}$	$3 \cdot 10^{-2}$	(a)
ρ	Biofilm density	$kg(COD)\ m^{-3}$	37	[84]
λ	Constant detachment coefficient	$m^{-1}\ d^{-1}$	50	(a)
V	Reactor volume	m^3	400	(a)
N_G	Number of granules in the reactor	$--$	$2.4 \cdot 10^{10}$	(a)
τ	Duration of the cycle	d	0.25	(a)
γ	Fraction of suspended biomass lost during the emptying	$--$	0.2	(a)
ω	Emptying/relling ratio	$--$	0.5	(a)

(a) Assumed

Table 5.2: Other model parameters

be specified later. Cyanobacteria play a key role in the formation of photogranules thanks to their properties. Such role is modelled by setting the attachment velocity of cyanobacteria an order of magnitude higher than the attachment velocity of the other species. The number of granules N_G is calculated in order to have a reactor filled by biofilm biomass for approximately 25% of volume once the granules have reached the steady-state dimension. All parameters used in this model are reported in Tables 5.1 and 5.2.

The same composition is considered for the influent of each treatment cycle. In particular, no suspended biomass is supposed to be present in the influent, while the concentration of soluble substrates varies from case to case and will be specified in each

study as appropriate. The initial concentration of soluble substrates within the reactor has been set equal to the concentration within the influent. Furthermore, a phototrophic inoculum of suspended cyanobacteria and microalgae is considered, where suspended heterotrophic and nitrifying bacteria are present in smaller amounts: $\psi^*_{A,0} = \psi^*_{C,0} = 300\ g\ m^{-3}$, $\psi^*_{H,0} = \psi^*_{N,0} = 50\ g\ m^{-3}$.

5.3.1 Study 1 - OPGs-based system fed with a typical municipal wastewater

In this study, the treatment process within the OPG-based system and the distribution of biomass within the photogranules are investigated in the case of a typical municipal wastewater. For this purpose, the following influent composition is considered: $S^{in}_{IC} = 180\ g\ m^{-3}$, $S^{in}_{DOC} = 500\ g\ m^{-3}$, $S^{in}_{NH_3} = 50\ g\ m^{-3}$, $S^{in}_{NO_3} = S^{in}_{O_2} = 0\ g\ m^{-3}$. The results are shown in Figs. 5.1-5.5.

Fig. 5.1 reports the distribution of biomass within the photogranules, after 50 days of simulation, while Fig. 5.2 presents the distribution of soluble substrates and the trend of light intensity along the granule radius at $T = 50\ d$ (before the emptying and refilling). From Fig. 5.1, it can be seen that photogranules are composed of a significant fraction of cyanobacteria, expecially in the external layers due to optimal light conditions, while they reduces by going towards the center, where light intensity decreases due to attenuation phenomena (see Fig. 5.2). On the other hand, microalgae are present in small amounts and confined to the outermost layers. In addition, optimal conditions for the growth of heterotrophic bacteria occur: the influent is rich in DOC and phototrophic organisms (microalgae and cyanobacteria) produce large amounts of O_2. As well as cyanobacteria, the fraction of heterotrophic bacteria is high in the external layers and reduces toward the granule nucleus, due to the DOC concentration gradients occurring along the granules (Fig. 5.2). Indeed, the high DOC concentration deriving from the liquid medium reduces along the granule due to diffusion and consumption in

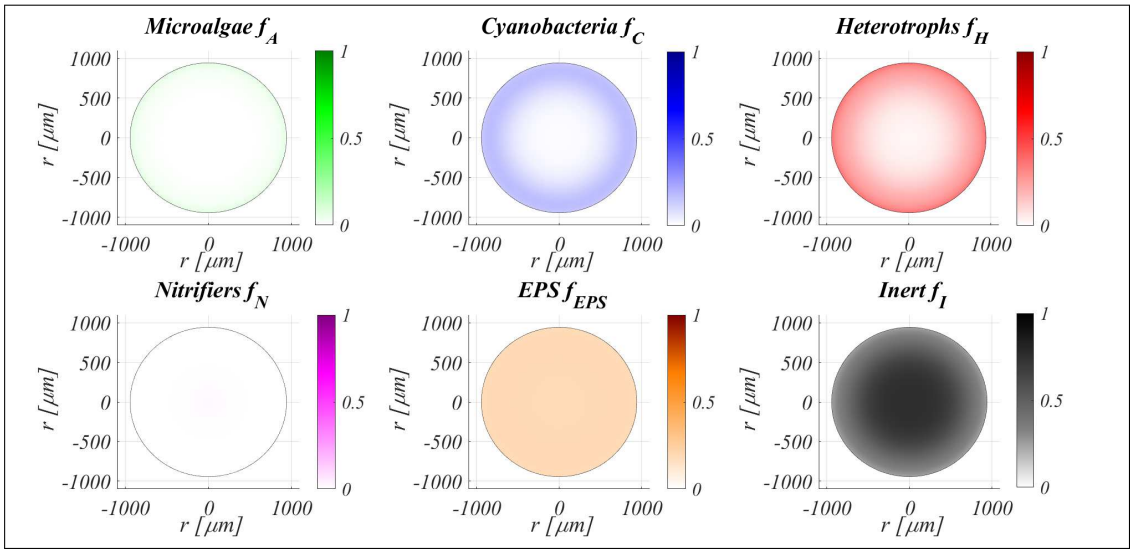

Figure 5.1: Study 1 - Microbial species distribution in the diametrical section, at $T = 50\ d$. Wastewater influent composition: $S_{IC}^{in} = 180\ g\ m^{-3}$ (inorganic carbon), $S_{DOC}^{in} = 500\ g\ m^{-3}$ (organic carbon), $S_{NH_3}^{in} = 50\ g\ m^{-3}$ (ammonia), $S_{NO_3}^{in} = 0\ g\ m^{-3}$ (nitrates), $S_{O_2}^{in} = 0\ g\ m^{-3}$ (oxygen). Incident light intensity: $I_0 = 0.008\ kmol\ m^{-2}\ d^{-1}$.

the outermost layers. Nitrifying bacteria are almost absent, because have lower maximum growth rates than heterotrophic bacteria which, consequently, in the presence of DOC are more competitive in the use of O_2. All active species contribute to the secretion of EPS, which has a homogeneous distribution throughout the granule. Finally, large quantities of inert material deriving by decay processes are found in the granule, especially in the internal layers.

Fig. 5.3 reports the evolution of the photogranule radius $R(t)$ over time. In the initial phase the intense attachment process lead to a linear increase of the radius over time. Subsequently, detachment processes become more relevant as the granule dimension increases, and limit the growth of the granule, which reaches its steady-state dimension after 40-50 days.

Fig. 5.4 shows how the concentration of substrates within the reactor varies over time. The observation period reported goes from day 49 to day 50, which is likely to describe the treatment process under operating conditions. Indeed, it is observed that the start-up of the system is completed before this time: photogranules have reached a

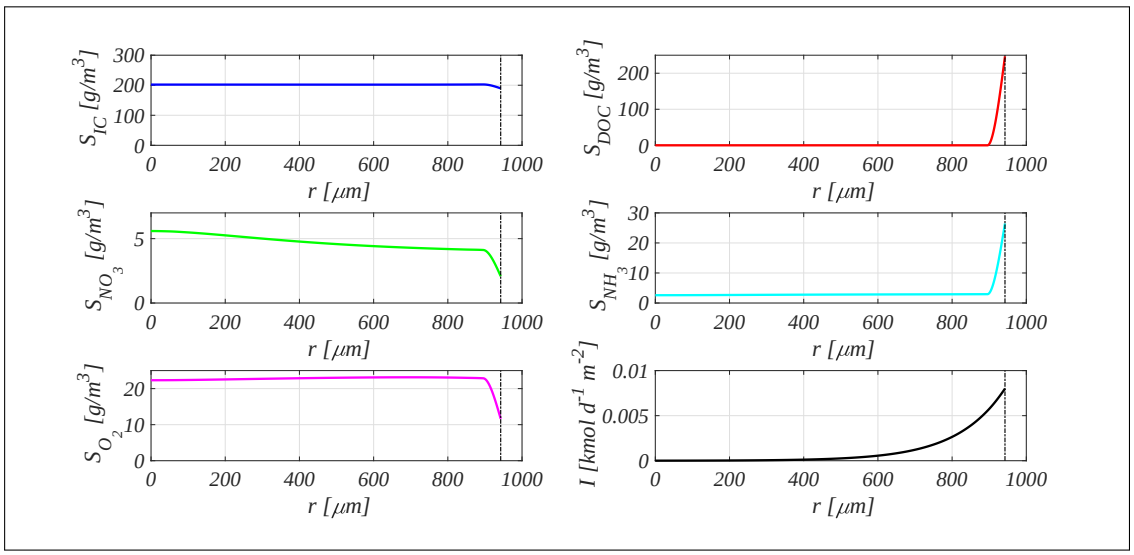

Figure 5.2: Study 1 - Distribution of soluble substrates and trend of light intensity along the granule radius at $T = 50\ d$ (before the emptying and refilling). Wastewater influent composition: $S^{in}_{IC} = 180\ g\ m^{-3}$ (inorganic carbon), $S^{in}_{DOC} = 500\ g\ m^{-3}$ (organic carbon), $S^{in}_{NH_3} = 50\ g\ m^{-3}$ (ammonia), $S^{in}_{NO_3} = 0\ g\ m^{-3}$ (nitrates), $S^{in}_{O_2} = 0\ g\ m^{-3}$ (oxygen). Incident light intensity: $I_0 = 0.008\ kmol\ m^{-2}\ d^{-1}$.

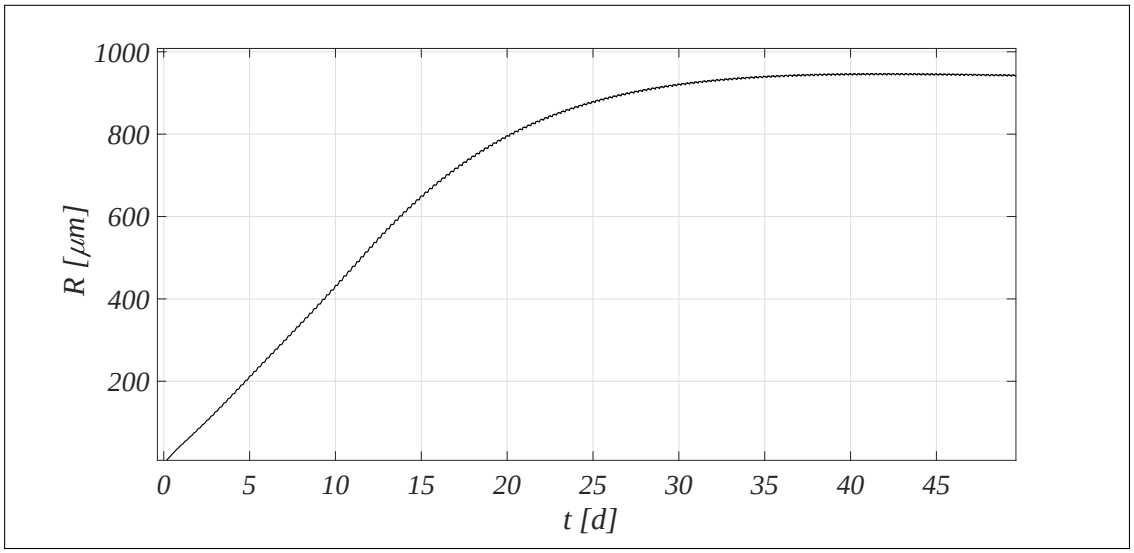

Figure 5.3: Study 1 - Evolution of biofilm radius over time. Wastewater influent composition: $S^{in}_{IC} = 180\ g\ m^{-3}$ (inorganic carbon), $S^{in}_{DOC} = 500\ g\ m^{-3}$ (organic carbon), $S^{in}_{NH_3} = 50\ g\ m^{-3}$ (ammonia), $S^{in}_{NO_3} = 0\ g\ m^{-3}$ (nitrates), $S^{in}_{O_2} = 0\ g\ m^{-3}$ (oxygen). Incident light intensity: $I_0 = 0.008\ kmol\ m^{-2}\ d^{-1}$.

steady-state dimension and the trend of the substrates concentration and the final composition of the effluent are repeated identically in each cycle. Since all cycles last six hours, Fig. 5.4 shows four consecutive cycles, where a dark phase (grey portion of the graphic) and a light phase (white portion of the graphic) are distinguished. At the end of each cycle there is a discontinuity in the graphs, which indicates the emptying of the reactor and refilling with a new wastewater volume to be treated. At the beginning of the cycle, a very rapid reduction of DOC and NH_3 is observed, due to all aerobic processes of microbial growth. In particular, the large amount of O_2 produced in the previous cycle leads to optimal conditions for the growth of aerobic heterotrophic bacteria, nitrifying bacteria, microalgae and cyanobacteria (in the absence of light the last two species adopt heterotrophic metabolic pathways). When O_2 concentration reduces, anoxic heterotrophs grow by consuming the small amount of NO_3 remained within the reactor from the previous cycle. However, the amount of NO_3 is extremely low and therefore the contribution that anoxic processes provide to the consumption of DOC and NH_3 is pratically negligible. When oxidized substrates drop to very low concentrations, they become limiting for microbial kinetics and a clear change in slope is observed in the trends of DOC, NH_3 and IC: growth rates are very low and lead to a slight consumption of DOC and NH_3 and a slight production of IC. This trend marks the remaining dark period. After it, the light source is provided in the reactor. Both cyanobacteria and microalgae adopt photoautotrophic metabolic strategies and produce large amounts of O_2. Aerobic heterotrophic and nitrifying bacteria find again optimal conditions for their metabolic growth and consequently, the consumption rates of DOC and NH_3 increases. As long as DOC is present in the reactor, heterotrophic bacteria govern the treatment process, being more competitive than nitrifying bacteria in using the O_2 produced by cyanobacteria and microalgae. To confirm this, no production of NO_3 is observed. When DOC tends to deplete, the growth of the heterotrophs slows down, their consumption of O_2 and NH_3 reduces, and nitrifying bacteria take over the process. Indeed, NH_3 continues to be consumed with a different rate and a slight pro-

duction of NO_3 is observed. Anyway, as already observed in Fig. 5.1, the fraction of nitrifying bacteria within the granule and their growth rate are very low, therefore the production of NO_3 is limited and the O_2 concentration increases again because the autotrophic consumption does not balance the photoautotrophic production. Regarding the IC concentration, it is associated to the trend of DOC: when DOC is present in the reactor, IC increases over time, because heterotrophic bacteria are the most competitive species and their IC production prevails over consumption processes, while IC reduces over time when DOC finishes, because the heterotrophic growth is inhibited and the photosynthetic activity of cyanobacteria and microalgae prevails. As can be seen in the Fig. 5.4, the trends of the substrates concentration described above are repeated identically in each cycle and are representative of the treatment cycle of an OPG-based system under operating conditions. The concentrations of the substrates at the end of the cycle are representative of the effluent composition. In this case, the removal efficiency is high: DOC has been completely removed and very low concentrations of nitrogen compounds are observed (less than $5\ g\ m^{-3}$ of NO_3). Obviously the operation of this system and the evolution of the granules are strongly influenced by the type of wastewater influent. For this reason, in the second study the treatment process will be investigated in the case of different compositions of the influent.

Fig. 5.5 reports the concentration of suspended biomasses within the reactor over time. It should be noted that the concentration trends have a discontinuity every six hours, at the end of each cycle, when 20% of each suspended biomass is supposed to be lost during the emptying phase, due to not perfect settling properties. Consequently, phenomena leading to the reduction of suspended biomass within the SBR are the attachment (the biomass swich its phenotype from suspended to sessile, going to constitute the biofilm granules), the emptying of the reactor and the decay processes, while the processes of metabolic growth lead to an increase of the suspended biomass.

Heterotrophic bacteria have higher maximum growth rates than other microbial species and their concentration significantly increases during the start-up phase of the

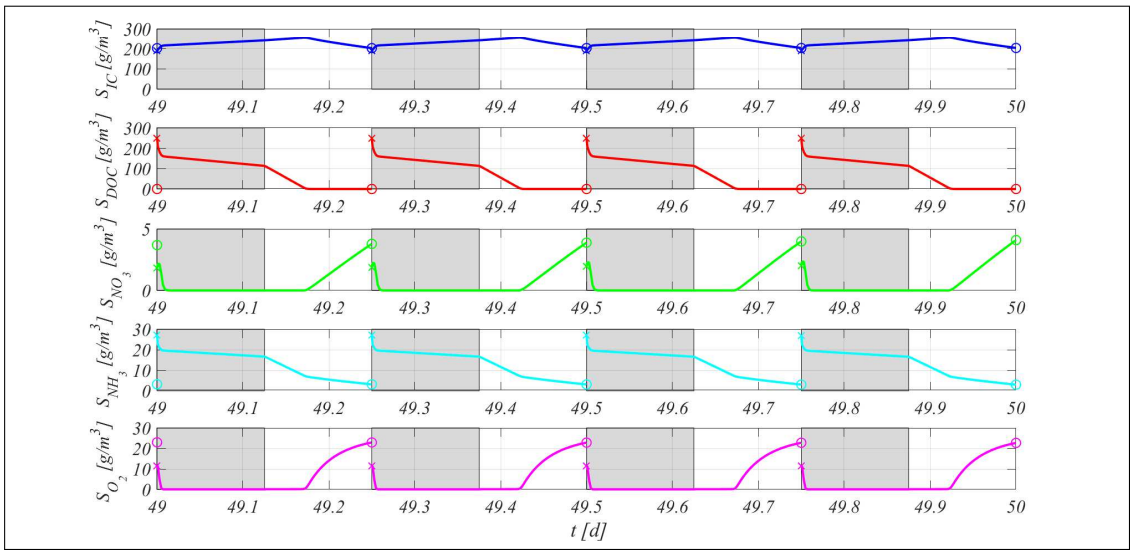

Figure 5.4: Study 1 - Evolution of soluble substrates concentration within the reactor, from $T = 49\ d$ to $T = 50\ d$ (four consecutive six-hours treatment cycles). Wastewater influent composition: $S_{IC}^{in} = 180\ g\ m^{-3}$ (inorganic carbon), $S_{DOC}^{in} = 500\ g\ m^{-3}$ (organic carbon), $S_{NH_3}^{in} = 50\ g\ m^{-3}$ (ammonia), $S_{NO_3}^{in} = 0\ g\ m^{-3}$ (nitrates), $S_{O_2}^{in} = 0\ g\ m^{-3}$ (oxygen). Incident light intensity: $I_0 = 0.008\ kmol\ m^{-2}\ d^{-1}$. Grey portions indicate the dark phases, white portions indicate the light phases.

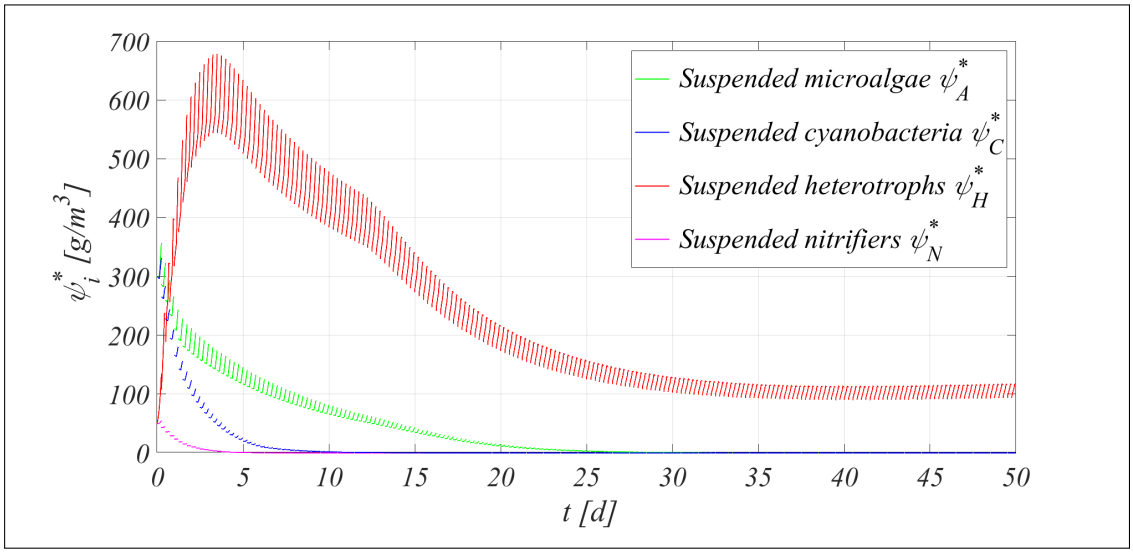

Figure 5.5: Study 1 - Evolution of suspended biomasses concentration within the reactor. Wastewater influent composition: $S_{IC}^{in} = 180\ g\ m^{-3}$ (inorganic carbon), $S_{DOC}^{in} = 500\ g\ m^{-3}$ (organic carbon), $S_{NH_3}^{in} = 50\ g\ m^{-3}$ (ammonia), $S_{NO_3}^{in} = 0\ g\ m^{-3}$ (nitrates), $S_{O_2}^{in} = 0\ g\ m^{-3}$ (oxygen). Incident light intensity: $I_0 = 0.008\ kmol\ m^{-2}\ d^{-1}$.

reactor, when the granules are small and higher amounts of substrates are available for the suspended biomass. Later, photogranules grow and the contribution of sessile biomass to the consumption of soluble substrates increases. As a result, the amount of substrates available for suspended biomass reduces and the concentration of suspended heterotrophs decreases cycle after cycle until to reach a final trend which is repeated identically over time. Other species have low maximum growth rates and are all washed out over time, due to the processes described above. Suspended nitrifying bacteria are the slowest species to grow due to their low maximum growth rate and to the competition with heterotrophs for O_2, and are the first to be washed out. Suspended cyanobacteria and microalgae have similar metabolic activities but the first have better attachment properties and the higher attachment flux explains the faster reduction observed.

5.3.2 Study 2 - Effects of wastewater influent composition on the process

The performances of the OPG-based system are strongly influenced by the composition of the wastewater influent, which governs the evolution and the microbial composition of photogranules and consequently, the treatment process. The carbon and nitrogen loads and their ratio affect the metabolic activity of microbial species populating the granules and the purifying ability of these biomass assemblies. Therefore, it is interesting to compare the results of the previous study with other case study, where different types of influent wastewater are considered: an higher strength carbon wastewater (case 1), an ammonia wastewater (case 2) and a municipal wastewater with the presence of nitrates (case 3). The results of this study are summarized in Figs. 5.6-5.9. In particular, Figs. 5.6-5.8 focus on the concentration of soluble substrates in the system in the three cases, while the microbial composition of photogranules in such cases is reported in Fig. 5.9, and compared with the results of the first study.

Fig. 5.6 reports the concentration of soluble substrates within the reactor over time, in the period between 49 and 50 days, in the case of a high strength organic wastewater (case 1: $S_{IC}^{in} = 180\ g\ m^{-3}$, $S_{DOC}^{in} = 1000\ g\ m^{-3}$, $S_{NH_3}^{in} = 50\ g\ m^{-3}$, $S_{NO_3}^{in} = S_{O_2}^{in} = 0$). As in the case presented in the previous study, at the beginning of the cycle there is a rapid heterotrophic consumption of O_2 which is still in the reactor from the previous cycle. When this concentration approaches zero, the trend of substrate concentrations does not show high variations until the end of the dark period: a slight reduction of DOC and NH_3 concentration and a slight increase of IC concentration are observed, caused by the metabolic activities of aerobic heterotrophic bacteria, microalgae and cyanobacteria. When the light period begins, cyanobacteria and microalgae carry out their photosynthetic activity and produce O_2 necessary for heterotrophs. As a result, a clear change in slope is observed in the trends of DOC and NH_3 concentrations, which reduce due to the fast consumption by heterotrophic bacteria growing in optimal conditions. In the last part of the cycle, NH_3 runs out, hence, the heterotrophic kinetics slow down again and the O_2 concentration increases up to $3\ g\ m^{-3}$. As can be seen, in this case NO_3 concentration is nearly zero throughout the cycle and suggests that the amount of nitrifying bacteria populating the photogranule is negligible. Indeed, as already mentioned in Study 1, compared to heterotrophs, nitrifying bacteria have lower maximum growth rates and are less competitive in the use of O_2, and develop only in poor-DOC environments. In this case the high DOC amounts present throughout the cycle do not allow their growth. At the end of the cycle, although NH_3 has been completely removed, large concentrations of DOC are still present in the effluent.

Fig. 5.7 presents the trend of the substrates concentration within the reactor in the case of an ammonia wastewater influent (case 2: $S_{IC}^{in} = 180\ g\ m^{-3}$, $S_{NH_3}^{in} = 100\ g\ m^{-3}$, $S_{DOC}^{in} = S_{NO_3}^{in} = S_{O_2}^{in} = 0$). In this case, the process is strongly influenced by the absence of DOC in the influent. Indeed, DOC concentration is extremely low and limiting for the heterotrophic growth throughout the cycle, and the process is mainly driven by nitrifying bacteria, microalgae and cyanobacteria. In dark conditions, the growth rate

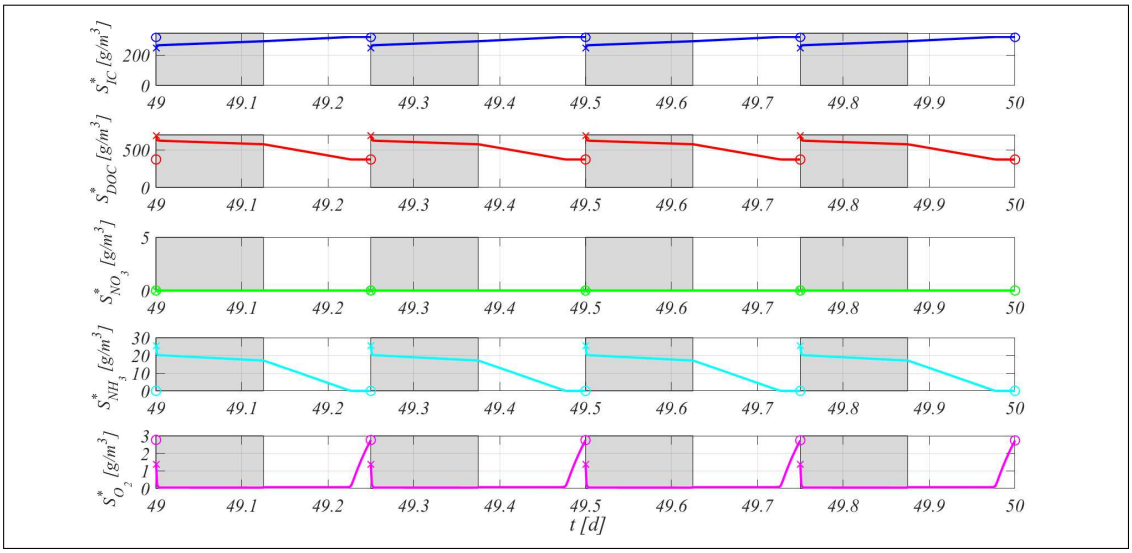

Figure 5.6: Study 2 (Case 1) - Evolution of soluble substrates concentration within the reactor, from $T = 49\ d$ to $T = 50\ d$ (four consecutive six-hours treatment cycles). Wastewater influent composition: $S^{in}_{IC} = 180\ g\ m^{-3}$ (inorganic carbon), $S^{in}_{DOC} = 1000\ g\ m^{-3}$ (organic carbon), $S^{in}_{NH_3} = 50\ g\ m^{-3}$ (ammonia), $S^{in}_{NO_3} = 0\ g\ m^{-3}$ (nitrates), $S^{in}_{O_2} = 0\ g\ m^{-3}$ (oxygen). Incident light intensity: $I_0 = 0.008\ kmol\ m^{-2}\ d^{-1}$. Grey portions indicate the dark phases, white portions indicate the light phases.

of microalgae, cyanobacteria and nitrifying bacteria is very low due to the DOC and O_2 shortage. For this reason, the concentration of DOC, IC and $O2$ is almost constant throughout the dark period and only a slight consumption of NH_3 and a slight production of NO_3 are observed. As light conditions within the system change, microbial growth rates increase. In particular, photoautotrophic processes in the presence of light lead to the production of O_2; consequently the growth rate of nitrifying bacteria also increases. NH_3 and IC reduce due to the combined effect of these growth processes, while the growth of nitrifying bacteria also induces an increase in the concentration of NO_3. In the final phase of the cycle, a change in the slope of the O_2 concentration trend is observed, which increases again because IC runs out and limits the activity of nitrifying bacteria and their O_2 consumption. The photosynthetic activity of microalgae and cyanobacteria involve a low release of DOC which, however, is immediately degraded by heterotrophs. As can be seen from the concentrations at the end of the cycles, in this case nitrogen is not effectively removed from the wastewater, since about

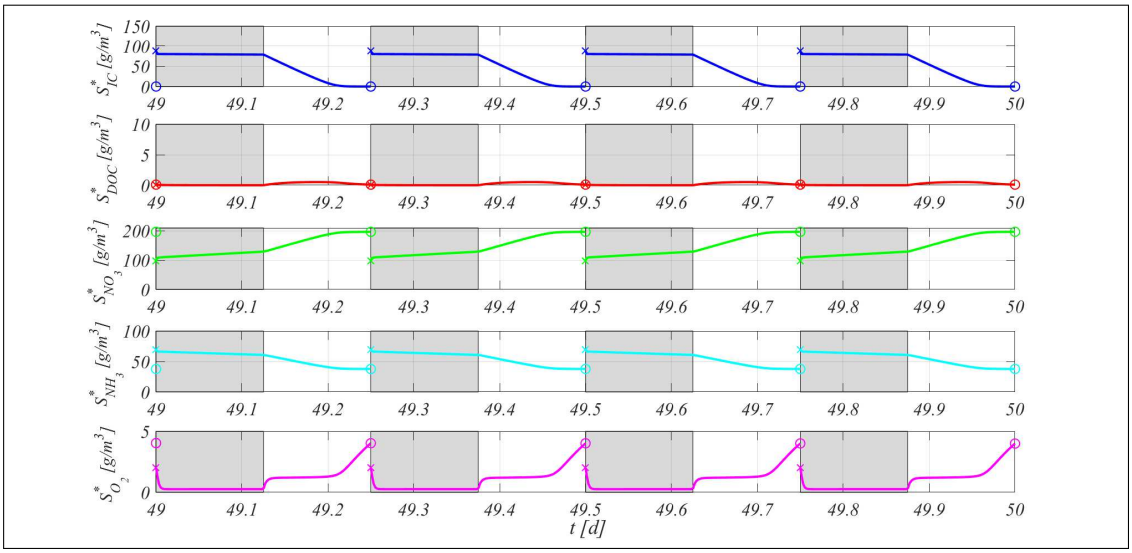

Figure 5.7: Study 2 (Case 2) - Evolution of soluble substrates concentration within the reactor, from $T = 49\ d$ to $T = 50\ d$ (four consecutive six-hours treatment cycles). Wastewater influent composition: $S^{in}_{IC} = 180\ g\ m^{-3}$ (inorganic carbon), $S^{in}_{DOC} = 0\ g\ m^{-3}$ (organic carbon), $S^{in}_{NH_3} = 100\ g\ m^{-3}$ (ammonia), $S^{in}_{NO_3} = 0\ g\ m^{-3}$ (nitrates), $S^{in}_{O_2} = 0\ g\ m^{-3}$ (oxygen). Incident light intensity: $I_0 = 0.008\ kmol\ m^{-2}\ d^{-1}$. Grey portions indicate the dark phases, white portions indicate the light phases.

50% of NH_3 influent concentration is still present in the effluent and another significant nitrogen amount is found in the form of NO_3.

Finally, the trend of the concentration of soluble substrates within the SBR over time in the case of a municipal wastewater with presence of nitrates is shown in Fig. 5.8 (case 3: $S^{in}_{IC} = 180\ g\ m^{-3}$, $S^{in}_{DOC} = 500\ g\ m^{-3}$, $S^{in}_{NO_3} = 100\ g\ m^{-3}$, $S^{in}_{NH_3} = 50\ g\ m^{-3}$, $S^{in}_{O_2} = 0$). At the beginning of the cycle, there is a high concentration of DOC and oxidized compounds (O_2 and NO_3) in the reactor and therefore there are optimal conditions for the growth of heterotrophs, first aerobic and then anoxic (when O_2 runs out). Consequently, the conversion of most of DOC and NH_3 present is observed in the initial phase of the dark period. When concentrations of O_2 and NO_3 reduce, they limit heterotrophic kinetics and the consumption rate of DOC and NH_3 slows down. However, as can be seen, DOC has been almost completely removed from the system at the end of the dark period. When light conditions change, the photosynthetic activity of microalgae and cyanobacteria leads to the consumption of NH_3 and the increase of O_2

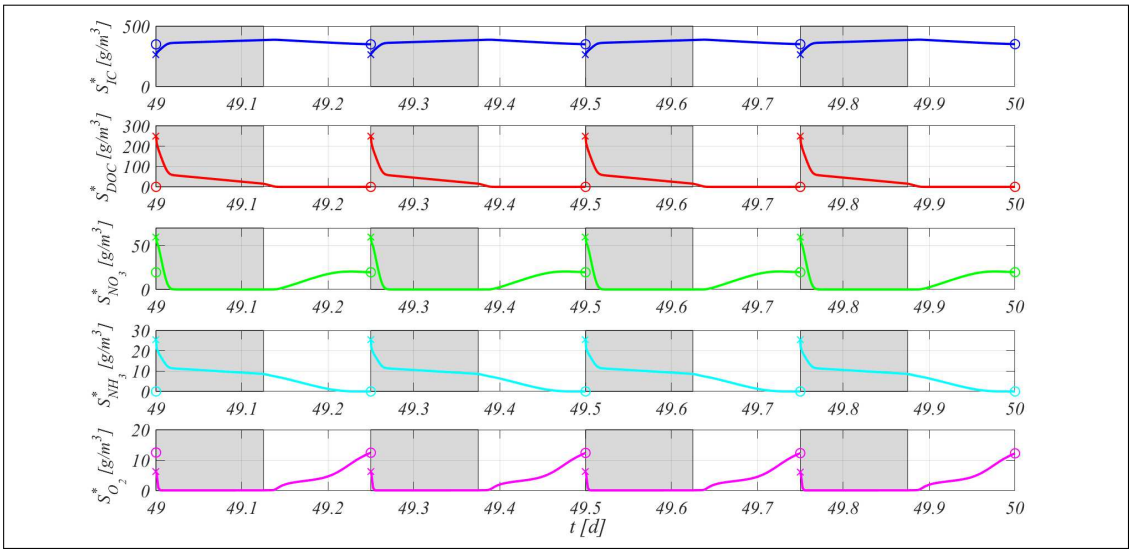

Figure 5.8: Study 2 (Case 3) - Evolution of soluble substrates concentration within the reactor, from $T = 49\ d$ to $T = 50\ d$ (four consecutive six-hours treatment cycles). Wastewater influent composition: $S^{in}_{IC} = 180\ g\ m^{-3}$ (inorganic carbon), $S^{in}_{DOC} = 500\ g\ m^{-3}$ (organic carbon), $S^{in}_{NH_3} = 50\ g\ m^{-3}$ (ammonia), $S^{in}_{NO_3} = 100\ g\ m^{-3}$ (nitrates), $S^{in}_{O_2} = 0\ g\ m^{-3}$ (oxygen). Incident light intensity: $I_0 = 0.008\ kmol\ m^{-2}\ d^{-1}$. Grey portions indicate the dark phases, white portions indicate the light phases.

concentration. Since DOC concentration is low, heterotrophic bacteria are not competitive and the oxygen produced is partially consumed by nitrifying bacteria, which convert the remaining NH_3 into NO_3. By observing the concentration of the soluble substrates at the end of the cycle, it is clear that the treatment cycle lead to the complete removal of DOC and NH_3, while a NO_3 concentration of about 20 $g\ m^{-3}$ is found in the effluent.

Fig. 5.9 shows the biomass distribution along the granule radius at 50 days, in the four cases described until now. In the case of a typical municipal wastewater (top left) and in the case of a higher strength carbon wastewater (top right) the microbial distribution is very similar. To explain this result it is necessary to note that the two influent wastewaters differ only in the DOC load. In the latter case, the growth kinetics of heterotrophic bacteria slow down during the light period, due to the depletion of NH_3 (as can be seen in Fig. 5.6). Consequently, most of additional amount of DOC present in this case is not consumed due to the lack of NH_3 and does not lead to significant

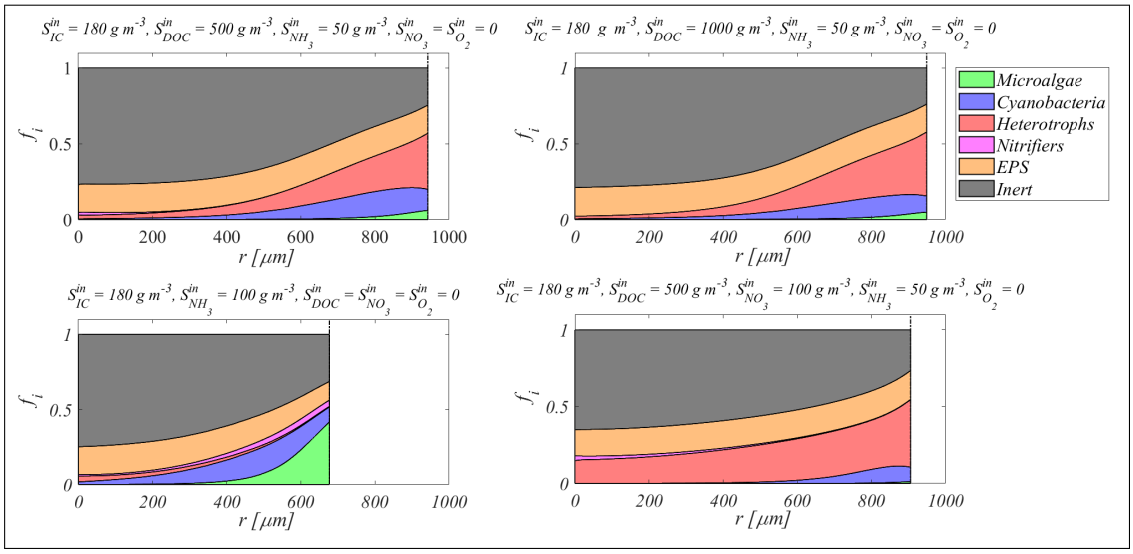

Figure 5.9: Study 2 - Microbial species distribution across the radius of the granule at $T = 50\ d$, in the four cases reported in Study 1 and Study 2. Incident light intensity: $I_0 = 0.008\ kmol\ m^{-2}\ d^{-1}$.

differences in the growth and distribution of biomass within the photogranule reported in the case of a typical municipal wastewater. In the case of an ammonia wastewater (bottom left), results are totally different. DOC is not present in the influent, hence, the only available carbon source for heterotrophs derives from the photoautotrophic release during the light period. However, such release is limited and just allows the growth of small amounts of heterotrophic biomass. Conversely, as there is no spatial competition with heterotrophs, high fractions of both cyanobacteria and microalgae are observed, and a small fraction of nitrifying bacteria, which is almost zero in the other cases, is also visible.

Anyway, due to the shortage of DOC and the low heterotrophic contribution to the growth process, granules which develop in this case are reasonably smaller than in the other cases. Lastly, in the case of a municipal wastewater with presence of nitrates (bottom right), granules are populated by high fractions of heterotrophs, higher than previous cases, while microalgae are almost absent and cyanobacteria fraction is low and limited to the outermost layers. This is due to the high concentration of NO_3 present in the influent which, in anoxic conditions, replaces O_2 as the oxidized substrate for the

metabolic activity of anoxic heterotrophs. Consequently, the growth of heterotrophs is not related exclusively to the production of O_2 by microalgae and cyanobacteria, but also occurs when there is no O_2, such as during the dark period (Fig. 5.8). The sum of aerobic and anoxic growth processes leads to larger fractions of heterotrophs than the previous cases. In conclusion, in the first three cases, the formation and evolution of photogranules is strongly related to the photosynthetic activity, while in the last case the denitrification processes become dominant and take over the photoautotrophic processes.

5.3.3 Study 3 - Effects of light conditions on the process

Light governs the metabolic activity of phototrophic organisms and the photogranules evolution, and therefore represents a key factor in the OPG-based system. Moreover, light conditions affect the relative abundance of cyanobacteria and microalgae within the granule and also their ratio. As reported in Section 5.1, microalgae and cyanobacteria have distinct modes of light harvesting and utilization which lead to different ecological niches. Specifically, under high light intensities the growth of microalgae is favored over cyanobacteria, which, however, are able to grow even in unfavorable light conditions. In this framework, such numerical study is aimed to prove that the model can correctly describe the effects of light on microalgae and cyanobacteria growth and on the performances of the system. For this purpose, various simulations have been carried out by varying the incident light intensity I_0. The same influent composition of the first study is considered: $S_{IC}^{in} = 180\ g\ m^{-3}$, $S_{DOC}^{in} = 500\ g\ m^{-3}$, $S_{NH_3}^{in} = 50\ g\ m^{-3}$, $S_{NO_3}^{in} = S_{O_2}^{in} = 0$.

Fig. 5.10 and Fig. 5.11 report results on the microbial composition within the photogranule under different light conditions. Specifically, Fig. 5.10 shows the overall mass of phototrophs and the mass of cyanobacteria and microalgae, while Fig. 5.11 shows the relative abundance (top) and mass (bottom) of sessile microbial species within the

granule. The numerical results of both figures refer to $T = 50\ d$. The overall phototrophic mass (sum of cyanobacteria and microalgae) increases with light conditions (Fig. 5.10), while the masses of cyanobacteria and microalgae are highly variable. The mass of microalgae increases with I_0, because their light dependency coefficient is directly proportional to I_0 in the range of values investigated (photoinhibition phenomena do not occur at these I_0 values). However, the mass of microalgae is very low up to $I_0 = 0.008\ kmol\ m^{-2}\ d^{-1}$ and limited by the competition with cyanobacteria, which have the ability to adapt to not optimal light conditions. The mass of cyanobacteria reaches the maximum value for $I_0 = 0.008\ kmol\ m^{-2}\ d^{-1}$ and decreases for higher values due to two reasons: optimal light conditions for cyanobacteria are supposed to be lower than these light conditions, hence, photoinhibition phenomena occur and limit the cyanobacterial growth; in addition, at these high light intensities, cyanobacteria suffer the competition with microalgae, which find optimal conditions to grow. Finally, in the case of $I_0 = 0.001\ kmol\ m^{-2}\ d^{-1}$, light conditions are too poor even for cyanobacterial metabolic activity and small amounts of phototrophic mass and small granule dimension are observed. Indeed, due to a very low incident light intensity, the photosynthetic activity of microalgae and cyanobacteria is limited and leads to low O_2 productions. This also influences the growth of the other active biomasses. The result is the formation of small granules and little microbial mass. Finally, in Fig. 5.11, it is noted that high fractions of heterotrophic bacteria and EPS are found in the photogranule for all I_0 values, while in no case the fraction of nitrifying bacteria is visible.

Fig. 5.12 reports the trend of the substrates concentration in the reactor under four different light conditions ($I_0 = 0.001 - 0.004 - 0.008 - 0.013\ kmol\ m^{-2}\ d^{-1}$). The period shown is one complete cycle (six hours), starting from day 49. Results of the four simulations differ in the light conditions which are provided in the second phase of the cycle (light period), while there are no differences during the dark phase, when a null value of I_0 is set for all cases. For this reason, trends of the substrates concentration are very similar during the dark period and differ mainly in the values at the beginning

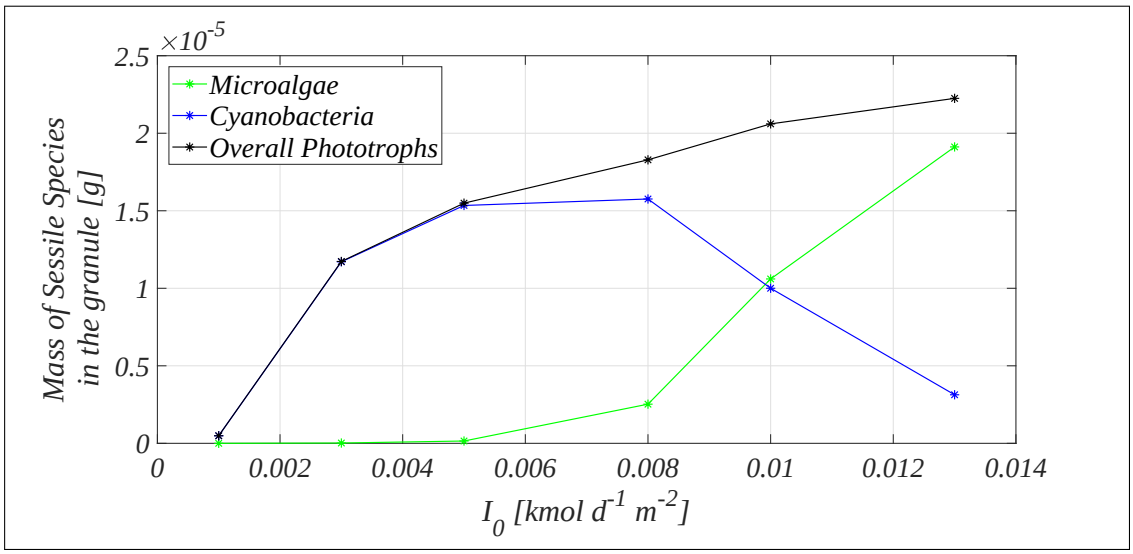

Figure 5.10: Study 3 - Mass of overall phototrophs, cyanobacteria and microalgae within the granule at $T = 50\ d$ to vary the incident light intensity I_0. Wastewater influent composition: $S^{in}_{IC} = 180\ g\ m^{-3}$ (inorganic carbon), $S^{in}_{DOC} = 500\ g\ m^{-3}$ (organic carbon), $S^{in}_{NH_3} = 50\ g\ m^{-3}$ (ammonia), $S^{in}_{NO_3} = 0\ g\ m^{-3}$ (nitrates), $S^{in}_{O_2} = 0\ g\ m^{-3}$ (oxygen).

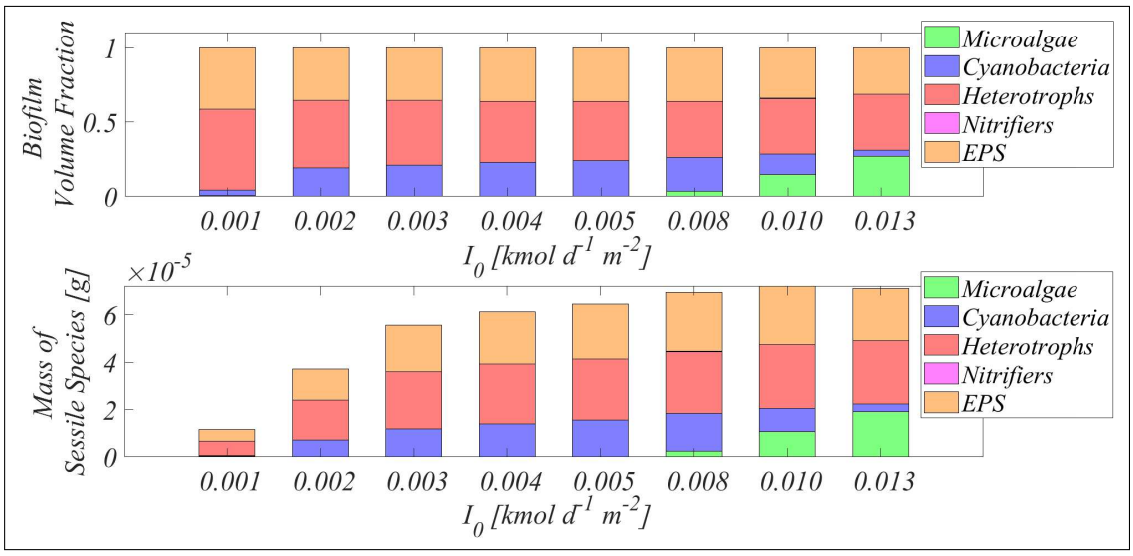

Figure 5.11: Study 3 - Relative abundances (bottom) and mass (top) of microbial species within the granule at $T = 50\ d$ under different light conditions. Wastewater influent composition: $S^{in}_{IC} = 180\ g\ m^{-3}$ (inorganic carbon), $S^{in}_{DOC} = 500\ g\ m^{-3}$ (organic carbon), $S^{in}_{NH_3} = 50\ g\ m^{-3}$ (ammonia), $S^{in}_{NO_3} = 0\ g\ m^{-3}$ (nitrates), $S^{in}_{O_2} = 0\ g\ m^{-3}$ (oxygen).

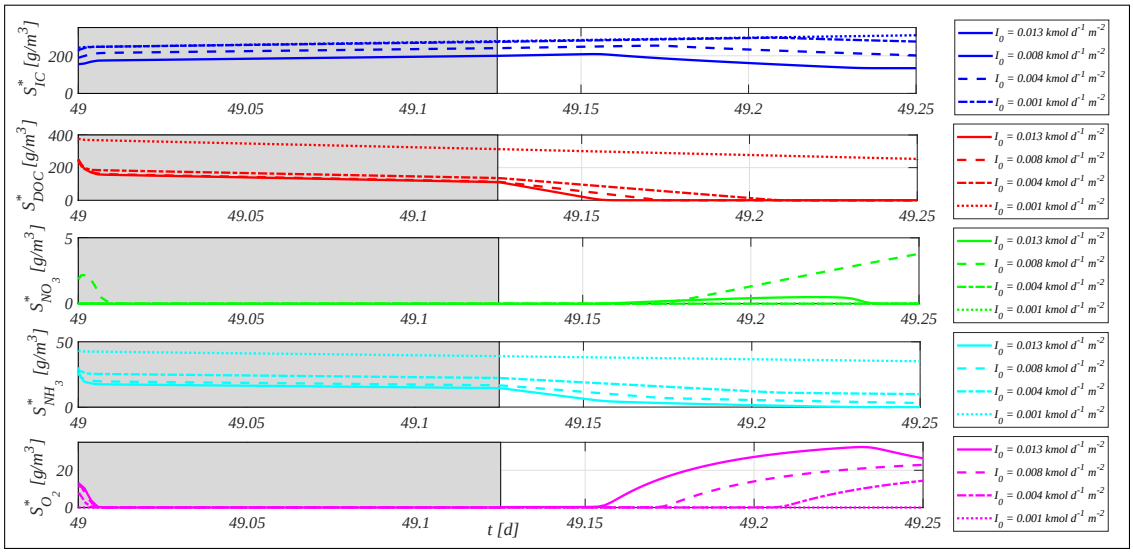

Figure 5.12: Study 3 - Evolution of soluble substrates concentration within the reactor, from $T = 49\ d$ to $T = 50\ d$ (four consecutive six-hours treatment cycles), under four different light conditions. Wastewater influent composition: $S^{in}_{IC} = 180\ g\ m^{-3}$ (inorganic carbon), $S^{in}_{DOC} = 500\ g\ m^{-3}$ (organic carbon), $S^{in}_{NH_3} = 100\ g\ m^{-3}$ (ammonia), $S^{in}_{NO_3} = 0\ g\ m^{-3}$ (nitrates), $S^{in}_{O_2} = 0\ g\ m^{-3}$ (oxygen). Grey portions indicate the dark phases, white portions indicate the light phases.

of the cycle, while significant differences are evident during the light phase. As I_0 increases going from 0.001 to $0.013\ kmol\ m^{-2}\ d^{-1}$, the rate of photosynthetic processes increases, hence, more O_2 is produced and more IC is consumed. The greater production of O_2 favors the microbial activity of heterotrophic bacteria and leads to the faster consumption of DOC and NH_3. In the case of $I_0 = 0.001\ kmol\ m^{-2}\ d^{-1}$, the treatment cycle does not take place efficiently and large quantities of DOC and NH_3 are found in the effluent, while in the other three cases, DOC is totally removed and NH_3 remains in low or null amounts. The trend of NO_3 needs some observations. Although in small quantities, NO_3 is produced in the case of $I_0 = 0.008\ kmol\ m^{-2}\ d^{-1}$, while in the other cases NO_3 is nearly zero throughout the cycle. When light conditions are poor ($I_0 = 0.001 - 0.004\ kmol\ m^{-2}\ d^{-1}$), DOC and NH_3 are present in the reactor throughout the cycle or almost, therefore the activity of heterotrophic bacteria strongly limits the nitrifying bacteria growth, and NO_3 production is not observed. On the other hand, when light conditions are high ($I_0 = 0.013\ kmol\ m^{-2}\ d^{-1}$), the consumption

of DOC and NH_3 is faster and is completed before the end of the cycle. Again, nitrifying bacteria are unable to grow and to produce NO_3 because they are limited by the absence of NH_3. In conclusion, $I_0 = 0.008\ kmol\ m^{-2}\ d^{-1}$ is the only case in which DOC runs out and not NH_3, and optimal conditions for the growth of nitrifying bacteria and the production of small amounts of NO_3 occur within the system. In the case of $I_0 = 0.013\ kmol\ m^{-2}\ d^{-1}$, a reduction of O_2 concentration is observed in the final part of the light phase. This occurs when both NH_4 and NO_3 are depleted and the photoautotrophic activity is limited by the lack of nutrients. Thus, the O_2 production reduces and the O_2 concentration decreases due to the effect of the gas transfer from liquid medium to the atmosphere.

5.4 Discussion and conclusions

In this section the results shown above are discussed, with the aim of outlining the main aspects of OPGs and the OPGs-based system and drawing general conclusions from the numerical studies carried out.

This model allows to simulate the formation and evolution of oxygenic photogranules within an SBR reactor and describe the microbial composition of such granular biofilms. In the case of a OPG-based system fed with a typical municipal wastewater, granules are populated by high amounts of cyanobacteria. Their fraction is highest in the most superficial layers, and reduces towards the center of the granule, where disadvantageous light conditions occur due to attenuation phenomena. However, their presence is also found in the middle layers of the granule because, as it is known, cyanobacteria have the ability to proliferate even under poor or non-optimal light conditions [120]. On the other hand, adaptation of microalgae to non-optimal light conditions is lower [120], and consequently their fraction is smaller than cyanobacteria and confined to the outermost layers of the granule. These results reflect what has been observed in [2, 3] under the same light and operating conditions used in this numerical

study. Moreover, large amounts of heterotrophs are observed while nitrifying bacteria are barely visible. This is due to the higher maximum growth rate of heterotrophs which, in presence of DOC, are more competitive of nitrifiers in the use of O_2 produced during the photosynthetic activity. Since the metabolic activity of nitrifying bacteria is negligible, concentration of NO_3 in the system is nearly zero throughout the cycle. Finally, a significant fraction of EPS is found throughout the granule, produced by all active microbial species and representing the "glue" that gives solidity and robustness to the aggregate. In conclusion, as suggested in [79, 7], the model confirm that the treatment process is governed by the symbiotic interaction between heterotrophs and phototrophs: phototrophs produce O_2 necessary for heterotrophs, which degrade the polluting compounds from the wastewater. The metabolic activity of heterotrophs is especially relevant in the light phase, when the photosynthetic activity of phototrophs guarantees high concentrations of O_2 in the system. Conversely, during the dark phase, all microbial growth processes slow down. The DOC/NH_3 ratio in the influent is the key parameter to achieve the efficient treatment of the wastewater and simultaneously remove DOC and NH_3 in the desired quantities. If such ratio is too high (Study 2, case 1), NH_3 runs out during the cycle (when DOC is still present), becomes limiting for the kinetics of heterotrophs and phototrophs, and DOC removal does not take place efficiently. If such ratio is too low (Study 2, case 2), excess NH_3 feed the metabolic pathway of nitrifying bacteria, converting into NO_3, and a nitrogen amount remains in the effluent in oxidized form.

The granule microbial composition just described in the case of a typical municipal wastewater can totally change as the composition of the influent changes. For example, in the case of an ammonia wastewater in which DOC is not present (Study 2, case 3), the growth of heterotrophs is severely limited and is exclusively supported by the low phototrophic DOC release during the photosynthetic activity. Consequently, the heterotrophic fraction is very small and, on the other hand, higher fractions of cyanobacteria and microalgae are observed. Without heterotrophic competition, nitrifying bacteria

find optimal conditions to grow and this time they are visible in the granule, albeit in very low fractions due to their low growth rate. An intense metabolic activity of nitrifying bacteria does not allow the effective removal of nitrogen from the wastewater, because it leads to the production of high NO_3 amounts which are found in the effluent.

In the case of a municipal wastewater with high presence of NO_3 (Study 2, case 3), heterotrophic growth is supported especially during the dark period. Indeed, in the absence of light and photosynthetic activity, O_2 runs out quickly and the subsequent anoxic conditions favor the growth of denitrifying heterotrophs, through the oxidation of high NO_3 amounts present within the reactor. The result is a photogranule constituted by high fractions of heterotrophs which take over cyanobacteria and microalgae, present in extremely modest fractions and limited to the most superficial layers. Therefore, in this case the treatment cycle is mostly governed by denitrification processes and not by aerobic processes. It should be emphasized that the latter is a theoretical result suggested by the model, that should be supported by experimental evidence. Indeed, as it is known, cyanobacteria play a key role in the formation of photogranules and preservation of the spherical structure, but in such case their modest presence may not guarantee the development and the preservation of the granular structure.

Furthermore, the model outlines the key role of light conditions on the treatment process occurring in OPG-based systems, by analyzing their effects on the evolution of the granules, on the growth of the overall phototrophic biomass, on the relative abundance of cyanobacteria and microalgae and on the performances of the system. Poor light conditions severely affect the metabolic activity of all active biomasses: they limit the photosynthetic activity and the phototrophic growth, and lead to low O_2 productions, not sufficient to support the growth of heterotrophic and nitrifying bacteria. Therefore, granules formed have small dimension and the global biomass present in the system only partially remove the polluting compounds from the influent wastewater. Under better light conditions, the photosynthetic activity takes place more effectively and leads to the optimal growth of phototrophs and high productions of O_2, necessary

for the metabolism of aerobic species. All this leads to the development of larger granules, mainly governed by heterotrophs, cyanobacteria and microalgae. In particular, due to their different light harvesting and utilization, the relative abundance of cyanobacteria and microalgae within the granule is highly variable to vary light conditions. Appreciable light conditions ($I_0 = 0.008\ kmol\ m^{-2}\ d^{-1}$) guarantee the proliferation of cyanobacteria, which have a lower maximum growth rate than microalgae but greater abilities to adapt to not optimal light conditions. Instead, very high incident light intensities favor the photosynthetic activity of microalgae, which take over the cyanobacteria. The described result confirms that the model is able to reproduce the behaviour of cyanobacteria and microalgae reported by several experimental studies [2, 3].

A significant drawback of the model is that it is not suitable to describe the uncertainty of the granulation phenomenon. As reported by [55, 38], photogranulation is an extremely complex process that is not always successful. Sometimes, it fails, without leading to the genesis of the granule, and the suspended inoculum remains in its original form. In this context, as specified in Section 5.1, chances of success are deeply affected by the cyanobacteria concentration: high concentration of cyanobacteria in the system considerably increases the chances of photogranule formation. The model presented in this Chapter describes the granulation process using a deterministic approach, through an attachment flux dependent on the concentration of cyanobacteria in suspended form. Such concentration is the discriminating factor in the realization of the process: assuming a non-zero initial value leads to a non-zero attachment flux and the granule is formed, while assuming a zero value has the effect that all biomass present in the system remains in suspended form. In conclusion, in this model the initial concentration of cyanobacteria in suspended form determines the occurrence of the photogranulation and quantitatively affects the growth rate of the granule, but cannot affect the probability that the granule is formed.

In summary, it is possible to draw a number of conclusions from the numerical results presented:

- The OPG-based system seems to be a very interesting technology for the wastewater treatment, because it allows to remove aerobically the polluting compounds thanks to the production of O_2 by phototrophic microorganisms, without the use of external aeration sources.

- In this system, the removal of polluting compounds from the wastewater is based on the mechanisms of symbiotic interaction established between different microbial species. Among these, the most relevant is certainly the photoautotrophic production of O_2 by cyanobacteria and microalgae, necessary for the metabolic activity of heterotrophs.

- The influent composition and the influent carbon/nitrogen ratio strongly affect the efficiency of the system. As this ratio varies, carbon or nitrogen can become limiting for microbial kinetics and compromise the purifying efficiency of the photogranules.

- The influent composition radically influences the dynamics and the development of photogranules. Different concentrations of DOC, NH_4 and NO_3 lead to different microbial compositions within the photogranules. Phototrophic microorganisms (cyanobacteria and microalgae) and heterotrophic bacteria are the most present species in photogranules. However, nitrifying bacteria can proliferate in the case of poor DOC wastewaters.

- Main biological processes involved in the OPG-based system are photosynthetic processes and aerobic growth processes. However, high concentrations of NO_3 in the influent can lead to intense denitrification processes during the dark phase.

- Light conditions play a key role in the process by regulating the photosynthetic activity of phototrophic microorganisms, the production of O_2 and, indirectly, the growth of other microbial species. Consequently, light conditions significantly affects the dimension of photogranules and the performances of the system.

5.5 Appendix A

All reaction terms of the model are written below. The kinetic expressions of the biological processes (in the biofilm ν and in the bulk liquid ν^*) and the stoichiometric coefficients (in the biofilm α and in the bulk liquid α^*) are reported in Tables 5.3, 5.4, 5.5 and 5.6.

$$r_{M,A} = \alpha_{A,1}\,\nu_{A,1} + \alpha_{A,2}\,\nu_{A,2} + \alpha_{A,3}\,\nu_{A,3} - k_{d,A}\,f_A, \tag{5.20}$$

$$r_{M,C} = \alpha_{C,1}\,\nu_{C,1} + \alpha_{C,2}\nu_{C,2} + \alpha_{C,3}\nu_{C,3} - k_{d,C}\,f_C, \tag{5.21}$$

$$r_{M,H} = \alpha_{H,1}\,\nu_{H,1} + \alpha_{H,2}\,\nu_{H,2} - k_{d,H}\,f_H, \tag{5.22}$$

$$r_{M,N} = \alpha_{N,1}\,\nu_N - k_{d,N}\,f_N, \tag{5.23}$$

$$r_{M,EPS} = \alpha_{EPS,1}\,\nu_{A,1} + \alpha_{EPS,2}\,\nu_{A,2} + \alpha_{EPS,3}\,\nu_{C,1} + \alpha_{EPS,4}\,\nu_{C,2} + \alpha_{EPS,5}\,\nu_{H,1} +$$

$$+\alpha_{EPS,6}\,\nu_{H,2} + \alpha_{EPS,7}\,\nu_N, \tag{5.24}$$

$$r_{M,I} = k_{d,A}\,f_A + k_{d,C}\,f_C + k_{d,H}\,f_H + k_{d,N}\,f_N, \tag{5.25}$$

$$r_{S,IC} = \alpha_{IC,1}\,\nu_{A,1}\rho + \alpha_{IC,2}\,\nu_{A,2}\rho + \alpha_{IC,3}\,\nu_{A,3}\rho + \alpha_{IC,4}\,\nu_{C,1}\rho +$$

$$+\alpha_{IC,5}\,\nu_{C,2}\rho+\alpha_{IC,6}\,\nu_{C,3}\rho+\alpha_{IC,7}\,\nu_{H,1}\rho+\alpha_{IC,8}\,\nu_{H,2}\rho+\alpha_{IC,9}\,\nu_N\rho, \tag{5.26}$$

$$r_{S,DOC}=\alpha_{DOC,1}\,\nu_{A,1}\rho+\alpha_{DOC,2}\,\nu_{A,2}\rho+\alpha_{DOC,3}\,\nu_{A,3}\rho+\alpha_{DOC,4}\,\nu_{C,1}\rho+$$

$$+\alpha_{DOC,5}\,\nu_{C,2}\rho+\alpha_{DOC,6}\,\nu_{C,3}\rho+\alpha_{DOC,7}\,\nu_{H,1}\rho+\alpha_{DOC,8}\,\nu_{H,2}\rho, \tag{5.27}$$

$$r_{S,NO3}=\alpha_{NO3,1}\,\nu_{A,2}\rho+\alpha_{NO3,2}\,\nu_{C,2}\rho+\alpha_{NO3,3}\,\nu_{H,2}\rho+\alpha_{NO3,4}\,\nu_N\rho, \tag{5.28}$$

$$r_{S,NH3}=\alpha_{NH3,1}\,\nu_{A,1}\rho+\alpha_{NH3,2}\,\nu_{A,3}\rho+\alpha_{NH3,3}\,\nu_{C,1}\rho+\alpha_{NH3,4}\,\nu_{C,3}\rho+$$

$$+\alpha_{NH3,5}\,\nu_{H,1}\rho+\alpha_{NH3,6}\,\nu_{H,2}\rho+\alpha_{NH3,7}\,\nu_N\rho, \tag{5.29}$$

$$r_{S,O2}=\alpha_{O2,1}\,\nu_{A,1}\rho+\alpha_{O2,2}\,\nu_{A,2}\rho+\alpha_{O2,3}\,\nu_{A,3}\rho+\alpha_{O2,4}\,\nu_{C,1}\rho+$$

$$+\alpha_{O2,5}\,\nu_{C,2}\rho+\alpha_{O2,6}\,\nu_{C,3}\rho+\alpha_{O2,7}\,\nu_{H,1}\rho+\alpha_{O2,8}\,\nu_N\rho, \tag{5.30}$$

$$r^*_{\psi,A}=\alpha^*_{A,1}\,\nu^*_{A,1}+\alpha^*_{A,2}\nu^*_{A,2}+\alpha^*_{A,3}\nu^*_{A,3}-k_{d,A}\,\psi^*_A, \tag{5.31}$$

$$r^*_{\psi,C}=\alpha^*_{C,1}\nu^*_{C,1}+\alpha^*_{C,2}\nu^*_{C,2}+\alpha^*_{C,3}\nu^*_{C,3}-k_{d,C}\,\psi^*_C, \tag{5.32}$$

$$r^*_{\psi,H} = \alpha^*_{H,1}\,\nu^*_{H,1} + \alpha^*_{H,2}\nu^*_{H,2} - k_{d,H}\,\psi^*_H, \tag{5.33}$$

$$r^*_{\psi,N} = \alpha^*_{N,1}\nu^*_N - k_{d,N}\,\psi^*_N, \tag{5.34}$$

$$r^*_{S,IC} = \alpha^*_{IC,1}\nu^*_{A,1} + \alpha^*_{IC,2}\,\nu^*_{A,2} + \alpha^*_{IC,3}\,\nu^*_{A,3} + \alpha^*_{IC,4}\,\nu^*_{C,1} + \alpha^*_{IC,5}\,\nu^*_{C,2}+$$

$$+\alpha^*_{IC,6}\,\nu^*_{C,3} + \alpha^*_{IC,7}\,\nu^*_{H,1} + \alpha^*_{IC,8}\,\nu^*_{H,2} + \alpha^*_{IC,9}\,\nu^*_N, \tag{5.35}$$

$$r^*_{S,DOC} = \alpha^*_{DOC,1}\,\nu^*_{A,1} + \alpha^*_{DOC,2}\,\nu^*_{A,2} + \alpha^*_{DOC,3}\,\nu^*_{A,3} + \alpha^*_{DOC,4}\,\nu^*_{C,1}+$$

$$+\alpha^*_{DOC,5}\,\nu^*_{C,2} + \alpha^*_{DOC,6}\,\nu^*_{C,3} + \alpha^*_{DOC,7}\,\nu^*_{H,1} + \alpha^*_{DOC,8}\,\nu^*_{H,2}, \tag{5.36}$$

$$r^*_{S,NO3} = \alpha^*_{NO3,1}\,\nu^*_{A,2} + \alpha^*_{NO3,2}\,\nu^*_{C,2} + \alpha^*_{NO3,3}\,\nu^*_{H,2} + \alpha^*_{NO3,4}\,\nu^*_N, \tag{5.37}$$

$$r^*_{S,NH3} = \alpha^*_{NH3,1}\,\nu^*_{A,1} + \alpha^*_{NH3,2}\,\nu^*_{A,3} + \alpha^*_{NH3,3}\,\nu^*_{C,1} + \alpha^*_{NH3,4}\,\nu^*_{C,3}+$$

$$+\alpha^*_{NH3,5}\,\nu^*_{H,1} + \alpha^*_{NH3,6}\,\nu^*_{H,2} + \alpha^*_{NH3,7}\,\nu^*_N, \tag{5.38}$$

$$r^*_{S,O2} = \alpha^*_{O2,1}\,\nu^*_{A,1} + \alpha^*_{O2,2}\,\nu^*_{A,2} + \alpha^*_{O2,3}\,\nu^*_{A,3} + \alpha^*_{O2,4}\,\nu^*_{C,1}+$$

$$+\alpha^*_{O2,5}\,\nu^*_{C,2} + \alpha^*_{O2,6}\,\nu^*_{C,3} + \alpha^*_{O2,7}\,\nu^*_{H,1} + \alpha^*_{O2,8}\,\nu^*_{N} + k_{La}\,(S_{O2,sat} - S^*_{O_2}). \qquad (5.39)$$

Table 5.3: Kinetic expressions of the growth processes within biofilm granules.

Process	**Expression**
Photoautotrophic growth of microalgae on NH_3	$\nu_{A,1} = q_{max,A} \frac{S_{IC}}{K_{A,IC}+S_{IC}} \frac{S_{NH3}}{K_{A,NH3}+S_{NH3}} \frac{K^{in}_{A,O2}}{K^{in}_{A,O2}+S_{O2}} (\frac{I}{I_{opt,A}})^{\eta_A} \, e^{(1-(\frac{I}{I_{opt,A}})^{\eta_A})} \, f_A$
Photoautotrophic growth of microalgae on NO_3	$\nu_{A,2} = q_{max,A} \frac{S_{IC}}{K_{A,IC}+S_{IC}} \frac{S_{NO3}}{K_{A,NO3}+S_{NO3}} \frac{K^{in}_{A,NH3}}{K^{in}_{A,NH3}+S_{NH3}} \frac{K^{in}_{A,O2}}{K^{in}_{A,O2}+S_{O2}} (\frac{I}{I_{opt,A}})^{\eta_A} \, e^{(1-(\frac{I}{I_{opt,A}})^{\eta_A})} \, f_A$
Heterotrophic growth of microalgae	$\nu_{A,3} = 0.1 \, q_{max,A} \frac{S_{DOC}}{K_{A,DOC}+S_{DOC}} \frac{S_{O2}}{K_{A,O2}+S_{O2}} \frac{K^{in}_{A,I}}{K^{in}_{A,I}+I} \, f_A$
Photoautotrophic growth of cyanobacteria on NH_3	$\nu_{C,1} = q_{max,C} \frac{S_{IC}}{K_{C,IC}+S_{IC}} \frac{S_{NH3}}{K_{C,NH3}+S_{NH3}} \frac{K^{in}_{C,O2}}{K^{in}_{C,O2}+S_{O2}} (\frac{I}{I_{opt,C}})^{\eta_C} \, e^{(1-(\frac{I}{I_{opt,C}})^{\eta_C})} \, f_C$
Photoautotrophic growth of cyanobacteria on NO_3	$\nu_{C,2} = q_{max,C} \frac{S_{IC}}{K_{C,IC}+S_{IC}} \frac{S_{NO3}}{K_{C,NO3}+S_{NO3}} \frac{K^{in}_{C,NH3}}{K^{in}_{C,NH3}+S_{NH3}} \frac{K^{in}_{C,O2}}{K^{in}_{C,O2}+S_{O2}} (\frac{I}{I_{opt,C}})^{\eta_C} \, e^{(1-(\frac{I}{I_{opt,C}})^{\eta_C})} \, f_C$
Heterotrophic growth of cyanobacteria	$\nu_{C,3} = 0.1 \, q_{max,C} \frac{S_{DOC}}{K_{C,DOC}+S_{DOC}} \frac{S_{O2}}{K_{C,O2}+S_{O2}} \frac{K^{in}_{C,I}}{K^{in}_{C,I}+I} \, f_C$
Aerobic growth of heterotrophic bacteria	$\nu_{H,1} = \mu_{max,H} \frac{S_{DOC}}{K_{H,DOC}+S_{DOC}} \frac{S_{NH3}}{K_{H,NH3}+S_{NH3}} \frac{S_{O2}}{K_{H,O2}+S_{O2}} \, f_H$
Anoxic growth of heterotrophic bacteria	$\nu_{H,2} = \mu_{max,H} \frac{S_{DOC}}{K_{H,DOC}+S_{DOC}} \frac{S_{NO3}}{K_{H,NO3}+S_{NO3}} \frac{S_{NH3}}{K_{H,NH3}+S_{NH3}} \frac{K_{H,O2}}{K_{H,O2}+S_{O2}} \, f_H$
Growth of nitrifying bacteria	$\nu_N = \mu_{max,N} \frac{S_{IC}}{K_{N,IC}+S_{IC}} \frac{S_{NH3}}{K_{H,NH3}+S_{NH3}} \frac{S_{O2}}{K_{H,O2}+S_{O2}} \, f_N$

where $K^{in}_{A,O2} = K^{in}_{C,O2} = K^{in}_{O2,max} \, \frac{\frac{S_{IC}}{S_{O2}}}{\frac{S_{IC}}{S_{O2}}+K_{R_{CO2/O2}}}$

Table 5.4: Kinetic expressions of the growth processes within the liquid medium.

Process	**Expression**
Photoautotrophic growth of microalgae on NH_3	$\nu^*_{A,1} = q_{max,A} \frac{S^*_{IC}}{K_{A,IC}+S^*_{IC}} \frac{S^*_{NH3}}{K_{A,NH3}+S^*_{NH3}} \frac{K^{in,*}_{A,O2}}{K^{in,*}_{A,O2}+S^*_{O2}} (\frac{I_0}{I_{opt,A}})^{\eta_A} \, e^{(1-(\frac{I_0}{I_{opt,A}})^{\eta_A})} \, \psi^*_A$
Photoautotrophic growth of microalgae on NO_3	$\nu^*_{A,2} = q_{max,A} \frac{S^*_{IC}}{K_{A,IC}+S^*_{IC}} \frac{S^*_{NO3}}{K_{A,NO3}+S^*_{NO3}} \frac{K^{in}_{A,NH3}}{K^{in}_{A,NH3}+S^*_{NH3}} \frac{K^{in,*}_{A,O2}}{K^{in,*}_{A,O2}+S^*_{O2}} (\frac{I_0}{I_{opt,A}})^{\eta_A} \, e^{(1-(\frac{I_0}{I_{opt,A}})^{\eta_A})} \, \psi^*_A$
Heterotrophic growth of microalgae	$\nu^*_{A,3} = 0.1 \, q_{max,A} \frac{S^*_{DOC}}{K_{A,DOC}+S^*_{DOC}} \frac{S^*_{O2}}{K_{A,O2}+S^*_{O2}} \frac{K^{in}_{A,I}}{K^{in}_{A,I}+I_0} \psi^*_A$
Photoautotrophic growth of cyanobacteria on NH_3	$\nu^*_{C,1} = q_{max,C} \frac{S^*_{IC}}{K_{C,IC}+S^*_{IC}} \frac{S^*_{NH3}}{K_{C,NH3}+S^*_{NH3}} \frac{K^{in,*}_{C,O2}}{K^{in,*}_{C,O2}+S^*_{O2}} (\frac{I_0}{I_{opt,C}})^{\eta_C} \, e^{(1-\frac{I_0}{I_{opt,C}})^{\eta_C}} \, \psi^*_C$
Photoautotrophic growth of cyanobacteria on NO_3	$\nu^*_{C,2} = q_{max,C} \frac{S^*_{IC}}{K_{C,IC}+S^*_{IC}} \frac{S^*_{NO3}}{K_{C,NO3}+S^*_{NO3}} \frac{K^{in}_{C,NH3}}{K^{in}_{C,NH3}+S^*_{NH3}} \frac{K^{in,*}_{C,O2}}{K^{in,*}_{C,O2}+S^*_{O2}} (\frac{I_0}{I_{opt,C}})^{\eta_C} \, e^{(1-(\frac{I_0}{I_{opt,C}})^{\eta_C})} \, \psi^*_C$
Heterotrophic growth of cyanobacteria	$\nu^*_{C,3} = 0.1 \, q_{max,C} \frac{S^*_{DOC}}{K_{C,DOC}+S^*_{DOC}} \frac{S^*_{O2}}{K_{C,O2}+S^*_{O2}} \frac{K^{in}_{C,I}}{K^{in}_{C,I}+I_0} \, \psi^*_C$
Aerobic growth of heterotrophic bacteria	$\nu^*_{H,1} = \mu_{max,H} \frac{S^*_{DOC}}{K_{H,DOC}+S^*_{DOC}} \frac{S^*_{NH3}}{K_{H,NH3}+S^*_{NH3}} \frac{S^*_{O2}}{K_{H,O2}+S^*_{O2}} \, \psi^*_H$
Anoxic growth of heterotrophic bacteria	$\nu^*_{H,2} = \mu_{max,H} \frac{S^*_{DOC}}{K_{H,DOC}+S^*_{DOC}} \frac{S^*_{NO3}}{K_{H,NO3}+S^*_{NO3}} \frac{S^*_{NH3}}{K_{H,NH3}+S^*_{NH3}} \frac{K_{H,O2}}{K_{H,O2}+S^*_{O2}} \, \psi^*_H$
Growth of nitrifying bacteria	$\nu^*_N = \mu_{max,N} \frac{S^*_{IC}}{K_{N,IC}+S^*_{IC}} \frac{S^*_{NH3}}{K_{H,NH3}+S^*_{NH3}} \frac{S^*_{O2}}{K_{H,O2}+S^*_{O2}} \, \psi^*_N$

where $K^{in,*}_{A,O2} = K^{in,*}_{C,O2} = K^{in}_{O2,max} \, \frac{\frac{S^*_{IC}}{S^*_{O2}}}{\frac{S^*_{IC}}{S^*_{O2}}+K_{R_{CO2/O2}}}$

Stoich. coefficient	Expression	Stoich. coefficient	Expression
$\alpha_{A,1}$	$\frac{32}{1+\phi_{EPS,A}+k_{DOC}}$	$\alpha_{DOC,2}$	$\frac{32\ k_{DOC}}{1.3409+\phi_{EPS,A}+k_{DOC}}$
$\alpha_{A,2}$	$\frac{32}{1.3409+\phi_{EPS,A}+k_{DOC}}$	$\alpha_{DOC,3}$	$\frac{-32}{1-Y_{DOC}}$
$\alpha_{A,3}$	$\frac{32\ Y_{DOC}}{1-Y_{DOC}}$	$\alpha_{DOC,4}$	$\frac{32\ k_{DOC}}{1.3409+\phi_{EPS,C}+k_{DOC}}$
$\alpha_{C,1}$	$\frac{32}{1+\phi_{EPS,C}+k_{DOC}}$	$\alpha_{DOC,5}$	$\frac{32\ k_{DOC}}{1.3409+\phi_{EPS,C}+k_{DOC}}$
$\alpha_{C,2}$	$\frac{32}{1.3409+\phi_{EPS,C}+k_{DOC}}$	$\alpha_{DOC,6}$	$\frac{-32}{1-Y_{DOC}}$
$\alpha_{C,3}$	$\frac{32\ Y_{DOC}}{1-Y_{DOC}}$	$\alpha_{DOC,7}$	$-\frac{1}{Y_H}$
$\alpha_{H,1}$	$1-k_{EPS,H}$	$\alpha_{DOC,8}$	$-\frac{1}{Y_H}$
$\alpha_{H,2}$	$1-k_{EPS,H}$	$\alpha_{NO3,1}$	$-\frac{0.1704}{1.3409+\phi_{EPS,A}+k_{DOC}}$
$\alpha_{N,1}$	$1-k_{EPS,N}$	$\alpha_{NO3,2}$	$-\frac{0.1704}{1.3409+\phi_{EPS,C}+k_{DOC}}$
$\alpha_{EPS,1}$	$\frac{32\ \phi_{EPS,A}}{1+\phi_{EPS,A}+k_{DOC}}$	$\alpha_{NO3,3}$	$-\frac{0.8}{32\ Y_H}+0.02857$
$\alpha_{EPS,2}$	$\frac{32\ \phi_{EPS,A}}{1.3409+\phi_{EPS,A}+k_{DOC}}$	$\alpha_{NO3,4}$	$+\frac{1}{14\ Y_N}$
$\alpha_{EPS,3}$	$\frac{32\ \phi_{EPS,C}}{1+\phi_{EPS,C}+k_{DOC}}$	$\alpha_{NH3,1}$	$-\frac{0.1704}{1+\phi_{EPS,A}+k_{DOC}}$
$\alpha_{EPS,4}$	$\frac{32\ \phi_{EPS,C}}{1.3409+\phi_{EPS,C}+k_{DOC}}$	$\alpha_{NH3,2}$	$-\frac{0.1704}{1-Y_{DOC}}$
$\alpha_{EPS,5}$	$k_{EPS,H}$	$\alpha_{NH3,3}$	$-\frac{0.1704}{1+\phi_{EPS,C}+k_{DOC}}$
$\alpha_{EPS,6}$	$k_{EPS,H}$	$\alpha_{NH3,4}$	$-\frac{0.1704}{1-Y_{DOC}}$
$\alpha_{EPS,7}$	$k_{EPS,N}$	$\alpha_{NH3,5}$	$-\frac{0.2}{33.6}$
$\alpha_{IC,1}$	$-\frac{1.0025+\phi_{EPS,A}+k_{DOC}}{1+\phi_{EPS,A}+k_{DOC}}$	$\alpha_{NH3,6}$	$-\frac{0.2}{33.6}$
$\alpha_{IC,2}$	$-\frac{1.0025+\phi_{EPS,A}+k_{DOC}}{1.3409+\phi_{EPS,A}+k_{DOC}}$	$\alpha_{NH3,7}$	$-\frac{1}{14\ Y_N}-0.00593$
$\alpha_{IC,3}$	$\frac{1-1.0025\ Y_{DOC}}{1-Y_{DOC}}$	$\alpha_{O2,1}$	1
$\alpha_{IC,4}$	$-\frac{1.0025+\phi_{EPS,C}+k_{DOC}}{1+\phi_{EPS,C}+k_{DOC}}$	$\alpha_{O2,2}$	1
$\alpha_{IC,5}$	$-\frac{1.0025+\phi_{EPS,C}+k_{DOC}}{1.3409+\phi_{EPS,C}+k_{DOC}}$	$\alpha_{O2,3}$	-1
$\alpha_{IC,6}$	$\frac{1-1.0025\ Y_{DOC}}{1-Y_{DOC}}$	$\alpha_{O2,4}$	1
$\alpha_{IC,7}$	$\frac{1}{32\ Y_H}-0.02976$	$\alpha_{O2,5}$	1
$\alpha_{IC,8}$	$\frac{1}{32\ Y_H}-0.02976$	$\alpha_{O2,6}$	-1
$\alpha_{IC,9}$	$-\frac{1}{33.6}$	$\alpha_{O2,7}$	$-\frac{1}{32\ Y_H}+0.03125$
$\alpha_{DOC,1}$	$\frac{32\ k_{DOC}}{A.3409+\phi_{EPS,A}+k_{DOC}}$	$\alpha_{O2,8}$	$-\frac{1}{7\ Y_N}+\frac{1}{32}$

Table 5.5: Stoichiometric coefficients used in the model biological processes within biofilm granules

Stoich. coefficient	Expression	Stoich. coefficient	Expression
$\alpha^*_{A,1}$	$\frac{32}{1+k_{DOC}}$	$\alpha^*_{DOC,6}$	$\frac{-32}{1-Y_{DOC}}$
$\alpha^*_{A,2}$	$\frac{32}{1.3409+k_{DOC}}$	$\alpha^*_{DOC,7}$	$-\frac{1}{Y_H}$
$\alpha^*_{A,3}$	$\frac{32\ Y_{DOC}}{1-Y_{DOC}}$	$\alpha^*_{DOC,8}$	$-\frac{1}{Y_H}$
$\alpha^*_{C,1}$	$\frac{32}{1+k_{DOC}}$	$\alpha^*_{NO3,1}$	$-\frac{0.1704}{1.3409+k_{DOC}}$
$\alpha^*_{C,2}$	$\frac{32}{1.3409+k_{DOC}}$	$\alpha^*_{NO3,2}$	$-\frac{0.1704}{1.3409+k_{DOC}}$
$\alpha^*_{C,3}$	$\frac{32\ Y_{DOC}}{1-Y_{DOC}}$	$\alpha^*_{NO3,3}$	$-\frac{0.8}{32\ Y_H}+0.02857$
$\alpha^*_{H,1}$	1	$\alpha^*_{NO3,4}$	$+\frac{1}{14\ Y_N}$
$\alpha^*_{H,2}$	1	$\alpha^*_{NH3,1}$	$-\frac{0.1704}{1+k_{DOC}}$
$\alpha^*_{N,1}$	1	$\alpha^*_{NH3,2}$	$-\frac{0.1704}{1-Y_{DOC}}$
$\alpha^*_{IC,1}$	$-\frac{1.0025+k_{DOC}}{1+k_{DOC}}$	$\alpha^*_{NH3,3}$	$-\frac{0.1704}{1+k_{DOC}}$
$\alpha^*_{IC,2}$	$-\frac{1.0025+k_{DOC}}{1.3409+k_{DOC}}$	$\alpha^*_{NH3,4}$	$-\frac{0.1704}{1-Y_{DOC}}$
$\alpha^*_{IC,3}$	$\frac{1-1.0025\ Y_{DOC}}{1-Y_{DOC}}$	$\alpha^*_{NH3,5}$	$-\frac{0.2}{33.6}$
$\alpha^*_{IC,4}$	$-\frac{1.0025+k_{DOC}}{1+k_{DOC}}$	$\alpha^*_{NH3,6}$	$-\frac{0.2}{33.6}$
$\alpha^*_{IC,5}$	$-\frac{1.0025+k_{DOC}}{1.3409+k_{DOC}}$	$\alpha^*_{NH3,7}$	$-\frac{1}{14\ Y_N}-0.00593$
$\alpha^*_{IC,6}$	$\frac{1-1.0025\ Y_{DOC}}{1-Y_{DOC}}$	$\alpha^*_{O2,1}$	1
$\alpha^*_{IC,7}$	$\frac{1}{32\ Y_H}-0.02976$	$\alpha^*_{O2,2}$	1
$\alpha^*_{IC,8}$	$\frac{1}{32\ Y_H}-0.02976$	$\alpha^*_{O2,3}$	-1
$\alpha^*_{IC,9}$	$-\frac{1}{33.6}$	$\alpha^*_{O2,4}$	1
$\alpha^*_{DOC,1}$	$\frac{32\ k_{DOC}}{1.3409+k_{DOC}}$	$\alpha^*_{O2,5}$	1
$\alpha^*_{DOC,2}$	$\frac{32\ k_{DOC}}{1.3409+k_{DOC}}$	$\alpha^*_{O2,6}$	-1
$\alpha^*_{DOC,3}$	$\frac{-32}{1-Y_{DOC}}$	$\alpha^*_{O2,7}$	$-\frac{1}{32\ Y_H}+0.03125$
$\alpha^*_{DOC,4}$	$\frac{32\ k_{DOC}}{1.3409+k_{DOC}}$	$\alpha^*_{O2,8}$	$-\frac{1}{7\ Y_N}+\frac{1}{32}$
$\alpha^*_{DOC,5}$	$\frac{32\ k_{DOC}}{1.3409+k_{DOC}}$		

Table 5.6: Stoichiometric coefficients used in the model for biological processes within the liquid medium

Chapter 6

Conclusion and future perspectives

Mathematical modelling represents a widely used approach to study biofilms, as it allows to achieve a double objective: it supports the experimental research in the analysis and understanding of these complex biological aggregates and provides auxiliary tools useful in industrial applications. In this context, the present work of thesis proposes new mathematical models able to comprehensively describe unexplored physical and biochemical aspects of biofilms.

In Chapter 2, a 1D model on the interaction of sessile and planktonic phenotypes in biofilm lifestyle has been presented. The phenomenon of initial attachment is modelled in a deterministic way, as a continuous flux of suspended biomass from the surrounding environment to the biofilm. The numerical study reported in this chapter highlights a criticism of Wanner and Gujer type models, which lead to restrictions on the ecological structure in specific situations. Indeed, in particular cases such models might not correctly describe the growth of microbial species which do not participate in the initial formation of the biofilm but attach later to a pre-existing aggregate. In this regard, it is shown how the modelling of invasion phenomena (modelled as a diffusive process) allows to overcome this criticism. A theorem that proves the existence and uniqueness of the solutions is also presented for this model. A numerical study is carried out for conceptual purposes and therefore refers to an ideal but realistic biological apparatus.

Anyway, the mathematical structure of the model is suitable to describe the microbial interactions between generic planktonic and sessile species and the formation and evolution of any type of biofilms. Consequently, it can be applied to any biological and engineering case study by correctly define model components and kinetic rates of the processes involved.

Chapter 3 presents a 1D model describing the ecology of phototrophic-heterotrophic biofilms. Numerical studies show that the model is able to simulate the growth of phototrophic-heterotrophic biofilms and reproduces accurately the main symbiotic mechanisms between phototrophs and heterotrophs reported in literature, such as the positive effect of heterotrophic pioneers and their EPS production on phototrophic growth and the effects of phototrophic organic carbon release on the invasion and growth of heterotrophic bacteria. Such microbial interactive mechanisms appear to be the element which governs and allows the development of these biofilm ecosystems. Moreover, model results confirm that light is the most significant factor in the growth process and highlight the role played by heterotrophic species under photoinhibition conditions, which provide a positive shading contribution to phototrophic growth.

In Chapter 4, a multiscale mathematical model on granular biofilms is derived in order to represent the evolution process of biofilm granules within a continuous reactor, including their initial formation. The model predicts the granule formation from the initial granulation process to the maturation and achievement of the steady-state configuration. Moreover, the model also takes into account the transformation processes occurring in the bulk liquid and mass exchanges between granules and bulk liquid, due to attachment, detachment, invasion of microbial species and diffusion of soluble substrates. This multiscale approach allows to accurately predict both the development of biofilm granules, their dimension and microbial composition, and the biological treatment process taking place in the wastewater treatment system. Consequently, after adequate procedures of calibration and validation, this model can represent an auxiliary tool for various engineering practices in the field of wastewater treatment. In particu-

lar, as the model is able to simulate the initial granulation, it can be used productively in the start up activity of full-scale granular biofilm systems, which is the most sensitive and delicate among the operating phases of such systems, due to the complexity of the granulation process. Furthermore, the model is applied to an anaerobic granular system in order to test its qualitative behavior and explore main aspects of *de novo* anaerobic granulation. Numerical studies reveal that the model is able to simulate the operation of this system, by describing the anaerobic treatment process, predicting the microbial composition of granules observed in the literature and reproducing the role and the effects that key factors, such as wastewater influent composition, shear forces, hydrodynamic conditions, have on the process.

Finally, the multiscale model introduced in Chapter 5 describes for the first time oxygenic photogranules (OPGs), their genesis and growth within a sequencing batch reactor (SBR). Nowadays, OPGs-based systems have not yet been implemented in full-scale reactors, therefore the first purpose of the model is to provide information on the effectiveness and applicability of this technology in the field of water treatment. From the numerical results presented, it can be concluded that oxygenic photogranules represent an interesting innovative technology for treating municipal wastewaters, as the mechanisms of symbiotic interaction which develop between phototrophs (cyanobacteria and microalgae) and heterotrophs lead to the degradation of carbon and nitrogen pollutants from wastewaters. The influent carbon/nitrogen ratio, the influent composition and light conditions turn out crucial factors for this biological system, as they influence the growth of photogranules and the treatment performances. The model is suitable for describing the photogranulation process and its main aspects, including the key role played by cyanobacteria. The modelling of the differences between cyanobacteria and microalgae in the metabolic activity and light harvesting and utilization allows to correctly describe the growth of these phototrophic species and their behavior under different light regimes. As the previous model, this model is based on a multiscale approach which allows to simulate both the growth process of biofilm granules and the

treatment process occurring within the treatment system. Consequently, after calibration and validation, it can be a useful tool for start-up and management activities of future full-scale OPGs-based plants.

The models presented here on phototrophic biofilms describe the growth of submerged biofilms, which develop in liquid environments, where the amount of water required by the microbial metabolic activities is always guaranteed. However, particular phototrophic biofilms, known as subaerial biofilms, can develop on humid solid surfaces in contact with air. The formation of these biofilms is governed by cyanobacteria, which manage to survive in environments where not optimal conditions of light and humidity are expected. In this context, it would be interesting to develop a mathematical model able to simulate the evolution of subaerial phototrophic biofilms.

Furthermore, all models proposed here consider the biofilm as a homogeneous domain, characterized by the same density at every point. Starting from this, a future modelling work, which takes into account the biofilm heterogeneity, could be developed by including porosity and density among the model variables, with the aim of modelling the effects of such factors on microbial invasion phenomena.

Numerical studies carried out here lead to a number of conclusions which are qualitatively in agreement with the experimental evidences present in the literature and confirm the potential of the models introduced. However, no quantitative comparison between numerical results and experimental data has been performed to definitively prove the accuracy of the model. Moreover, some model parameters have been introduced here for the first time and their value has been assumed. For these reasons, future works should focus on activities of sensitivity analysis, calibration and validation of these models. Specifically, the achievement of uncertainty quantification and global sensitivity analysis, through the use of the Sobol' indices and the development of surrogate models, would allow to identify the most influential model parameters and to quantify their effects on the biofilm structure and evolution, and on the treatment process. Then, the calibration and validation of the models by using experimental data would

lead to numerical tools suitable to provide quantitatively reliable results, and applicable for the start-up, monitoring, management and sizing of full-scale wastewater treatment systems.

Bibliography

[1] ABBAS, F., SUDARSAN, R., AND EBERL, H. J. Longtime behavior of one-dimensional biofilm models with shear dependent detachment rates. *Math. Biosc. Eng 9*, 2 (2012), 215–239.

[2] ABOUHEND, A. S., MCNAIR, A., KUO-DAHAB, W. C., WATT, C., BUTLER, C. S., MILFERSTEDT, K., HAMELIN, J., SEO, J., GIKONYO, G. J., EL-MOSELHY, K. M., ET AL. The oxygenic photogranule process for aeration-free wastewater treatment. *Environmental science & technology 52*, 6 (2018), 3503–3511.

[3] ABOUHEND, A. S., MILFERSTEDT, K., HAMELIN, J., ANSARI, A. A., BUTLER, C., CARBAJAL-GONZÁLEZ, B. I., AND PARK, C. Growth progression of oxygenic photogranules and its impact on bioactivity for aeration-free wastewater treatment. *Environmental Science & Technology 54*, 1 (2019), 486–496.

[4] AHMAD, J. S. M., CAI, W., ZHAO, Z., ZHANG, Z., SHIMIZU, K., LEI, Z., AND LEE, D.-J. Stability of algal-bacterial granules in continuous-flow reactors to treat varying strength domestic wastewater. *Bioresource technology 244* (2017), 225–233.

[5] ALPKVISTA, E., AND KLAPPER, I. A multidimensional multispecies continuum model for heterogeneous biofilm development. *Bulletin of mathematical biology 69*, 2 (2007), 765–789.

[6] AMIN, S. A., PARKER, M. S., AND ARMBRUST, E. V. Interactions between diatoms and bacteria. *Microbiol. Mol. Biol. Rev. 76*, 3 (2012), 667–684.

[7] ANSARI, A. A., ABOUHEND, A. S., AND PARK, C. Effects of seeding density on photogranulation and the start-up of the oxygenic photogranule process for aeration-free wastewater treatment. *Algal Research 40* (2019), 101495.

[8] ARCAND, Y., GUIOT, S., DESROCHERS, M., AND CHAVARIE, C. Impact of the reactor hydrodynamics and organic loading on the size and activity of anaerobic granules. *The Chemical Engineering Journal and the Biochemical Engineering Journal 56*, 1 (1994), B23–B35.

[9] BAETEN, J. E., BATSTONE, D. J., SCHRAA, O. J., VAN LOOSDRECHT, M. C., AND VOLCKE, E. I. Modelling anaerobic, aerobic and partial nitritation-anammox granular sludge reactors-a review. *Water research 149* (2019), 322–341.

[10] BATHE, S., DE KREUK, M. K., MCSWAIN, B., AND SCHWARZENBECK, N. *Aerobic granular sludge*. IWA Publishing, 2005.

[11] BATSTONE, D. J., KELLER, J., ANGELIDAKI, I., KALYUZHNYI, S., PAVLOSTATHIS, S., ROZZI, A., SANDERS, W., SIEGRIST, H., AND VAVILIN, V. The iwa anaerobic digestion model no 1 (adm1). *Water Science and technology 45*, 10 (2002), 65–73.

[12] BATSTONE, D. J., KELLER, J., AND BLACKALL, L. The influence of substrate kinetics on the microbial community structure in granular anaerobic biomass. *Water Research 38*, 6 (2004), 1390–1404.

[13] BECK, A. E., BERNSTEIN, H. C., AND CARLSON, R. P. Stoichiometric network analysis of cyanobacterial acclimation to photosynthesis-associated stresses identifies heterotrophic niches. *Processes 5*, 2 (2017), 32.

[14] BERMAN, T., AND HOLM-HANSEN, O. Release of photoassimilated carbon as dissolved organic matter by marine phytoplankton. *Marine Biology 28*, 4 (1974), 305–310.

[15] BERTILSSON, S., AND JONES JR, J. B. Supply of dissolved organic matter to aquatic ecosystems: autochthonous sources. In *Aquatic Ecosystems*. Elsevier, 2003, pp. 3–24.

[16] BEUN, J., HENDRIKS, A., VAN LOOSDRECHT, M., MORGENROTH, E., WILDERER, P., AND HEIJNEN, J. Aerobic granulation in a sequencing batch reactor. *Water research 33*, 10 (1999), 2283–2290.

[17] BHARTI, A., VELMOUROUGANE, K., AND PRASANNA, R. Phototrophic biofilms: diversity, ecology and applications. *Journal of Applied Phycology 29*, 6 (2017), 2729–2744.

[18] BOELEE, N. C., TEMMINK, H., JANSSEN, M., BUISMAN, C. J., AND WIJFFELS, R. H. Scenario analysis of nutrient removal from municipal wastewater by microalgal biofilms. *Water 4*, 2 (2012), 460–473.

[19] BOROWITZKA, M. A., BEARDALL, J., RAVEN, J. A., ET AL. *The physiology of microalgae*, vol. 6. Springer, 2016.

[20] BURMØLLE, M., REN, D., BJARNSHOLT, T., AND SØRENSEN, S. J. Interactions in multispecies biofilms: do they actually matter? *Trends in microbiology 22*, 2 (2014), 84–91.

[21] CLARELLI, F., DI RUSSO, C., NATALINI, R., AND RIBOT, M. A fluid dynamics model of the growth of phototrophic biofilms. *Journal of mathematical biology 66*, 7 (2013), 1387–1408.

[22] CLARELLI, F., DI RUSSO, C., NATALINI, R., AND RIBOT, M. A fluid dynamics multidimensional model of biofilm growth: stability, influence of environ-

ment and sensitivity. *Mathematical medicine and biology: a journal of the IMA 33*, 4 (2016), 371–395.

[23] COCLITE, G. M., COCLITE, M. M., AND MISHRA, S. On a model for the evolution of morphogens in a growing tissue. *SIAM Journal on Mathematical Analysis 48*, 3 (2016), 1575–1615.

[24] COGAN, N. Two-fluid model of biofilm disinfection. *Bulletin of mathematical biology 70*, 3 (2008), 800–819.

[25] COLE, J. J., LIKENS, G. E., AND STRAYER, D. L. Photosynthetically produced dissolved organic carbon: An important carbon source for planktonic bacteria1. *Limnology and oceanography 27*, 6 (1982), 1080–1090.

[26] COLLINS, G., MAHONY, T., MCHUGH, S., GIESEKE, A., DE BEER, D., AND O'FLAHERTY, V. Distribution, dynamics and in situ ecophysiology of crenarchaeota in anaerobic wastewater treatment granular biofilms. *Water science and technology 52*, 7 (2005), 233–239.

[27] D'ACUNTO, B., AND FRUNZO, L. Qualitative analysis and simulations of a free boundary problem for multispecies biofilm models. *Mathematical and computer modelling 53*, 9-10 (2011), 1596–1606.

[28] D'ACUNTO, B., FRUNZO, L., KLAPPER, I., AND MATTEI, M. Modeling multispecies biofilms including new bacterial species invasion. *Mathematical biosciences 259* (2015), 20–26.

[29] D'ACUNTO, B., FRUNZO, L., LUONGO, V., AND MATTEI, M. Free boundary approach for the attachment in the initial phase of multispecies biofilm growth. *Zeitschrift für angewandte Mathematik und Physik 70*, 3 (2019), 91.

[30] D'ACUNTO, B., FRUNZO, L., LUONGO, V., AND MATTEI, M. R. Invasion moving boundary problem for a biofilm reactor model. *European Journal of Applied Mathematics 29*, 6 (2018), 1079–1109.

[31] D'ACUNTO, B., FRUNZO, L., AND MATTEI, M. R. Moving boundary problem for the detachment in multispecies biofilms. *Ricerche di Matematica 67*, 2 (2018), 683–698.

[32] DE KREUK, M., PICIOREANU, C., HOSSEINI, M., XAVIER, J., AND VAN LOOSDRECHT, M. Kinetic model of a granular sludge sbr: influences on nutrient removal. *Biotechnology and bioengineering 97*, 4 (2007), 801–815.

[33] DE VRIEZE, J., AND VERSTRAETE, W. Perspectives for microbial community composition in anaerobic digestion: from abundance and activity to connectivity. *Environmental microbiology 18*, 9 (2016), 2797–2809.

[34] DI IACONI, C., RAMADORI, R., LOPEZ, A., AND PASSINO, R. Influence of hydrodynamic shear forces on properties of granular biomass in a sequencing batch biofilter reactor. *Biochemical Engineering Journal 30*, 2 (2006), 152–157.

[35] DI PIPPO, F., ELLWOOD, N. T. W., GUZZON, A., SILIATO, L., MICHELETTI, E., DE PHILIPPIS, R., AND ALBERTANO, P. B. Effect of light and temperature on biomass, photosynthesis and capsular polysaccharides in cultured phototrophic biofilms. *Journal of applied phycology 24*, 2 (2012), 211–220.

[36] DOLOMAN, A., VARGHESE, H., MILLER, C. D., AND FLANN, N. S. Modeling de novo granulation of anaerobic sludge. *BMC systems biology 11*, 1 (2017), 69.

[37] DONLAN, R. M. Biofilms: microbial life on surfaces. *Emerging infectious diseases 8*, 9 (2002), 881.

[38] DOWNES, S. The success, morphology, and performance of oxygenic photogranules under light-induced stress conditions.

[39] EBERL, H. J., PARKER, D. F., AND VANLOOSDRECHT, M. C. A new deterministic spatio-temporal continuum model for biofilm development. *Computational and Mathematical Methods in Medicine 3*, 3 (2001), 161–175.

[40] EL MOUSTAID, F., CARLSON, R., VILLA, F., AND KLAPPER, I. Photorespiration and rate synchronization in a phototroph-heterotroph microbial consortium. *Processes 5*, 1 (2017), 11.

[41] EMERENINI, B. O., HENSE, B. A., KUTTLER, C., AND EBERL, H. J. A mathematical model of quorum sensing induced biofilm detachment. *PloS one 10*, 7 (2015).

[42] FANG, F., LU, W.-T., SHAN, Q., AND CAO, J.-S. Characteristics of extracellular polymeric substances of phototrophic biofilms at different aquatic habitats. *Carbohydrate polymers 106* (2014), 1–6.

[43] FANG, H. Microbial distribution in uasb granules and its resulting effects. *Water science and technology 42*, 12 (2000), 201–208.

[44] FELDMAN, H., FLORES-ALSINA, X., RAMIN, P., KJELLBERG, K., JEPPSSON, U., BATSTONE, D. J., AND GERNAEY, K. V. Modelling an industrial anaerobic granular reactor using a multi-scale approach. *Water research 126* (2017), 488–500.

[45] FERRENTINO, R., FERRARO, A., MATTEI, M. R., ESPOSITO, G., AND ANDREOTTOLA, G. Process performance optimization and mathematical modelling of a sbr-mbbr treatment at low oxygen concentration. *Process Biochemistry 75* (2018), 230–239.

[46] FLEMMING, H.-C., AND WINGENDER, J. The biofilm matrix. *Nature reviews microbiology 8*, 9 (2010), 623.

[47] FLEMMING, H.-C., WINGENDER, J., SZEWZYK, U., STEINBERG, P., RICE, S. A., AND KJELLEBERG, S. Biofilms: an emergent form of bacterial life. *Nature Reviews Microbiology 14*, 9 (2016), 563.

[48] FLORA, J. R., SUIDAN, M. T., BISWAS, P., AND SAYLES, G. D. Modeling algal biofilms: role of carbon, light, cell surface charge, and ionic species. *Water Environment Research 67*, 1 (1995), 87–94.

[49] FRUNZO, L., AND MATTEI, M. Qualitative analysis of the invasion free boundary problem in biofilms. *Ricerche di Matematica 66*, 1 (2017), 171–188.

[50] FUENTES, J., GARBAYO, I., CUARESMA, M., MONTERO, Z., GONZÁLEZ-DEL VALLE, M., AND VÍLCHEZ, C. Impact of microalgae-bacteria interactions on the production of algal biomass and associated compounds. *Marine drugs 14*, 5 (2016), 100.

[51] GAEBLER, H. J., AND EBERL, H. J. A simple model of biofilm growth in a porous medium that accounts for detachment and attachment of suspended biomass and their contribution to substrate degradation. *European Journal of Applied Mathematics 29*, 6 (2018), 1110–1140.

[52] GIORDANO, M., DAVIS, J. S., AND BOWES, G. Organic carbon release by dunaliella salina (chlorophyta) under different growth conditions of co2, nitrogen, and salinity 1. *Journal of phycology 30*, 2 (1994), 249–257.

[53] GROSS, M., JARBOE, D., AND WEN, Z. Biofilm-based algal cultivation systems. *Applied microbiology and biotechnology 99*, 14 (2015), 5781–5789.

[54] GUIOT, S., TAWFIKI-HAJJI, K., AND LEPINE, F. Immobilization strategies for bioaugmentation of anaerobic reactors treating phenolic compounds. *Water science and technology 42*, 5-6 (2000), 245–250.

[55] HANN, M. Factors impacting the cultivation, structure, and oxygen profiles of oxygenic photogranules for aeration-free wastewater treatment.

[56] HENZE, M., GUJER, W., MINO, T., AND VAN LOOSDRECHT, M. C. *Activated sludge models ASM1, ASM2, ASM2d and ASM3*. IWA publishing, 2000.

[57] JIAN, C., AND SHI-YI, L. Study on mechanism of anaerobic sludge granulation in uasb reactors. *Water Science and Technology 28*, 7 (1993), 171–178.

[58] JIN, R.-C., ZHANG, Q.-Q., ZHANG, Z.-Z., LIU, J.-H., YANG, B.-E., GUO, L.-X., AND WANG, H.-Z. Bio-augmentation for mitigating the impact of transient oxytetracycline shock on anaerobic ammonium oxidation (anammox) performance. *Bioresource technology 163* (2014), 244–253.

[59] KLAPPER, I., AND SZOMOLAY, B. An exclusion principle and the importance of mobility for a class of biofilm models. *Bulletin of mathematical biology 73*, 9 (2011), 2213–2230.

[60] KOUZUMA, A., AND WATANABE, K. Exploring the potential of algae/bacteria interactions. *Current Opinion in Biotechnology 33* (2015), 125–129.

[61] KU, S.-B., AND EDWARDS, G. E. Oxygen inhibition of photosynthesis. *Planta 140*, 1 (1978), 1–6.

[62] LASPIDOU, C. S., AND RITTMANN, B. E. A unified theory for extracellular polymeric substances, soluble microbial products, and active and inert biomass. *Water research 36*, 11 (2002), 2711–2720.

[63] LEMAIRE, R., WEBB, R. I., AND YUAN, Z. Micro-scale observations of the structure of aerobic microbial granules used for the treatment of nutrient-rich industrial wastewater. *The ISME journal 2*, 5 (2008), 528–541.

[64] LETTINGA, G., VAN VELSEN, A., HOBMA, S. D., DE ZEEUW, W., AND KLAPWIJK, A. Use of the upflow sludge blanket (usb) reactor concept for biological wastewater treatment, especially for anaerobic treatment. *Biotechnology and bioengineering 22*, 4 (1980), 699–734.

[65] LI, J., ZHENG, X., GUO, X., QI, L., AND DONG, X. Characterization of an archaeal two-component system that regulates methanogenesis in methanosaeta harundinacea. *PloS one 9*, 4 (2014), e95502.

[66] LI, L., ZHENG, M., MA, H., GONG, S., AI, G., LIU, X., LI, J., WANG, K., AND DONG, X. Significant performance enhancement of a uasb reactor by using acyl homoserine lactones to facilitate the long filaments of methanosaeta harundinacea 6ac. *Applied microbiology and biotechnology 99*, 15 (2015), 6471–6480.

[67] LI, TONG AND PODOLA, BJÖRN AND MELKONIAN, MICHAEL. Investigating dynamic processes in a porous substrate biofilm photobioreactor-a modeling approach. *Algal research 13* (2016), 30–40.

[68] LIM, S. J., AND KIM, T.-H. Applicability and trends of anaerobic granular sludge treatment processes. *Biomass and bioenergy 60* (2014), 189–202.

[69] LIU, Y., AND TAY, J.-H. The essential role of hydrodynamic shear force in the formation of biofilm and granular sludge. *Water research 36*, 7 (2002), 1653–1665.

[70] LIU, Y., AND TAY, J.-H. State of the art of biogranulation technology for wastewater treatment. *Biotechnology advances 22*, 7 (2004), 533–563.

[71] LONG, S. P., HUMPHRIES, S., AND FALKOWSKI, P. G. Photoinhibition of photosynthesis in nature. *Annual review of plant biology 45*, 1 (1994), 633–662.

[72] MACLEOD, F., GUIOT, S., AND COSTERTON, J. Layered structure of bacterial aggregates produced in an upflow anaerobic sludge bed and filter reactor. *Applied and Environmental Microbiology 56*, 6 (1990), 1598–1607.

[73] MAŠIĆ, A., AND EBERL, H. J. Persistence in a single species cstr model with suspended flocs and wall attached biofilms. *Bulletin of mathematical biology 74*, 4 (2012), 1001–1026.

[74] MAŠIĆ, A., AND EBERL, H. J. A modeling and simulation study of the role of suspended microbial populations in nitrification in a biofilm reactor. *Bulletin of mathematical biology 76*, 1 (2014), 27–58.

[75] MATTEI, M., FRUNZO, L., D'ACUNTO, B., PECHAUD, Y., PIROZZI, F., AND ESPOSITO, G. Continuum and discrete approach in modeling biofilm development and structure: a review. *Journal of mathematical biology 76*, 4 (2018), 945–1003.

[76] MATTEI, M., FRUNZO, L., D'ACUNTO, B., PECHAUD, Y., PIROZZI, F., AND ESPOSITO, G. Continuum and discrete approach in modeling biofilm development and structure: a review. *Journal of Mathematical Biology 76*, 4 (2018), 945–1003.

[77] MCDOUGALD, D., RICE, S. A., BARRAUD, N., STEINBERG, P. D., AND KJELLEBERG, S. Should we stay or should we go: mechanisms and ecological consequences for biofilm dispersal. *Nature Reviews Microbiology 10*, 1 (2012), 39–50.

[78] MERKEY, B. V., RITTMANN, B. E., AND CHOPP, D. L. Modeling how soluble microbial products (smp) support heterotrophic bacteria in autotroph-based biofilms. *Journal of theoretical biology 259*, 4 (2009), 670–683.

[79] MILFERSTEDT, K., KUO-DAHAB, W. C., BUTLER, C. S., HAMELIN, J., ABOUHEND, A. S., STAUCH-WHITE, K., MCNAIR, A., WATT, C., CARBAJAL-GONZÁLEZ, B. I., DOLAN, S., ET AL. The importance of filamentous cyanobacteria in the development of oxygenic photogranules. *Scientific reports 7*, 1 (2017), 1–15.

[80] MIRANDA, A. F., RAMKUMAR, N., ANDRIOTIS, C., HÖLTKEMEIER, T., YASMIN, A., ROCHFORT, S., WLODKOWIC, D., MORRISON, P., RODDICK, F., SPANGENBERG, G., ET AL. Applications of microalgal biofilms for wastewater treatment and bioenergy production. *Biotechnology for biofuels 10*, 1 (2017), 120.

[81] MITRA, A., AND FLYNN, K. J. Modelling mixotrophy in harmful algal blooms: More or less the sum of the parts? *Journal of Marine Systems 83*, 3-4 (2010), 158–169.

[82] MOUGET, J.-L., DAKHAMA, A., LAVOIE, M. C., AND DE LA NOÜE, J. Algal growth enhancement by bacteria: is consumption of photosynthetic oxygen involved? *FEMS Microbiology Ecology 18*, 1 (1995), 35–43.

[83] MUELLER, B., DEN HAAN, J., VISSER, P. M., VERMEIJ, M. J., AND VAN DUYL, F. C. Effect of light and nutrient availability on the release of dissolved organic carbon (doc) by caribbean turf algae. *Scientific reports 6* (2016), 23248.

[84] MUÑOZ SIERRA, J., PICIOREANU, C., AND VAN LOOSDRECHT, M. Modeling phototrophic biofilms in a plug-flow reactor. *Water Science and Technology 70*, 7 (2014), 1261–1270.

[85] NANCHARAIAH, Y. V., JOSHI, H. M., HAUSNER, M., AND VENUGOPALAN, V. P. Bioaugmentation of aerobic microbial granules with pseudomonas putida carrying tol plasmid. *Chemosphere 71*, 1 (2008), 30–35.

[86] NATRAH, F. M., BOSSIER, P., SORGELOOS, P., YUSOFF, F. M., AND DEFOIRDT, T. Significance of microalgal–bacterial interactions for aquaculture. *Reviews in Aquaculture 6*, 1 (2014), 48–61.

[87] NICOLELLA, C., VAN LOOSDRECHT, M., AND HEIJNEN, J. Wastewater treatment with particulate biofilm reactors. *Journal of biotechnology 80*, 1 (2000), 1–33.

[88] ODRIOZOLA, M., LÓPEZ, I., AND BORZACCONI, L. Modeling granule development and reactor performance on anaerobic granular sludge reactors. *Journal of environmental chemical engineering 4*, 2 (2016), 1615–1628.

[89] O'TOOLE, G., KAPLAN, H. B., AND KOLTER, R. Biofilm formation as microbial development. *Annual Reviews in Microbiology 54*, 1 (2000), 49–79.

[90] PALMER, J., FLINT, S., AND BROOKS, J. Bacterial cell attachment, the beginning of a biofilm. *Journal of industrial microbiology & biotechnology 34*, 9 (2007), 577–588.

[91] PICIOREANU, C., BATSTONE, D. J., AND VAN LOOSDRECHT, M. Multidimensional modelling of anaerobic granules. *Water Science and Technology 52*, 1-2 (2005), 501–507.

[92] POL, L. H., DE CASTRO LOPES, S., LETTINGA, G., AND LENS, P. Anaerobic sludge granulation. *Water Research 38*, 6 (2004), 1376–1389.

[93] POLIZZI, B., BERNARD, O., AND RIBOT, M. A time-space model for the growth of microalgae biofilms for biofuel production. *Journal of theoretical biology 432* (2017), 55–79.

[94] POSADAS, E., GARCÍA-ENCINA, P.-A., SOLTAU, A., DOMÍNGUEZ, A., DÍAZ, I., AND MUÑOZ, R. Carbon and nutrient removal from centrates and

domestic wastewater using algal–bacterial biofilm bioreactors. *Bioresource technology 139* (2013), 50–58.

[95] PRONK, M., DE KREUK, M., DE BRUIN, B., KAMMINGA, P., KLEEREBEZEM, R. V., AND VAN LOOSDRECHT, M. Full scale performance of the aerobic granular sludge process for sewage treatment. *Water Research 84* (2015), 207–217.

[96] RAHMAN, K. A., SUDARSAN, R., AND EBERL, H. J. A mixed-culture biofilm model with cross-diffusion. *Bulletin of mathematical biology 77*, 11 (2015), 2086–2124.

[97] RAHMAN, K. A., SUDARSAN, R., AND EBERL, H. J. A mixed-culture biofilm model with cross-diffusion. *Bulletin of mathematical biology 77*, 11 (2015), 2086–2124.

[98] RAMANAN, R., KIM, B.-H., CHO, D.-H., OH, H.-M., AND KIM, H.-S. Algae–bacteria interactions: evolution, ecology and emerging applications. *Biotechnology advances 34*, 1 (2016), 14–29.

[99] RAS, M., LEFEBVRE, D., DERLON, N., PAUL, E., AND GIRBAL-NEUHAUSER, E. Extracellular polymeric substances diversity of biofilms grown under contrasted environmental conditions. *Water research 45*, 4 (2011), 1529–1538.

[100] ROESELERS, G., VAN LOOSDRECHT, M., AND MUYZER, G. Heterotrophic pioneers facilitate phototrophic biofilm development. *Microbial Ecology 54*, 3 (2007), 578–585.

[101] ROESELERS, G., VAN LOOSDRECHT, M. C., AND MUYZER, G. Phototrophic biofilms and their potential applications. *Journal of applied phycology 20*, 3 (2008), 227–235.

[102] ROHANIZADEGAN, Y., SONNER, S., AND EBERL, H. J. Discrete attachment to a cellulolytic biofilm modeled by an itô stochastic differential equation.

[103] ROMANI, A. M. Freshwater biofilms. *Biofouling. Wiley-Blackwell, Oxford* (2010), 137–153.

[104] ROOSTAEI, J., ZHANG, Y., GOPALAKRISHNAN, K., AND OCHOCKI, A. J. Mixotrophic microalgae biofilm: A novel algae cultivation strategy for improved productivity and cost-efficiency of biofuel feedstock production. *Scientific reports 8*, 1 (2018), 12528.

[105] ROSSI, F., AND DE PHILIPPIS, R. Role of cyanobacterial exopolysaccharides in phototrophic biofilms and in complex microbial mats. *Life 5*, 2 (2015), 1218–1238.

[106] RUMBAUGH, K. P., AND SAUER, K. Biofilm dispersion. *Nature Reviews Microbiology 18*, 10 (2020), 571–586.

[107] SEGHEZZO, L., ZEEMAN, G., VAN LIER, J. B., HAMELERS, H., AND LETTINGA, G. A review: the anaerobic treatment of sewage in uasb and egsb reactors. *Bioresource technology 65*, 3 (1998), 175–190.

[108] SEKIGUCHI, Y., KAMAGATA, Y., NAKAMURA, K., OHASHI, A., AND HARADA, H. Fluorescence in situ hybridization using 16s rrna-targeted oligonucleotides reveals localization of methanogens and selected uncultured bacteria in mesophilic and thermophilic sludge granules. *Applied and environmental microbiology 65*, 3 (1999), 1280–1288.

[109] SEOK, J., AND KOMISAR, S. J. Integrated modeling of anaerobic fluidized bed bioreactor for deicing waste treatment. i: Model derivation. *Journal of Environmental Engineering 129*, 2 (2003), 100–109.

[110] SHIBASAKI, S., AND MITRI, S. Controlling evolutionary dynamics to optimize microbial bioremediation. *BioRxiv* (2019), 705749.

[111] SKIADAS, I. V., AND AHRING, B. K. A new model for anaerobic processes of up-flow anaerobic sludge blanket reactors based on cellular automata. *Water science and technology 45*, 10 (2002), 87–92.

[112] SOLIMENO, A., PARKER, L., LUNDQUIST, T., AND GARCÍA, J. Integral microalgae-bacteria model (bio_algae): Application to wastewater high rate algal ponds. *Science of the total environment 601* (2017), 646–657.

[113] SORRELL, B. K., HAWES, I., SCHWARZ, A.-M., AND SUTHERLAND, D. Inter-specific differences in photosynthetic carbon uptake, photosynthate partitioning and extracellular organic carbon release by deep-water characean algae. *Freshwater Biology 46*, 4 (2001), 453–464.

[114] STAUCH-WHITE, K., SRINIVASAN, V. N., KUO-DAHAB, W. C., PARK, C., AND BUTLER, C. S. The role of inorganic nitrogen in successful formation of granular biofilms for wastewater treatment that support cyanobacteria and bacteria. *Amb Express 7*, 1 (2017), 1–10.

[115] STEELE, J. H. Environmental control of photosynthesis in the sea. *Limnology and oceanography 7*, 2 (1962), 137–150.

[116] STEWART, P. S. Diffusion in biofilms. *Journal of bacteriology 185*, 5 (2003), 1485–1491.

[117] SUTHERLAND, I. W. The biofilm matrix-an immobilized but dynamic microbial environment. *Trends in microbiology 9*, 5 (2001), 222–227.

[118] TAY, J.-H., LIU, Q.-S., AND LIU, Y. The effects of shear force on the formation, structure and metabolism of aerobic granules. *Applied microbiology and biotechnology 57*, 1-2 (2001), 227–233.

[119] TENORE, A., MATTEI, M., AND FRUNZO, L. Modelling the ecology of phototrophic-heterotrophic biofilms. *Communications in Nonlinear Science and Numerical Simulation 94*, 105577.

[120] TILZER, M. M. Light-dependence of photosynthesis and growth in cyanobacteria: Implications for their dominance in eutrophic lakes. *New Zealand Journal of Marine and Freshwater Research 21*, 3 (1987), 401–412.

[121] TING, C. S., ROCAP, G., KING, J., AND CHISHOLM, S. W. Cyanobacterial photosynthesis in the oceans: the origins and significance of divergent light-harvesting strategies. *Trends in microbiology 10*, 3 (2002), 134–142.

[122] TREGO, A. C., GALVIN, E., SWEENEY, C., DUNNING, S., MURPHY, C., MILLS, S., NZETEU, C., QUINCE, C., CONNELLY, S., IJAZ, U. Z., ET AL. De novo growth of methanogenic granules indicates a biofilm life-cycle with complex ecology. *bioRxiv* (2019).

[123] TREGO, A. C., MILLS, S., AND COLLINS, G. Granular biofilms: Formation, function, application, and new trends as model microbial communities.

[124] TRULEAR, M. G., AND CHARACKLIS, W. G. Dynamics of biofilm processes. *Journal (Water Pollution Control Federation)* (1982), 1288–1301.

[125] VAN DER STAR, W. R., ABMA, W. R., BLOMMERS, D., MULDER, J.-W., TOKUTOMI, T., STROUS, M., PICIOREANU, C., AND VAN LOOSDRECHT, M. C. Startup of reactors for anoxic ammonium oxidation: experiences from the first full-scale anammox reactor in rotterdam. *Water research 41*, 18 (2007), 4149–4163.

[126] VANDERHAEGEN, B., YSEBAERT, E., FAVERE, K., VAN WAMBEKE, M., PEETERS, T., PANIC, V., VANDENLANGENBERGH, V., AND VERSTRAETE,

W. Acidogenesis in relation to in-reactor granule yield. *Water Science and Technology 25*, 7 (1992), 21–30.

[127] VANGSGAARD, A. K., MAURICIO-IGLESIAS, M., GERNAEY, K. V., SMETS, B. F., AND SIN, G. Sensitivity analysis of autotrophic n removal by a granule based bioreactor: Influence of mass transfer versus microbial kinetics. *Bioresource technology 123* (2012), 230–241.

[128] VÁZQUEZ-NION, D., RODRÍGUEZ-CASTRO, J., LÓPEZ-RODRÍGUEZ, M., FERNÁNDEZ-SILVA, I., AND PRIETO, B. Subaerial biofilms on granitic historic buildings: microbial diversity and development of phototrophic multi-species cultures. *Biofouling 32*, 6 (2016), 657–669.

[129] VOLCKE, E., PICIOREANU, C., DE BAETS, B., AND VAN LOOSDRECHT, M. Effect of granule size on autotrophic nitrogen removal in a granular sludge reactor. *Environmental technology 31*, 11 (2010), 1271–1280.

[130] VOLCKE, E., PICIOREANU, C., DE BAETS, B., AND VAN LOOSDRECHT, M. The granule size distribution in an anammox-based granular sludge reactor affects the conversion-implications for modeling. *Biotechnology and bioengineering 109*, 7 (2012), 1629–1636.

[131] WÁGNER, D. S., VALVERDE-PÉREZ, B., SÆBØ, M., DE LA SOTILLA, M. B., VAN WAGENEN, J., SMETS, B. F., AND PLOSZ, B. G. Towards a consensus-based biokinetic model for green microalgae–the asm-a. *Water research 103* (2016), 485–499.

[132] WANNER, O., AND GUJER, W. A multispecies biofilm model. *Biotechnology and bioengineering 28*, 3 (1986), 314–328.

[133] WANNER, O., AND REICHERT, P. Mathematical modeling of mixed-culture biofilms. *Biotechnology and bioengineering 49*, 2 (1996), 172–184.

[134] WARD, J. P., AND KING, J. R. Thin-film modelling of biofilm growth and quorum sensing. *Journal of Engineering Mathematics 73*, 1 (2012), 71–92.

[135] WATNICK, P., AND KOLTER, R. Biofilm, city of microbes. *Journal of bacteriology 182*, 10 (2000), 2675–2679.

[136] WEISSBRODT, D. G., NEU, T. R., KUHLICKE, U., RAPPAZ, Y., AND HOLLIGER, C. Assessment of bacterial and structural dynamics in aerobic granular biofilms. *Frontiers in microbiology 4* (2013), 175.

[137] WIEGANT, W. The spaghetti theory on anaerobic granular sludge formation, or the inevitability of granulation. *Granular anaerobic sludge* (1988), 146–152.

[138] WOLF, G., PICIOREANU, C., AND VAN LOOSDRECHT, M. C. Kinetic modeling of phototrophic biofilms: The phobia model. *Biotechnology and bioengineering 97*, 5 (2007), 1064–1079.

[139] WUERTZ, S., BISHOP, P. L., AND WILDERER, P. A. *Biofilms in wastewater treatment*. IWA publishing, 2003.

[140] XAVIER, J. B., DE KREUK, M. K., PICIOREANU, C., AND VAN LOOSDRECHT, M. C. Multi-scale individual-based model of microbial and bioconversion dynamics in aerobic granular sludge. *Environmental science & technology 41*, 18 (2007), 6410–6417.

[141] ZHANG, G., ZHANG, F., DING, G., LI, J., GUO, X., ZHU, J., ZHOU, L., CAI, S., LIU, X., LUO, Y., ET AL. Acyl homoserine lactone-based quorum sensing in a methanogenic archaeon. *The ISME journal 6*, 7 (2012), 1336–1344.

[142] ZHENG, D., ANGENENT, L., AND RASKIN, L. Monitoring granule formation in anaerobic upflow bioreactors using oligonucleotide hybridization probes. *Biotechnology and bioengineering 94*, 3 (2006), 458–472.

[143] ZHUANG, L.-L., AZIMI, Y., YU, D., WANG, W.-L., WU, Y.-H., DAO, G.-H., AND HU, H.-Y. Enhanced attached growth of microalgae scenedesmus. lx1 through ambient bacterial pre-coating of cotton fiber carriers. *Bioresource technology 218* (2016), 643–649.

[144] ZLOTNIK, I., AND DUBINSKY, Z. The effect of light and temperature on doc excretion by phytoplankton. *Limnology and Oceanography 34*, 5 (1989), 831–839.